# Evaluating the involvement of metallothionein I in complex I deficiency: an *in vitro* study

**M Mereis**

orcid.org 0000-0002-0112-0691

Dissertation submitted in partial fulfilment of the requirements for the degree *Master of Science in Biochemistry* at the North-West University

Supervisor: Prof FH van der Westhuizen

Co-supervisor: Prof R Louw

Graduation May 2018

23114126

*“I can do all things through Christ who strengthens me.”*
Philippians 4:13

# ACKNOWLEDGEMENTS

Firstly, I would like to thank my supervisor, **Prof Francois van der Westhuizen**, for his unfaltering patience, support, and guidance. His belief in me and his willingness to help will always motivate me to strive for greatness. He continues to inspire me to challenge myself and excel in this field.

Secondly, I would like to thank my co-supervisor, **Prof Roan Louw**, for his insight, advice, and enthusiasm. His example of perseverance is inspiring.

I would also like to thank the following people and institutions whose contribution enabled the completion of this dissertation:

- The financial assistance of the **National Research Foundation (NRF)** towards this research is hereby acknowledged. Opinions expressed and conclusions arrived at, are those of the author and are not necessarily to be attributed to the NRF.
- The **North-West University (NWU)**, for financial support.
- The **staff at the Preclinical Drug Development Platform (PCDDP)** of the NWU, Potchefstroom Campus, for their care and assistance with the mice used in this study.
- The **staff at the Jackson Laboratory**, for their assistance with the SNP genotyping.
- **Prof Albert Quintana**, previously from the University of Washington (Seattle, WA, USA), for his input in this study and gracious donation of *Ndufs4*$^{+/-}$ mice.
- **Prof Lissinda du Plessis**, for her expertise and help with the flow cytometric analyses.
- **Mari van Reenen**, for her invaluable assistance with regards to the statistical analyses.
- **Helgard Jordaan**, for his impeccable service in language and grammar editing.
- My **colleagues at the Mitochondrial Laboratory**, NWU, Potchefstroom Campus, for their laughter, friendship, and support.

I especially want to thank **my parents**, without whom none of this would have been possible. Their endless love and support throughout the years have meant more to me than I will ever be able to say. Their example and motivation has always carried me and will continue to encourage me to be the best I can possibly be. Furthermore, I would like to thank my **brother** for his continued willingness to listen and for his motivation.

I would also like to thank my best friend, **Driaan**, for putting up with me when I didn't even want to put up with myself, for wiping my tears and encouraging me, for putting my needs before his own, and for his unconditional love and support.

Finally, and most importantly, I would like thank the **Lord** for all the blessings He has given me, for the amazing people He has put in my life, for all the opportunities I have been allowed to have, and for His unfailing love. This dissertation was possible by His Grace alone.

# ABSTRACT

Among the inborn errors of energy metabolism, complex I (CI) deficiency is the most frequently encountered and debilitating disorder of the oxidative phosphorylation system. Hallmarks include an early onset, progressive and heterogeneous course resulting in mortality, as well as a lack of curative treatment. On a cellular level, CI deficiency exhibits various biochemical consequences, of which the most destructive is the excessive production of reactive oxygen species (ROS). Previous studies at this institution have investigated the adaptive cellular responses associated with CI deficiency, with special focus on the increased expression of metallothioneins (MTs). MTs are small, non-enzymatic, endogenously expressed proteins, which have been shown to be involved in mitochondrial energy modulation and the detoxification of ROS. Consequently, these proteins may provide a novel therapeutic option against CI deficiency. However, a suitable experimental model to investigate this has been lacking.

Therefore, this study aspired to realise two aims: Firstly, to produce and characterise (on a genetic and protein level) an *in vitro* model with which the effect of MTI overexpression on CI deficiency could be investigated; secondly, to perform an *in vitro* evaluation of the effect of MTI overexpression on the bioenergetics consequences of CI deficiency. To achieve the first, *Ndufs4* knockout (a CI-deficient model) and TgMTI (an MTI overexpressing model) mice were used. In comparing their genetic backgrounds to C57BL6/J, a clear match was revealed. Consequently, the two mouse strains were crossbred to obtain four genotypes [wildtype, CI-deficient, MTI overexpressing and CI-deficient MTI overexpressing (experimental model)] from which primary skin fibroblasts – used for the remainder of the study – were successfully established. Upon characterisation, each cell line was found to correspond to its expected Ndufs4 and TgMTI genotypes, while $TgMTI^{+/+}$ cell lines revealed *MtI* mRNA overexpression. CI deficiency could further be verified in the $Ndufs4^{-/-}$ cell lines, by the absence of the NDUFS4 [NADH dehydrogenase (ubiquinone) iron-sulphur protein 4] protein and instable and non-functional CI. Interestingly, these parameters were all increased in $Ndufs4^{+/+}$:$TgMTI^{+/+}$ cells. For the second aim, the effect of each genotype on cell viability, relative mitochondrial DNA copy number, cellular reduction-oxidation- and energy status, and ROS levels was determined. Finally, each genotype's bioenergetics profile was evaluated, using the Seahorse XF Analyser.

In this study, all objectives relating to the development and characterisation of primary mouse fibroblasts were thus successfully met. Since the four fibroblast models exhibited undeniable genetic and protein correspondence to the original mouse strains, they were regarded as suitable for further bioenergetics investigations. However, while the objectives of the second aim could be addressed using suitable methodologies, the results showed striking variation attributable to the process of cell culture, thereby making it impossible to accurately evaluate the effect of genotype

on the bioenergetics consequences of CI deficiency. In conclusion, while the model produced corresponded exactly to genetic and protein expectations, primary skin fibroblasts from these mouse models are not suitable to investigate MTI overexpression on CI deficiency. It is therefore recommended that robust conclusions involving these models can only be reached via an *in vivo* approach.

**Keywords:** adaptive response; complex I deficiency; Leigh syndrome; metallothionein; *Ndufs4* knockout mouse model; primary fibroblasts; reactive oxygen species; Seahorse XF Analyser; TgMTI mouse model

# CONTENTS

**ACKNOWLEDGEMENTS** ..... **i**

**ABSTRACT** ..... **iii**

**LIST OF FIGURES** ..... **xiii**

**LIST OF TABLES** ..... **xvi**

**LIST OF EQUATIONS** ..... **xvii**

**ABBREVIATIONS, SYMBOLS & UNITS** ..... **xviii**

**CHAPTER 1: INTRODUCTION** ..... **1**

**CHAPTER 2: LITERATURE REVIEW** ..... **3**

2.1 INTRODUCTION ..... 3

2.2 MITOCHONDRION ..... 3

2.2.1 STRUCTURE & ORGANIZATION ..... 3

2.2.2 FUNCTION & BIOLOGICAL SIGNIFICANCE ..... 4

2.2.3 MITOCHONDRIAL GENOME ..... 5

2.3 COMPLEX I ..... 6

2.3.1 STRUCTURE ..... 6

2.3.2 FUNCTION ..... 6

2.3.3 ASSEMBLY ..... 8

2.3.4 ACCESSORY SUBUNITS & THEIR FUNCTION ..... 8

2.3.5 THE NDUFS4 SUBUNIT ..... 9

2.4 MITOCHONDRIAL DYSFUNCTION ..... 10

2.4.1 INTRODUCTION ..... 10

2.4.2 GENETICS & CLINICAL PHENOTYPE OF MITOCHONDRIAL DYSFUNCTION ..... 11

2.4.3 COMPLEX I DEFICIENCY ..... 12

2.4.3.1 GENETICS ..... 12

2.4.3.2 CLINICAL PHENOTYPE ..... 13

2.4.4 LEIGH SYNDROME ..... 14

2.4.5 DIAGNOSIS & TREATMENT OF MITOCHONDRIAL DYSFUNCTION ..... 15

# CONTENTS (continued)

2.5 BIOCHEMICAL CONSEQUENCES OF MITOCHONDRIAL DYSFUNCTION ..... 16
2.5.1 INTRODUCTION ..... 16
2.5.2 REACTIVE OXYGEN SPECIES ..... 17
2.5.3 CELLULAR REDOX STATUS ..... 18
2.5.4 CELLULAR ENERGY STATUS ..... 19
2.5.5 $Ca^{2+}$ HOMEOSTASIS & MITOCHONDRIAL MEMBRANE POTENTIAL ..... 20
2.6 ADAPTIVE RESPONSES TO MITOCHONDRIAL DYSFUNCTION ..... 21
2.6.1 INTRODUCTION ..... 21
2.6.2 MITOCHONDRIAL BIOGENESIS ..... 22
2.6.3 REGULATION OF METABOLISM ..... 23
2.6.4 CELL DEATH ..... 24
2.6.4.1 BIOCHEMICAL THRESHOLD ..... 24
2.6.4.2 MECHANISMS OF CELL DEATH ..... 25
2.6.5 ANTIOXIDANT RESPONSE ..... 26
2.6.6 METALLOTHIONEINS ..... 27
2.6.6.1 GENERAL PROPERTIES ..... 27
2.6.6.2 INDUCTION & BIOLOGICAL FUNCTION ..... 29
2.6.6.2.a THE ROLE OF METALLOTHIONEIN IN METAL HOMEOSTASIS ..... 32
2.6.6.2.b THE ROLE OF METALLOTHIONEIN IN PROTECTION AGAINST OXIDATIVE DAMAGE ..... 33
2.7 EXPERIMENTAL MODELS TO INVESTIGATE CI DEFICIENCY & *MT* INDUCTION ..... 34
**CHAPTER 3: EXPERIMENTAL RATIONALE, AIMS, OBJECTIVES & STRATEGY .....37**
3.1 INTRODUCTION ..... 37
3.2 PROBLEM STATEMENT ..... 37
3.3 AIMS & OBJECTIVES ..... 38
3.3.1 AIMS ..... 38
3.3.2 OBJECTIVES ..... 39
3.4 EXPERIMENTAL STRATEGY ..... 40

# CONTENTS (continued)

**CHAPTER 4: MATERIALS & METHODS ..... 45**

4.1 INTRODUCTION ..... 45

4.2 ETHICS, HOUSING & IDENTIFICATION OF MICE ..... 45

4.3 PART 1: ESTABLISHING & CHARACTERISING Ndufs4:TgMTI MICE ..... 46

4.3.1 GENOTYPING THE WHOLE GENOME OF THE Ndufs4 & TgMTI STRAINS – *Objective 1.1* ..... 46

4.3.1.1 METHODS ..... 47

4.3.1.1.a SAMPLE PREPARATION ..... 47

4.3.1.1.b GENOTYPING THE WHOLE GENOME USING AN SNP PANEL ..... 48

4.3.2 CROSSBREEDING THE Ndufs4 & TgMTI MOUSE LINES – *Objective 1.2* ..... 49

4.3.2.1 METHODS ..... 50

4.3.3 ESTABLISHING & CULTURING PRIMARY MOUSE FIBROBLAST CELL LINES – *Objective 1.3* ..... 52

4.3.3.1 METHODS ..... 52

4.3.3.1.a EUTHANISING MICE & COLLECTING SAMPLES ..... 52

4.3.3.1.b ESTABLISHING PRIMARY CULTURES ..... 53

4.3.3.1.c STANDARD CULTURING TECHNIQUES ..... 54

4.3.4 GENOTYPING Ndufs4:TgMTI MICE – *Objectives 1.4 & 1.5* ..... 55

4.3.4.1 METHODS ..... 55

4.3.4.1.a SAMPLE COLLECTION ..... 55

4.3.4.1.b ISOLATING & QUANTIFYING DNA FROM TAIL-SNIPS & CELLS ..... 56

4.3.4.1.c CHARACTERISING THE Ndufs4 GENOTYPE – *Objective 1.4* ..... 57

4.3.4.1.d CHARACTERISING THE TgMTI GENOTYPE – *Objective 1.5* ..... 59

4.3.5 QUANTIFYING THE RELATIVE *MtI* mRNA – *Objective 1.6* ..... 60

4.3.5.1 METHODS ..... 60

4.3.5.1.a SAMPLE COLLECTION ..... 61

4.3.5.1.b ISOLATING & QUANTIFYING RNA FROM CELLS ..... 61

4.3.5.1.c QUANTIFYING THE RELATIVE *MtI* mRNA BY MULTIPLEX RT-qPCR ..... 62

# CONTENTS (continued)


4.3.6 EXTRACTING & QUANTIFYING PROTEIN FROM CELLS FOR NDUFS4 & CI PROTEIN ANALYSES ..... 63

4.3.6.1 METHODS ..... 63

4.3.6.1.a SAMPLE COLLECTION ..... 63

4.3.6.1.b PROTEIN EXTRACTION FROM CELLS ..... 64

4.3.6.1.c QUANTIFYING TOTAL PROTEIN CONTENT BY THE BICINCHONINIC ACID METHOD ..... 64

4.3.7 QUANTIFYING THE STEADY STATE LEVEL OF NDUFS4 WITH SDS-PAGE + WESTERN BLOT ANALYSIS – *Objective 1.7* ..... 65

4.3.7.1 METHODS ..... 65

4.3.7.1.a SDS-PAGE ANALYSIS OF NDUFS4 ..... 65

4.3.7.1.b WESTERN BLOT ANALYSIS OF NDUFS4 ..... 66

4.3.8 QUANTIFYING THE STEADY STATE LEVEL & ACTIVITY OF FULLY ASSEMBLED CI WITH BN-PAGE + WESTERN BLOT & IGA ANALYSES – *Objective 1.8* ..... 67

4.3.8.1 METHODS ..... 67

4.3.8.1.a BN-PAGE ANALYSIS OF CI ..... 67

4.3.8.1.b WESTERN BLOT ANALYSIS OF CI ..... 69

4.3.8.1.c IGA ANALYSIS OF CI ACTIVITY ..... 69

4.3.8.1.d COOMASSIE STAINING OF THE PROTEIN LADDER ..... 69

4.4 PART 2: INVESTIGATING THE EFFECT OF MTI OVEREXPRESSION ON THE BIOENERGETICS CONSEQUENCES OF CI DEFICIENCY ..... 70

4.4.1 DETERMINING CELL VIABILITY WITH THE MTT ASSAY – *Objective 2.1* ..... 70

4.4.1.1 METHODS ..... 70

4.4.1.1.a SEEDING CELLS ..... 71

4.4.1.1.b MTT ASSAY ..... 71

4.4.2 DETERMINING THE RMCN BY qPCR ANALYSIS – *Objective 2.2* ..... 72

4.4.2.1 METHODS ..... 72

4.4.3 QUANTIFYING THE RELATIVE NADH/$NAD^+$ RATIO – *Objective 2.3* ..... 73

4.4.3.1 METHODS ..... 73

# CONTENTS (continued)


4.4.3.1.a SEEDING CELLS ..... 73

4.4.3.1.b NAD/NADH-GLO™ ASSAY ..... 73

4.4.4 QUANTIFYING THE RELATIVE ATP/ADP RATIO – *Objective 2.4* ..... 74

4.4.4.1 METHODS ..... 74

4.4.4.1.a SEEDING CELLS ..... 74

4.4.4.1.b ADP/ATP RATIO ASSAY ..... 75

4.4.5 DETERMINING ROS LEVELS USING THE BD FACSVerse™ FLOW CYTOMETER – *Objective 2.5* ..... 76

4.4.5.1 FLUORESCENCE-BASED QUANTIFICATION OF ROS USING FLOW CYTOMETRY ..... 76

4.4.5.2 METHODS ..... 77

4.4.5.2.a SAMPLE PREPARATION ..... 77

4.4.5.2.b ANALYSING THE ROS LEVELS USING THE BD FACSVERSE™ FLOW CYTOMETER ..... 78

4.4.6 DETERMINING THE BIOENERGETICS PROFILE USING THE SEAHORSE XF$^{e}$96 ANALYSER – *Objective 2.6* ..... 79

4.4.6.1 OPERATION OF THE EXTRACELLULAR FLUX ANALYSER ..... 79

4.4.6.2 DESCRIPTION OF THE PARAMETERS EVALUATED ..... 82

4.4.6.3 METHODS ..... 83

4.4.6.3.a DETERMINING THE BIOENERGETICS PROFILE USING A MITO STRESS TEST ..... 83

4.4.6.3.b NORMALISING TO CELL NUCLEIC ACID CONTENT USING THE CYQUANT® CELL PROLIFERATION ASSAY KIT ..... 84

4.4.7 STATISTICAL ANALYSES & INTERPRETATION – *Objective 2.7.* ..... 85

4.4.7.1 STATISTICAL ANALYSES ..... 85

4.4.7.2 INTERPRETATION ..... 88

**CHAPTER 5: RESULTS & DISCUSSION PART 1: ESTABLISHING & CHARACTERISING Ndufs4:TgMTI MICE ..... 91**

5.1 INTRODUCTION ..... 91

# CONTENTS (continued)

5.2 GENOTYPING THE WHOLE GENOME OF THE Ndufs4 & TgMTI STRAINS – *Objective 1.1* ..... 92

5.2.1 INTRODUCTION ..... 92

5.2.2 RESULTS ..... 93

5.2.3 DISCUSSION ..... 93

5.3 CROSSBREEDING THE Ndufs4 & TgMTI MOUSE LINES & ESTABLISHING & CULTURING PRIMARY MOUSE FIBROBLAST CELL LINES – *Objectives 1.2 & 1.3* ..... 94

5.3.1 RESULTS & DISCUSSION ..... 94

5.4 GENOTYPING Ndufs4:TgMTI MICE – *Objectives 1.4 & 1.5* ..... 95

5.4.1 CHARACTERISING THE Ndufs4 GENOTYPE – *Objective 1.4* ..... 95

5.4.1.1 INTRODUCTION ..... 95

5.4.1.2 RESULTS ..... 96

5.4.1.3 DISCUSSION ..... 96

5.4.2 CHARACTERISING THE TgMTI GENOTYPE – *Objective 1.5* ..... 97

5.4.2.1 INTRODUCTION ..... 97

5.4.2.2 RESULTS ..... 98

5.4.2.3 DISCUSSION ..... 98

5.5 QUANTIFYING THE RELATIVE *MtI* mRNA – *Objective 1.6* ..... 99

5.5.1 INTRODUCTION ..... 99

5.5.2 RESULTS ..... 100

5.5.3 DISCUSSION ..... 101

5.6 QUANTIFYING THE STEADY STATE LEVEL OF NDUFS4 WITH SDS-PAGE + WESTERN BLOT ANALYSIS – *Objective 1.7* ..... 102

5.6.1 INTRODUCTION ..... 102

5.6.2 RESULTS ..... 103

5.6.3 DISCUSSION ..... 104

5.7 QUANTIFYING THE STEADY STATE LEVEL & ACTIVITY OF FULLY ASSEMBLED CI WITH BN-PAGE + WESTERN BLOT & IGA ANALYSES – *Objective 1.8* ..... 104

5.7.1 INTRODUCTION ..... 104

# CONTENTS (continued)

5.7.2 RESULTS ..... 106

5.7.3 DISCUSSION ..... 107

**CHAPTER 6: RESULTS & DISCUSSION PART 2: INVESTIGATING THE EFFECT OF MTI OVEREXPRESSION ON THE BIOENERGETICS CONSEQUENCES OF CI DEFICIENCY .. 111**

6.1 INTRODUCTION ..... 111

6.2 DETERMINING CELL VIABILITY WITH THE MTT ASSAY – *Objective 2.1* ..... 111

6.2.1 INTRODUCTION ..... 111

6.2.2 RESULTS ..... 112

6.2.3 DISCUSSION ..... 113

6.3 DETERMINING THE RMCN BY qPCR ANALYSIS – *Objective 2.2* ..... 115

6.3.1 INTRODUCTION ..... 115

6.3.2 RESULTS ..... 116

6.3.3 DISCUSSION ..... 116

6.4 QUANTIFYING THE RELATIVE NADH/$NAD^+$ RATIO – *Objective 2.3* ..... 117

6.4.1 INTRODUCTION ..... 117

6.4.2 RESULTS ..... 118

6.4.3 DISCUSSION ..... 119

6.5 QUANTIFYING THE RELATIVE ATP/ADP RATIO – *Objective 2.4* ..... 120

6.5.1 INTRODUCTION ..... 120

6.5.2 RESULTS ..... 121

6.5.3 DISCUSSION ..... 121

6.6 DETERMINING THE ROS LEVELS USING THE BD FACSVerse™ FLOW CYTOMETER – *Objective 2.5* ..... 122

6.6.1 INTRODUCTION ..... 122

6.6.2 RESULTS ..... 123

6.6.3 DISCUSSION ..... 124

6.7 DETERMINING THE BIOENERGETICS PROFILE USING THE SEAHORSE $XF^e96$ ANALYSER – *Objective 2.6* ..... 127

# CONTENTS (continued)

6.7.1 INTRODUCTION....127
6.7.2 RESULTS....128
6.7.3 DISCUSSION....130
**CHAPTER 7: SUMMARY & CONCLUSIONS....133**
7.1 INTRODUCTION....133
7.2 PART 1: ESTABLISHING & CHARACTERISING Ndufs4:TgMTI MICE – *Aim 1*....134
7.3 PART 2: INVESTIGATING THE EFFECT OF MTI OVEREXPRESSION ON THE BIOENERGETICS CONSEQUENCES OF CI DEFICIENCY – *Aim 2*....136
7.4 FINAL CONCLUSIONS & FUTURE PROSPECTS....140
**REFERENCES....143**
**APPENDIX A: PUNNETT SQUARES....169**
**APPENDIX B: OPTIMISATION OF THE qPCR AMPLIFICATION OF DNA & RNA....171**
INTRODUCTION....171
i. OPTIMISATION OF INPUT TEMPLATE DNA & RNA CONCENTRATION....171
ii. PCR AMPLIFICATION EFFICIENCY....173
iii. RELATIVE EFFICIENCY OF COMPARED qPCR REACTIONS....174
**APPENDIX C: PREPARATION OF SDS-PAGE GEL....176**
**APPENDIX D: 96-WELL MICROTITER PLATE LAYOUTS....177**
**APPENDIX E: OPTIMISATION OF THE SEAHORSE XF$^{e}$96 ANALYSER CONDITIONS....179**
INTRODUCTION....179
i. SEEDING CELLS & ANALYSING THE BIOENERGETICS PROFILE USING THE SEAHORSE XF$^{e}$96 ANALYSER....179
ii. OPTIMISING THE CELL SEEDING DENSITY & FCCP CONCENTRATION....180
**APPENDIX F: LANGUAGE EDITING CERTIFICATE....184**

# LIST OF FIGURES

**CHAPTER 2**

**Figure 2.1:** Mitochondrial OXPHOS system ..... 4

**Figure 2.2:** Surface structure representation of CI [based on the bovine CI structure (PDB ID: 4UQ8)] indicating subunits associated with human CI deficiency ..... 13

**Figure 2.3:** Three-dimensional representation of the tertiary structure of rat MTII ..... 28

**Figure 2.4:** Illustration of the biochemical consequences and adaptive responses associated with CI deficiency (indicated by letters), with special focus on *MT* induction and MT function (indicated by numbers) ..... 30

**CHAPTER 3**

**Figure 3.1:** Experimental strategy depicting the aims and objectives of the study ..... 42

**CHAPTER 4**

**Figure 4.1:** Illustration depicting the ear punch numbering system employed to identify mice used in this study ..... 46

**Figure 4.2:** Breeding strategy design used to obtain *Ndufs4*$^{+/+}$*:TgMTI*$^{+/+}$, *Ndufs4*$^{-/-}$*:TgMTI*$^{+/+}$, *Ndufs4*$^{+/+}$*:TgMTI*$^{-/-}$, and *Ndufs4*$^{-/-}$*:TgMTI*$^{-/-}$ genotypes ..... 51

**Figure 4.3:** Illustration of the BN-PAGE well layout ..... 68

**Figure 4.4:** Flow cytometric dot plots and histogram depicting the gating method employed for this study ..... 79

**Figure 4.5:** Mito Stress Test profile ..... 81

**Figure 4.6:** Strategy depicting the statistical analyses performed on the data obtained from Objectives 2.1 and 2.3 to 2.6 ..... 86

**CHAPTER 5**

**Figure 5.1:** Image depicting mouse skin fibroblasts with fusiform morphology, exiting the skin explant after three days of culture ..... 94

**Figure 5.2:** Agarose gel electrophoresis image depicting the bands produced by each sample and three Ndufs4 controls ..... 96

**Figure 5.3:** Bar chart depicting the nuclear *MtI* copy number, relative to *Actb*, for each sample and three TgMTI controls ..... 98

**Figure 5.4:** Bar chart depicting the mRNA expression of *Mtl*, relative to *B2m*, for each sample and four controls .....100

**Figure 5.5.a-b:** Western blot of NDUFS4 and VDAC1 following separation by SDS-PAGE, and a bar chart depicting normalised NDUFS4 band intensity. .....103

**Figure 5.6.a-b:** Western blot of CI and CII following separation by BN-PAGE, and a bar chart depicting normalised CI band intensity.....106

**Figure 5.7.a-b:** In-gel activity analysis of CI following separation by BN-PAGE, and a bar chart depicting normalised CI band intensity.....107

**CHAPTER 6**

**Figure 6.1.a-b:** Box plots depicting the percentage cell viability of two sets of cell lines, each comprising the four genotypes of interest.....112

**Figure 6.2.a-b:** Bar charts depicting the RMCN of two sets of cell lines, each comprising the four genotypes of interest.....116

**Figure 6.3.a-c:** Bar charts depicting the percentage NADH/$NAD^+$ ratio of two sets of cell lines, each comprising the four genotypes of interest, as well as the percentage $NAD^+$ of the positive control .....118

**Figure 6.4.a-c:** Bar charts depicting the percentage ATP/ADP ratio of two sets of cell lines, each comprising the four genotypes of interest, as well as the percentage ATP of the positive control.....121

**Figure 6.5.a-b:** Bar charts depicting the percentage ROS, expressed as the gMFI, of two sets of cell lines, each comprising the four genotypes of interest.....123

**Figure 6.6.a-c:** Histogram depicting the fluorescence of the cell- and positive controls, and two dot blots illustrating the differences in cell size between two genetically identical cell lines.....124

**Figure 6.7.a-b:** Box plots depicting the basal respiration of two sets of cell lines, each comprising the four genotypes of interest.....128

**Figure 6.7.c-d:** Box plots depicting the ATP production of two sets of cell lines, each comprising the four genotypes of interest.....129

**Figure 6.7.e-f:** Box plots depicting the maximal respiration of two sets of cell lines, each comprising the four genotypes of interest.....129

**APPENDIX A**

**Figure A.1:** Punnett squares depicting how the probability of each genotype was determined as a fraction of 4 or 16 ..... 169

**APPENDIX B**

**Figure B.1:** Standard curve depicting the results for *MtI*, *mt-Nd2* and *Actb* in Table B.2 .. 172

**Figure B.2:** Standard curve depicting the results for *MtI* (mRNA) and *B2m* (mRNA) in Table B.3 ..... 173

**Figure B.3:** Relative efficiency plot for *MtI* and *Actb* ..... 174

**Figure B.4:** Relative efficiency plot for *mt-Nd2* and *Actb* ..... 175

**Figure B.5:** Relative efficiency plot for *MtI* (mRNA) and *B2m* (mRNA) ..... 175

**APPENDIX D**

**Figure D.1:** Microtiter plate layout used for the MTT assay ..... 177

**Figure D.2:** Microtiter plate layout used for the NAD/NADH-Glo™ assay ..... 177

**Figure D.3:** Microtiter plate layout used for the ADP/ATP assay ..... 178

**Figure D.4:** Microtiter plate layout used for the Mito Stress Test ..... 178

**APPENDIX E**

**Figure E.1:** Microtiter plate layout depicting the different seeding densities and FCCP concentrations used for optimisation ..... 180

**Figure E.2:** Scatter plot depicting the relationship between the basal respiration (OCR taken at measurement 3) and cell seeding density ..... 181

**Figure E.3:** Scatter plot depicting the relationship between the basal respiration (OCR taken at measurement 3) and cell seeding density, normalised to the theoretical number of cells/well ..... 182

**Figure E.4:** Titration curve depicting the relationship between the maximal respiration (OCR taken at measurement 7) and FCCP concentration ..... 183

# LIST OF TABLES

**CHAPTER 4**

**Table 4.1:** Mice used for whole genome genotyping.....47

**Table 4.2:** Details of the mice used in this study.....52

**Table 4.3:** Mice used as controls for genotyping .....55

**Table 4.4:** Sequences of the primers used to genotype the *Ndufs4* gene.....57

**Table 4.5:** Mice used as controls for *MtI* mRNA quantification.....61

**Table 4.6:** Composition of the ATP- and ADP reagents required for one reaction .....75

**CHAPTER 5**

**Table 5.1:** Comparability of the Ndufs4 and TgMTI strains' genetic background to a reference C57BL6/J genome, as determined by SNP analysis.....93

**CHAPTER 6**

**Table 6.1:** Equations used by the Seahorse XF Cell Mito Stress Test Report Generator to obtain the reported parameters .....128

**APPENDIX B**

**Table B.1:** Mice used to optimise qPCR amplification.....171

**Table B.2:** Average $C_T$-values obtained for the *MtI*, *mt-Nd2* and *Actb* genes using a serial dilution of DNA .....172

**Table B.3:** Average $C_T$-values obtained for the *MtI* (mRNA) and *B2m* (mRNA) genes using a serial dilution of RNA.....172

**APPENDIX C**

**Table C.1:** Content of the stacking- and resolving components of the SDS-PAGE gel.....176

# LIST OF EQUATIONS

**CHAPTER 2**

**Equation 2.1:** Oxidation of NADH in the N module of CI ..... 7

**Equation 2.2:** Reduction of Q in the P module of CI ..... 7

**Equation 2.3:** Total reaction catalysed by CI ..... 7

**CHAPTER 4**

**Equation 4.1:** Calculation of protein concentration (in µg/µL) as used in the BCA method..... 65

**Equation 4.2:** Calculation of the ATP/ADP ratio..... 76

**Equation 4.3:** Calculation of the ROS gMFI ..... 78

**CHAPTER 5**

**Equation 5.1:** Calculation of the pooled SD by the Gauß error propagation..... 97

**Equation 5.2:** Calculation of the pooled CV% by the Gauß error propagation..... 100

**APPENDIX B**

**Equation B.1:** Calculation of the individual PCR amplification efficiency ..... 173

**Equation B.2:** Calculation of the percentage PCR amplification efficiency ..... 174

# ABBREVIATIONS, SYMBOLS & UNITS

| | |
|---|---|
| $^{-/-}$ | Wildtype genotype; gene of interest is unaltered in both alleles |
| [ ] | Concentration |
| ~ | Approximately |
| $^{+/-}$ | Heterozygous genotype; gene of interest is altered in one of the two alleles |
| $^{+/+}$ | Homozygous genotype; gene of interest is altered in both alleles |
| °C | Degrees Celsius |
| 143B | Human osteosarcoma cell line |
| $^1O_2$ | Singlet oxygen |
| 3’ | 3’-end of the polynucleotide chain |
| 5’ to 3’ | Polynucleotide directionality; from the 5’-end to the 3’-end |
| 5’ | 5’-end of the polynucleotide chain |
| α | Alpha |
| α-KG | α-ketoglutarate |
| α-KGDH | α-ketoglutarate dehydrogenase |
| α-value | The p threshold; the probability of making a Type I error |
| β | Beta |
| γ | Gamma |
| Δ | Delta |
| ΔpH | pH gradient |
| Δψ | Mitochondrial membrane potential |
| µg | Microgram |
| µL | Microlitre |
| µm | Micrometre |
| µM | Micromolar |
| $\rho^0$ | Rho0; mtDNA-depleted cells |

| | |
|---|---|
| A | Absorbance (followed by subscript) or ampere (following value) |
| *Actb* | β-actin gene |
| *ad libitum* | (Latin): without restraint; (consumption): food and water are available at all times |
| ADP | Adenosine diphosphate |
| Ag | Silver |
| AIDS | Acquired immune deficiency syndrome |
| AMP | Adenosine monophosphate |
| AMPK | Adenosine monophosphate-activated protein kinase |
| ANOVA | Analysis of variance |
| APS | Ammonium persulphate |
| ARE | Antioxidant response element |
| ATCC | American Type Culture Collection |
| ATP | Adenosine triphosphate |
| ATP5A | α-subunit of ATP synthase |
| *B2m* | β-2 microglobulin gene |
| BCA | Bicinchoninic acid |
| BN-PAGE | Blue-native polyacrylamide gel electrophoresis |
| bp | Base pairs |
| BSA | Bovine serum albumin |
| $Ca^{2+}$ | Calcium(II) ion |
| cAMP | Cyclic adenosine monophosphate |
| CAT | Catalase |
| Cat. no. | Catalogue number |
| CBB | Coomassie brilliant blue |
| CCO-Va | Cytochrome c oxidase-Va |
| Cd | Cadmium |
| $Cd^{2+}$ | Cadmium(II) ion |
| C-DCFH-DA-AM | 6-Carboxy-2',7'-dichlorodihydrofluorescein diacetate di(acetoxymethyl ester) |

| | |
|---|---|
| $CdCl_2$ | Cadmium chloride |
| cDNA | Complementary DNA |
| chr | Chromosome |
| CI | Complex I; NADH:ubiquinone oxidoreductase; EC 1.6.5.3 |
| CII | Complex II; succinate:ubiquinone oxidoreductase; EC 1.3.5.1 |
| CIII | Complex III; ubiquinol:ferricytochrome c oxidoreductase; EC 1.10.2.2 |
| CIV | Complex IV; ferrocytochrome-c:oxygen oxidoreductase; EC 1.9.3.1 |
| cm | Centimetre |
| $CO_2$ | Carbon dioxide |
| COX17 | Cytochrome c oxidase copper chaperone |
| COXIV | Cytochrome c oxidase subunit IV |
| CPEO | Chronic progressive external ophthalmoplegia |
| CT or $C_T$ | Threshold cycle |
| Cu | Copper |
| Cu/ZnSOD | Copper and zinc-containing superoxide dismutase |
| $Cu^+$ | Copper(I) ion |
| $Cu^{2+}$ | Copper(II) ion |
| $CuSO_4$ | Copper(II) sulphate |
| $CuSO_4 \cdot 5H_2O$ | Copper(II) sulphate pentahydrate |
| CV | Complex V; ATP synthase; EC 3.6.1.3 |
| CV% | Coefficient of variance |
| Cys | Cysteine |
| cyt c | Cytochrome c |
| DCF | 2',7'-Dichlorofluorescein |
| DCFH | 2',7'-Dichlorodihydrofluoroscein |
| DCFH-DA | 2',7'-Dichlorodihydrofluorescein diacetate |
| DDM | *n*-dodecyl-β-D-maltoside |
| *de novo* | (Latin): anew; from the beginning |

| | |
|---|---|
| DMEM | Dulbecco's Modified Eagle Medium |
| DMSO | Dimethyl sulfoxide |
| DNA Pol | Deoxyribonucleic acid polymerase |
| DNA | Deoxyribonucleic acid |
| dNTP | Deoxyribonucleotide triphosphate |
| DOB | Date of birth |
| DTAB | Dodecyltrimethylammonium bromide |
| $e^-$ | Electron |
| E | PCR amplification efficiency |
| ECAR | Extracellular acidification rate |
| ECL | Enhanced chemiluminescence |
| EDTA | Ethylenediaminetetraacetic acid |
| ELISA | Enzyme-linked immunosorbent assay |
| ER | Endoplasmic reticulum |
| *et al.* | *et alii* (Latin): and others |
| ETF:QO | Electron transfer flavoprotein-ubiquinone oxidoreductase |
| FACS | Fluorescence-activated cell sorting |
| $FADH_2$ | Reduced flavin adenine dinucleotide |
| FAM or 6-FAM | 6-Carboxyfluorescein |
| FBS | Fetal bovine serum |
| FCCP | Carbonyl cyanide-4-(trifluoromethoxy)phenylhydrazone |
| Fe-S | Iron-sulphur |
| FILA | Fatal infantile lactic acidosis |
| FITC | Green fluorescence |
| FMN | Oxidised flavin mononucleotide |
| $FMNH_2$ | Reduced flavin mononucleotide |
| FRET | Fluorescence resonance energy transfer |
| FSC | Forward scatter |

| | |
|---|---|
| g | Gram |
| G-6-P | Glucose-6-phosphate |
| gMFI | Geometric mean fluorescence intensity |
| GPDH | *s*,*n*-glycerophosphate dehydrogenase |
| GPx | Glutathione peroxidase |
| GR | Glutathione reductase |
| GSH | Reduced glutathione |
| GSSG | Oxidised glutathione; glutathione disulfide |
| GTPase | Guanosine triphosphatase |
| h | Hour(s) |
| $H^+$ | Hydrogen ion; proton |
| $H_2O$ | Water |
| $H_2O_2$ | Hydrogen peroxide |
| HCl | Hydrogen chloride |
| HeLa | Human cervical adenocarcinoma cell line |
| HEPA | High-efficiency particulate air |
| HEX | Hexachloro-6-carboxyfluorescein |
| Hg | Mercury |
| $Hg^{2+}$ | Mercury(II) ion |
| HOO· | Hydroperoxyl radical |
| HRP | Horse radish peroxidase |
| Hsc | Heat shock cognate |
| Hsp | Heat shock protein |
| ID | Identification number |
| IGA | In-gel activity |
| IMM | Inner mitochondrial membrane |
| IMS | Intermembrane space |
| *in utero* | (Latin): in the uterus; before birth |

| | |
|---|---|
| *in vitro* | (Latin): in the glass; (of a process): performed or taking place outside a living organism |
| *in vivo* | (Latin): in life; (of any biological process, reaction, or experiment): occurring or made to occur within a living organism |
| $IP_3$ | Inositol 1,4,5-triphosphate |
| $IP_3R$ | Inositol 1,4,5-triphosphate receptor |
| $K^+$ | Potassium ion |
| kb | Kilobase |
| KCl | Potassium chloride |
| kDa | Kilodalton |
| KO OVER | *Ndufs4* knockout MTI overexpressing sample (specific to this study) |
| KO | Knockout; *Ndufs4* knockout sample (specific to this study) |
| KSS | Kearns-Sayre syndrome |
| L | Litre |
| L· | Lipid radical |
| LDH | Lactate dehydrogenase |
| LDS | Lithium dodecyl sulphate |
| LHON | Leber's hereditary optic neuropathy |
| LLS | Leigh-like syndrome |
| LO· | Lipid alkoxyl radical |
| log | Logarithm |
| LOO· | Lipid peroxyl radical |
| *loxP* | Locus of X(cross)-over in P1 |
| LS | Leigh syndrome |
| M | Molar |
| *m*-aconitase | Mitochondrial aconitase |
| MELAS | Mitochondrial encephalopathy, lactic acidosis, and stroke-like episodes |
| MERRF | Mitochondrial encephalopathy with ragged red fibres |
| mg | Milligram |
| $Mg^{2+}$ | Magnesium(II) ion |

| | |
|---|---|
| MGB | Minor groove binder |
| $MgCl_2$ | Magnesium chloride |
| MILS | Maternally inherited Leigh syndrome |
| min | Minute(s) |
| mL | Millilitre |
| mm | Millimetre |
| mM | Millimolar |
| Mn | Manganese |
| MnSOD | Manganese-containing superoxide dismutase |
| mol | Mole |
| mpH | Milli pH |
| MRE | Metal response element |
| mRNA | Messenger ribonucleic acid |
| MT | Metallothionein |
| mtDNA | Mitochondrial DNA |
| *MtI to MtIV* | Metallothionein isoforms I to IV genes |
| MTI* | Minimally marked metallothionein isoform I |
| *MtI** | Minimally marked metallothionein isoform I gene |
| MTI to MTIV | Metallothionein isoforms I to IV |
| *mt-Nd2* | Mitochondrial *Nd2* gene |
| MTT | 3-(4,5-Dimethylthiazolyl-2)-2,5-diphenyltetrazolium bromide |
| N module | NADH binding module |
| N | Normal |
| n | Number of samples or replicates analysed |
| $Na^+$ | Sodium ion |
| NaCl | Sodium chloride |
| NAD | Nicotinamide adenine dinucleotide |
| $NAD^+$ | Oxidised nicotinamide adenine dinucleotide |

| | |
|---|---|
| NADH | Reduced nicotinamide adenine dinucleotide |
| $NADP^+$ | Oxidised nicotinamide adenine dinucleotide phosphate |
| NADPH | Reduced nicotinamide adenine dinucleotide phosphate |
| NaOH | Sodium hydroxide |
| NARP | Neuropathy, ataxia, and retinitis pigmentosa |
| NBT | Nitro-blue tetrazolium |
| NCBI | National Center for Biotechnology Information |
| ND | NADH dehydrogenase subunit |
| nDNA | Nuclear DNA |
| NDUF | NADH:ubiquinone oxidoreductase subunit or core subunit *(if it is a core subunit, e.g. NDUFS1: NADH:ubiquinone oxidoreductase* core *subunit S1)* |
| NDUFAF | NADH:ubiquinone oxidoreductase complex assembly factor |
| NDUFS4 | NADH dehydrogenase (ubiquinone) iron-sulphur protein 4 |
| Ndufs4 mouse | *Ndufs4* knockout mouse |
| *Ndufs4* | NADH dehydrogenase (ubiquinone) iron-sulphur protein 4 gene |
| NFQ | Non-fluorescent quencher |
| ng | Nanogram |
| nm | Nanometre |
| nM | Nanomolar |
| NP-40 | Nonidet P40 |
| NR | Nuclear receptor |
| NTC | No template control |
| NUYM | Orthologue (from *Yarrowia lipolytica*) of human and mouse NDUFS4 |
| NWU | North-West University |
| $O_2$ | Oxygen |
| $O_2^{\cdot -}$ | Superoxide anion radical |
| OCR | Oxygen consumption rate |
| $OH^{\cdot}$ | Hydroxyl radical |
| OMIM | Online Mendelian Inheritance in Man |

| | |
|---|---|
| OMM | Outer mitochondrial membrane |
| OVER | MTI overexpressing sample (specific to this study) |
| OXPHOS | Oxidative phosphorylation |
| P module | Proton pumping module |
| P | Postnatal day (e.g. P21 means day 21 following birth) |
| P/N | Part number |
| P/S | Penicillin:Streptomycin |
| $p66^{Shc}$ | Isoform of the SHC-transforming protein 1 |
| PBS | Phosphate buffered saline |
| PCDDP | Preclinical Drug Development Platform |
| PCR | Polymerase chain reaction |
| PDB | Protein Data Bank |
| PDH | Pyruvate dehydrogenase |
| PGC-1 | Peroxisome proliferator-activated receptor γ co-activator 1 |
| PGC-1α | Peroxisome proliferator-activated receptor γ co-activator 1α |
| pH | Potential of hydrogen; the negative of the log 10 of the $H^+$ molar concentration |
| $P_i$ | Inorganic phosphate |
| PMD | Primary mitochondrial disease |
| pmf | Proton motive force |
| pmol | Picomole |
| PMSF | Phenylmethylsulphonyl fluoride |
| *Polg* | DNA polymerase γ gene |
| p-value | Significance value |
| PVDF | Polyvinylidene difluoride |
| Q module | Ubiquinone binding module |
| q | Long (q) arm of a chromosome |
| Q | Ubiquinone; oxidised coenzyme Q |
| Q1 | First quartile; $25^{th}$ percentile |

| | |
|---|---|
| Q2 | Second quartile; 50$^{th}$ percentile; median |
| Q3 | Third quartile; 75$^{th}$ percentile |
| QH· | Semiquinone intermediate |
| $QH_2$ | Ubiquinol; reduced coenzyme Q |
| qPCR | Real-time PCR |
| $R^2$ | Linearity of the data; how well the experimental data fits the regression line |
| RC | Respiratory chain |
| Redox | Reduction-oxidation |
| REST© | Relative expression software tool© |
| RLU | Relative light unit |
| RMCN | Relative mitochondrial DNA copy number |
| RNA | Ribonucleic acid |
| ROS | Reactive oxygen species |
| ROX | 6-Carboxy-X-rhodamine |
| rpm | Revolutions per minute |
| rRNA | Ribosomal ribonucleic acid |
| RT | Room temperature |
| RT-qPCR | Reverse transcription-real-time PCR |
| RVSTK | Arginine-valine-serine-threonine-lysine |
| s | Second(s) |
| S/HPEM | Slowly/highly progressive encephalomyopathy |
| SAM | Signal accumulation mode |
| SD | Standard deviation |
| SDHA | Succinate dehydrogenase complex flavoprotein subunit A |
| SDS | Sodium dodecyl sulphate |
| SDS-PAGE | Sodium dodecyl sulphate polyacrylamide gel electrophoresis |
| SMD | Secondary mitochondrial disease |
| SNP | Single nucleotide polymorphism |

| | |
|---|---|
| SOD | Superoxide dismutase |
| SOP | Standard operating procedure |
| SSC | Side scatter |
| T | Thionein |
| *Taq* | *Thermus aquaticus* (recombinant) |
| TBS | Tris buffered saline |
| TCA cycle | Tricarboxylic acid cycle |
| TEMED | *N,N,N',N'*-tetramethylethylenediamine |
| TF | Transcription factor |
| TgMTI mouse | Metallothionein I overexpressing transgenic mouse |
| $T_m$ | Melting temperature |
| tRNA | Transfer ribonucleic acid |
| UQCRC2 | Ubiquinol-cytochrome c reductase core protein II |
| UV | Ultraviolet |
| UW | University of Washington |
| V | Volt |
| v | Version |
| v/v | Volume (of solute) per volume (of solvent) |
| VDAC1 | Voltage dependent anion channel subunit 1 |
| w/v | Weight (of solute) per weight (of solvent) |
| WT | Wild type; genetically unaltered sample (specific to this study) |
| x | Times |
| x *g* | Relative centrifugal field |
| XF | Extracellular flux |
| Zn | Zinc |
| $Zn^{2+}$ | Zinc(II) ion |

# CHAPTER 1:

## INTRODUCTION

Present in nearly all eukaryotic cells, *mitochondria* are classified as highly specialised organelles, tasked with the responsibility of providing the majority of cellular energy in the form of adenosine triphosphate (ATP). This function is achieved via the concerted action of five multimeric complexes (CI to CV), collectively termed the oxidative phosphorylation (OXPHOS) system. In addition, mitochondria control numerous physiological processes including, but not limited to, various forms of metabolism, cellular reduction-oxidation (redox) status, $Ca^{2+}$ signalling, the generation of reactive oxygen species (ROS), and cell death via apoptosis and necrosis (Koopman *et al.*, 2010). Given its multifaceted involvement in cells, the mitochondrion's dysfunction has therefore been implicated in numerous rare as well as common human disorders.

Overall, mitochondrial dysfunction has a prevalence of 1 in ~4 300, the greater part of which is due to *complex I (CI) deficiency* (Gorman *et al.*, 2015; Hoefs *et al.*, 2012). The same tendency has been observed in the South African patient population, where CI deficiencies represent ~67% of all diagnosed cases (unpublished data). Due to its large structure and sizeable involvement in energy production, a deficiency of CI can have a profound and detrimental effect on physiological cell function. The defect is associated with a variety of biochemical abnormalities [including an altered redox status, decreased energy production, intracellular $Ca^{2+}$ imbalance and disrupted mitochondrial membrane potential ($\Delta\psi$)], of which the most destructive involves the excessive production of ROS (Distelmaier *et al.*, 2009). In general, CI deficiency has an early onset, followed by a short and devastating course which ultimately ends in mortality. In addition, these disorders may be specific or multi-systemic and are accompanied by exceptional genetic and clinical heterogeneity. Altogether, these factors impede the development of curative treatment, with current disease management being largely empirical and primarily symptomatic (Rodenburg, 2016).

To promote survival in the face of CI deficiency, the cell employs various adaptive responses to restore homeostasis. These include, mitochondrial biogenesis, metabolic regulation, autophagy, controlled cell death, and defensive (e.g. antioxidant) responses. Previous studies at this institution have identified the *increased expression of metallothioneins* (MTs) as a novel adaptation to CI deficiency (van der Westhuizen *et al.*, 2003). MTs are small, cysteine-rich, non-enzymatic proteins, primarily involved in metal homeostasis, heavy metal detoxification, and free radical scavenging. Of particular interest to this study are the numerous reports linking MT's action to the mitochondrion. Specifically, MTs have been shown to modulate mitochondrial energy production (Babula *et al.*, 2012). In addition, research at this facility has provided *in vitro* evidence

for the protein's protective effect against ROS-mediated cell damage and -death (Reinecke *et al.*, 2006). Since ROS is one of the primary initiators of CI deficiency, antioxidants like MTs may offer a favourable endogenously expressed therapeutic intervention. Indeed, current therapeutic studies researching the potential of antioxidants have shown great promise (de Haas *et al.*, 2017). Thus, the critical question put forward was whether MTs display a protective effect against CI deficiency *in vivo*.

In order to investigate this treatment option, a *suitable experimental model* was required. To this end, previous studies at this institution have involved the use of various MT models [e.g. transformation-induced MTIB and MTIIA overexpressing HeLa cells, as well as *MtI, MtII* and *MtIII* knockout (KO) mice] in which CI deficiency had been induced by inhibition with rotenone. The use of chemical inhibition, however, failed to mimic the full spectrum of the disorder, displayed clear secondary effects, and was therefore considered to be limited with regards to disease model studies (Lindeque, 2011; Pretorius, 2011). A more dependable alternative is the use of animal genetic models. Of these, mice are especially valued, owing to their genetic, physiological, and phenotypic similarities to humans (Breuer *et al.*, 2013b). In 2015, the first genetic model of CI deficiency [produced in 2008 by Kruse *et al.* (2008)] became commercially available to the general scientific community. This model, referred to in this study as the Ndufs4 mouse, was developed by knocking out the NADH dehydrogenase (ubiquinone) iron-sulphur protein 4 (NDUFS4) subunit of CI, producing a pathophysiological phenotype corresponding to that of the CI deficiency, Leigh syndrome. Additionally, in 1993, an MTI overexpressing transgenic model, referred to in this study as the TgMTI mouse, was developed (Palmiter *et al.*, 1993). Both models were therefore acquired for a larger project at this facility, of which the final aim was to obtain a more comprehensive understanding of the effect of MTI (and its overexpression) on CI deficiency.

As a first step towards the larger project, the *first aim of this study* was thus to crossbreed the Ndufs4 and TgMTI mouse strains in order to develop a model with which the effects of MTI overexpression on CI deficiency could be studied and confirmed *in vitro* [similar to Reinecke *et al.* (2006)]. Primary fibroblasts were then to be cultured from these mice and characterised on a genetic and protein level. *Secondly,* this study aimed to investigate the effects of MTI overexpression on the bioenergetics consequences of CI deficiency, using the fibroblasts mentioned.

In Chapter 2, a comprehensive overview of the literature relevant to this study is provided. The problem statement, aims and objectives, as well as the experimental strategy are summarised in Chapter 3, whereas Chapter 4 contains a detailed description of the methodologies used for each objective. The results pertaining to the first and second aims of this study are presented in Chapters 5 and 6, respectively. Lastly, Chapter 7 provides a short summary of the results as well as the main conclusions reached, while additional information is given in Appendices A to E.

# CHAPTER 2:

# LITERATURE REVIEW

## 2.1 INTRODUCTION

All biochemical reactions require the exchange of some or other form of energy. In aerobic eukaryotic cells, this primarily involves the hydrolysis of adenosine triphosphate (ATP) to its constituents, adenosine diphosphate (ADP) and inorganic phosphate ($P_i$). The continued synthesis of ATP is therefore vital to maintain the energetic integrity, and thus survival, of the cell. While soluble enzyme systems (i.e. glycolysis) catalyse the production of some ATP via substrate-level phosphorylation, by far the greatest percentage (± 90%) is generated by the mitochondrion (Marquez *et al.*, 2016; Nicholls & Ferguson, 2002a:3).

In this chapter, the reader will be provided with a theoretical framework of the fundamental aspects addressed in this dissertation. This will include a description of the mitochondrion, its structure and role in energy production, as well as a detailed examination of mitochondrial complex I (CI) and the purpose of its accessory subunits (like NDUFS4). The focus will then be shifted to mitochondrial dysfunction, paying special attention to CI deficiency and Leigh syndrome. A comprehensive overview will then be given of the biochemical consequences accompanying these disorders, as well as the adaptive responses employed by the cell (e.g. metallothionein expression). Finally, the chapter will be concluded by reviewing the experimental models used to investigate CI deficiency and metallothionein induction.

## 2.2 MITOCHONDRION

### 2.2.1 STRUCTURE & ORGANIZATION

The typical mammalian cell contains 800 to 2 500 mitochondria, while high-energy tissues such as the brain, endocrine system, liver, kidneys, muscles, and heart exhibit an even greater abundance (Koopman *et al.*, 2005; Vasava & Mashiyava, 2016). *Mitochondria* may be classified as multifunctional organelles consisting of a relatively porous outer membrane (OMM) and contrastingly impermeable inner membrane (IMM). The latter serves as the barrier between the intermembrane space (IMS) and matrix, and folds inwards to create an intricate series of internal compartments, termed *cristae* (Gropper & Smith, 2013:6-8; Mannella, 2006).

Mitochondrial ATP is generated by the combined action of the respiratory chain (RC), an electron transfer system composed of four multiprotein enzyme complexes (CI to CIV) and two electron carriers (ubiquinone and cytochrome c), and the protein complex, ATP synthase (CV). Collectively these are called the oxidative phosphorylation (OXPHOS) system of which all the components

except for cytochrome c (cyt c) are embedded in the IMM. The organisation of the RC complexes, however, remains a highly debated matter. For years the prevailing opinion viewed these complexes as individual diffusants in the IMM with electron transport depending on their random collision with electron carriers. However, the *random collision* model has recently been challenged by both the *solid state* and *plasticity models* (Acin-Perez & Enriquez, 2014; Calvaruso *et al.*, 2012; Hackenbrock *et al.*, 1986; Hoefs *et al.*, 2012; Schagger & Pfeiffer, 2000; Seelert *et al.*, 2009). The former states that the RC complexes are instead arranged into supercomplexes, capable of containing CI and $CIII^2$ or CI, $CIII^2$ and $CIV^{1-4}$, whereas the latter accepts that the complexes may exist as both supercomplexes and individual entities.

### 2.2.2 FUNCTION & BIOLOGICAL SIGNIFICANCE

ATP synthesis starts with the production of the reducing equivalents NADH (reduced nicotinamide adenine dinucleotide) and $FADH_2$ (reduced flavin adenine dinucleotide) from carbohydrate-, amino acid- and fatty acid catabolism. The electrons acquired from their oxidation at CI and CII respectively, as well as those supplied by the electron transfer flavoprotein-ubiquinone oxidoreductase (ETF:QO), dihydroorotate dehydrogenase and *s*,*n*-glycerophosphate dehydrogenase (GPDH), are then collected by ubiquinone (Q) and passed to CIII. CIII subsequently transfers the electrons to cyt c (located in the IMS), which carries them to CIV. Here, they finally react with the terminal electron acceptor, $O_2$, to yield $H_2O$ (see Figure 2.1) (Koopman *et al.*, 2013; Sazanov, 2015).

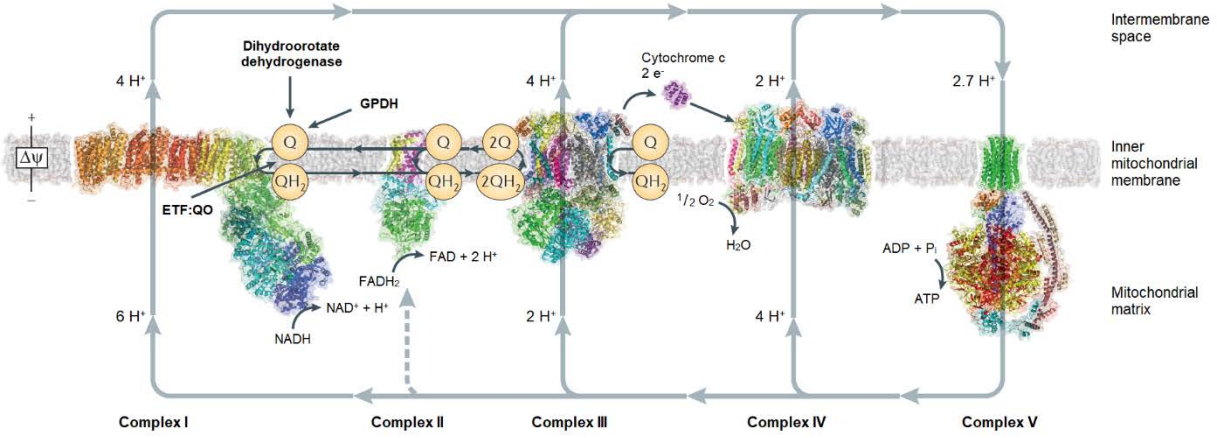


**Figure 2.1: Mitochondrial OXPHOS system.** Electrons are donated to complex I from NADH, to complex II from $FADH_2$, and to Q by complex I and II, ETF:QO, dihydroorotate dehydrogenase and GPDH. Adapted by permission from Macmillan Publishers Ltd.: Nature Reviews Molecular Cell Biology, Sazanov (2015:376), copyright 2015.

The energy liberated by this primary pump (i.e. the RC) is consequently utilised to translocate protons from the matrix to the IMS via CI, CIII and CIV. This produces an electrochemical gradient

across the IMM and thereby a matrix-directed proton motive force (pmf). In turn, the pmf enables the synthesis of ATP from ADP and $P_i$ via the secondary pump, CV (Nicholls & Ferguson, 2002a:4-5). This combined effect of proton translocation and ATP production defines Mitchell's *chemiosmotic theory* (Mitchell, 1961). Besides proton re-entry via CV, mitochondria also display an endogenous proton leak, which generally completes the proton circuit in the absence of ATP synthesis. In this way, the mitochondrion prevents membrane dielectric breakdown, restricts the pmf, and limits singular electron leakage which may otherwise lead to the excessive production of reactive oxygen species (ROS) (Brand & Nicholls, 2011).

Apart from acting as the cell's central "powerhouse", the mitochondrion also controls and regulates numerous other physiological processes. These include various forms of metabolism (e.g. amino acid-, lipid- and metal-metabolism), $Ca^{2+}$ signalling, cellular reduction-oxidation (redox) status ($NADH/NAD^+$ ratio), ROS generation and release, apoptosis and necrosis, as well as several other cell signalling pathways, and therefore preserves the delicate balance between life and death in the cell (Acin-Perez & Enriquez, 2014; Lindeque *et al.*, 2010).

### 2.2.3 MITOCHONDRIAL GENOME

The functional complexity of the mitochondrion is supported by its dependence on an equally complex bigenomic system: Aside from the nuclear genome, it also receives genetic input from its own deoxyribonucleic acid (DNA) (Lagouge & Larsson, 2013).

Mitochondrial DNA (mtDNA) is a strictly maternally inherited, double-stranded, closed circular molecule (Bibb *et al.*, 1981; Chinnery & Hudson, 2013; Lagouge & Larsson, 2013). The typical somatic mammalian cell contains between 1 000 and 10 000 copies, which may vary in accordance with its energetic need. Similar to nuclear DNA (nDNA), mtDNA combines with various proteins to form mitochondrial matrix-associated structures called *nucleoids*. Moreover, mtDNA is species-specific. As an example, the mitochondrial genome of the group E inbred mouse strain (C57BL6/J) used in this study, is 16 299 base pairs (bp) in size compared to its 16 569 bp human counterpart (Bayona-Bafaluy, 2003; NCBI, 2017a). Nonetheless, a likeness exists in overall sequence and gene organization, with both encoding 37 genes. These include two ribosomal ribonucleic acids (rRNAs), 22 transfer ribonucleic acids (tRNAs), and 13 polypeptides which, when translated, form 13 of the core subunits of CI, CIII, CIV and CV of the OXPHOS system (Bibb *et al.*, 1981; Park & Larsson, 2011; Sharpley *et al.*, 2012).

Although mitochondria possess some of the machinery required for basic cellular functions like replication, transcription and translation, these processes are only semi-autonomous, since the necessary enzymes and proteins are nuclear-encoded and require mitochondrial import (Asin-Cayuela & Gustafsson, 2007). Accordingly, the mouse mitochondrial proteome is encoded

by an estimated ~1 200 nuclear genes (as specified by MitoCarta2.0), which include the 92 genes encoding the remaining structural subunits of the OXPHOS system (Calvo *et al.*, 2016; Chinnery & Hudson, 2013; Mootha *et al.*, 2003).

## 2.3 COMPLEX I

### 2.3.1 STRUCTURE

The first RC complex, complex I (CI; NADH:ubiquinone oxidoreductase; EC 1.6.5.3), is encoded by nearly half of the structural mtDNA genes, underscoring its undeniable importance in the mitochondrion. With 45 (44 unique) subunits and a combined molecular mass of ~980 kDa, CI is considered the largest and most complicated multiheteromeric assembly of the mitochondrial OXPHOS system (Balsa *et al.*, 2012; Fiedorczuk *et al.*, 2016; Hunte *et al.*, 2010; Mimaki *et al.*, 2012). The L-shaped molecule possesses an evolutionarily conserved catalytic core made up of seven mitochondrial-encoded and seven nuclear-encoded polypeptides. The former are imbedded in the IMM and constitute the hydrophobic membrane arm, whereas the latter protrude into the mitochondrial matrix to produce a hydrophilic peripheral arm of equal size (Hoefs *et al.*, 2012). Thirty-one (30 unique) nuclear-encoded polypeptides, called *supernumerary-* or *accessory subunits*, conclude the structure by enveloping this central catalytic formation (Fiedorczuk *et al.*, 2016; Stroud *et al.*, 2016).

On a functional level, CI may further be divided into three modules or domains that cooperate to yield approximately 40% of the pmf responsible for CV-generated ATP (Hoefs *et al.*, 2012; Hunte *et al.*, 2010). The first two, known as the *N* (NADH binding) and *Q* (ubiquinone binding) *modules*, are located in the peripheral arm, whereas the third, termed the *P* (proton pumping) *module,* comprises the membrane arm (Sanchez-Caballero *et al.*, 2016).

### 2.3.2 FUNCTION

Despite recent progress, CI is still considered the least characterised OXPHOS system enzyme. Existing structural studies on bacterial, yeast and mammalian models have however greatly aided the elucidation of its function (Fiedorczuk *et al.*, 2016; Kahlhofer *et al.*, 2017; Sanchez-Caballero *et al.*, 2016; Stroud *et al.*, 2016). Consequently, CI has become well-known as the primary entry point for electrons into the RC and is therefore considered as the pacemaker of mitochondrial OXPHOS. Since the IMM is impermeable to NADH, it seems only fitting that the majority of the reducing equivalents are produced within the mitochondrial matrix (Bakker *et al.*, 2000; Papa *et al.*, 2010; Sazanov, 2015).

This, in turn, enables the first step of CI's function, which involves the binding and oxidation of matrix-produced NADH at specific redox centres located in the N module. Each NADH molecule

donates two electrons to the primary electron acceptor flavin mononucleotide (FMN), effectively reducing it to $FMNH_2$ (see Equation 2.1) (Hoefs *et al.*, 2012):

$$\mathrm{NADH} + [\mathrm{FMN}] + \mathrm{H}^+ \rightarrow [\mathrm{FMNH_2}] + \mathrm{NAD}^+ \qquad (2.1)$$

Step two proceeds across both the N and Q modules and encompasses the sequential transfer of electrons from $FMNH_2$ to a series of eight iron-sulphur (Fe-S) clusters. The final step occurs within the P module, during which the Fe-S clusters are oxidised to donate two electrons to the hydrophobic, mobile electron transporter Q, thereby producing ubiquinol ($QH_2$) (see Equation 2.2) (Hoefs *et al.*, 2012; Sazanov, 2015).

$$\mathrm{Q} + \mathrm{e}^- + \mathrm{H}^+ \rightarrow \mathrm{QH}\cdot + \mathrm{e}^- + \mathrm{H}^+ \rightarrow \mathrm{QH_2} \qquad (2.2)$$

$QH_2$ may then freely diffuse through the IMM to donate its electrons to CIII (Nicholls & Ferguson, 2002b:116; Sazanov, 2015).

Part of the energy liberated by the successive redox reactions of CI's functional components is ultimately used to transfer matrix-derived protons across the IMM (Hoefs *et al.*, 2012). Available evidence suggests a stoichiometry of four protons to two electrons ($4H^+/2e^-$) and proton translocation presumably takes place via four antiporter-like domains located in the P module (Baradaran *et al.*, 2013; Fiedorczuk *et al.*, 2016). Over the years, different mechanisms have been proposed to describe the process, including the direct coupling mechanism, active proton pumping mechanism, a combination of the two and the conformation-driven, semiquinone (QH·)-gated mechanism (Brandt, 1997; Brandt *et al.*, 2003; Friedrich, 2001; Ohnishi & Salerno, 2005).

Efremov and Sazanov (2012) suggested a new model called the *conformational coupling mechanism*. In this model electron transport from NADH to Q is coupled to conformational changes in the hydrophilic arm, which lead to a change in the conformation of ionisable residue in three of the proton channels when propagated. This subsequently results in the translocation of three protons, followed by a fourth from the junction between the two arms.

In this manner CI contributes to the pmf required for ATP synthesis, with the total reaction being (Equation 2.3) (Baradaran *et al.*, 2013):

$$\mathrm{NADH} + \mathrm{H}^+ + \mathrm{Q} + 4\mathrm{H}^+_{\mathrm{matrix}} \rightarrow \mathrm{NAD}^+ + \mathrm{QH_2} + 4\mathrm{H}^+_{\mathrm{IMS}} \qquad (2.3)$$

Although the RC primarily uses matrix-derived NADH, it may also utilise cytosolic NADH by means of meticulously developed shuttling systems that bypass the transmembrane transport of

this reducing equivalent from the cytosol to the mitochondrial matrix. These systems include the irreversible glycerophosphate- and reversible malate-aspartate shuttles. In the first, cytosolic NADH may be converted to matrix $FADH_2$, which circumvents CI and enters the RC by its direct reduction of Q. The second system utilises the cytosolic oxidation of oxaloacetate and the subsequent reduction of matrix malate to produce one molecule of NADH, which may enter CI and proceed as usual (Nicholls & Ferguson, 2002c:229-230). Both shuttling systems provide a means of replenishing cytosolic and matrix oxidised nicotinamide adenine dinucleotide ($NAD^+$) and mainly occur when the cytosolic NADH/$NAD^+$ ratio is higher than that of the mitochondrial matrix (Garrett & Grisham, 2013a:671-672).

### 2.3.3 ASSEMBLY

The effective functioning of CI is governed by its successful assembly. This process comprises a multifaceted, coordinated compilation of CI's core and supernumerary subunits, together with cofactors, and is transiently assisted by at least 14 established assembly factors (Guerrero-Castillo *et al.*, 2017; Mimaki *et al.*, 2012; Stroud *et al.*, 2016).

CI assembly may be explained by the *modular assembly model*. This states that CI's assembly is a stepwise procedure, starting with the independent construction of small molecular mass submodules that correspond to the three functional domains of the enzyme. These may then associate with each other, as well as cofactors, to form larger intermediates which combine to produce the CI holoenzyme (Kahlhofer *et al.*, 2017; Sanchez-Caballero *et al.*, 2016). Stroud *et al.* (2016) state that the vast majority of mature CI then associates with RC CIII or CIII and CIV to produce supercomplexes, which may be used for ATP generation.

Following its production, CI homeostasis is continuously maintained by exchanging pre-existing, incorporated nDNA subunits for newly synthesised, imported ones, thereby averting the accumulation of damaged proteins (Mimaki *et al.*, 2012; Papa *et al.*, 2010). Its assembly and upkeep is thus regarded as strictly interconnected and regulated (Sanchez-Caballero *et al.*, 2016).

### 2.3.4 ACCESSORY SUBUNITS & THEIR FUNCTION

Unlike the 14 core subunits, which coordinate the cofactors and execute the function of CI, the relevance of the accessory subunits is less clear (Sazanov, 2015). However, their association with assembly factors and consequent incorporation into the complex is energetically expensive, suggesting an importance of some sort.

A study by Stroud *et al.* (2016), in which knockout (KO) cell lines were created for each of the 31 accessory subunits, proved this to be true. Using blue-native polyacrylamide gel

electrophoresis (BN-PAGE) and immunoblot analysis against proteins located in different parts of the enzyme (NDUFA9, NDUFA13, and NDUFB11), they revealed that 25 of these subunits were required for CI's assembly and that one was indispensable for cell viability. Using quantitative proteomic analysis, this group further showed that the loss of an individual subunit may influence the stability of those subunits sharing its module.

Many other studies concur with these findings, proposing that the accessory subunits also provide structural stability for the entire complex, assist in its biogenesis and regulate its function via signal transduction pathways. More putative functions include anchoring CI to the IMM, the prevention of and protection against the effects of ROS, and the formation of supercomplexes (Friedrich & Bottcher, 2004; Hoefs *et al.*, 2012; Sazanov, 2015; Stroud *et al.*, 2016).

Although the production of supercomplexes greatly improves the function of the RC (by reducing substrate diffusion times, limiting enzyme competition and lessening ROS production), research has also shown it to be required for the stabilisation of the enzyme complexes (Hoefs *et al.*, 2012). For example, a study by Acin-Perez *et al.* (2008) on human cell lines demonstrated a decrease in the level of RC complexes when their containing supercomplex was not produced.

### 2.3.5 THE NDUFS4 SUBUNIT

Of particular importance to this study is the CI accessory subunit, *NADH dehydrogenase (ubiquinone) iron-sulphur protein 4* (NDUFS4). This non-enzymatic 18 kDa protein is expressed in all cells and encoded by either the eight- or five-exon nuclear gene, located on human chromosome (chr) 5 [gene ID: 4724 (*NDUFS4*)] or mouse chr 13 [gene ID: 17993 (*Ndufs4*)] respectively[1] (Kruse *et al.*, 2008; NCBI, 2017b; NCBI, 2017c).

An important feature explaining some of the function of NDUFS4 is the presence of the canonical RVSTK sequence located within its highly conserved carboxyl terminus (Papa *et al.*, 2010). This sequence is recognised by either mitochondrial (and cytosolic) cyclic adenosine monophosphate (cAMP)-dependent protein kinase, or mitochondrial phosphatase, which correspondingly allow NDUFS4 to be phosphorylated or dephosphorylated. The former permits its import into and maturation within the mitochondrion, while the latter possibly plays a role in its degradation. In this manner, NDUFS4 is able to regulate CI's activity (and consequently the activity of the OXPHOS system) by continuously exchanging (possibly oxidatively) damaged, pre-existing NDUFS4 for newly synthesised subunits (Papa *et al.*, 2010; Scacco *et al.*, 2003).

[1] Throughout this dissertation, distinction is made between genes and proteins by the use of italics [e.g. *NDUFS4* (gene) and NDUFS4 (protein)], and between human and mouse genes by capitalisation [e.g. *NDUFS4* (human) and *Ndufs4* (mouse)].

Although NDUFS4 does not directly participate in electron transport, studies have shown that the protein has other additional functions within CI (Quintana *et al.*, 2010). According to BN-PAGE analysis and protein modelling, NDUFS4 forms part of the N module and, as such, the protein is added during the later stages of CI's biogenesis (Calvaruso *et al.*, 2012; Kahlhofer *et al.*, 2017). Despite its late insertion, its location seems to be significant as its impairment results in the defective assembly of intact CI, compromised complex stability, and reduced CI activity (Lamont *et al.*, 2017).

To investigate this, Kahlhofer *et al.* (2017) utilised an *NUYM* [a human (and mouse) *NDUFS4* orthologue] KO strain of the aerobic yeast *Yarrowia lipolytica*. Their study showed that in the absence of NUYM, two CI Fe-S cluster binding sites were distorted, the N module was destabilised, and CI's activity was suppressed. Interestingly, their results supported an increase in ROS release, suggesting that human NDUFS4 might provide physical protection in CI by shielding the core subunits. From these and many other papers it is evident that the NDUFS4 subunit plays a vital role in producing and maintaining intact and functional CI (Alam *et al.*, 2015; Andrews *et al.*, 2013; Calvaruso *et al.*, 2012; Kahlhofer *et al.*, 2017; Lamont *et al.*, 2017; Papa *et al.*, 2010; Quintana *et al.*, 2010; Scacco *et al.*, 2003). It is therefore not surprising that its gene is considered a mutational hot spot.

## 2.4 MITOCHONDRIAL DYSFUNCTION

### 2.4.1 INTRODUCTION

Given the mitochondrion's significant involvement in some of the most vital cellular operations, its strict dependence on the nucleus, and the complicated nature of its OXPHOS system components, it stands to reason that its dysfunction can result in devastating disease (Chinnery & Hudson, 2013; Kruse *et al.*, 2008).

*Mitochondrial disease* may be defined as a heterogeneous group of conditions arising from, or introducing, chronic deficient cellular energy production which manifests in a clinical phenotype (Carroll *et al.*, 2014; Chinnery & Hudson, 2013; Niyazov *et al.*, 2016). These disorders may be brought about by germline mutations in genes that encode subunits of the OXPHOS proteins, as well as mutations that alter the machinery involved in their production. In both cases the resulting defect is referred to as a *primary mitochondrial disease (PMD)* (Niyazov *et al.*, 2016).

By contrast, *secondary mitochondrial disease (SMD)* can develop as a result of inherited mutations in non-OXPHOS genes, but may also be acquired as a consequence of pre-existing, hereditary non-mitochondrial pathologies or environmental factors (including viral and chemical) (Carroll *et al.*, 2014; Niyazov *et al.*, 2016). Examples of adult-onset SMDs include those that develop in conjunction with neurodegenerative disorders (e.g. Alzheimer's and Parkinson's

disease), cardiovascular and kidney disease, diabetes, cancer, inborn errors of metabolism (e.g. propionic aciduria), ageing, as well as acquired immune deficiency syndrome (AIDS) and its therapies (Kalman, 2006; Lindeque *et al.*, 2010; Niyazov *et al.*, 2016).

### 2.4.2 GENETICS & CLINICAL PHENOTYPE OF MITOCHONDRIAL DYSFUNCTION

The dual genetic control of the mitochondrion evidently means that deficiencies thereof may be caused by mutations in either the mtDNA or nDNA (Gorman *et al.*, 2016). mtDNA mutations were first linked to mitochondrial myopathies in 1988 (Holt *et al.*, 1988; Lestienne & Ponsot, 1988; Wallace *et al.*, 1988). Today, pathogenic variants have been found in all the mtDNA genes (Porcelli *et al.*, 2016; Wortmann *et al.*, 2017). Generally, abnormalities of this nature are more often encountered in adults and, although mitochondrial-encoded OXPHOS genes are few in comparison to their nuclear counterparts, their mutations may be associated with wide-ranging phenotypes[2] (Alston *et al.*, 2017; Niyazov *et al.*, 2016).

Conversely, the role of nDNA in mitochondrial disease was not elucidated until 1995, when Bourgeron *et al.* (1995) identified a mutation in the nuclear-encoded CII as the underlying cause of a case of Leigh syndrome. Mutations have since been found in ≥250 nuclear gene loci (Alston *et al.*, 2017). Altogether nDNA mutations result in three quarters of infantile- and a third of all adult mitochondrial disease, collectively making the nuclear genome the chief culprit of mitochondrial dysfunction. While some nuclear PMDs may occur *de novo,* the majority are transmitted via Mendelian inheritance[3] (Niyazov *et al.*, 2016). Furthermore, since the relationship between the mitochondrion and the nucleus stresses a need for interorganelle cooperation, nuclear mutations often include those resulting in intergenomic communication disorders and mtDNA depletion (Almeida *et al.*, 2012:293-294; Park & Larsson, 2011). More frequently however, the affected genes comprise those encoding the five OXPHOS complexes (Niyazov *et al.*, 2016). Nonetheless, mitochondrial dysfunction as a whole is considered among the most common adult inherited neurological disorders, with an incidence of 1 in ~4 300 (Gorman *et al.*, 2015).

[2] Examples include LHON, MILS, NARP (mutated protein-coding genes), MELAS, MERRF (mutated tRNA-coding genes), syndromic deafness (mutated rRNA-coding genes), CPEO, KSS, and Pearson's syndrome (mtDNA deletions and duplications) (Kalman, 2006; Niyazov *et al.*, 2016).

[3] Nuclear PMDs are predominantly inherited in an autosomal recessive manner, although autosomal dominant and X-linked patterns have also been reported (Niyazov *et al.*, 2016).

### 2.4.3 COMPLEX I DEFICIENCY

Due to CI's enormous structure and sizeable involvement in ATP production, it follows that CI deficiency (OMIM 252010) is regarded as the most frequently encountered human mitochondrial disorder (responsible for 30% thereof, where 70% to 80% of cases include nDNA mutations) (Alston *et al.*, 2017; OMIM, 2016b; Rodenburg, 2016). Accordingly, the condition affects as many as 1 in 10 000 new-borns, accounting for up to 23% of all paediatric RC disorder cases (Hoefs *et al.*, 2012; Smeitink *et al.*, 2001).

Defects of this nature may present as neonatal, infantile, childhood, or adult-onset disorders and range from very mild to fatal (Chinnery & Hudson, 2013; Hoefs *et al.*, 2012). A fatal phenotype, however, is considered to be more common, with approximately 75% of all affected individuals succumbing before the age of ten years, of which 50% die before the age of 24 months (Rodenburg, 2016).

#### 2.4.3.1 GENETICS

As with mitochondrial dysfunction, the majority of CI deficiencies are caused by errors in the nDNA sequence. Disorders of this kind are consequently transmitted via Mendelian inheritance with the autosomal recessive pattern of heredity being the most common (Hoefs *et al.*, 2012). Of all the mitochondrial disorders, CI deficiency possesses the most complicated aetiology, and while various causative genes have been identified, many challenges remain (Gorman *et al.*, 2016; Haack *et al.*, 2012; Wortmann *et al.*, 2017).

In 1998, Loeffen *et al.* (1998) described the first pathogenic mutation (resulting in Leigh syndrome) in a nuclear-encoded subunit of CI. Since then, disease-causing mutations[4] have been found in the seven nDNA core subunits (NDUFS1 to NDUFS3, NDUFS7, NDUFS8, NDUFV1 and NDUFV2) and 13 of the 31 nuclear-encoded CI accessory subunits (NDUFS4, NDUFS6, NDUFA1, NDUFA2, NDUFA9 to NDUFA13, NDUFB3 and NDUFB9 to NDUFB11) as depicted in Figure 2.2. Since these proteins are directly involved in the complex's function and structure, mutations of this nature can lead to catalytic defects. That being said, the majority of CI mutations usually rather affect the assembly and stability of the complex, thereby reducing the quantity of CI (Rodenburg, 2016; Wortmann *et al.*, 2017).

[4] Mutations have also been identified in all seven of the mitochondrial-encoded subunits (ND1 to ND6 and ND4L) (Rodenburg, 2016).

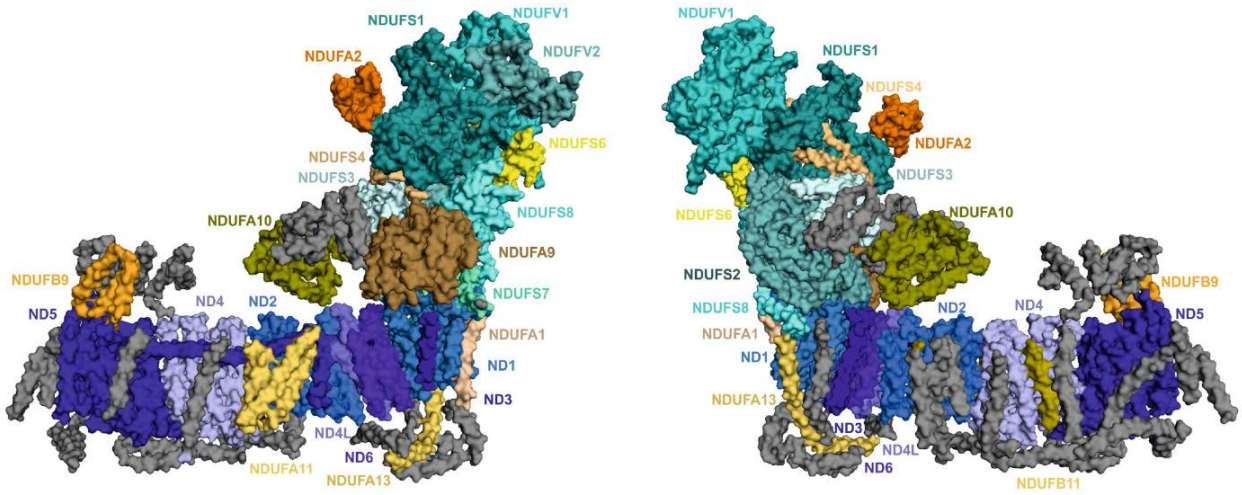


**Figure 2.2: Surface structure representation of CI [based on the bovine CI structure (PDB ID: 4UQ8)] indicating subunits associated with human CI deficiency.** Subunits in which mutations are known are depicted in colour (core subunits in the N and Q modules, and P module are in shades of green and purple, respectively), while others are grey. Three known mutated subunits, NDUFA12, NDUFB3, and NDUFB10, are not shown. Adapted by permission from Elsevier: BBA Bioenergetics, Rodenburg (2016:940), copyright 2016.

More specific to this dissertation, recent reports suggest that there is a total of 13 different human *NDUFS4* mutations. These include missense-, nonsense-, splicing-, frameshift- and point mutations, as well as a multi-exon deletion. Of these, all but one are considered loss of function alleles (Kahlhofer *et al.*, 2017; Lamont *et al.*, 2017).

#### 2.4.3.2 CLINICAL PHENOTYPE

The energetic importance of CI means that disorders thereof can either be specific or multi-systemic (Jain *et al.*, 2016). As may be expected, the typically affected tissues include those with a high-energy demand and/or the inability to adapt to the consequences of decreased energy capacity (Carroll *et al.*, 2014; Koopman *et al.*, 2005). In support hereof, the observed phenotype usually includes muscle weakness, cardiomyopathy, hepatopathy with renal tubulopathy, respiratory failure, macrocephaly with leukodystrophy, neurodegenerative- and/or neuromuscular disease (including Huntington's, Alzheimer's or Parkinson's disease and LHON) (Alam *et al.*, 2015; Hoefs *et al.*, 2012; Kahlhofer *et al.*, 2017; Koopman *et al.*, 2005; Valsecchi *et al.*, 2012). CI deficiency has further been found to be implicated in less suspected diseases, like bipolar disorder, Down syndrome, schizophrenia, and even multiple sclerosis. Three of the most prevalent clinical presentations, however, include slowly/highly progressive encephalomyopathy (S/HPEM), fatal infantile lactic acidosis (FILA) and Leigh syndrome (LS) (the latter is discussed in Section 2.4.4) (Hoefs *et al.*, 2012; Loeffen *et al.*, 2000).

From the vast array of phenotypes, it may consequently be gathered that the clinical spectrum of CI deficiency is exceptionally diverse (Gorman *et al.*, 2016). No single symptom, apart from hypotonia which affects 60% of patients, is present in more than 35% of CI deficiency cases. While this heterogeneity may once again be partially explained by the structural and functional complexity of the enzyme, it remains mostly unclear why different or even identical mutations in the same gene may lead to a completely different clinical presentation. Despite thorough investigation of the medical, biochemical and cellular aspects, there appears to simply be no definite genotype-phenotype correlation (Rodenburg, 2016; Wortmann *et al.*, 2017). However, it is feasible that the environmental aspects (epigenetics) and genetic background of the individual could contribute to the expression and progression of the disease (Hudson *et al.*, 2005; Johnson *et al.*, 2001; Papa *et al.*, 2010).

### 2.4.4 LEIGH SYNDROME

Notwithstanding the heterogeneity that accompanies the disease, more than 80% of CI-deficient patients will present with signs of LS or Leigh-like syndrome (LLS)[5] (Hoefs *et al.*, 2012; Rodenburg, 2016; Smeitink *et al.*, 2004).

LS, or subacute necrotising encephalopathy (OMIM 256000), is a severe neurodegenerative disorder. It is regarded as the most prevalent paediatric manifestation of mitochondrial- or CI disease, and affects 1 in 40 000 new-borns (Darin *et al.*, 2001; Lake *et al.*, 2015; OMIM, 2016a). Although infants appear relatively healthy at birth, clinical symptoms may develop as early as one month of age. The disease course that follows includes a progressive, irreversible, and episodic pattern of neurodegeneration which usually ends in death, due to central respiratory failure, before the age of three years (Lake *et al.*, 2015; Lamont *et al.*, 2017). While adult-onset LS is not unheard of, late presentation of the disease is very rare (Hoefs *et al.*, 2012). LS has been associated with >35 gene mutations affecting the mitochondrial RC; three quarters of which are attributable to nuclear-encoded errors. Although this incorporates deficiencies in all of the RC complexes, in Q or pyruvate biosynthesis, as well as other secondary proteins, mutations have specifically been identified in 25 of the genes encoding CI (Lamont *et al.*, 2017; Rodenburg, 2016). This includes numerous mutations in the *NDUFS4* gene, a few of which, when expressed, may result in some of the more severe autosomal recessive forms of LS (Jain *et al.*, 2016; Kalman, 2006).

Whereas LS patients primarily exhibit central nervous system malfunction, deficient CI may reside in various other tissues and present with different degrees of severity, depending on the mutation and/or energy requirement (Quintana *et al.*, 2010). Consequently, symptoms of the disorder are widespread and include feeding difficulties, hypotonia, dystonia, failure to thrive, developmental

[5] LLS is analogous to LS, apart from exhibiting pathological symptoms of the brain.

delay and -regression, psychomotor retardation, central respiratory compromise (bilateral, symmetrical lesions in the basal ganglia and brainstem, with gliosis and changes in the thalamus), seizures, lactic acidosis, respiratory problems, and ophthalmologic abnormalities (vision impairment or nystagmus) (Hoefs *et al.*, 2012; Jain *et al.*, 2016; Lake *et al.*, 2015; Lamont *et al.*, 2017). Like CI deficiency, LS presents with significant genetic, clinical, and biochemical heterogeneity. This has not only complicated research into the underlying molecular mechanisms, but as with other mitochondrial disorders, set hurdles for the diagnosis and successful treatment of patients (Carroll *et al.*, 2014; Lake *et al.*, 2015; Lamont *et al.*, 2017).

### 2.4.5 DIAGNOSIS & TREATMENT OF MITOCHONDRIAL DYSFUNCTION

Considering the severity and poor prognosis of mitochondrial- and specifically CI disease, early and effectual diagnosis is of the utmost importance (Quintana *et al.*, 2010). As may be expected however, the process is greatly hindered by the disorders' heterogeneous nature (Rodenburg, 2016). Overall, diagnosing mitochondrial disease is very similar to establishing other conditions. The process generally involves family and patient history, clinical assessment (neurological and physical), tissue biopsies, and laboratory testing (histopathological and metabolic). Findings may then be confirmed by molecular genetic- or biochemical evaluation, the order of which depends on the nature of the suspected mutation (Almeida *et al.*, 2012:308; Niyazov *et al.*, 2016).

While next-generation sequencing has become a very promising tool in pathogenic diagnosis and gene discovery, biochemical analysis is considered the cornerstone of diagnosis (van den Heuvel *et al.*, 2004; Wortmann *et al.*, 2017). Using this approach, the enzymatic defect may be established by assessing RC enzyme activity [by spectrophotometry or BN-PAGE and in-gel activity (IGA) analysis], structure and quantity (by immunochemical detection with dipsticks or BN-PAGE + western blot analysis), as well as by evaluating the OXPHOS system as a whole (by respirometry) (Hoefs *et al.*, 2012; Rodenburg, 2016). Ideally, these analyses are performed in fresh, or otherwise frozen, patient muscle biopsies. However, due to the inconvenience of its collection and the fatal phenotype associated with OXPHOS disorders, muscle biopsy material is not always available for diagnosis; even more so when it is required for research purposes (Distelmaier *et al.*, 2009; Hoefs *et al.*, 2012; van den Heuvel *et al.*, 2004).

Since a simple skin biopsy provides a far less invasive method, a widely used alternative is to perform these analyses on fibroblasts. One advantage of using skin fibroblasts is that they are easily cultured to large quantities and little starting material is therefore required. Additionally, these cells are reported to provide a more reproducible experimental milieu and can be stored and re-cultured for future research purposes (e.g. when new technology or knowledge becomes available) (Breuer *et al.*, 2013b; Hoefs *et al.*, 2012; van den Heuvel *et al.*, 2004; Voets *et al.*, 2012). It should however be kept in mind that different tissues are not always affected similarly

and, as a result, the possibility exists that the presumed disorder may not manifest in fibroblasts. Therefore, fibroblasts are usually analysed together with muscle biopsies for a more comprehensive diagnosis (Hoefs *et al.*, 2012).

Considering the rapid and progressive nature of most mitochondrial disorders, therapeutic development is critical. Regrettably, however, disease management is largely empirical and primarily symptomatic (Rodenburg, 2016). No cure currently exists and, although next-generation sequencing aids in patient identification, attempts at therapeutic development have been impeded by the lack of sufficiently sized homogeneous patient cohorts (Carroll *et al.*, 2014). Although mostly unsatisfactory, treatment options are numerous and combination therapies have been developed. Of the available agents, vitamin- and cofactor treatments have become the mainstay of disease management (Distelmaier *et al.*, 2009; Jain *et al.*, 2016; Niyazov *et al.*, 2016). Other options include dietary adjustments (regular caloric intake- and ketogenic diets) and exercise, the latter of which is considered a standard effective remedy. Since mitochondrial disease, and especially CI deficiency, is further frequently accompanied and exacerbated by the production of ROS, these molecules serve as potential therapeutic targets (Rodenburg, 2016). To this end, Q, many forms thereof ($QH_2$, mitoquinone, and idebenone), as well as other antioxidants have become popular agents against mitochondrial disease. Several antioxidant therapeutic trials are currently being tested, as well as those that employ mitochondrial-targeted peptides, gene therapy, and the allotopic expression of wildtype (WT) mitochondrial genes (Niyazov *et al.*, 2016; Rodenburg, 2016). An example includes the vitamin E analogue Trolox, as well as derivatives thereof (especially KH176), which has shown promising results in research trials (de Haas *et al.*, 2017).

Much research has shown that different cases of mitochondrial disease require different treatment strategies (Almeida *et al.*, 2012:306-308). Thus, in order to promote therapeutic development, a comprehensive understanding of CI, the OXPHOS system, as well as mitochondrial function under physiological and pathological conditions is required (Valsecchi *et al.*, 2013).

## 2.5 BIOCHEMICAL CONSEQUENCES OF MITOCHONDRIAL DYSFUNCTION

### 2.5.1 INTRODUCTION

Due to the versatile nature of the mitochondrion, it stands to reason that PMD will be associated with critical alterations in cellular function (Distelmaier *et al.*, 2009). To further our understanding of mitochondrial disease, many researchers have therefore turned their attention to the cell biological consequences of OXPHOS deficiency (Breuer *et al.*, 2013a).

Apart from influencing the activity of the affected complex, PMDs may bring about a myriad of direct and secondary biochemical insults. Once again, these responses vary between patients

and tissues, but most often the biochemical phenotype includes elevated ROS, altered redox status ($NADH/NAD^+$ ratio), decreased energy production (ATP/ADP ratio), changes in intracellular $Ca^{2+}$ homeostasis, and/or the disruption of the mitochondrial membrane potential (Reinecke *et al.*, 2009; Rodenburg, 2016; Smeitink *et al.*, 2001; van der Westhuizen *et al.*, 2003).

### 2.5.2 REACTIVE OXYGEN SPECIES

One of the primary initiators of the immediate and downstream effects of mitochondrial dysfunction is the formation of ROS (Reinecke *et al.*, 2009). *In vivo*, ROS species are considered as the most important group of radicals[6], with the mitochondrion being regarded as their main point of origin (Valko *et al.*, 2007).

Briefly stated, mitochondrial ROS production begins with the ineffective transfer of electrons through the RC components (CI to CIV) as well as the ineffective transfer of electron carriers (Q and cyt c) through the IMM, resulting in electron accumulation in the matrix. Since mitochondrial $O_2$ delivery continues despite most OXPHOS defects, these electrons can subsequently leak and react with $O_2$ (Jain *et al.*, 2016; Koopman *et al.*, 2010; Lindeque *et al.*, 2010). In this manner, between 0.1% and 0.5% of mitochondrial consumed $O_2$ may be converted to primary ROS in the form of the superoxide anion radical ($O_2^{\bullet -}$) (Koopman *et al.*, 2010).

Depending on the source and supply of reducing equivalents, mitochondrial ROS may be produced by CI (on the matrix side, at the bound flavin), CII, CIII (at the $QH_2$ oxidation site), ETF:QO (of the fatty acid β-oxidation pathway), GPDH, α-ketoglutarate dehydrogenase [α-KGDH; of the tricarboxylic acid (TCA) cycle], isoform $p66^{Shc}$ of the SHC-transforming protein 1, and pyruvate dehydrogenase (PDH)[7] (Koopman *et al.*, 2013; Reinecke *et al.*, 2009). Of particular importance to this dissertation, however, is the fact that CI is considered as the major site of cellular ROS formation and, contrariwise, that ROS is regarded to be the central regulator in CI deficiency (Distelmaier *et al.*, 2009; Papa *et al.*, 2010).

Under physiological conditions, cells rely on the generation of small amounts of ROS to ensure their viability and natural death. This steady state of redox balance and its associated consequences may be referred to as *oxidative stress* (Cutler *et al.*, 2005). In this case, ROS may play a considerable role in the signaling pathways involved in cell growth, -death and

[6] *Radicals* may be defined as molecules or fragments having one or more unpaired electrons in their molecular or atomic orbitals (Valko *et al.*, 2007).

[7] It should be noted that, apart from the mitochondrion (mitochondrial ROS), the cell is capable of producing ROS from various other sources, including the peroxisomes, endoplasmic reticulum (ER), cytosol, plasma membrane (cellular ROS), and the extracellular space (extracellular ROS) (Koopman *et al.*, 2013).

-transformation, mitochondrial biogenesis, -morphology and -removal (mitophagy), protein function regulation, and gene induction (e.g. the antioxidant response) (Koopman *et al.*, 2005; Papa *et al.*, 2010; Reinecke *et al.*, 2009; Valsecchi *et al.*, 2013). It is only when ROS production becomes uncontrolled, thereby exceeding the cells' capacity to effectively remove it and regain homeostasis, that cells are said to enter a state of *increased oxidative stress* (Cutler *et al.*, 2005).

While ROS includes a variety of secondary species [for instance hydrogen peroxide ($H_2O_2$), the hydroxyl radical (OH·), $^1O_2$, HOO·, L·, LO·, LOO·, and peroxides], the most prominent members are $O_2^{\cdot -}$, $H_2O_2$ and OH· (the latter of which is mainly produced by the Fenton reaction) (Koopman *et al.*, 2010; Lindeque *et al.*, 2010; Smeitink *et al.*, 2001; Valko *et al.*, 2007). As a whole, ROS are considered highly reactive and capable of readily extracting electrons from other indiscriminately targeted molecules. Consequently, those structures directly surrounding the site of ROS production are damaged or modified first (Koopman *et al.*, 2013). This includes important biomolecules, especially mitochondrial components (like the RC, Fe-S clusters and mtDNA), proteins, lipids, trace elements, and even whole organelles. Of particular note is the genotoxic effect of ROS on mtDNA. Since seven of the 13 mitochondrial structural genes encode for CI, ROS-induced mutations may present an additional threat to the function of this complex (Lindeque *et al.*, 2010; Smeitink *et al.*, 2004).

Altogether, the uncontrolled increase in ROS production, subsequent rise in mtDNA mutation rate, and the concomitant decrease in OXPHOS function result in a vicious cycle, which, through accumulation, may set into motion or worsen the pathology of mitochondrial- and especially CI deficiency (Hoefs *et al.*, 2012; Indo *et al.*, 2007).

### 2.5.3 CELLULAR REDOX STATUS

Another important parameter that affects various aspects of cellular functioning during CI deficiency, is the NADH/$NAD^+$ ratio (Bilan & Belousov, 2016; Smeitink *et al.*, 2004). In the cell, energy homeostasis is determined by the redox status of the NAD (nicotinamide adenine dinucleotide) pool, which in turn hinges on the balance between NAD's biosynthesis and consumption. As stated in Section 2.2.2, $NAD^+$ is reduced to NADH when glucose is collectively oxidised via the glycolytic pathway, PDH and the TCA cycle. Though the first half of this process takes place in the cytosol, the mitochondrial matrix ultimately houses a higher NADH concentration under physiological conditions. Here, NADH binds to the NDUFV1 subunit of CI to be re-oxidised to $NAD^+$. While $NAD^+$ may also be recycled via lactate dehydrogenase (LDH), as well as the glycerophosphate- and malate-aspartate shuttles, the RC is considered to be its main consumer (Bilan & Belousov, 2016; Smeitink *et al.*, 2004).

In theory then, CI dysfunction will upset the total cellular NAD pool (the free and protein-bound forms), with its reduced activity leading to the accumulation of NADH and, consequently, to an augmented NADH/$NAD^+$ redox status. Depending on the severity of the disorder, this may occur at the cellular, tissue, or organismal level (Barrow *et al.*, 2016; Bilan & Belousov, 2016; Reinecke *et al.*, 2009; Smeitink *et al.*, 2004). In addition to its regulatory role in energy metabolism, the redox couple may partake in several other interconnected biological processes. For example, research exists that implicates $NAD^+$ and NADH in the supervision of $Ca^{2+}$ homeostasis; either directly or via the use of their metabolites. A disturbance in the NADH/$NAD^+$ ratio may therefore lead to the disruption of intracellular $Ca^{2+}$ signalling. The NADH/$NAD^+$ ratio is further associated with two other essential redox parameters, namely the reduced/oxidised glutathione- (2GSH/GSSG) and reduced/oxidised nicotinamide adenine dinucleotide phosphate (NADPH/$NADP^+$) ratios (Bilan & Belousov, 2016; Lindeque *et al.*, 2010). Together, these three couples make up an intricate and strictly controlled redox network which defines the cell's general redox status and maintains its oxidant production, antioxidant systems, and reductive biosynthesis. As an example, some studies have revealed a link between increased NADH/$NAD^+$ and α-KGDH- or CI-stimulated $O_2^{\bullet -}$ production (Koopman *et al.*, 2010).

Evidence also indicates that $NAD^+$ and NADH may function as mediators of cell death by modulating the cellular energy status, the mitochondrial permeability transition, or the apoptosis-inducing factor (Koopman *et al.*, 2010). Finally, it is important to note that, throughout their production and use, $NAD^+$ and NADH may act as rate-limiting factors in various metabolic reactions (Bilan & Belousov, 2016). Indeed these metabolites operate as cofactors for many different enzymes (Smeitink *et al.*, 2004). As an example, increased mitochondrial NADH/$NAD^+$ has been shown to inhibit α-KGDH, resulting in the accumulation of α-ketoglutarate (α-KG), which in turn inhibits the degradation of the transcription factor, hypoxia-inducible factor 1α. This leads to its build-up and to the activation of a cellular "glycolytic switch", which directs the metabolism away from OXPHOS (Rossignol, 2015). It is thus clear that a significant disturbance in the NADH/$NAD^+$ couple can have detrimental effects on the cell, with potential consequences on a genomic, proteomic, and/or metabolic scale (Bilan & Belousov, 2016).

### 2.5.4 CELLULAR ENERGY STATUS

Since CI deficiency is usually accompanied by decreased CI activity and a possible increase in the NADH/$NAD^+$ ratio, the disorder may present with impaired mitochondrial ATP generation and, as a result, a disturbed ATP/ADP homeostasis (Reinecke *et al.*, 2009; Rodenburg, 2016). As previously stated, ATP is considered the primary source of cellular chemical energy and is produced according to the demand imposed by the cell's diverse collection of ATP-consuming reactions (Maldonado & Lemasters, 2014; Parker, 2001:115). Following its synthesis by the

OXPHOS system (as described in Section 2.2.2), a portion of the product may be used by the mitochondrion itself. The majority of ATP will however be transported from the mitochondrial matrix to the cytosol in exchange for ADP in a 1:1 molar ratio; a process driven by the mitochondrial membrane potential and enabled by the adenine nucleotide transporter located in the IMM (Maldonado & Lemasters, 2014; Rodenburg, 2011; Smeitink *et al.*, 2001).

It should be noted that ATP is not used to store energy, but rather to transiently capture and transfer it by means of its hydrolysis to ADP and $P_i$. Within the cell, ATP's importance may be illustrated by its two main functions: Firstly, ATP may act as an allosteric effector by kinetically controlling the regulatory enzymes located at essential points within the metabolism, e.g. hexokinase, phosphofructokinase, and pyruvate kinase in glycolysis (Garrett & Grisham, 2013c:923). Secondly, by coupling the free energy released upon its hydrolysis to reactions, ATP can enable thermodynamically unfavourable metabolic sequences, thereby playing a stoichiometric role. The latter is exemplified in various cellular processes.

For instance, ATP can maintain ion gradients and partake in cellular biogenesis by assisting in targeting various charged and sterically cumbersome compounds to their correct locales (subcellular or extracellular) via the process of primary active transport (Alder & Theg, 2003). ATP's hydrolysis may further be used to ensure the dynamic turnover of actin filaments and to enable the folding and mitochondrial import of hydrophobic precursor proteins by ATP-dependent chaperones (e.g. Hsc70, Hsp70 and Hsp90) (Alder & Theg, 2003; Ghiasi *et al.*, 2012; Gourlay & Ayscough, 2005). Another illustration of ATP's value, is its role in anabolism, where it provides the energy (or substrates) required to produce nucleotides, lipids, carbohydrates, and aminoacyl-tRNAs (required for protein synthesis) (Garrett & Grisham, 2013b:892-893; Parker, 2001:116; Woese *et al.*, 2000). Finally, it is also important to note ATP's involvement in cell signalling via its reaction with protein kinases (Day *et al.*, 2016). It is therefore understandable that the improper functioning of the ATP/ADP system will contribute to the disease phenotype of CI deficiency.

### 2.5.5 $Ca^{2+}$ HOMEOSTASIS & MITOCHONDRIAL MEMBRANE POTENTIAL

Two additional parameters that are related to impaired ATP production and have been shown to be affected by CI malfunction are $Ca^{2+}$ homeostasis and the mitochondrial membrane potential ($\Delta\psi$) (Distelmaier *et al.*, 2009; Rossignol, 2015).

In cells, $Ca^{2+}$ is regarded as the most common signalling molecule. It regulates numerous cellular activities like proliferation, secretion, and muscle contraction, but is also crucially involved in ATP homeostasis. When the work load and thus the energetic need of the cell increases (e.g. upon hormonal-, nutrient- or electrical stimulation), $Ca^{2+}$ can operate as a secondary messenger to enhance ATP synthesis (Koopman *et al.*, 2010; Willems *et al.*, 2009). This is initiated by the

production and binding of inositol 1,4,5-triphosphate ($IP_3$) to its endoplasmic reticulum (ER) membrane receptor, $IP_3R$, and leads to $Ca^{2+}$'s release from the ER (the primary $Ca^{2+}$-storage organelle) to the cytosol. $Ca^{2+}$ is then swiftly taken up by the mitochondrion and transferred to the mitochondrial matrix where it activates dehydrogenases and stimulates ATP synthesis by the OXPHOS system. Following this, ATP may be transported to the cytosol to fuel ATP-requiring reactions. When the ATP imbalance has been remedied, $Ca^{2+}$ will be returned to its pre-stimulatory levels by ATP's reaction with the ER membrane's $Ca^{2+}$-sequestering adenosine triphosphatase (Tarasov *et al.*, 2012; Willems *et al.*, 2009).

As described in Section 2.2.2, this ATP production requires an inside-negative potential difference which is established and maintained by the RC. This potential difference is referred to as the Δψ and makes up the majority of the pmf, with its second component, ΔpH, contributing a mere ~15% (Koopman *et al.*, 2010). Besides its rate-determining role in energy production, the Δψ further governs mitochondrial $Ca^{2+}$ influx, ATP/ADP exchange, the assembly of mitochondrial transport systems, the import of nuclear-encoded proteins, and $Na^+$ and $K^+$ transfer across the IMM. The Δψ therefore serves as a measure of mitochondrial function, metabolism, and health (Alder & Theg, 2003; Koopman *et al.*, 2010).

Still, conflicting evidence exists regarding CI activity as a contributing factor of the Δψ. For example, in a paediatric study of 15 patients with isolated CI deficiency, Distelmaier *et al.* (2009) assert that nine patients (including three patients with *NDUFS4* mutations) displayed significantly depolarised Δψ in comparison to healthy controls. By contrast, Koopman *et al.* (2010) state that the Δψ is not drastically affected by rotenone-induced CI dysfunction. Both groups however agree that even small changes in the Δψ may significantly decrease ATP production. They further explain that elevated ROS may hamper the Δψ due to its damaging effect on protein and membrane integrity (Distelmaier *et al.*, 2009; Koopman *et al.*, 2010).

While impaired OXPHOS may affect the Δψ, the cell can maintain this parameter as long as it is able to provide ATP via alternative metabolic pathways (e.g. glycolysis) (Maldonado & Lemasters, 2014).

## 2.6 ADAPTIVE RESPONSES TO MITOCHONDRIAL DYSFUNCTION

### 2.6.1 INTRODUCTION

Although the biochemical consequences of OXPHOS deficiency can be a direct detriment to cellular function, it is important to note that the affected metabolites (i.e. ROS, $NADH/NAD^+$, ATP/ADP and $Ca^{2+}$) are considered key components of the cell's adaptive response programme (Cagin & Enriquez, 2015; Jones *et al.*, 2012). In effect, these molecules are continuously monitoring the cell's metabolic status and mitochondrial performance, and relaying any changes

to the nucleus via a wealth of signal transduction pathways[8]. This mitochondrion-to-nucleus communication is referred to as *retrograde signalling* and results in the transcription of nuclear genes that can reprogram cellular metabolism or defend the cell against stress (Quiros *et al.*, 2016).

Conversely, the nucleus may control the mitochondrion in a process called *anterograde signalling* (nucleus-to-mitochondrion communication) by varying the expression of the nuclear-encoded mitochondrial proteome (to alter mitochondrial activity) or by regulating the number and volume of mitochondria (i.e. influencing mitochondrial biogenesis) (Quiros *et al.*, 2016). Therefore, the adaptive response programme employs both genomes in an attempt to re-establish cellular homeostasis and promote cell survival, the failure of which results in cell death (Reinecke *et al.*, 2009).

Collectively, retrograde- and anterograde signalling are known as *mito-nuclear communication*. They may share various signalling pathways and generally function in a hormetic and bidirectional manner (Quiros *et al.*, 2016). The process is therefore extremely complex, includes innumerous cell functions, and the mechanisms involved are, as of yet, poorly understood (Rub *et al.*, 2017). Since the entire adaptive response programme falls outside the scope of this dissertation, only the most applicable areas will be discussed, including mitochondrial biogenesis, metabolism regulation, cell death, the antioxidant response, and, in particular, the induction of metallothionein.

### 2.6.2 MITOCHONDRIAL BIOGENESIS

To meet the varying energy demands imposed by its continual molecular turnover, the cell must maintain an adequate population of functional mitochondria (Jones *et al.*, 2012). This is especially true in the face of OXPHOS dysfunction, where cells are subjected to both energy deficiency *and* mitochondrial damage (e.g. misfolded or impaired mitochondrial proteins and mtDNA damage). While procedures exist to clear away mitochondrial debris (e.g. protein degradation by mitochondrial proteases and mtDNA segregation via fission), an equally active system is required to replenish the mitochondrial network and return the cell to homeostasis (Jones *et al.*, 2012).

This system is referred to as *mitochondrial biogenesis* and entails the increased production of all the mitochondrial components, including the double phospholipid membrane, mitochondrial proteome, and mtDNA (Andreu *et al.*, 2009; Cagin & Enriquez, 2015; Jones *et al.*, 2012). As is evidenced in a review by Reinecke *et al.* (2009), the expression of genes involved in mitochondrial biogenesis is clearly influenced in various *in vivo* and *in vitro* models of OXPHOS disorders. These

[8] Although, these aspects are continuously being monitored under physiological conditions, the process is upregulated during pathogenesis, e.g. during CI deficiency.

reports display both increased and decreased mtDNA copy number[9] and/or mitochondrial proteome transcription, and differ with respect to the type of tissue and OXPHOS defect (Reinecke *et al.*, 2009; van der Westhuizen *et al.*, 2003).

Since the mitochondrion depends on two genomes (Section 2.2.3), the regulation of mitochondrial biogenesis requires their coordination and is therefore diverse, extremely complex, and tightly controlled (Cagin & Enriquez, 2015; Jones *et al.*, 2012; Reinecke *et al.*, 2009). In short, stimuli like energy deprivation or cellular stress can lead to the activation of co-activators via various signal transduction pathways. By acting as part of multiprotein complexes, these co-activators can then directly or indirectly promote or suppress the activity of a wealth of nuclear receptors (NRs) and transcription factors (TFs). NRs and TFs may then further influence the transcription potency of genes involved in mitochondrial biogenesis through their combined action or interaction on the DNA (Jones *et al.*, 2012).

The master regulator of mitochondrial biogenesis is the peroxisome proliferator-activated receptor γ co-activator 1 (PGC-1) family of co-activators, which includes PGC-1α among others. During energy deprivation, the decreased ratio of ATP/adenosine monophosphate (AMP) may lead to the activation of AMP activated protein kinase (AMPK), which in turn will stimulate PGC-1α and promote mitochondrial biogenesis (Jones *et al.*, 2012). AMPK has also been shown to promote sirtuin activity by increasing $NAD^+$ levels. $NAD^+$ then activates sirtuins 1 and 3 which may respectively stimulate PGC-1α (via deacetylation) or AMPK to promote mitochondrial proliferation. Additionally, augmented cytosolic $Ca^{2+}$ (the result of decreased ATP or the loss of $\Delta\psi$) will activate both calcineurin and calcium/calmodulin-dependent protein kinase IV which may increase PGC-1α levels, mitochondrial mass, and mtDNA (Brenmoehl & Hoeflich, 2013).

Finally, the close proximity of the mitochondrial components to ROS (as mentioned in Section 2.5.2), as well as mtDNA's lack of histones and less efficient DNA repair mechanisms, increase the mitochondrion's sensitivity to ROS-mediated damage and may enhance mitochondrial proliferation (Butow & Avadhani, 2004; Hock & Kralli, 2009). A study by Lee *et al.* (2000) substantiated this claim by demonstrating that $H_2O_2$-treatment increased both mitochondrial mass and mtDNA in a cell cycle- and concentration-dependent manner.

### 2.6.3 REGULATION OF METABOLISM

To adapt to the sub-optimum energy-output associated with mitochondrial deficiency, a cell or organism may alter its energy-yielding metabolic pathways (Cagin & Enriquez, 2015). With the

[9] The mtDNA copy number may be defined as the number of mtDNA molecules present per cell, as expressed by the mtDNA/nDNA ratio.

advent of sequencing and systems biology tools, researchers have turned their attention to transcriptomics and metabolomics investigations in an attempt to better understand these metabolic adaptations. Accordingly, many studies have described the induction of the OXPHOS components, accompanied by the varied expression of the many metabolic pathways preceding, or interfacing with, the OXPHOS system (Reinecke *et al.*, 2009; Reznik *et al.*, 2015; van der Lee *et al.*, 2015). In an extensive review on the metabolomics changes associated with mitochondrial disease, Esterhuizen *et al.* (2017) report alterations in the glycolytic pathway, TCA cycle, urea cycle, fatty acid-, nucleotide-, one carbon-, and amino acid (including branched chain amino acids) metabolism of various models. It may therefore be gathered that, despite some consistent changes, the metabolome is typically not influenced in a localised manner, due mainly to the complex nature and wide-ranging implications of mitochondrial dysfunction (Esterhuizen *et al.*, 2017). However, many other aspects can complicate studies of this nature, including the variation observed with regards to the genetic background, cell-, tissue- or mutation type, and experimental design (Reinecke *et al.*, 2009).

One of the more consistent changes accompanying decreased OXPHOS function is the proportionate increase in glycolytic flux to lactate (Cagin & Enriquez, 2015; Esterhuizen *et al.*, 2017; Rossignol *et al.*, 2003). Under normal physiological conditions, the cell drives a high cytosolic ATP/ADP ratio, with the relative amounts of each component remaining constant. In this case, aerobic oxidative metabolism is favoured while glycolysis is less active. Conversely, when mitochondrial ATP production is compromised, the cytosolic ATP/ADP ratio is diminished. Cells may then upregulate glycolysis as an alternative energy-producing pathway, converting its product, pyruvate, to lactate, during which $NAD^+$ is also replenished (Ghiasi *et al.*, 2012; Maldonado & Lemasters, 2014). This shift is normally observed for cancer cells where it is referred to as the Crabtree- (temporary) or Warburg (more permanent) effect (Crabtree, 1929; Rossignol *et al.*, 2003; Warburg *et al.*, 1927). The same change is seen in patient cells with mitochondrial deficiencies. For example, fibroblasts with deficient OXPHOS can proliferate at a rate equal to that of control cells when cultured in glucose, while their growth is greatly restricted by galactose medium (which forces the use of mitochondrial OXPHOS for ATP production) (Hofhaus *et al.*, 1996). A limitation of the use of glycolysis, however, is its lower ATP yield in comparison to OXPHOS (i.e. glycolysis yields 2 mol ATP, whereas OXPHOS produces 36 to 38 mol ATP) (Maldonado & Lemasters, 2014; Tarasov *et al.*, 2012).

### 2.6.4 CELL DEATH

#### 2.6.4.1 BIOCHEMICAL THRESHOLD

An important concept to take note of before examining the mechanisms of cell death, is the existence of the *biochemical threshold* (Rossignol *et al.*, 2003). The biochemical threshold is

defined as the maximum extent to which a given OXPHOS complex needs to be inhibited in order to collapse the overall respiratory flux and result in cell damage (Obre & Rossignol, 2015). While CI to CV are often viewed as individual entities, mitochondrial OXPHOS is in essence a system. Furthermore, as seen in the previous sections, mitochondrial function is intricately connected to the nucleus and other metabolic pathways. As a result, mitochondrial respiration is controlled by the collective action of *all* these components (Rossignol *et al.*, 2003).

Therefore, a significant genetic defect of CI (kinetic or not) does not always assure the biochemical expression of, and detrimental effects associated with, mitochondrial dysfunction. On the contrary, cell fate is ultimately determined by the extent to which protective mechanisms can ameliorate cell injury and redirect the cell back to homeostasis. The efficiency of the adaptive responses employed therefore determines the biochemical threshold, which allows the cell greater stability against nDNA and mtDNA mutations (Rossignol *et al.*, 2003). For each complex the biochemical threshold value is usually high (~70%) but, as before, it exhibits considerable variability regarding mutation and tissue type, as well as experimental conditions (Obre & Rossignol, 2015).

#### 2.6.4.2 MECHANISMS OF CELL DEATH

When the cell's injury surpasses its ability to restore balance, the biochemical threshold is exceeded and cell death may ensue (Galluzzi *et al.*, 2012). This can proceed via one of two pathways, termed *apoptosis* or *necrosis*, although some papers suggest autophagy as a possible third (Baehrecke, 2003; Edinger & Thompson, 2004).

*Apoptosis* can be described as an energy-dependent form of cell suicide involving the elimination of single or small groups of cells in a morphologically distinct and programmed manner. It is considered the principle mechanism of cell death and occurs physiologically during development and ageing to ensure normal cellular turnover and to defend against cell damage (Elmore, 2007; Kerr *et al.*, 1972). During the process, cells are neatly carved up by the action of caspases, packed into apoptotic bodies, and released to the extracellular environment without invoking an inflammatory response (Edinger & Thompson, 2004). The intrinsic apoptotic pathway is governed by the mitochondrion and can be stimulated by altered ROS status, increased $Ca^{2+}$ levels, collapsed $\Delta\psi$, as well as the action of stress kinases and/or the pro-apoptotic Bcl-2 family (Barrientos & Moraes, 1999; Reinecke *et al.*, 2009; Smeitink *et al.*, 2004). These stimuli further support the involvement of apoptosis in CI deficiency. For example, a study by Danielson *et al.* (2005) showed that the combined effects of increased ROS and osmotic stress, exhibited by the cells of LHON patients, resulted in the reduced expression of pro-survival and proliferation factors, while pro-apoptotic genes were upregulated.

By contrast, *necrosis* is classified as an uncontrolled and energy-independent mode of cell death, affecting large clusters of cells (Elmore, 2007; Galluzzi *et al.*, 2012). It is almost always regarded as detrimental, though some authors have suggested programmed methods that might serve a physiological purpose. Stimuli are much more severe and include direct damage to the cell's membranes (e.g. via toxic insult) as well as bioenergetics catastrophe resulting from acutely decreased ATP (Chan *et al.*, 2003; Holler *et al.*, 2000). Additionally, the process may stem from ongoing apoptosis when caspase availability decreases and/or ATP is depleted. Ultimately, necrosis involves the loss of $\Delta\psi$, followed by the sudden swelling and rupture of cell organelles, as well as plasma membrane breakdown. This leads to the uncontrolled release of cellular constituents to the extracellular environment and initiates inflammation (Edinger & Thompson, 2004; Jones *et al.*, 2012). Research by Quintana *et al.* (2010) of a neuronal *Ndufs4* KO mouse model showed that apoptosis (brought on by increased oxidative stress) was redirected to necrosis due to insufficient ATP, and thus supports the role of necrosis in CI deficiency.

Another relevant process is *autophagy*. Its function has been the topic of much debate with research describing it as a survival mechanism (by providing energy), death promoter (by mediating apoptosis) or distinct form of cell suicide (by digesting the cell to death). During autophagy, cell constituents, cytoplasm and/or organelles are enveloped by double-membrane vesicles and catabolised by lysosomes (Edinger & Thompson, 2004; Galluzzi *et al.*, 2012; Yonekawa & Thorburn, 2013). In this manner, autophagy may play a degradative or recycling role by enabling the turnover of long-lived proteins and/or damaged organelles (e.g. defective mitochondria possibly containing mutated mtDNA; termed *mitophagy*). Similarly, it may offer a means of ATP production during times of energy deficiency (Clay Montier *et al.*, 2009; Edinger & Thompson, 2004). Aptly, the process is stimulated by conditions of nutrient deprivation and bioenergetics stress and, as such, has been observed during CI deficiency (Galluzzi *et al.*, 2012). In support hereof, Carilla-Latorre *et al.* (2013) reported that mutations in the *NDUFAF5* and *NDUFAF7* genes of CI led to increased autophagy in the amoeba, *Dictyostelium discoideum.*

### 2.6.5 ANTIOXIDANT RESPONSE

Due to its widespread involvement in cellular function (Section 2.5.2), as well as its contribution to cell damage and -death (Sections 2.5.2 and 2.6.4), ROS is considered key in determining the cell's survival. It is therefore vitally important that its quantity be strictly regulated (Koopman *et al.*, 2013). However, as mentioned, this control is often lost during CI deficiency.

To clear the excessive ROS and restore oxidative homeostasis, the cell may respond to CI dysfunction by upregulating the gene expression of a wide array of endogenous antioxidant systems (Reinecke *et al.*, 2009; Weydert & Cullen, 2010). These systems may be initiated via the influence of $Ca^{2+}$, the $NADH/NAD^{+}$ redox status, or ROS itself on retrograde signalling, and

include both enzymatic and non-enzymatic (GSH, vitamin C and E, carotenoids, flavonoids, $QH_2$ and metallothioneins) components (Kelso *et al.*, 2001; Koopman *et al.*, 2010). Three of the main antioxidant enzymes that are increased in response to enhanced ROS, are superoxide dismutase (SOD), catalase (CAT), and glutathione peroxidase (GPx) (Weydert & Cullen, 2010). In the mitochondrial matrix, Mn-containing SOD (MnSOD) functions as a first line of defense by dismutating the $O_2^{\bullet -}$ to the less reactive $H_2O_2$. Cu and Zn-containing SODs (Cu/ZnSODs) perform the same reaction in the cytosol and, to a lesser extent, in the lysosomes, peroxisomes, nucleus and mitochondrial IMS. The resultant $H_2O_2$ may then further be reduced to $H_2O$ and $O_2$ by CAT, an enzyme situated primarily in the cytosol and peroxisomes, with small fractions occurring in the mitochondrion. However, a more effective and frequently employed method, that eliminates $O_2$ as a substrate for further $O_2^{\bullet -}$ formation, is the reduction of $H_2O_2$ to only $H_2O$ by nuclear or mitochondrial GPx in conjunction with GSH (Weydert & Cullen, 2010). The involvement of GPx and GSH in CI deficiency is made clear by a study by Voets *et al.* (2012) which showed that the fibroblasts of CI-deficient patients with nDNA mutations responded to increased oxidative stress by upregulating genes of the GSH antioxidant system.

GSH is considered the most important and best characterised antioxidant metabolite and, although it acts with GPx, it may also independently reduce ROS (Forman *et al.*, 2009). Following its synthesis in the cytosol, it can be distributed to the nucleus or mitochondrion (Koopman *et al.*, 2010; Kulinsky & Kolesnichenko, 2007). However, despite its high cellular concentration, GSH may become limited during OXPHOS deficiency when it is oxidised to GSSG (Lindeque *et al.*, 2010). While the cell normally counters this by recycling GSSG to GSH via the combined action of glutathione reductase (GR), glucose-6-phosphate dehydrogenase, and the cofactors NADPH and glucose-6-phosphate (G-6-P), the method might not always be sufficient to restore homeostasis during increased oxidative stress (Weydert & Cullen, 2010).

### 2.6.6 METALLOTHIONEINS

#### 2.6.6.1 GENERAL PROPERTIES

Among the genes that are upregulated during CI- and other mitochondrial disorders are those encoding for a family of small (6 to 7 kDa), metal-binding proteins, termed *metallothioneins* (MTs) (Mehus *et al.*, 2014). These proteins are highly conserved, non-enzymatic, and found in all eukaryotes, many prokaryotes and plants (Freisinger, 2008). At the level of their primary structure, mammalian MTs are typically 61 to 68 amino acids in length and characterised by a lack of histidine and aromatic amino acids, as well as a distinctly high cysteine (Cys) content[10] (Banerjee

[10] MTs contain 20 invariant Cys residues occurring in Cys-X-Cys, Cys-X-X-Cys and Cys-Cys sequences, with X denoting any non-Cys amino acid (Kagi & Schaffer, 1988).

*et al.*, 1982; Hunziker & Kagi, 1985; Kagi & Schaffer, 1988; Mehus *et al.*, 2014). These Cys residues, in turn, are arranged into two globular domains separated by a Cys-free spacer region to yield a protein with a dumbbell-like tertiary structure (Figure 2.3) (Babula *et al.*, 2012).

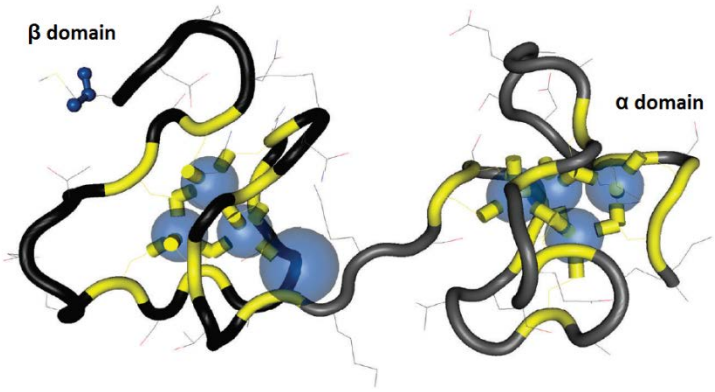


**Figure 2.3: Three-dimensional representation of the tertiary structure of rat MTII.** Dumbbell-like structure of MT with its α and β domains. Adapted from Babula *et al.* (2012:740) with permission of The Royal Society of Chemistry.

It is the high sulphur content and external orientation of these Cys residues that allow the domains to bind metal ions (thereby forming metal-thiolate clusters) and scavenge oxygen radicals (Babula *et al.*, 2012; Rigby & Stillman, 2004). Accordingly, the protein can occur in the unbound state (apoform) as "*thionein*", metal-bound state (holoform) as "*metallothionein*", or oxidised state as "*thionin*" (Krezel & Maret, 2007). Research has shown MTs to be capable of binding Group 11 and 12 metals with stoichiometries of 7, 12, or 18 (Wong *et al.*, 2017:243). It is further believed that the specific metal ion defines certain aspects of the protein's tertiary structure, endowing it with a higher stability. As a result, the protein usually occurs with a complete or incomplete complement of metal ions, leaving the cell with only small amounts of thioneins under physiological conditions (Ma, 2005; Penkowa *et al.*, 2006).

Since their discovery in 1957 by Margoshes and Vallee (1957), four MT isoforms (encoded by *MtI* to *MtIV*, located on a 60 kb region on chr 8) have been described in mice, with humans housing 14 (11 *MTI* isoforms and one *MTIIA*, *MTIII,* and *MTIV* isoform genes on chr 16q13) (Babula *et al.*, 2012; Penkowa *et al.*, 2006). Of these, MTI and MTII are ubiquitously expressed in all vital organs (especially the brain, intestines, pancreas, kidneys and liver), while MTIII and MTIV are respectively confined to the neurons and squamous epithelial cells (Wong *et al.*, 2017:244). Though slight differences have been reported, the isoforms are generally homologous and functionally similar (Haq *et al.*, 2003; Quaife *et al.*, 1994). MTI, which is the focus of this dissertation, has been found in the cytoplasm, nucleus, mitochondrion, lysosome and extracellular environment (Babula *et al.*, 2012; Penkowa *et al.*, 2006). As MTs lack organelle targeting sequences, it has been proposed that they enter the nucleus by means of free diffusion through the nuclear pore complex or via the action of cytosolic factors and guanosine

triphosphatases (GTPases), while their retention is ATP-dependent (Breeuwer & Goldfarb, 1990; Nagano *et al.*, 2000; Woo *et al.*, 2000). Furthermore, although MTs are not officially part of the mitochondrial proteome, studies have revealed their presence in the mitochondrial IMS. As before, the import mechanism is not certain, but is thought to occur via passive diffusion through the OMM (which has a 10 kDa exclusion limit), or according to the mechanism employed by the structurally similar cytochrome c oxidase copper chaperone (COX17) (Ye *et al.*, 2001).

#### 2.6.6.2 INDUCTION & BIOLOGICAL FUNCTION

Studies have shown that MT expression can be induced by several stimuli, ranging from physical (cold and irradiation) or chemical stress (toxins, drugs, radical generating agents, and metals) to endogenous factors (endogenous ROS, metals, and hormonal- and immune responses) (Babula *et al.*, 2012; Penkowa *et al.*, 2006). Of these, however, the most studied and pertinent to this dissertation are metals and ROS.

Consequently, *MTI*'s dose dependent induction may be regulated via the TF-trans-activation of six *cis*-acting metal response elements (MREs; a to f) and one antioxidant response element (ARE), located in the genes' proximal promoter. This results in a negative-feedback response, in which MTs bind the stressor (metals or ROS) with the intent of decreasing its concentration to pre-stimulatory levels (Haq *et al.*, 2003; Penkowa *et al.*, 2006). Accordingly, the majority of research (ranging from environmental to medical) describes MTs as having a primarily protective effect on cells in times of disease or stress (Babula *et al.*, 2012; Hauser-Davis *et al.*, 2014). This same protective effect has been shown to occur during mitochondrial- and CI dysfunction (Voets *et al.*, 2012). For example, van der Westhuizen *et al.* (2003) observed an increased expression of various MT isoforms in the fibroblasts of patients with nDNA CI mutations when directing their metabolism towards mitochondrial ATP production via galactose culture conditions.

Despite decades of research, MT's main biological function is still unclear. Based on the wide range of stimuli affecting its production, most researchers instead agree that MT functions as a multipurpose protein, affecting a myriad of cellular processes in its wake (Andrews, 2000). According to Vasak (2005), this characteristic property is ascribable to the metal-thiolate clusters of the protein. To simplify this multifunctionality, the biological roles of MTs may be divided into three major categories, namely (i) detoxification of heavy metals (e.g. Hg, Cd and Ag), (ii) metal (Zn and Cu) homeostasis, and (iii) protection against oxidative damage via free radical scavenging (Lindeque *et al.*, 2010). The latter two functions are particularly applicable in mitochondrial disorders. A summary of the cellular functions of MTs which are described in the following Sections (2.6.6.2.a and 2.6.6.2.b), as well as the processes discussed in Sections 2.5 and 2.6, are illustrated in Figure 2.4.

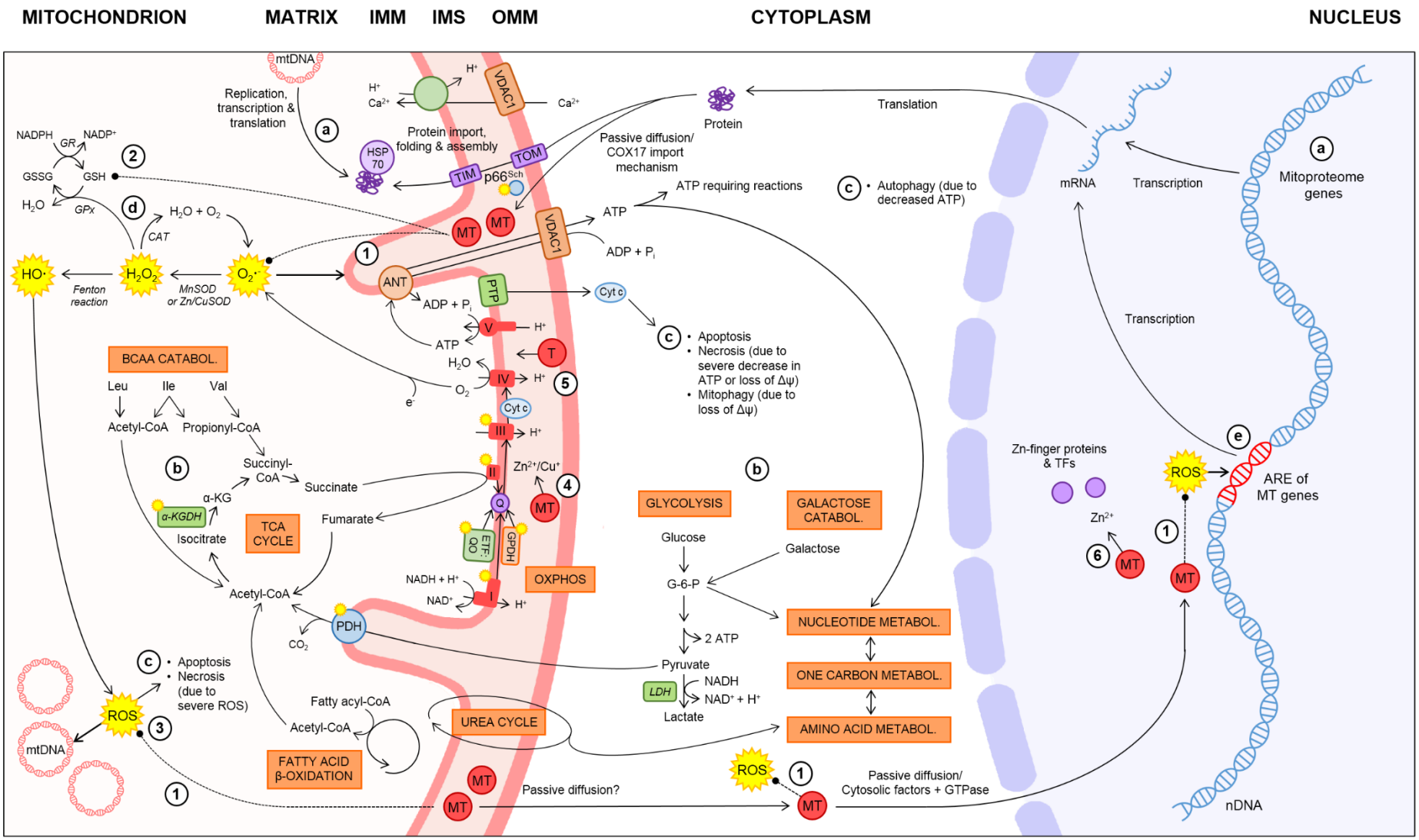


**Figure 2.4: Illustration of the biochemical consequences and adaptive responses associated with CI deficiency (indicated by letters), with special focus on *MT* induction and MT function (indicated by numbers).**

**Figure 2.4: Illustration of the biochemical consequences and adaptive responses associated with CI deficiency (indicated by letters), with special focus on *MT* induction and MT function (indicated by numbers). (a)** Mitochondrial biogenesis is influenced by increased ROS and $Ca^{2+}$ levels and decreased ATP/ADP (Brenmoehl & Hoeflich, 2013; Jones *et al.*, 2012; Koopman *et al.*, 2005; Reinecke *et al.*, 2009). **(b)** Changes in the metabolome may result from elevated ROS, decreased ATP/ADP and increased NADH/$NAD^+$ (orange boxes indicate affected pathways) (Bilan & Belousov, 2016; Cagin & Enriquez, 2015; Esterhuizen *et al.*, 2017; Maldonado & Lemasters, 2014; Smeitink *et al.*, 2004; Woese *et al.*, 2000). **(c)** If left unchecked, elevated ROS, NADH/$NAD^+$, and $Ca^{2+}$ levels, as well as decreased ATP/ADP and/or Δψ loss can lead to apoptosis (via the intrinsic pathway) (Barrientos & Moraes, 1999; Elmore, 2007; Koopman *et al.*, 2010; Reinecke *et al.*, 2009; Smeitink *et al.*, 2004). Similarly, a severe increase in ROS, decrease in ATP/ADP, and the sudden loss of Δψ may result in necrosis (Chan *et al.*, 2003; Holler *et al.*, 2000; Jones *et al.*, 2012; Quintana *et al.*, 2010). Autophagy is primarily caused by lowered ATP/ADP (Galluzzi *et al.*, 2012), whereas mitophagy may result from Δψ loss (Clay Montier *et al.*, 2009; Koopman *et al.,* 2013). **(d)** The antioxidant response is influenced by altered $Ca^{2+}$ levels and increased ROS and NADH/$NAD^+$ (Bilan & Belousov, 2016; Kelso *et al.*, 2001; Koopman *et al.*, 2010; Weydert & Cullen, 2010). **(e)** ROS stimulates the induction of *MT* (Babula *et al.*, 2012; Penkowa *et al.*, 2006). Points of origin for ROS production are indicated in yellow (Koopman *et al.*, 2013; Reinecke *et al.*, 2009).

**(1)** MTs may protect the mitochondrion, mtDNA, and nDNA by scavenging ROS (Babula *et al.*, 2012; Merten *et al.*, 2005; Min *et al.*, 2005; Pretorius, 2011) and can thereby **(2)** preserve GSH (Cai *et al.*, 2006; Ding *et al.*, 2002; Wu & Kang, 1998). MTs may potentially replenish GSH via the MT-GSH cycle (Brouwer *et al.*, 1993; Rofe *et al.*, 1996). **(3)** MTs may protect against apoptosis (Aiuchi *et al.*, 1998; Reinecke *et al.*, 2006; Shimoda *et al.*, 2003) and **(4)** interact with mitochondrial proteins (specifically proteins of the OXPHOS system) via direct or indirect $Zn^{2+}$ and $Cu^+$ donation (Costello *et al.*, 2004; Feng *et al.*, 2005; Lindeque *et al.*, 2010; Maret, 1994). **(5)** The putative restoration of inhibited OXPHOS by thioneins has been reported (Ye *et al.*, 2001). **(6)** MTs may affect gene transcription by supplying or removing $Zn^{2+}$ to and from TFs and Zn-finger proteins (Babula *et al.*, 2012; Hathout *et al.*, 2001). Metabol. = metabolism, catabol. = catabolism, ANT = adenine nucleotide transporter, PTP = permeability transition pore, CoA = coenzyme A, Leu = leucine, Ile = isoleucine, Val = valine, MT = metallothionein, T = thionein (a clarification of the remaining abbreviations may be found in the abbreviation list).

#### 2.6.6.2.a THE ROLE OF METALLOTHIONEIN IN METAL HOMEOSTASIS

Research has shown that MTs can act as metal chaperones by primarily binding the biologically essential metal ions $Zn^{2+}$, followed by $Cu^{+}$, with a high thermodynamic stability under physiological conditions[11] (Babula *et al.*, 2012; Haq *et al.*, 2003). Additionally, studies have described MTs' role in $Zn^{2+}$ and $Cu^{+}$ removal, trafficking (intra- and intercellular), release, and storage (although to a lesser extent). Consequently, this keen association has designated MTs as major players in the regulation of metal homeostasis (Babula *et al.*, 2012; Penkowa *et al.*, 2006; Wong *et al.*, 2017:247).

MTs' participation in mitochondrial energy metabolism is of particular interest (Molto *et al.*, 2007). Over 300 cellular enzymes depend on metal ion cofactors like $Zn^{2+}$ and $Cu^{+}$ for their structure and function (Coyle *et al.*, 2002; Das *et al.*, 2006; Rubio-Osornio *et al.*, 2017). In spite of MT's strong hold on metal ions, their sulphhydryl groups are highly reactive, thereby enabling the donation of $Zn^{2+}$ or $Cu^{+}$ to proteins. Since MTs can translocate to the mitochondrial IMS, a direct interaction between these proteins and members of the OXPHOS system (CI, CIII to CV and cyt c) seems possible (Lindeque *et al.*, 2010). By contrast, MTs have also been shown to donate $Zn^{2+}$ to the mitochondrial matrix despite not being able to cross the IMM, suggesting their possible interaction with GSH (discussed in Section 2.6.6.2.b) or transporters (Costello *et al.*, 2004; Feng *et al.*, 2005; Maret, 1994).

While MTs may mediate the activation of mitochondrial proteins, it should be noted that they are also capable of regulating them via inhibition (Rubio-Osornio *et al.*, 2017). As MTs are unable to remove metal ions from the catalytic sites of enzymes, the process likely proceeds via their donation of metals to specific inhibitory sites (Jacob *et al.*, 1998; Maret *et al.*, 1999). In this manner, it has been shown that MTs can partake in the inhibition of all four the RC complexes, two of the TCA cycle enzymes [mitochondrial aconitase (*m*-aconitase) and α-KGDH], and mitochondrial respiration as a whole (Brown *et al.*, 2000; Feng *et al.*, 2005; Ye *et al.*, 2001). The fact that mitochondrial respiration can subsequently be restored with thionein suggests the potential cooperation of MT and thioneins to modulate mitochondrial energy production (Ye *et al.*, 2001). Furthermore, as stated previously, MT is found in the nucleus. One possible reason might be to enable its collaboration with metal-dependent TFs and Zn-finger proteins. By supplying or removing metal ions to or from these proteins, MTs can therefore partake in the transcriptional activation or -inhibition of nuclear-, and perhaps also mitochondrial-, encoded genes. The functional changes observed on the metabolic level may therefore be influenced or determined by MTs' regulatory role in gene transcription (Babula *et al.*, 2012; Hathout *et al.*, 2001).

[11] If present, the protein may exhibit an even greater affinity towards toxic heavy metal ions, like $Cd^{2+}$ and $Hg^{2+}$ (*in vivo*) (Babula *et al.*, 2012; Penkowa *et al.*, 2006).

#### 2.6.6.2.b THE ROLE OF METALLOTHIONEIN IN PROTECTION AGAINST OXIDATIVE DAMAGE

Another main function of MT is to protect against ROS and associated oxidative damage (Babula *et al.*, 2012). Over the years, various cell-free and *in vitro* experiments have substantiated this claim by demonstrating that MTs can act as scavengers to $O_2^{\cdot -}$, $OH^{\cdot}$, $H_2O_2$, and nitric oxide (Choi, 2003; Hussain *et al.*, 1996; Kang, 1999; Quesada *et al.*, 1996). Additionally, evidence supporting MT's antioxidant role *in vivo* exists (Penkowa *et al.*, 2006).

Recall that the mitochondrion is regarded as the main producer of ROS (Section 2.5.2). Since highly reactive ROS have poor diffusion properties, MTs would have to be close to their site of production to successfully protect mitochondrial structures (Koopman *et al.*, 2013). Though MTs do not have access to the mitochondrial matrix, they might offer remote protection by their interaction with antioxidants (e.g. GSH, as explained later) (Pretorius, 2011). Moreover, Merten *et al.* (2005) propose that MTs might prevent additional ROS formation by modulating the RC components. Apart from the mitochondrion, MTs can also protect other parts of the cell such as the nucleus and nDNA (Min *et al.*, 2005). One suggestion is that MTs' localisation (i.e. IMS, cytoplasmic, and nuclear MTs) essentially forms "barriers" which slow or eliminate the effects of both internal and external migrating ROS (Lindeque *et al.*, 2010; Min *et al.*, 2005). Owing to the inaccessibility of MT's inwardly directed thiol groups, thioneins are more readily oxidised than their metal-bound counterparts (Haase & Maret, 2008). However, interestingly, thioneins are not targeted for destruction or inactivated like other proteins upon oxidation. Instead, they are easily restored to their original form and function by reducing agents (like metals or GSH) (Lindeque *et al.*, 2010). While thionein's quaternary structure may be influenced by oxidation or metal-binding *in vitro,* thereby producing higher-order thionin- or MT aggregates with intermolecular disulfide bonds, no evidence exists for this polymerisation occurring *in vivo* (Babula *et al.*, 2012; Haase & Maret, 2008). Should this be possible, however, Haase and Maret (2008) have suggested various positive roles for MT-polymerisation[12]. Therefore, except for possibly increasing the cellular metal level (which could lead to enzyme inhibition), no known adverse side effects have been reported for the *in vivo* oxidation of MTs (Lindeque *et al.*, 2010).

As previously stated (in Section 2.6.5), the effectiveness of GSH becomes limited during increased oxidative stress. In such a case, MTs may take over as the primary cellular antioxidants, scavenging ROS ~300 times better than GSH (Cai *et al.*, 2006; Ding *et al.*, 2002; Wu & Kang, 1998). In this manner, MTs may rescue the cell by preserving GSH levels and thus effectively saving GSH to function where they cannot (e.g. in the matrix). The oxidation of some GSH to GSSG is, however, unavoidable (Weydert & Cullen, 2010). As MT has been shown to bind to

[12] Putative MT-polymerisation could possibly aid in the protein's function, help with its organellar retention, store it to avoid *de novo* synthesis and protect it against degradation.

GSH, it stands to reason that it might also bind GSSG and possibly aid GR in replenishing GSH via an MT-GSH cycle (Brouwer *et al.*, 1993; Rofe *et al.*, 1996). MTs' role in ROS scavenging has further led researchers to investigate its involvement in apoptosis. Consequently, it has been reported that MTs exhibit a protective effect against this form of cell death. For example, in a rotenone-generated model of CI deficiency, MTIIA overexpression has been found to promote the maintenance of $\Delta\psi$, as well as nucleosome enrichment and lower caspase 3/7 activation (Reinecke *et al.*, 2006). Interestingly, it has also been reported that MTs can act against the extrinsic pathway of apoptosis, which is not stimulated by ROS, via their metal-donating ability (Aiuchi *et al.*, 1998; Shimoda *et al.*, 2003). Since MTs actively partake in mitochondrial function and are capable of protecting the cell against the consequences of its dysfunction, they offer an interesting therapeutic option against the effects of CI deficiency. Indeed, the potential therapeutic use of MTs in CI deficiency has been a particular interest of this institution since 2003 (van der Westhuizen *et al.*, 2003).

## 2.7 EXPERIMENTAL MODELS TO INVESTIGATE CI DEFICIENCY & *MT* INDUCTION

One of the main factors determining the success of a study, is the reliability of the experimental model used. With respect to CI deficiency and MTs, both chemical and genetic models exist (Koene *et al.*, 2011; Lindeque *et al.*, 2010).

Over the years, CI deficiency has been studied using various inhibitors of the enzyme, with rotenone, piericidin A, and acetogenins being the most popular (Fato *et al.*, 2009; Murai *et al.*, 2015). Similarly, numerous chemicals, ranging from endotoxins and metals to plant-derivatives and medicines, have been used to induce the expression of MTs (Agarwal *et al.*, 2010; Iszard *et al.*, 1995; Miyahara *et al.*, 1991; Yousuf *et al.*, 2009). However, these types of models have many drawbacks. An example of this is that CI inhibitors are non-specific and influence many additional metabolic pathways that are usually unaffected in patients (e.g. cell proliferation and proteasome formation inhibition) (Irwin *et al.*, 2013; Koene *et al.*, 2011). Likewise, *MT* inducers have been shown to affect systems that protect cells against increased oxidative stress (e.g. antioxidant enzyme induction), thereby complicating the elucidation of their own protective roles (Iszard *et al.*, 1995). The uptake and distribution of CI inhibitors and *MT* inducers can also be impaired by the mode of administration and endogenous detoxification systems (e.g. hepatic cytochrome P450) of the research animal (Alessandrini, 2003; Iszard *et al.*, 1995).

A more dependable alternative, then, is the use of cell or animal genetic models (Koene *et al.*, 2011). While the former can yield considerable information with minimal starting material, mouse models are especially valued because of their genetic, physiological, and phenotypic similarity to humans (Breuer *et al.*, 2013; Koene *et al.*, 2011; Torraco *et al.*, 2009). As of yet, no stable genetically engineered mice exist that harbour mutations in the mitochondrial-encoded CI subunit

genes (Irwin *et al.*, 2013). Nonetheless, there are models that indirectly mutate or delete mtDNA genes, including CI genes, due to their own mutated nDNA (Torraco *et al.*, 2009; Vempati *et al.*, 2008). Examples include the mutator mouse, the *Polg* KO mouse (with a mutated DNA polymerase γ gene) and the transgenic Twinkle mouse (with a mutated Twinkle helicase gene). However, since these models affect the transcriptional machinery of mtDNA, the resulting mutations occur at random (Hance *et al.*, 2005; Trifunovic *et al.*, 2004; Tyynismaa *et al.*, 2005). Additionally, the proportion of induced mtDNA mutations decline with each generation (owing to mitochondrial dynamics). For this reason, it is preferential to use genetic models that directly target nuclear subunits of CI, especially if these mutations are known to cause disease. To date, the only nuclear-encoded CI subunit gene that has been successfully mutated in mice is *Ndufs4* (Irwin *et al.*, 2013). In 2009, an *Ndufs4* point mutation mouse model was created that resulted in mice with a truncated form of NDUFS4. Unfortunately, homozygous mutants died *in utero*, and while the heterozygous mutants displayed features of CI deficiency, they did not present with the intended LS symptoms (Ingraham *et al.*, 2009).

The first and best characterised genetic KO model of CI deficiency was developed by the Palmiter group in 2008 (Irwin *et al.*, 2013; Kruse *et al.*, 2008). This model, called the *Ndufs4* whole-body KO mouse (B6.129S4-*Ndufs4*$^{tm1.1Rpa}$/J; hereafter referred to as the Ndufs4 mouse), was produced by flanking exon two of the *Ndufs4* gene with *loxP* (locus of X(cross)-over in P1) sites, deleting it from the germline via Cre-lox recombination and interbreeding the resulting heterozygous mice to create a homozygous mutant. The mice were then backcrossed on a C57BL6/J genetic background. Since the second exon of *Ndufs4* encodes the first 17 amino acids of the protein, as well as the final part of the mitochondrial targeting sequence, deletion thereof resulted in a frameshift mutation and lack of mature NDUFS4 (JAX, 2017b; Kruse *et al.*, 2008). This led to significantly reduced levels of intact CI and decreased CI activity, as seen in patients with *NDUFS4* mutations. Whereas heterozygous (*Ndufs4*$^{+/-}$) mice were indistinguishable from WTs (*Ndufs4*$^{+/+}$), homozygous mice (*Ndufs4*$^{-/-}$) displayed a stable clinical phenotype with extensive similarities to CI-deficient LS patients (Koene *et al.*, 2011). For example, the *Ndufs4*$^{-/-}$ mice exhibited a retarded growth rate, failure to thrive, elevated serum lactate, loss of motor skills, respiratory problems, encephalopathy, basal ganglia abnormalities, epilepsy, hypothermia, deafness, blindness, and death before adulthood [at a median age of postnatal day 50 (P50)] (Johnson *et al.*, 2013; Kruse *et al.*, 2008; Valsecchi *et al.*, 2012). Contrary to LS patients, the *Ndufs4*$^{-/-}$ mice additionally displayed ataxia, normal muscle morphology and reversible hair loss (at P21) (Kruse *et al.*, 2008).

nDNA-targeted MT mutants are plentiful and include gene KO mice (*MtI* + *MtII* KO, and *MtIII* KO mice), overexpressing transgenic mice (*MtI*, heart-specific *MtIIA* and *MtIII* mice), gene knockdown cells [small interfering ribonucleic acid silenced *MTIIA* cells], and transformation-induced overexpressing (*MTIB* and *MTIIA* cells) or null cells (*MTI* + *MTII* immortalised cells) (Erickson *et*

*al.*, 1997; Erickson *et al.*, 1995; Kang *et al.*, 1997; Kondo *et al.*, 1999; Lim *et al.*, 2009; Masters *et al.*, 1994; Michalska & Choo, 1993; Palmiter *et al.*, 1993; Reinecke *et al.*, 2006). Previous studies at this institution have already focussed on *Mt* KO mice and transformation-induced MT overexpressing cells (Lindeque, 2011; Pretorius, 2011; Reinecke, 2004). Additionally, since MTIII and MTIV are not ubiquitously expressed, nor enhanced by the same stimuli as MTI and MTII, these isoforms are not applicable (Haq *et al.*, 2003). A particularly interesting model, however, is the MTI overexpressing transgenic mouse [B6.Cg-Tg(Mt1)174Bri/J; hereafter referred to as the TgMTI mouse] (JAX, 2017a).

As before, the model was developed by the Palmiter group. In short, the TgMTI mouse was produced by inserting a 4 kb minimally marked *MtI* gene (*MtI**)[13] in-between two DNA regions (a 10 kb and 7 kb sequence, located upstream of the *MtII* gene and downstream of the *MtI* gene, respectively) and excising the complete ~21 kb transgene for microinjection into fertilised ova obtained from mating C57BL/6 x SJL males and females (Palmiter *et al.*, 1993). Of the resulting transgenic founder mice, a heterozygote [Tg(Mt1)174Bri] containing 56 randomly inserted copies of the transgene in addition to its two endogenous *MtI* genes, was then backcrossed on a C57BL6/J genetic background for commercial use (JAX, 2017a; Penkowa *et al.*, 2003). The DNA sequences used to flank *MtI** behave similarly to locus control regions that flank other genetic loci (Palmiter *et al.*, 1993). These regions are thought to enhance the successful expression of the enclosed gene by establishing a chromosomal domain which protects it from neighbouring chromosomal interference and facilitates the recognition of promotor or enhancer sequences by TFs (Felsenfeld, 1992; Palmiter *et al.*, 1993). Accordingly, TgMTI mice displayed copy number-dependent and position-independent expression of fully functional and inducible MTI. Ultimately each transgene yielded half the amount of *MtI* messenger ribonucleic acid (mRNA) normally expressed by the endogenous gene, and no ill effects were observed.

In conclusion, the Ndufs4 and TgMTI mouse models appear to be very promising and theoretically meet the requirements set by the proposed project (described in Chapter 3). It has therefore been decided to use both models to evaluate the role of MTI in CI deficiency.

[13] The *MtI** gene was marked by two additional nucleotides located nine nucleotides upstream of the translation initiation codon.

# CHAPTER 3:

# EXPERIMENTAL RATIONALE, AIMS, OBJECTIVES & STRATEGY

## 3.1 INTRODUCTION

In this chapter, the rationale (problem statement) behind this dissertation, along with the envisioned aims of the study, will be presented (Sections 3.2 and 3.3.1). This will be followed by the objectives and the experimental strategy proposed to achieve the aims (Sections 3.3.2 and 3.4). For detailed methods describing each objective, the reader is referred to Chapter 4.

## 3.2 PROBLEM STATEMENT

Given the mitochondrion's role in energy production, as well as its substantial contribution to cellular function, its dysfunction is frequently accompanied by devastating disease. Of these disorders, those concerning CI of the mitochondrial RC are considered the most common. Due to the enzyme's size and energetic importance, CI's deficiency can have profound and detrimental effects on normal cellular operation (Chinnery & Hudson, 2013). Furthermore, the disorder has been shown to be accompanied by a variety of biochemical abnormalities (e.g. increased ROS, an altered redox status, intracellular $Ca^{2+}$ imbalance, reduced energy production, and disrupted $\Delta\psi$). While many studies agree that the increased production of ROS and ensuing oxidative damage are among the most destructive of these, not all cases of CI deficiency will present with elevated ROS. This heterogeneity is further mimicked on the phenotypic level where a clear genotype-phenotype correlation is absent (Hoefs *et al.*, 2012). Additionally, the disorder has an early onset, an extremely rapid and progressive course, and ultimately proves fatal at a very young age. This not only complicates research into the pathophysiological mechanisms of CI deficiency, but impedes the development of successful treatment. As such, existing therapies are largely symptomatic and not completely curative as of yet (Rodenburg, 2016). While not always detectable, the production of ROS is regarded as one of the primary initiators of the disease phenotype, and studies researching the development of antioxidant therapies have shown great promise (de Haas *et al.*, 2017). An example includes KH176 (a chemical entity derivative of the vitamin E analogue Trolox), which is currently undergoing phase II clinical trials and is used in the treatment of LS (www.Khondrion.com). The fact that this product's pre-clinical development employed *fibroblasts* from patients with LS is of particular relevance to this study (Koopman *et al.*, 2016).

To restore homeostasis and promote their overall survival in times of stress or disease, cells are further equipped with a series of adaptive response programs (e.g. mitochondrial biogenesis, metabolic adaptations, autophagy, controlled cell death and antioxidant systems) (Reinecke *et*

*al.*, 2009). As shown at this institution by van der Westhuizen *et al.* (2003), one of these responses involves the upregulation of genes encoding for MTs. While the main function of these molecules remains elusive, numerous studies have linked their action to the mitochondrion. Accordingly, MTs have been shown to modulate mitochondrial energy production via their role as metal chaperones. Additionally, many studies have elaborated on their ROS scavenging capabilities, suggesting that MTs can protect the cell against oxidative damage and apoptosis. It should however be noted that contradicting evidence exists (Lindeque *et al.*, 2010). Regardless, it seems that MTs might offer an interesting therapeutic option against the effects of CI deficiency. *A problem that is of more relevance to this study, however, is the lack of literature regarding MTs' role in CI deficiency.*

Elucidating the position of MTs in CI deficiency has been a focus area of this institution since 2003 (van der Westhuizen *et al.*, 2003). To this end, numerous experimental models have been used, including transformation-induced MTIB and MTIIA overexpressing HeLa cells, as well as *MtI, MtII* and *MtIII* KO mice (Lindeque, 2011; Lindeque *et al.*, 2010; Pretorius, 2011; Reinecke, 2004; Reinecke *et al.*, 2006). *Because of the lack of a suitable genetic model at that time,* CI deficiency was generated by rotenone treatment in each case. Although effective, chemical inhibition did not mimic the full spectrum of the disorder as envisioned (Lindeque, 2011; Pretorius, 2011). The first genetic model of CI deficiency, namely the Ndufs4 mouse [developed by Kruse *et al.* (2008)] became commercially available in 2015. Additionally, the same group had previously developed an MTI overexpressing mouse model in 1993, called the TgMTI mouse (Palmiter *et al.*, 1993). Since genetic models are more commensurable with the physiological setting in human patients, *a more facile investigation of the effect of MTI on CI deficiency might thus be obtained from models generated by crossbreeding the Ndufs4 and TgMTI mice.* An undertaking of this nature will, of course, *necessitate a thorough characterisation of the model on a genetic, protein, and bioenergetics level.*

## 3.3 AIMS & OBJECTIVES

### 3.3.1 AIMS

It should be noted that the research presented here forms part of a much larger study of which the *overall aim* is to investigate the biochemical *(in vitro* and *in vivo)*, metabolic (*in vivo*), and phenotypic (*in vivo*) effects of MTI on CI deficiency, with the intention of demonstrating a protective effect[14].

For the purpose of this study however, the following *two aims* have been formulated:

[14] The other aspects of this study were conducted by various post-graduate colleagues.

- The **first aim** is to develop mouse models with which the effects of MTI overexpression on CI deficiency can be studied, by crossbreeding the Ndufs4 and TgMTI mouse strains. The models are then to be characterised on a genetic and protein level by using primary fibroblast cells lines, cultured from these mice (Objectives 1.1 to 1.8).
- The **second aim** is to investigate the effect of MTI overexpression on the bioenergetics consequences of CI deficiency by using the aforementioned established primary fibroblast cell lines (Objectives 2.1 to 2.7).

### 3.3.2 OBJECTIVES

To achieve the proposed aims, this *in vitro* study has been divided into two parts (referred to below as one and two). The first will entail setting up a successful crossbreeding strategy to obtain mice of four specific genotypes. From these mice, primary mouse fibroblast cell lines will then be established and characterised. The second part of this study will involve evaluating the biochemical profile of each fibroblast cell line, thereby investigating the effect of MTI overexpression on the bioenergetics consequences of CI deficiency.

Therefore, the *objectives* of part one of this study are to:

1.1. Verify the C57BL6/J genetic background of the individual mouse strains.

1.2. Develop a successful crossbreeding strategy and obtain mice corresponding to the following confirmed genotypes:
   i. WT mice (*Ndufs4*$^{+/+}$*:TgMTI*$^{-/-}$)
   ii. *Ndufs4* KO mice (*Ndufs4*$^{-/-}$*:TgMTI*$^{-/-}$)
   iii. MTI overexpressing mice (*Ndufs4*$^{+/+}$*:TgMTI*$^{+/+}$)
   iv. *Ndufs4* KO mice overexpressing MTI (*Ndufs4*$^{-/-}$*:TgMTI*$^{+/+}$)

1.3. Culture primary fibroblasts from skin samples obtained from each of the four mouse genotypes mentioned in Objective 1.2.

In order to characterise each primary fibroblast cell line, it will then be necessary to:

1.4. Genotype the *Ndufs4* gene by evaluating the absence or presence of exon two.

1.5. Genotype the *MtI** transgene by determining the relative copy number of *MtI*.

1.6. Measure the relative quantity of *MtI* mRNA.

1.7. Relatively quantify the level of NDUFS4 protein.

1.8. Determine the relative activity and quantity of intact CI.

Furthermore, to evaluate the effect of MTI overexpression on the bioenergetics consequences of CI deficiency (part two of the study), the *objectives* are to:

2.1 Assess the cell viability.

2.2 Determine the RMCN (relative mitochondrial DNA copy number).

2.3 Analyse the cellular redox status (NADH/$NAD^+$ ratio).

2.4 Evaluate the energy status (ATP/ADP ratio) of the cell.

2.5 Quantify the cellular ROS levels.

2.6 Determine the mitochondrial bioenergetics profile.

2.7 Perform the necessary statistical analyses on the obtained results.

### 3.4 EXPERIMENTAL STRATEGY

Figure 3.1 depicts the experimental strategy employed in this study. To achieve the *first aim*, a single nucleotide polymorphism (SNP) panel was used to compare the genetic background of the individual mouse strains (*Ndufs4*$^{+/-}$ and *TgMTI*$^{+/-}$ or *TgMTI*$^{+/+}$) to the C57BL6/J background, with the purpose of confirming that these mice differed only with respect to their individual genetic modifications (Objective 1.1). Hereafter, the animals were crossbred according to a specific breeding strategy to obtain mice with the following genotypes: *Ndufs4*$^{+/+}$*:TgMTI*$^{-/-}$, *Ndufs4*$^{-/-}$*:TgMTI*$^{-/-}$, *Ndufs4*$^{+/+}$*:TgMTI*$^{+/+}$, and *Ndufs4*$^{-/-}$*:TgMTI*$^{+/+}$ (Objective 1.2)[15].

*At this point, it is important to note that although the mice of a specific genotype group are essentially identical, slight genetic variations and the process of cell culture could nevertheless produce a degree of variability, even between putative identical samples. To get an estimation of the effect of these factors on the reproducibility of the results, it was decided to use two – and not one as is common practice – cell lines from each genotype in this study.* Eight mice were thus obtained and euthanised between P49 and P51, after which skin biopsies were collected. From these samples, primary fibroblast cell lines were then established in glucose-containing medium and cryopreserved for the upcoming experiments (Objective 1.3).

To genetically characterise each fibroblast cell line (cultured to passage four), samples were then genotyped by conventional polymerase chain reaction (PCR; for the *Ndufs4* gene; Objective 1.4) and real-time PCR [qPCR; for the *MtI* (both *MtI* and *MtI**) genes; Objective 1.5] analyses. Hereafter, the relative quantity of the *MtI* mRNA was measured via a multiplex reverse transcription-qPCR (RT-qPCR) reaction to corroborate the transcription of the *MtI** transgenes (Objective 1.6). For protein characterisation, one fibroblast cell line of each genotype was cultured to passage six. Using cell lysates, the relative quantity of the NDUFS4 protein was measured via sodium dodecyl sulphate polyacrylamide gel electrophoresis (SDS-PAGE) + western blot analysis (Objective 1.7). The role of NDUFS4 in CI's stability and function was then evaluated by examining the relative quantity and activity of fully assembled CI, from enriched mitochondrial

[15] Throughout Objectives 1.1 and 1.2, mice were selected based on genotyping results acquired from tail-snip samples, according to the methods mentioned below.

fractions of the fibroblast cell lines, via BN-PAGE + western blot and IGA analyses (Objective 1.8).

In fulfilment of the *second aim*, the eight fibroblast cell lines were cultured to passage four. To overcome any secondary effects stemming from the fibroblasts' glycolytic nature, the culture medium was replaced by a galactose-containing medium one to two days prior to each analysis. Cells were then analysed to determine whether cell viability was influenced by the genotype (Objective 2.1). To evaluate if and how mitochondrial biogenesis was affected, the RMCN was measured by qPCR analysis (Objective 2.2). Hereafter, the effect of the genotype on the redox- ($NADH/NAD^+$ ratio; Objective 2.3) and energy status (ATP/ADP ratio; Objective 2.4) was determined by using two bioluminescent assays. To quantitatively determine the cellular ROS level of each primary fibroblast culture, flow cytometry was employed (Objective 2.5), while the mitochondrial bioenergetics profile was evaluated using the Seahorse $XF^e96$ Analyser (Objective 2.6). Finally, statistical analyses were performed where necessary (Objective 2.7) and the biochemical profiles were compared to determine the effect of MTI overexpression on the bioenergetics consequences of CI deficiency.

## PART 1: ESTABLISH & CHARACTERISE Ndufs4:TgMTI MICE (AIM 1)

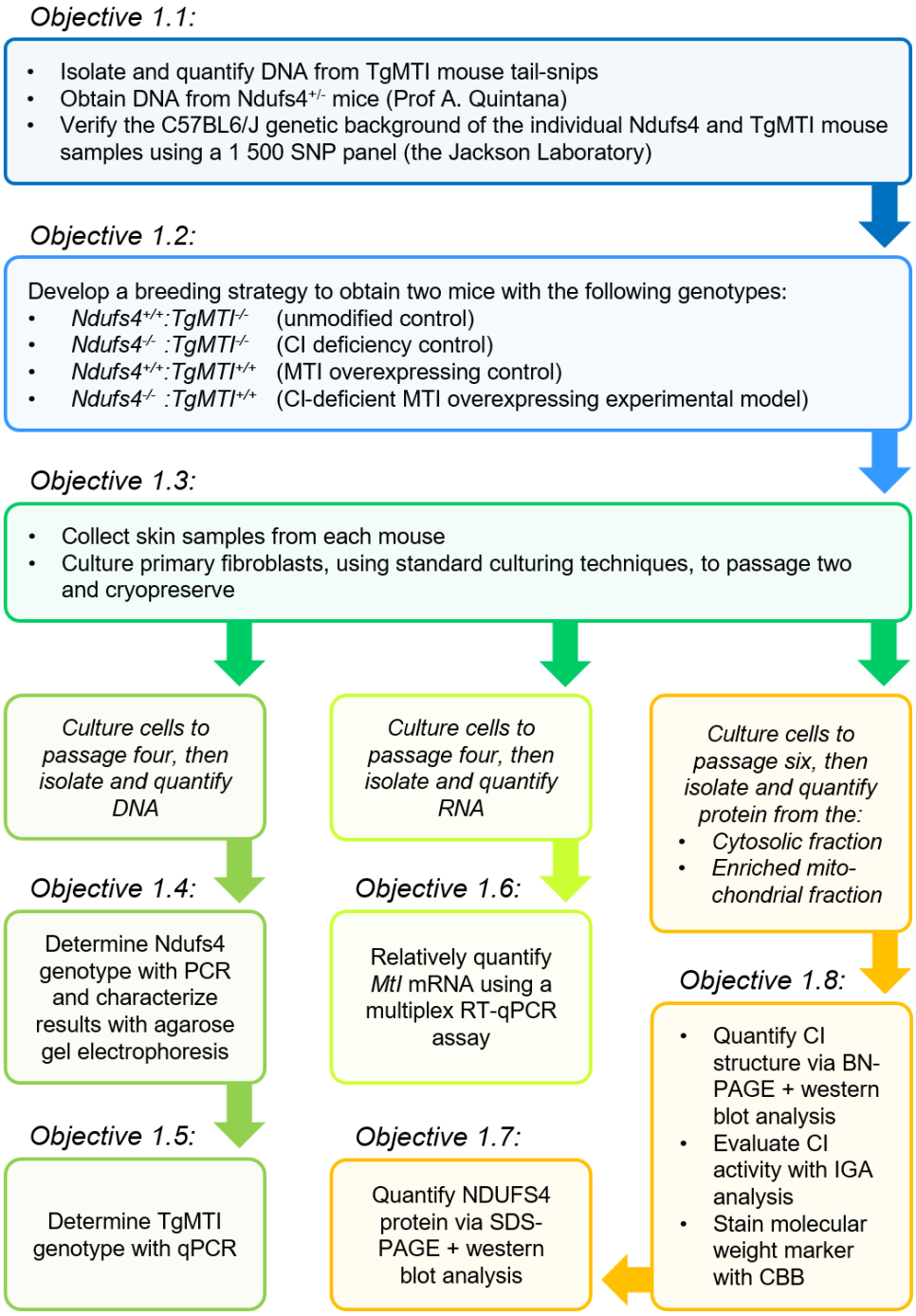

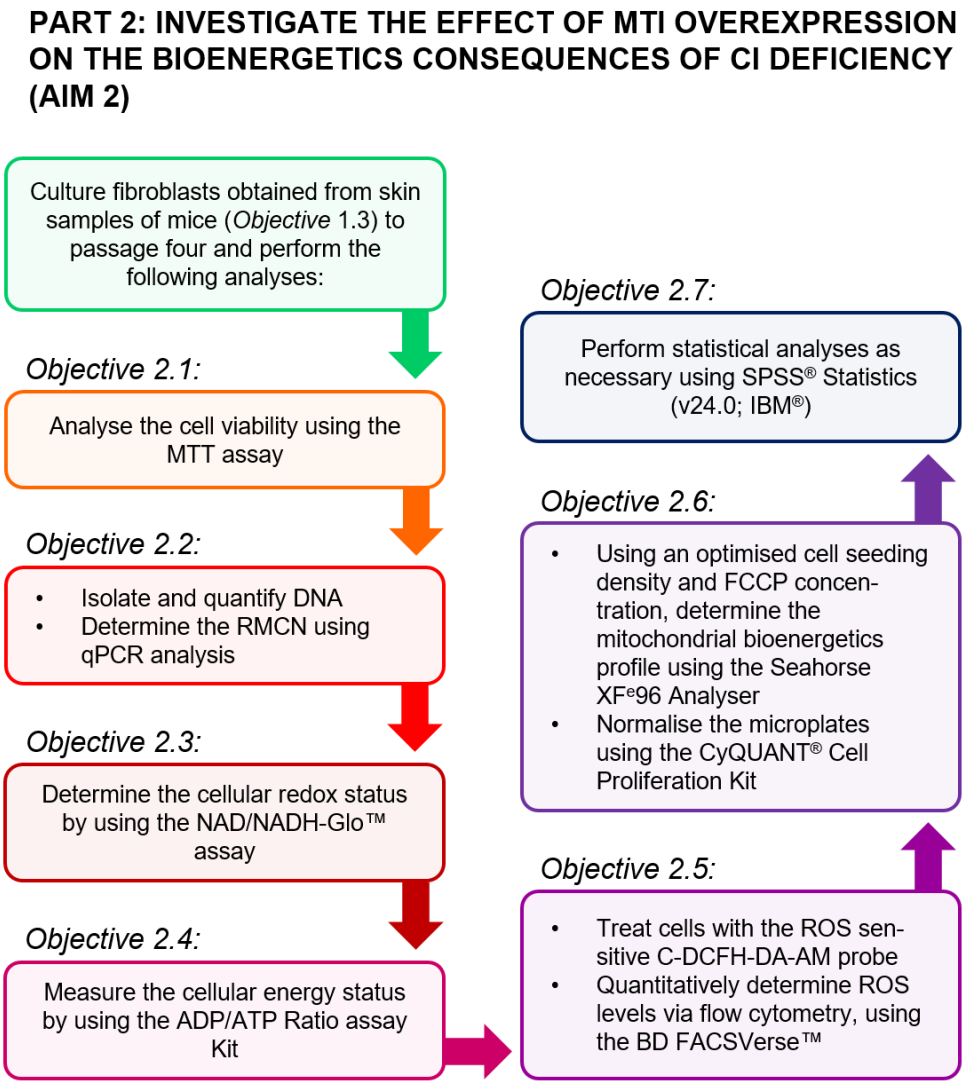


**Figure 3.1: Experimental strategy depicting the aims and objectives of the study.** This study was divided into two parts. Part one (the first aim) consisted of Objectives 1.1 to 1.8 and involved the development and characterisation of genetic mouse fibroblast models, with which the effect of MTI overexpression on the bioenergetics consequences of CI deficiency could be evaluated. In part two (the second aim) this effect was subsequently investigated using the methods depicted in Objectives 2.1 to 2.7.

# CHAPTER 4:

# MATERIALS & METHODS

## 4.1 INTRODUCTION

In this study, the effect of MTI overexpression on CI deficiency was investigated by means of defined crossbred mouse models. Prior to producing the models, the genetic background of each contributing strain (Ndufs4 and TgMTI) was compared. A breeding strategy was then set up to obtain two mice with a WT- (*Ndufs4*$^{+/+}$*:TgMTI*$^{-/-}$; unmodified control), CI-deficient- (*Ndufs4*$^{-/-}$*:TgMTI*$^{-/-}$; CI deficiency control), MTI overexpressing- (*Ndufs4*$^{+/+}$*:TgMTI*$^{+/+}$; MTI overexpressing control), and CI-deficient MTI overexpressing (*Ndufs4*$^{-/-}$*:TgMTI*$^{+/+}$; experimental model) genotype. By using primary fibroblast cell lines generated from these mice, the models were then characterised on the genetic and protein level. The study was concluded by evaluating the biochemical profile of each fibroblast culture to determine the effect of MTI overexpression on the bioenergetics consequences of CI deficiency.

In the following chapter the methods employed to achieve the objectives listed in Section 3.3.2 are given. Unless otherwise stated, methods have been described in detail and adhere to the specifications as recommended by the supplier or relevant publications. All materials have been recorded as used, while the Punnett squares, initial optimisation procedures, gel preparations, and microtiter plate layouts may be found in Appendices A to E.

## 4.2 ETHICS, HOUSING & IDENTIFICATION OF MICE

The necessary ethical approval for this study was obtained from the AnimCare Ethics Committee of the North-West University (NWU) in 2014 (approval number: NWU-00001-15-S1). As mentioned in Section 2.7, the mouse strains required to produce the *Ndufs4*$^{-/-}$*:TgMTI*$^{+/+}$ model included B6.129S4-*Ndufs4*$^{tm1.1Rpa}$/J (Ndufs4) and B6.Cg-Tg(Mt1)174Bri/J (TgMTI). While the DNA of two *Ndufs4*$^{+/-}$ mice were kindly provided by Prof Albert Quintana [previously from the University of Washington (UW), Seattle, WA, USA], the purpose of which is explained in Section 4.3.1, mice used in the breeding program were acquired from the Jackson Laboratory (ME, USA) in 2015. This included three male and six female *Ndufs4*$^{+/-}$ mice, as well as seven male and five female *TgMTI*$^{+/-}$ or *TgMTI*$^{+/+}$ mice. To import these animals, permits were acquired from the South African Department of Agriculture and the mice were subsequently housed, bred and crossbred at the specific pathogen-free unit of the Preclinical Drug Development Platform (PCDDP) at the NWU, Potchefstroom Campus.

Here, mice received *ad libitum* access to standard laboratory chow (Laboratory animal food: Rodent Breeder, #RM1845, purchased from LabChef, Nutritionhub, Western Cape)[16] and tap water, while being kept under the following conditions: A 12 h light/dark cycle, temperature of 22°C ± 2°C, relative humidity of 55% ± 10%, positive air pressure in the animal rooms maintained by airtight doors between departments, air quality maintained by high-efficiency particulate air (HEPA) filters, and a minimum air exchange of 18 to 20 times the volume fresh uncirculated air per hour. Furthermore, mice were weaned and identified at P21 to P23. Identification entailed assigning each mouse a unique identification number (ID) by punching holes into different positions of one or both ears (Figure 4.1). In turn, each position signified a specific digit and combinations thereof allowed mice to be numbered from 1 to 99. Mice were further sorted according to their date of birth (DOB) and litter number (1a to z, 2a to z, etc.), and strict records were kept on their parental lineage.


**Figure 4.1: Illustration depicting the ear punch numbering system employed to identify mice used in this study.** When the animal is viewed from the front, the first digit (tens position) of its ID is obtained by summing the numbers designated by the holes on its right ear, while the second digit (ones position) is acquired by doing so for the left. For example, mouse 62 is indicated by a 20 and 40 hole in the right ear, and a 2 hole in the left. Adapted by permission from John Wiley & Sons, Inc.: In book: Mouse Models of Human Cancer, Chapter 1, Boggess *et al.* (2004:1-14), copyright 2004.

## 4.3 PART 1: ESTABLISHING & CHARACTERISING Ndufs4:TgMTI MICE

### 4.3.1 GENOTYPING THE WHOLE GENOME OF THE Ndufs4 & TgMTI STRAINS – *Objective 1.1*

In the context of experimental mouse models, the *background genome* (also called the *genetic background*) may be defined as the genetic makeup of the organism, excluding the modified gene(s) of interest (JAX, 2006). Differences in this background have been reported to affect the phenotype of research animals by altering the expression or consequences of the genetic modification (Schauwecker, 2011). Therefore, one of the first steps of this study was to confirm

[16] In this chapter, numbers following a # symbol in brackets indicate the catalogue numbers of reagents.

that each individual strain (Ndufs4 and TgMTI) possessed a genetic background comparable to the C57BL6/J genome. To accomplish this, DNA of mice from each strain was sent to the Jackson Laboratory in 2015 for analysis against a set of C57BL6/J-specific SNPs.

#### 4.3.1.1 METHODS

##### 4.3.1.1.a SAMPLE PREPARATION

In preparation for the assay, DNA was isolated from the tail-snip samples of nine TgMTI mice (collected as described in Section 4.3.4.1.a), according to the method discussed in Section 4.3.4.1.b. To avoid potential downstream interference from the DNA Elution Buffer, the purified DNA was instead eluted in 25 µL of nuclease-free $H_2O$ (#129114, purchased from Qiagen, Whitehead Scientific, Cape Town). The quantity and purity of each sample were subsequently determined, as described in Section 4.3.4.1.b, by using the NanoDrop® 1000 Spectrophotometer (purchased from NanoDrop Technologies, Thermo Fisher Scientific™, MA, USA) and Operating Software (v3.8.1). If necessary, samples were then concentrated by using the Savant™ ISS110 Speedvac™ Concentrator (Thermo Electron Corporation, NC, USA), after which concentrations were adjusted to ~100 ng/µL with nuclease-free $H_2O$. Since the TgMTI mice analysed were those originally purchased from the Jackson Laboratory, there was no need genotype them.

For the Ndufs4 strain, DNA of two *Ndufs4*$^{+/-}$ mice were kindly provided by Prof Albert Quintana, as the Ndufs4 colony had not yet been established at this facility at the time of the assay. In total, then, the DNA of 11 mice were sent (at -4°C) to the Jackson Laboratory for analysis on the 1 500 SNP Panel (item number: GES0028). Table 4.1 lists the details of each sample analysed.

**Table 4.1: Mice used for whole genome genotyping**

| Animal ID | Genotype | Gender | DOB | Institution supplying sample |
|---|---|---|---|---|
| 7964 | *TgMTI*$^{+/-}$ or $^{+/+}$ | Male | 2014-03-12 | PCDDP (NWU) |
| 2282 | *TgMTI*$^{+/-}$ or $^{+/+}$ | Male | 2014-03-12 | PCDDP (NWU) |
| 2273 | *TgMTI*$^{+/-}$ or $^{+/+}$ | Male | 2014-03-12 | PCDDP (NWU) |
| 7691 | *TgMTI*$^{+/-}$ or $^{+/+}$ | Male | 2014-03-12 | PCDDP (NWU) |
| 2278 | *TgMTI*$^{+/-}$ or $^{+/+}$ | Female | 2014-03-12 | PCDDP (NWU) |
| 2277 | *TgMTI*$^{+/-}$ or $^{+/+}$ | Female | 2014-03-12 | PCDDP (NWU) |
| 2269 | *TgMTI*$^{+/-}$ or $^{+/+}$ | Female | 2014-03-12 | PCDDP (NWU) |
| 2271 | *TgMTI*$^{+/-}$ or $^{+/+}$ | Female | 2014-03-12 | PCDDP (NWU) |
| 2279 | *TgMTI*$^{+/-}$ or $^{+/+}$ | Female | 2014-03-12 | PCDDP (NWU) |
| Q4036 | *Ndufs4*$^{+/-}$ | Female | Unknown | UW |
| Q4037 | *Ndufs4*$^{+/-}$ | Female | Unknown | UW |

The table displays the identification number (ID), genotype, gender, and date of birth (DOB) of the mice, as well as the institution supplying the DNA samples.

#### 4.3.1.1.b GENOTYPING THE WHOLE GENOME USING AN SNP PANEL

*Single nucleotide polymorphisms* (SNPs) – defined as single base pair variations occurring at specific loci within the DNA in >1% of a population – are considered one of the most abundant groups of genetic markers (Petkov *et al.*, 2004). Since SNPs are generally conserved, found across all chromosomes, and enable the distinction of closely related strains, they provide a successful means to monitor the genetic quality of laboratory animals. Consequently, the Jackson Laboratory offers SNP genotyping services to aid researchers in comparing the background genomes of various strains. Accordingly, the samples listed in Table 4.1 were analysed using the 1 500 SNP Panel service provided by the Jackson Laboratory. This entailed comparing the SNPs of each sample against 1 453 validated and polymorphic (i.e. highly informative) SNP markers, spaced evenly across all 19 autosomes, as well as the X chromosome of the C57BL6/J genetic background (JAX, 2014). Since the Y chromosome is considered to be fixed via backcrossing, the panel excluded SNP markers thereof.

To analyse each sample, competitive allele-specific PCR (KASP™ genotyping technology, LGC Ltd.) was performed in 1 536-well microtiter plates, according to the manufacturer's instructions (LGC Ltd.: KASP™ genotyping technology, 4227/CB/0415). Each 1 µL reaction consisted of sample template DNA, KASP™ Assay mix (containing two allele-specific forward primers[17] and one common reverse primer) and KASP™ Master mix [containing two FRET (fluorescence resonance energy transfer) reporter cassettes[18], Hot Start KASP™ *Taq* deoxyribonucleic acid polymerase (DNA Pol), deoxyribonucleotide triphosphates (dNTPs), ROX passive dye and $MgCl_2$ in an optimised buffer]. In addition, a no template control (NTC) was prepared to monitor reagent contamination (i.e. a KASP™ reaction lacking template DNA). Following reaction preparation, the plates were securely sealed and each reaction was amplified according to a KASP™ thermocycling protocol.

During the first stage, an increased temperature allowed for the denaturation of double stranded template DNA, as well as the activation of KASP™ *Taq* DNA Pol. This was followed by various cycles consisting of a DNA denaturation step (step one) and a combined annealing/extension

[17] Each allele-specific forward primer consisted of a 5'-tail sequence, complimentary to one of the reporter cassettes, and a 3'-target sequence, complimentary to the template DNA.

[18] Each FRET reporter cassette consisted of two complimentary oligonucleotides. While the first oligonucleotide contained a 5'-fluorophore, the second contained a 3'-quencher. Thus, the cassette was non-fluorescent in its bound form. Each cassette was further complimentary to only one of the 5'-tail sequences of the forward primer, and possessed a different fluorophore (FAM or HEX).

step (step two)[19]. To simplify the explanation of the cycles, the events occurring at only one of the two strands of the original template DNA are discussed: in the second step of the first cycle, the target sequence of one of the forward primers was allowed to anneal to one strand of the template DNA. Since the forward primers were each specific to the same DNA sequence, but differed in terms of their 3'-nucleotides (the nucleotide complimentary to the SNP), the SNP in the template DNA determined which forward primer would bind. Hereafter, the strand was extended by KASP™ *Taq* DNA Pol. In the second step of the second cycle, the common reverse primer was allowed to anneal to the complimentary strand now containing the incorporated forward primer (the new template strand). Once again, the strand was extended via KASP™ *Taq* DNA Pol. However, this time, the 5'-tail sequence of the forward primer contained in the new template strand, was also amplified. Consequently, only the fluorophore-labelled oligonucleotide (from the FRET reporter cassette) complimentary to the amplified tail sequence, was allowed to bind to the new strand in the second step of the third cycle. The subsequent extension of the fluorophore-labelled oligonucleotide by KASP™ *Taq* DNA Pol, therefore led to its incorporation into a new complimentary DNA strand, thus causing it to permanently dissociate from its original cassette compliment containing the 3'-quencher. As a result, this new strand of DNA produced fluorescence indicative of the SNP incorporated in one of the alleles of the original template DNA. Following various cycles, the fluorescence increased according to the proportion of incorporated fluorophore-labelled oligonucleotides.

Once the PCR reaction was completed, it was cooled to below 40°C in order to quench any unincorporated fluorophore-labelled oligonucleotides. The fluorescence of the incorporated fluorophore-labelled oligonucleotides was then measured. Depending on the SNPs present in both alleles of the original DNA template, either FAM- or HEX-fluorescence, or both FAM- and HEX-fluorescence was present. Cluster analysis was then performed using the Karken software and a genotype was assigned to each SNP of all 11 samples. Using this approach, the KASP™ chemistry was able to yield a >99.8% genotyping accuracy, based on independent measurements.

### 4.3.2 CROSSBREEDING THE Ndufs4 & TgMTI MOUSE LINES – *Objective 1.2*

After confirming the lack of significant genetic variance between the C57BL6/J backgrounds of the Ndufs4 and TgMTI mouse strains (Section 4.3.1), a breeding strategy was developed as a specific objective, with which the genotypes required for this study could be obtained. Since other aspects of the larger project (not discussed in this dissertation) would also investigate these

[19] Each step occurred at a specific temperature and for a specific period, as optimised by the manufacturer. Since the analysis was not performed at this institution, these details are unknown.

genotypes, the breeding strategy was designed to produce the required mice at the highest possible probability and efficiency.

#### 4.3.2.1 METHODS

In order to crossbreed the Ndufs4 and TgMTI strains, the breeding strategy depicted in Figure 4.2 was followed, while Punnett squares (Appendix A) were used to determine the genetic probability of the offspring. The first step entailed obtaining mice of a specific genotype from each individual strain. As *Ndufs4*$^{-/-}$ mice developed a fatal phenotype before reaching sexual maturity (six to eight weeks), they were considered unsuited for breeding (Kruse *et al.*, 2008). Therefore, *Ndufs4*$^{+/-}$ males were selected from the Ndufs4 colony. From the TgMTI strain, it was decided to use *TgMTI*$^{+/+}$ females. Although, theoretically, both *TgMTI*$^{+/-}$ and *TgMTI*$^{+/+}$ mice were healthy, and while the possibility existed that there would be no difference in their MTI* protein expression level (not determined in this study), *TgMTI*$^{+/+}$ was the most effective starting genotype. To obtain *Ndufs4*$^{+/-}$ males and *TgMTI*$^{+/+}$ females, heterozygous males and females were mated within each strain (intra-strain mating) in a ratio of 1:2 per breeding cage (Figure 4.2, Steps 1 and 2). The same ratio was maintained throughout the breeding program.

Once enough founder mice had become available, they were paired up with the purpose of producing dihybrid (*Ndufs4*$^{+/-}$*:TgMTI*$^{+/-}$) pups (Figure 4.2, Step 3). Upon reaching maturity, the dihybrid males and females were mated (Figure 4.2, Step 4). While this allowed a 6.25% chance of obtaining mice with one of the four intended genotypes, this percentage was regarded too low to yield the sizeable gender-specific group of mice required for the studies of the overall project (not discussed in this dissertation). It was therefore decided to include two additional steps in the breeding program. To this end, *Ndufs4*$^{+/-}$*:TgMTI*$^{+/+}$ males and females, and *Ndufs4*$^{+/-}$*:TgMTI*$^{-/-}$ males and females (each obtained from Step 3 with a 12.5% genetic probability) were mated. As this alternative resulted in a 25% chance of obtaining mice with the required genotype, i.e. *Ndufs4*$^{+/+}$*:TgMTI*$^{+/+}$ and *Ndufs4*$^{-/-}$*:TgMTI*$^{+/+}$ mice (Figure 4.2, Step 5), and *Ndufs4*$^{+/+}$*:TgMTI*$^{-/-}$ and *Ndufs4*$^{-/-}$*:TgMTI*$^{-/-}$ mice (Figure 4.2, Step 6), it was regarded as more acceptable.

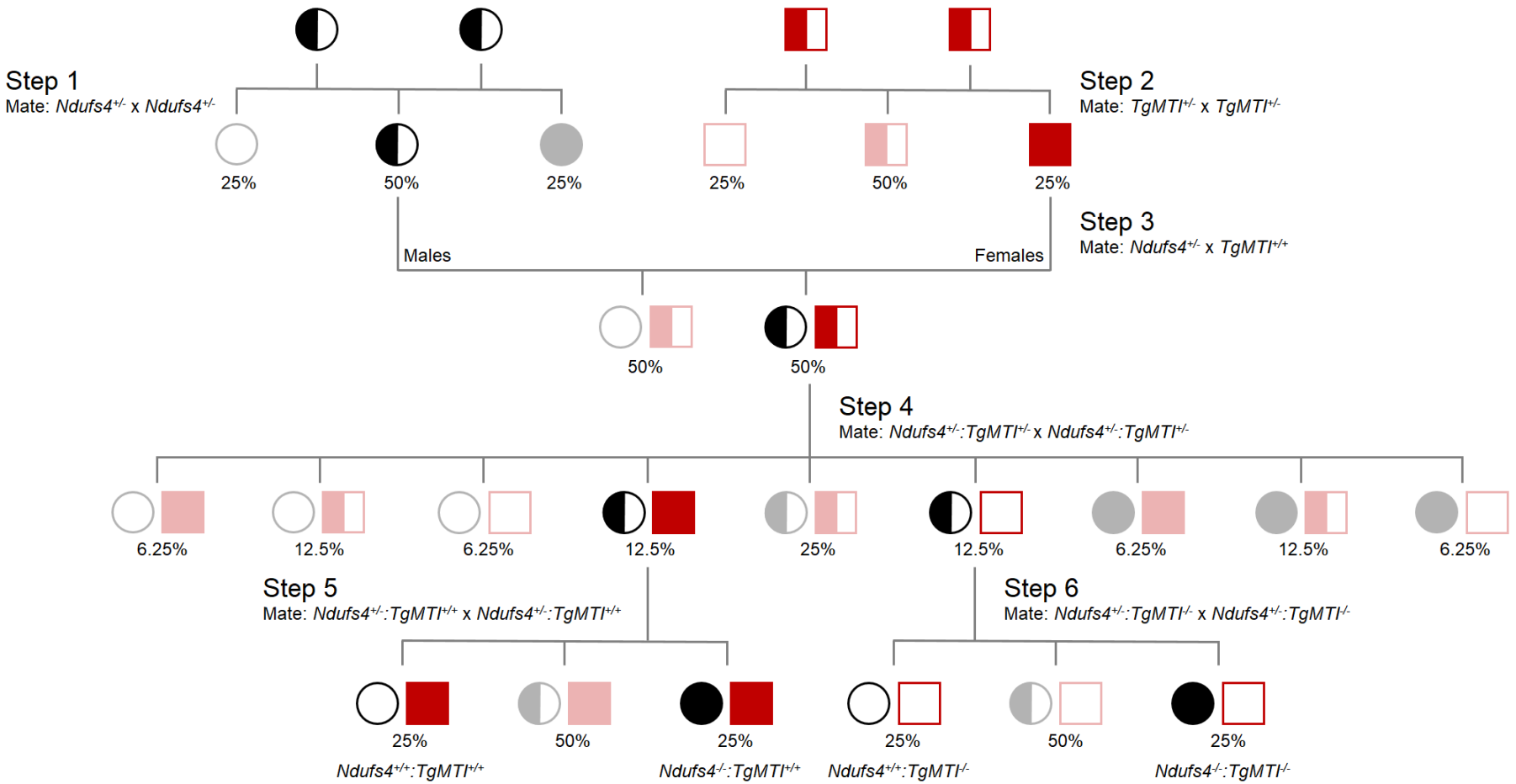


**Figure 4.2: Breeding strategy design used to obtain *Ndufs4$^{+/+}$:TgMTI$^{+/+}$*, *Ndufs4$^{-/-}$:TgMTI$^{+/+}$*, *Ndufs4$^{+/+}$:TgMTI$^{-/-}$*, and *Ndufs4$^{-/-}$:TgMTI$^{-/-}$* genotypes.** Black circles signify the Ndufs4 genotype, while red squares represent the TgMTI genotype. Open, half-filled and filled shapes refer to wild type, heterozygous and homozygous genotypes, respectively. Each step represents a new generation. Percentage probabilities were obtained using Punnett squares (Appendix A).

Considering the severely inbred nature of the mice used in the breeding program, as well as the similarity of their C57BL6/J genetic backgrounds, it was further acceptable to use mice as soon as they became available, i.e. the mice used came from different steps of the breeding strategy. Additionally, since these mice would be utilised to establish fibroblast cultures and the genetic modifications were not X-linked, gender was not of importance in the present study.

**Table 4.2: Details of the mice used in this study**

| Animal ID | Sample name | Set | Genotype | Gender | Litter number | Parental lineage | Age (days) |
|---|---|---|---|---|---|---|---|
| 11 | WT 1 | 1 | *Ndufs4*$^{+/+}$:*TgMTI*$^{-/-}$ | Male | 1v | Step 2 | 50 |
| 62 | OVER 1 | 1 | *Ndufs4*$^{+/+}$:*TgMTI*$^{+/+}$ | Male | 1m | Step 3 | 50 |
| 85 | KO 1 | 1 | *Ndufs4*$^{-/-}$:*TgMTI*$^{-/-}$ | Female | 2h | Step 5 | 50 |
| 72 | KO OVER 1 | 1 | *Ndufs4*$^{-/-}$:*TgMTI*$^{+/+}$ | Male | 2f | Step 4 | 49 |
| 12 | WT 2 | 2 | *Ndufs4*$^{+/+}$:*TgMTI*$^{-/-}$ | Male | 1v | Step 2 | 50 |
| 65 | OVER 2 | 2 | *Ndufs4*$^{+/+}$:*TgMTI*$^{+/+}$ | Female | 1m | Step 3 | 51 |
| 86 | KO 2 | 2 | *Ndufs4*$^{-/-}$:*TgMTI*$^{-/-}$ | Female | 2h | Step 5 | 50 |
| 84 | KO OVER 2 | 2 | *Ndufs4*$^{-/-}$:*TgMTI*$^{+/+}$ | Female | 2g | Step 4 | 50 |

The table displays the ear punch identification number (ID), sample name, genotype, gender, litter number, parental lineage, and age of the mice. The set to which each sample belonged, is also shown. While parental lineage refers to the step of the breeding program (Figure 4.2) to which the parents of the mouse in question belonged, age denotes the age of the mouse upon euthanasia.

### 4.3.3 ESTABLISHING & CULTURING PRIMARY MOUSE FIBROBLAST CELL LINES – *Objective 1.3*

Section 2.4.5 underscored some of the advantages of using fibroblast cultures as an alternative to muscle biopsies during patient diagnosis. Similarly, primary fibroblast cultures have been widely applied as models to study biochemical and/or functional abnormalities in both KO and transgenic animals (Takashima, 1998:2.1.1). Since cultures of this nature are often reported to closely mimic the physiological state of cells *in vivo*, it was decided, for the purpose of this study, to evaluate the effect of MTI overexpression in CI deficiency by using primary fibroblast models, established from skin biopsies of the mice of interest (ATCC®: Primary cell culture guide, P/N PC-0813-02).

#### 4.3.3.1 METHODS

##### 4.3.3.1.a EUTHANISING MICE & COLLECTING SAMPLES

Mice corresponding to the four genotypes of interest were euthanised between P49 and P51 via cervical dislocation. Hereafter, the hide of the dorsal trunk was sterilised with 70% (v/v) ethanol, wiped clean and shaved using a sterile surgical blade (Takashima, 1998:2.1.11). From this area, a 1.2 $cm^2$ region of skin was aseptically removed and temporarily stored at 0°C in a 15 mL

polypropylene tube containing 10 mL complete growth medium [Dulbecco's Modified Eagle Medium (DMEM, #41966029) with 20% (v/v) fetal bovine serum (FBS, #10270106) and 100 units/mL penicillin and 100 µg/mL streptomycin (Penicillin:Streptomycin; P/S, #15140122), purchased from Gibco®, Thermo Fisher Scientific™].

#### 4.3.3.1.b ESTABLISHING PRIMARY CULTURES

Primary skin fibroblast cultures were subsequently set up via a skin explant culture system. This type of method was selected as it is technically simpler, requires minimal reagents and is much more rapid (30 min to 60 min) than the alternative dissociated fibroblast culture system (2 h to 4 h) (Takashima, 1998:2.1.1). Since the technique had to be developed, it will be described in full.

Working in a laminar flow hood under sterile conditions, the skin biopsy was washed twice in complete growth medium and placed in a petri dish containing 500 µL of the same liquid. The sample was then cut into 32x 2 $mm^2$ pieces using forceps and a surgical blade. Hereafter, eight biopsies were placed near each other in the centre of four T25 cell culture flasks with the subcutaneous layer facing down, and allowed to adhere in the laminar flow hood for 1 h (Keira *et al.*, 2004). The biopsies were then carefully overlaid with 500 µL FBS/flask and incubated at 37°C in a humidified atmosphere of 5% $CO_2$. These standard culture incubation conditions were used throughout the study, unless otherwise stated. Over a period of two days, the volume in each flask was steadily adjusted by first adding 500 µL DMEM containing 100 units/mL penicillin and 100 µg/mL streptomycin at 24 h, followed by 2 mL complete growth medium at 48 h. The biopsies were incubated until fibroblasts, identified by their fusiform morphology, finally emerged from and completely surrounded the skin samples (± five days following initial sample processing). Despite the skin's complexity, it was possible to obtain relatively pure primary fibroblast cell lines, since fibroblasts are known to overgrow and outcompete other skin cell types (e.g. keratinocytes) at very early passages (first and second) when using conventional culture medium, such as DMEM (Takashima, 1998:2.1.11). For this reason, characterisation of the cell type was not deemed necessary (Takashima, 1998:2.1.10).

In addition to the antibacterial P/S present in the complete growth medium, any potential mycoplasma was removed from these cultures by prophylactic treatment with a BM Cyclin regime (#10799050001, purchased from Roche, Sigma-Aldrich, MO, USA). Accordingly, the spent culture medium was replaced with 3 mL complete growth medium containing 5 µg/mL of BM Cyclin's pleuromutilin derivative. Cells were incubated under standard conditions for three days, after which the medium was once again replaced with 3 mL complete growth medium containing 2.5 µg/mL of BM Cyclin's tetracycline derivative. Following four days of incubation, the tissue fragments were carefully removed with forceps and the entire antibiotics course was repeated with 4 mL volumes. If necessary, the cells could be sub-cultured during this time

(according to the method explained in Section 4.3.3.1.c), provided that BM Cyclin-containing medium was used instead of complete growth medium. Alternatively, cells were sub-cultured following the BM Cyclin regime.

#### 4.3.3.1.c STANDARD CULTURING TECHNIQUES

To maintain cultures in the exponential growth phase, it is necessary to sub-culture, or passage, cells upon reaching a density of ± 80% to 90% of confluence (ATCC®: Primary cell culture guide, P/N PC-0813-02). To achieve this, cells are lifted from the culture vessel by breaking the inter- and intracellular cell-to-surface bonds via a proteolytic enzymatic reaction (trypsinisation). The procedure is then concluded by splitting the culture into smaller proportions (Jin *et al.*, 2017).

Throughout this study each primary culture was passaged upon reaching a ± 90% confluency (every three days). This was accomplished via trypsinisation according to an established standard operating procedure (SOP), by using 1x phosphate buffered saline (PBS; 0.01 M phosphate buffer, 0.0027 M KCl and 0.137 M NaCl, pH 7.4; #P4417, Sigma-Aldrich) prepared in Milli-Q® $H_2O$[20] and 1x trypsin-EDTA [0.05% (w/v) trypsin-EDTA; #15400054, Gibco®, Thermo Fisher Scientific™] prepared in 1x PBS. Following this, complete growth medium was added to inhibit the enzymatic reaction, and cells were split and incubated in a total of 5 mL complete growth medium (Seluanov *et al.*, 2010).

Since primary cell lines have been shown to exhibit a predetermined number of cell divisions, as described by the Hayflick limit, it is suggested that initial aliquots be frozen at low (second or third) passage numbers to ensure higher cell viability and to optimise their use in research (ATCC®: Primary cell culture guide, P/N PC-0813-02) (Hayflick, 1965; Takashima, 1998:2.1.4). Therefore, primary cultures were cryopreserved at the second passage, upon reaching ± 90% confluency. To achieve this, cells were trypsinised and frozen at -80°C in complete growth medium containing 5% (v/v) dimethyl sulfoxide (DMSO, #D2650, Sigma-Aldrich) as cryoprotectant.

In preparation for each experiment and to limit time-related differences, all eight cell lines were restarted for culture at the same time in complete growth medium from frozen aliquots, according to an established SOP. To allow cells a sufficient recovery period from the effects of cryopreservation with DMSO, and to exclude the variability observed when using cells with different passage numbers, each cell line was sub-cultured to passage four (unless otherwise stated) before experimental evaluation (ATCC®: Primary cell culture guide, P/N PC-0813-02). This early passage number was chosen to limit the accumulation of cell damage, as well as the

[20] Milli-Q® $H_2O$ refers to water that has been purified by the Milli-Q® system (purchased from Millipore™, Merck, MA, USA).

senescence-associated changes observed in the cell morphology and proliferation rate of primary cultures (Jin *et al.*, 2017; Keira *et al.*, 2004; Rubin, 1997). Throughout the study, the cell lines were cultured under identical conditions (to limit obvious culture-related differences) in T25 flasks containing 5 mL complete growth medium.

### 4.3.4 GENOTYPING Ndufs4:TgMTI MICE – *Objectives 1.4 & 1.5*

Since each of the six steps of the crossbreeding strategy had the potential to yield pups with at least two possible Ndufs4 and/or TgMTI genotypes, all mice had to be genotyped before inclusion into the breeding strategy[21] and project.

#### 4.3.4.1 METHODS

##### 4.3.4.1.a SAMPLE COLLECTION

The eight mice used in this study (see Table 4.2) were genotyped on two occasions: Firstly, as a means of initial identification by using tail-snip tissue samples and, secondly, to verify the genetic make-up of the established primary fibroblast cultures prior to their experimental use. For the former, tail-snip samples of each mouse and those mice serving as genotyping controls (see Table 4.3) were collected upon weaning via sterile techniques, by cutting the tip (5 mm) of the mouse tail and storing it in a 1.5 mL microcentrifuge tube at 4°C for immediate use. For the latter, each cell line was cultured to passage four as described in Section 4.3.3. Upon reaching ± 90% confluency, each culture was trypsinised. Following this, complete growth medium was added and the cell pellets were collected by centrifugation at 600 x *g* and 20°C for 5 min. Hereafter, the supernatant was discarded and the cell pellets were frozen at -20°C until use.

**Table 4.3: Mice used as controls for genotyping**

| Animal ID | Genotype | Gender | DOB |
|---|---|---|---|
| 65 | *Ndufs4*$^{+/+}$*:TgMTI*$^{-/-}$ | Male | 2016-06-30 |
| 43 | *Ndufs4*$^{+/-}$*:TgMTI*$^{-/-}$ | Female | 2016-06-02 |
| 41 | *Ndufs4*$^{-/-}$*:TgMTI*$^{-/-}$ | Female | 2016-08-15 |
| 67 | *Ndufs4*$^{+/+}$*:TgMTI*$^{-/-}$ | Male | 2016-06-28 |
| 10 | *Ndufs4*$^{+/+}$*:TgMTI*$^{+/-}$ | Male | 2016-08-01 |
| 13 | *Ndufs4*$^{+/+}$*:TgMTI*$^{+/+}$ | Female | 2016-08-01 |

The table displays the ear punch identification number (ID), genotype, gender, and date of birth (DOB) of the mice.

[21] While it exceeds the scope of this dissertation, it should be noted that mice used in the breeding program were also genotyped from tail-snip samples, by using the same methods described in Section 4.3.4.

#### 4.3.4.1.b ISOLATING & QUANTIFYING DNA FROM TAIL-SNIPS & CELLS

DNA was isolated from the abovementioned samples and controls via the ZR Genomic DNA™-Tissue MiniPrep Kit (#D3051, purchased from Zymo Research, Inqaba Biotec, Pretoria), in accordance with the manufacturer's instructions for solid tissue and cell monolayers. While the tissue and cell digestion methods differed, the remainder of the procedure was similar for both sample types. Briefly, tail-snip digestion included incubating each sample in a sterile 1.5 mL microcentrifuge tube containing a mixture of 95 µL nuclease-free $H_2O$, 95 µL 2x Digestion Buffer and 10 µL Proteinase K, at 55°C[22] for 2.5 h. Conversely, thawed cell pellets were first resuspended in 1 mL 1x PBS, transferred to a sterile 1.5 mL microcentrifuge tube and centrifuged[23] at 500 x *g* for 5 min. Cells were then digested by replacing the supernatant with a mixture of 95 µL nuclease-free $H_2O$, 95 µL 2x Digestion Buffer and 5 µL Proteinase K, and resuspending and incubating each sample at 55°C for 20 min.

Following incubation, the binding conditions were adjusted with 700 µL Genomic Lysis Buffer (containing chaotropic salts which disrupt nucleic acid-$H_2O$ interaction) to later allow the DNA's binding to the silica column. Samples were then mixed by vortexing and centrifuged at 10 000 x *g* for 1 min to pellet the insoluble cell debris. Hereafter, the supernatant was transferred to a Zymo-Spin™ IIC Column in a Collection Tube and centrifuged at 10 000 x *g* for 1 min. The flow-through, containing the bulk of the impurities, was then discarded[24] and any remaining contaminants were removed from the silica column in two wash steps [both with solutions containing 70% (v/v) ethanol to remove chaotropic salts and improve sample yield and purity]. For the first, 200 µL DNA Pre-Wash Buffer was added and the column was centrifuged at 10 000 x *g* for 1 min. The second included the addition of 400 µL of g-DNA Wash Buffer, followed by another 1 min centrifugation step at 10 000 x *g.* The Zymo-Spin™ IIC Column was then transferred to a sterile 1.5 mL microcentrifuge tube and 25 µL of a pre-warmed (to 65°C) DNA Elution Buffer was carefully added to the silica matrix. To allow the DNA to detach from the silica matrix and dissolve in the added buffer, the tube was incubated at room temperature (RT) for 5 min, after which the purified DNA was eluted from the column by centrifugation at 16 000 x *g* for 1 min. To increase the DNA yield, the elution step was repeated with another 25 µL volume of pre-warmed DNA Elution Buffer.

Purified DNA samples were subsequently quantified by measuring their absorbance at 260 nm (the wavelength at which DNA most strongly absorbs light) using the NanoDrop® 1000

[22] All >room temperature (RT; 21°C ± 1°C) incubations were performed in a heating block, unless otherwise stated.

[23] Centrifugation was performed at RT, unless otherwise stated.

[24] The capacity of the Collection Tubes was 1 mL.

Spectrophotometer and Operating Software (v3.8.1). In order to further assess the purity of each sample, the ratio of sample absorbance at 260 nm and 280 nm ($A_{260}/A_{280}$) was determined. Generally, DNA with a ratio of ~1.8 was accepted as pure. Conversely, the presence of impurities that strongly absorb at or near 280 nm (e.g. protein) was indicated by considerably lower $A_{260}/A_{280}$ ratios, while a ratio ≥2.0 signified ribonucleic acid (RNA) contamination.

#### 4.3.4.1.c CHARACTERISING THE Ndufs4 GENOTYPE – *Objective 1.4*

##### i AMPLIFYING DNA BY PCR ANALYSIS

Since the Ndufs4 mouse was created by deleting the second exon of the *Ndufs4* gene (as described in Section 2.7), amplicons spanning this area differ in size between homozygous WTs (*Ndufs4*$^{+/+}$), homozygous KOs (*Ndufs4*$^{-/-}$) and mice heterozygous for the *Ndufs4* gene (*Ndufs4*$^{+/-}$). As such, it was possible to use conventional PCR, as first described by Mullis *et al.* (1986), to differentiate between the three potential genotypes. To achieve this, primers, corresponding to the introns flanking exon two, were purchased from Inqaba Biotec, as presented in Table 4.4.

**Table 4.4: Sequences of the primers used to genotype the *Ndufs4* gene**

| Primer | Cat. no. | Primer sequence (5' to 3') | $T_m$ (°C) | Size (bp) |
|---|---|---|---|---|
| NDUFS4 1060 (Forward) | S32E6 | AGC CTG TTC TCA TAC CTC GG | 62.45 | 20 |
| NDUFS4 Rev (Reverse) | S3424 | TTG TGC TTA CAG GTT CAA AGT GA | 59.2 | 23 |

The table displays the name, catalogue number (cat. no.), sequence, melting temperature ($T_m$), and size of the forward and reverse primers used to genotype the *Ndufs4* gene. The primers used corresponded to those designed by Valsecchi *et al.* (2012).

PCR amplification was performed using the Phire™ Tissue Direct PCR Master Mix (#F170L, Thermo Fisher Scientific™), which employs the Phire Hot Start II DNA Pol. It was decided to use a Hot Start DNA Pol since the high degree of specificity it provided decreased most of the non-specific amplification and allowed for better distinction between the genotypes. For each sample, a 10 µL volume, consisting of 1x Phire Tissue Direct PCR Master Mix (2x), 0.5 µM forward primer, 0.5 µM reverse primer, nuclease-free $H_2O$, and a total of 25 ng DNA (previously diluted with nuclease-free $H_2O$[25]), was set up at 0°C[26] in a PCR tube. In addition, three control samples

[25] All DNA and RNA dilutions where prepared with nuclease-free $H_2O$, unless otherwise stated.

[26] Although Hot Start DNA Pol is inactive at RT, reactions were still prepared at 0°C as a precaution to maintain DNA and primer integrity.

corresponding to an *Ndufs4*$^{+/+}$, *Ndufs4*$^{-/-}$ and *Ndufs4*$^{+/-}$ genotype were prepared (mice 65, 41 and 43 in Table 4.3). Following this, samples were amplified in a T100™ Thermal cycler (#1861096, Bio-Rad, Pretoria) according to the following cycling conditions: An initial denaturation step (at 98°C for 5 min) was performed to guarantee complete denaturation of the double stranded template DNA and to activate the Phire Hot Start II DNA Pol. This step was followed by 35 cycles of DNA denaturation (at 98°C for 5 s), primer annealing (at 57.3°C for 5 s), and DNA extension (at 72°C for 20 s). The annealing temperature was optimised using a temperature gradient (not shown), while the DNA extension period was selected as advised by the manufacturer, according to the maximum size of the obtained amplicons (20 s/kb). PCR amplification was concluded with a final DNA extension step (at 72°C for 1 min), ensuring the completion of all amplicons, and the samples were cooled and stored at 4°C until use.

### ii CHARACTERISING DNA WITH AGAROSE GEL ELECTROPHORESIS

Hereafter, 10 µL of the amplified products (i.e. the three controls and eight samples), diluted 3:10 in nuclease-free $H_2O$, were loaded into the wells of a 1% (w/v) agarose gel (#8100-CONDA, purchased from Conda Laboratories, Thermo Fisher Scientific™) prepared in 1x Bionic™ Buffer (10x; #B6185, Sigma-Aldrich), with 5 µg/mL ethidium bromide (#46065, purchased from Fluka® Analytical, Sigma-Aldrich) acting as nucleic acid stain. Since the Phire™ Tissue Direct PCR Master Mix contained a pre-mixed gel loading dye, no additional loading dye was required. Furthermore, 10 µL of the GeneRuler™ 100 bp DNA Ladder[27] (#SM0241, Thermo Fisher Scientific™), diluted 3:10 in nuclease-free $H_2O$, was loaded on both sides of the gel as a DNA size marker. The gel was then run at 80 V in a Sub-Cell® GT Cell Horizontal Electrophoresis System (#1704401, Bio-Rad) until the electrophoretic front had travelled half the gel length. Due to the absence of the second *Ndufs4* exon, amplification of the KO allele yielded an amplicon of ~429 bp, whereas that of the WT allele was ~1 229 bp. As a result, the cathode-to-anode migration of the WT band occurred at a much slower rate than that of the KO.

Finally, the gel was photographed under ultraviolet (UV) light, using the ChemiDoc™ MP system (#17001402, Bio-Rad) and the Image Lab software (v5.2.1). While the *Ndufs4*$^{+/+}$ and *Ndufs4*$^{-/-}$ genotypes respectively corresponded to the ~1 229 bp and ~429 bp band, both bands were present in the *Ndufs4*$^{+/-}$ genotype.

[27] The GeneRuler™ 100 bp DNA Ladder contained a 2:1:3 ratio of DNA ladder:6x DNA loading dye (#SM0242, Thermo Fisher Scientific™):nuclease-free $H_2O$.

#### 4.3.4.1.d CHARACTERISING THE TgMTI GENOTYPE – *Objective 1.5*

Heterozygotes of the TgMTI mouse model used in this study contained 56 randomly inserted copies of the *MtI** transgene, as explained in Section 2.7. While there are conventional end-point PCR methods which allow distinction between homozygous WT mice (*TgMTI*$^{-/-}$) and mice containing the *MtI** transgene [homozygous MTI overexpressing mice (*TgMTI*$^{+/+}$) and heterozygous MTI overexpressing mice (*TgMTI*$^{+/-}$)], no published method existed at the start of this study with which all three genotypes could be distinguished (JAX, 2017a). Although the position of the *MtI** transgene insertion-sites have not been determined, it may be theorised that all 56 copies are transferred to the offspring together as one allele. This is supported by the knowledge that, despite various crosses (outbreeding and backcrossing), *TgMTI*$^{+/-}$ mice still carry the 56 copies of *MtI** (JAX, 2017a). By this reasoning, then, the *TgMTI*$^{+/+}$ genome, which theoretically contains two *MtI**-containing alleles, should exhibit 112 copies of *MtI*.*

##### i QUANTIFYING THE RELATIVE *MtI* COPY NUMBER BY qPCR ANALYSIS

To distinguish between the three possible TgMTI genotypes, a novel method was developed with which the collective copy number of the *MtI** and *MtI* genes (hereafter collectively referred to as *MtI*) could be determined. To achieve this, the nuclear *MtI* (target) gene was relatively quantified to the nuclear β-actin (*Actb*; reference) gene via qPCR analysis. The relative *MtI* copy number was subsequently resolved by processing the obtained data according to a simplification of the $2^{-\Delta\Delta CT}$ method (Applied Biosystems: User Bulletin No. 2, P/N 4303859), called $2^{-\Delta CT}$ (Schmittgen & Livak, 2008). In short, the $\Delta C_T$-value was calculated by subtracting the mean $C_T$ (threshold cycle) of the reference gene from that of the target gene. This value was then substituted into the $2^{-\Delta CT}$ formula to obtain the *MtI* copy number relatively quantified to that of a single copy of the reference gene. However, since somatic mouse nDNA contains two copies of the *Actb* gene, the final *MtI* copy number was calculated by multiplying the answer by two (Elder *et al.*, 1988).

The qPCR method employed in this study was similar to that previously described by Meissner-Roloff (2009) for RMCN determination, while samples were prepared in line with the TaqMan® Gene Expressions Assay Protocol (P/N 4333458). Accordingly, reactions of 20 µL were set up in a MicroAmp® Optical 96-well Reaction Plate (#N8010560, purchased from Life Technologies™, Thermo Fisher Scientific™), in separate and triplicate wells, for both the target gene and reference gene. All reactions were prepared in a DNA-free PCR workstation at 0°C, and each 20 µL volume contained the following: 1x TaqMan® Gene Expression Master Mix (2x; #4369016, purchased from Applied Biosystems, Thermo Fisher Scientific™), either 1x TaqMan® Copy Number Assay (20x) for mouse *MtI* (#4400291, Mm00256362_cn, Applied Biosystems, Thermo Fisher

Scientific™) or 1x TaqMan® Gene Expression Assay (20x)[28] for mouse *Actb* (#4331182, Mm02619580_g1, Applied Biosystems, Thermo Fisher Scientific™), nuclease-free $H_2O$ and a total of 10 ng sample- or 10 ng control DNA (including *TgMTI*$^{+/+}$, *TgMTI*$^{-/-}$ and *TgMTI*$^{+/-}$; mice 13, 67 and 10 in Table 4.3). Reagent contamination was monitored by the use of an NTC, prepared as described above, but containing nuclease-free $H_2O$ instead of DNA. Finally, the plate was sealed with a MicroAmp® Optical Adhesive Cover (#4360954, Life Technologies™, Thermo Fisher Scientific™) after which amplification was performed using the QuantStudio™ 5 Real-Time PCR system (#A28139, Applied Biosystems, Thermo Fisher Scientific™) and QuantStudio™ Design and Analysis Desktop Software (v1.4).

The cycling conditions included an initial hold stage (at 95°C for 10 min) during which the double stranded template DNA was denatured and *Taq* DNA Pol was activated. This was followed by 40 cycles consisting of a DNA denaturation step (at 95°C for 15 s) and combined annealing/extension step (at 60°C for 1 min). During the latter, the primer pair and TaqMan® probe were allowed to anneal to the template DNA. While *Taq* DNA Pol then extended the primers to produce new copies of DNA, its 5' to 3' exonuclease activity would cleave the 5'-fluorescent reporter from the TaqMan® probe. As a result, the reporter would be spatially separated from the probe's 3'-non fluorescent quencher (NFQ), allowing an increase in the fluorescent emission spectra that is proportional to the quantity of amplified DNA (Bio-Rad: Bulletin No. 5279) (Heid *et al.*, 1996). Following amplification, mice with a *TgMTI*$^{-/-}$, *TgMTI*$^{+/-}$, or *TgMTI*$^{+/+}$ genotype exhibited copy numbers of approximately 2 (two inherent *MtI* genes), 58 (two inherent *MtI* genes and 56 *MtI** genes), or 114 (two inherent *MtI* genes and 2x 56 *MtI** genes) respectively.

It should be noted that prior to utilising the $2^{-\Delta CT}$ method, the optimal concentration of input template DNA, the PCR amplification efficiency percentage of each gene, and the relative efficiency of the target and reference qPCR amplification reactions had to be determined. The results, which agree with the advised values, as well as a short description thereof, may be found in Appendix B.

### 4.3.5 QUANTIFYING THE RELATIVE *MtI* mRNA – *Objective 1.6*

#### 4.3.5.1 METHODS

Prior to evaluating the biochemical profile of the eight primary fibroblast cell lines (Section 4.4), it was necessary to characterise the level of MTI in order to verify its overexpression in those cells

[28] The TaqMan® Gene Expression Assay (20x) and TaqMan® Copy Number Assay (20x) used, contains two primers (18 µM each), a 6-FAM™ dye-labelled TaqMan® MGB (minor groove binder) probe (5 µM), and a non-fluorescent quencher (NFQ) in an optimised reaction mix.

homozygous for the transgene. Ideally, MTI expression is studied by quantifying the amount of MTI protein (Dabrio *et al.*, 2002). While enzyme-linked immunosorbent assays (ELISAs) and SDS-PAGE + western blot analyses were evaluated by the author as a first and second option, no method was successful in detecting MTI (results not shown). This was not surprising, since the protein is notorious for having a low detection sensitivity and selectivity (Dabrio *et al.*, 2002; Lindeque, 2007; Lindeque, 2011; Mehus *et al.*, 2014). Moreover, the outcome agreed with past experiments at this institution, using a different ELISA and antibodies (van der Westhuizen, 2017a, personal communication).

As an alternative, then, it was decided to measure the mRNA transcription of the *Mtl* and *Mtl** (hereafter collectively referred to as *Mtl*) genes by using multiplex RT-qPCR. While this technique has a high sensitivity and selectivity, it should be noted that *Mtl*'s mRNA transcripts do not necessarily translate quantitatively into protein since the process may be affected by many factors (Vasconcelos, 2002). Therefore, at best, this method provides only a semi-quantitative measure of MTI protein expression. As the goal of this experiment was to simply confirm overexpression, this technique was considered sufficient.

#### 4.3.5.1.a SAMPLE COLLECTION

Primary fibroblasts from each of the eight mice used in this study (see Table 4.2), as well as from two control mice (see Table 4.5), were collected as described in Section 4.3.4.1.a. The latter included *Ndufs4*$^{+/+}$*:TgMTI*$^{-/-}$ and *Ndufs4*$^{+/+}$*:TgMTI*$^{+/+}$ cells that were either untreated or treated with 12.5 µM $CdCl_2$ (a known *Mtl* inducer) for 24 h prior to trypsinisation (Palmiter *et al.*, 1993).

**Table 4.5: Mice used as controls for *Mtl* mRNA quantification**

| Animal ID | Genotype | Gender | DOB |
|---|---|---|---|
| 79 | *Ndufs4*$^{+/+}$*:TgMTI*$^{-/-}$ | Male | 2016-05-08 |
| 40 | *Ndufs4*$^{+/+}$*:TgMTI*$^{+/+}$ | Female | 2016-03-22 |

The table displays the ear punch identification number (ID), genotype, gender, and date of birth (DOB) of the mice.

#### 4.3.5.1.b ISOLATING & QUANTIFYING RNA FROM CELLS

From each cell pellet, the total RNA was isolated using TRIsure™ (#38032, purchased from Bioline, Inqaba Biotec). To achieve this, the reagent was added to each thawed sample at a concentration of 1 mL per 10 $cm^2$ cell culture vessel growth area and mixed by pipetting[29]. Each suspension was subsequently transferred to two sterile 1.5 mL microcentrifuge tubes and

[29] Since each cell pellet contained cells that covered a ~25 $cm^2$ growth area (a T25 flask), 2.5 mL TRIsure™ was added per sample.

homogenised with 60 strokes of a Teflon® Potter Elvehjem homogeniser. Hereafter, the manufacturer's instructions were followed (Bioline: PI-50260 V4): The cell suspensions were first incubated at RT for 5 min, after which chloroform was added in a ratio of 2:1 chloroform:initial TRIsure™ volume, per tube. Samples were then mixed, incubated at RT for 3 min and centrifuged at 12 000 x *g* and 4°C for 15 min. This allowed the solution to separate into a pale green, lower organic phase, a turbid interphase, and a colourless, upper aqueous phase containing the RNA. Per sample, the latter was carefully transferred from the two microcentrifuge tubes, to a single, clean 1.5 mL microcentrifuge tube. Hereafter, RNA was precipitated with isopropyl alcohol, added in a ratio of 0.5:1 isopropyl alcohol:initial TRIsure™ volume. Samples were then incubated at RT for 10 min, followed by a 10 min centrifugation step at 12 000 x *g* and 4°C. The resulting supernatant was discarded and the RNA pellet was washed with 75% (v/v) ethanol [obtained by diluting absolute ethanol (#E7023, Sigma-Aldrich) in nuclease-free $H_2O$] added in a ratio of 1:1 ethanol:initial TRIsure™ volume. Samples were then vortexed and centrifuged at 7 500 x *g* and 4°C for 5 min. Lastly, the RNA pellet was air-dried and redissolved in 30 µL nuclease-free $H_2O$ by careful pipetting.

The quantity and purity of each total RNA sample was then determined as described in Section 4.3.4.1.b, using the NanoDrop® 1000 Spectrophotometer and Operating Software (v3.8.1).

#### 4.3.5.1.c QUANTIFYING THE RELATIVE *Mtl* mRNA BY MULTIPLEX RT-qPCR

Following this, mRNA transcription of the nuclear *Mtl* (target) gene was quantified relative to that of the nuclear β-2 microglobulin (*B2m*; reference) gene via a multiplex RT-qPCR assay. As before, the $2^{-\Delta CT}$ method was employed to resolve the expression levels (Schmittgen & Livak, 2008). However, since mRNA quantity was being evaluated, the answer of $2^{-\Delta CT}$ was not multiplied by two.

To set up the multiplex RT-qPCR assay, the TaqMan® RNA-to-$C_T$™ 1-*Step* Kit protocol (P/N 4393463) was followed. This involved preparing 20 µL reactions in a MicroAmp® Optical 96-well Reaction Plate, in separate and triplicate wells, for both the target (*Mtl*) and reference (*B2m*) mRNA sequences. All reactions were set up in a DNA-free PCR workstation at 0°C, and each 20 µL volume contained the following: 1x TaqMan® RT Enzyme Mix (40x) and 1x TaqMan® RT-PCR Mix (2x; #4392938, Applied Biosystems, Thermo Fisher Scientific™), either 1x TaqMan® Gene Expression Assay (20x) for mouse *Mtl* mRNA (#4331182, Mm00496660_g1, Applied Biosystems, Thermo Fisher Scientific™) or 1x TaqMan® Gene Expression Assay (20x) for mouse *B2m* mRNA (#4331182, Mm00437762_m1, Applied Biosystems, Thermo Fisher

Scientific™)[30], nuclease-free $H_2O$ and a total of 100 ng[31] sample- or control RNA. Reagent contamination was evaluated and the plate was sealed as before (see Section 4.3.4.1.d.i), after which amplification was performed with the QuantStudio™ 5 Real-Time PCR system and QuantStudio™ Design and Analysis Desktop Software (v1.4).

The cycling protocol included a hold stage (at 48°C for 15 min), during which the target and reference mRNA sequences were converted to complementary DNA (cDNA) by reverse transcriptase. The cDNA templates were then amplified by following the cycling conditions described in Section 4.3.4.1.d.i. The optimal concentration of input template RNA, the PCR amplification efficiency percentage of each gene, and the relative efficiency of the target and reference qPCR amplification reactions may be found in Appendix B. While the results did not agree well with the recommended values, it was still regarded as sufficient for the purpose of this method.

### 4.3.6 EXTRACTING & QUANTIFYING PROTEIN FROM CELLS FOR NDUFS4 & CI PROTEIN ANALYSES

Exon two of the *Ndufs4* gene is responsible for encoding the first 17 amino acids of the protein's structure, as well as the last part of its mitochondrial targeting sequence. As shown by Kruse *et al.* (2008), its excision results in a lack of mature NDUFS4 protein and consequently reduces the quantity and activity of intact CI. While the Ndufs4 mouse is a whole-body KO model, it was still considered good practice to verify these results in the fibroblasts of mice carrying the KO mutation (*Ndufs4*$^{-/-}$). Therefore, the relative quantity of the NDUFS4 protein, as well as the effect of its absence on the structure and activity of intact CI, was evaluated.

#### 4.3.6.1 METHODS

##### 4.3.6.1.a SAMPLE COLLECTION

To assess each genotype, four representative cell lines (WT 1, OVER 1, KO 1, and KO OVER 1 from set one; see Table 4.2) were cultured to passage six and harvested as described in Section 4.3.4.1.a. Each cell pellet was then washed in 1x PBS to remove any residual protein (from left-over medium), transferred to two sterile 1.5 mL microcentrifuge tubes and centrifuged

[30] Each TaqMan® Gene Expression Assay (20x) contains two primers (18 µM each), a 6-FAM™ dye-labeled TaqMan® MGB probe (5 µM), and an NFQ in an optimised reaction mix.

[31] As recommended by the TaqMan® RNA-to-$C_T$™ 1-*Step* Kit, the concentration of input template total RNA, is up to 1 µg.

at 600 x *g* and 4°C for 5 min. After carefully removing the supernatant, the cell pellets were frozen at -20°C until use.

#### 4.3.6.1.b PROTEIN EXTRACTION FROM CELLS

Each cell pellet was subsequently processed by using one of two different protein extraction methods, each specific to the protein or protein complex of interest.

Since NDUFS4 is an organellar, membrane-bound protein (contained within CI, located within the IMM), its extraction required the use of a detergent (Seddon *et al.*, 2004). During trial experiments (not presented in this dissertation), the best results were obtained when using the mild non-ionic detergent, Nonidet P40 (NP-40). Protein isolation for SDS-PAGE + western blot analyses therefore entailed resuspending the thawed pellets in 60 µL cell lysis buffer, consisting of 50 mM Tris (pH 7.5), 100 mM NaCl, 5 mM $MgCl_2$, 0.5% (v/v) NP-40, 1x cOmplete™, Mini, EDTA-free Protease inhibitor Cocktail (#11836170001, Roche, Sigma-Aldrich) and 0.1 mM phenylmethylsulphonyl fluoride (PMSF) prepared in Milli-Q® $H_2O$. Following 20 min incubation at 0°C, cell debris was collected by centrifugation at 13 000 x *g* and 4°C for another 20 min. The supernatant, containing the cytosolic extract, was then transferred to a clean 1.5 mL microcentrifuge tube and kept at 4°C for immediate use (Abcam, 2016).

While a similar argument regarding the use of detergents could be given for the isolation of CI-containing samples, the protein complex was instead isolated by a method used at this institution. This included the preparation of enriched mitochondrial fractions by resuspending thawed pellets in 100 µL buffer consisting of only 1x PBS and 1x cOmplete™, Mini, EDTA-free Protease inhibitor Cocktail. The solution was then homogenised at 0°C with 60 strokes of a Teflon® Potter Elvehjem homogeniser. Hereafter, cell debris was collected by centrifugation at 600 x *g* and 4°C for 10 min. The supernatant was centrifuged at 20 000 x *g* and 4°C for 20 min to produce an enriched mitochondrial pellet. Lastly, each pellet was resuspended in 30 µL of the 1x PBS with 1x cOmplete™, Mini, EDTA-free Protease inhibitor Cocktail and kept at 4°C for immediate use.

#### 4.3.6.1.c QUANTIFYING TOTAL PROTEIN CONTENT BY THE BICINCHONINIC ACID METHOD

To ultimately compare the results of the samples analysed by the SDS-PAGE (or BN-PAGE) + western blot analysis, an equal quantity of protein had to be loaded in every lane of the same gel. Therefore, it was necessary to determine the total protein concentration of each sample, prior to further analysis. To accomplish this, it was decided to use the popular bicinchoninic acid (BCA) method, as first described by Smith *et al.* (1985). This method combines the traditional biuret reaction with the high sensitivity and selectivity of the colorimetric detection of $Cu^{+}$ by the BCA

reagent (Thermo Scientific™: Thermo Scientific Pierce Protein Assay Technical Handbook V.2, P/N 1602063). In the first reaction, $Cu^{2+}$ (from $CuSO_4$) is reduced to $Cu^{+}$ under alkaline conditions, due to its reaction with four to six nearby peptide bonds residing between the amino acids of proteins or peptides (containing at least three amino acids). The reaction is optimal at 37°C and the $Cu^{+}$-formation is directly proportional to the quantity of protein present. During the second reaction, each $Cu^{+}$ reacts with two molecules of BCA, to produce a purple, water-soluble chromogen, which exhibits a strong absorbance at 562 nm (Thermo Scientific™: Thermo Scientific Pierce Protein Assay Technical Handbook V.2, P/N 1602063) (Smith *et al.*, 1985).

The method was performed according to the manufacturer's instructions by preparing duplicate reactions of the following: A bovine serum albumin (BSA, #P0914, Sigma-Aldrich) protein standard series ranging from 0 µg to 20 µg protein, in 4 µg increments, was set up in a 96-well UV microtiter plate. To the same plate, 2 µL of each sample was added per well. Each well used was then topped up to a final volume of 20 µL with Milli-Q® $H_2O$. Hereafter, 200 µL of a 50:1 dilution of BCA (#B9643, Sigma-Aldrich):$CuSO_4 \cdot 5H_2O$ (#C2284, Sigma-Aldrich) was added to each well and the plate was incubated at 37°C for 30 min in a Synergy™ HT Multi-detection microtiter plate reader (BioTek® Instruments, VT, USA). Using the Gen5™ Data Analysis software (v1.11.5), the absorbance was measured at 562 nm and the protein concentration (in µg) was determined via linear regression analysis. The value of each sample or control was then converted to µg/µL by dividing the concentration (as determined by the instrument) by the initial volume of sample added, as shown in Equation 4.1:

$$\frac{\mu g \text{ protein}}{\mu L \text{ volume added}} = \mu g/\mu L \text{ protein} \qquad (4.1)$$

### 4.3.7 QUANTIFYING THE STEADY STATE LEVEL OF NDUFS4 WITH SDS-PAGE + WESTERN BLOT ANALYSIS – *Objective 1.7*

#### 4.3.7.1 METHODS

##### 4.3.7.1.a SDS-PAGE ANALYSIS OF NDUFS4

The cytosolic lysate protein preparations isolated for NDUFS4 detection, were separated by SDS-PAGE analysis, as first described by Laemmli (1970). To this end, samples containing 30 µg of protein, 1x Laemmli sample buffer (4x; #1610747, Bio-Rad)[32] and Milli-Q® $H_2O$ were prepared and boiled for 5 min at 100°C. The β-mercaptoethanol (added at a final concentration of 355 mM; #M-3148, Sigma-Aldrich) and lithium dodecyl sulphate (LDS; an anionic detergent that can be used in the place of SDS) contained in the 1x Laemmli sample buffer allowed the subsequent

[32] 4x Laemmli sample buffer contains 62.5 mM Tris-HCl (pH 6.8), 10% glycerol, 1% LDS, 0.005% bromophenol blue and requires the addition of β-mercaptoethanol.

reduction of protein disulfide bridges and the denaturation of the protein's structure, respectively. To separate the protein, a 1 mm SDS-PAGE gel (consisting of a 4% stacking- and 10% resolving gel; see Appendix C for preparation) and 1x Tris/Glycine/SDS buffer (10x; #1610732, Bio-Rad), were used together with the Mini-PROTEAN® Tetra Cell (#1658004; Bio-Rad). Samples were then added to the relevant wells of the SDS-PAGE gel, at 20 µL volumes. Additionally, 20 µL of a molecular weight marker [containing 9.6% (v/v) Precision Plus Protein™ WesternC™ Blotting Standard (#1610385, Bio-Rad), 1x Laemmli sample buffer and Milli-Q® $H_2O$] was loaded on both sides of the samples and the gel was run at 150 V. As the LDS in the 1x Laemmli sample buffer conferred each protein with a negative charge, proteins were allowed to migrate to the anode, while separating purely by virtue of their molecular mass. The gel was run until the electrophoretic dye front (indicated by bromophenol blue) had reached 1 cm from the bottom of the glass plates.

#### 4.3.7.1.b WESTERN BLOT ANALYSIS OF NDUFS4

Following SDS-PAGE, the separated proteins were electroblotted for 30 min by using the Trans-Blot® Turbo™ Blotting System (#1704155, Bio-Rad). During this semi-dry transfer, a current of up to 1.0 A (and 25 V) was passed at right angles to the gel, causing the separated proteins to electrophorese towards the anode and onto a 0.2 µm polyvinylidene difluoride (PVDF; Trans-Blot® Turbo™ Mini PVDF Transfer Pack, #1704156, Bio-Rad) membrane. The remaining hydrophobic binding sites on the blot were then blocked by incubation in blocking buffer [1x Tris buffered saline (TBS) with 1% (w/v) Casein; #1610782, Bio-Rad] for 1.5 h. During this time, and in all the subsequent steps, the blot was gently agitated on a waving platform shaker at 26 rpm. Additionally, this, and every succeeding, step was followed by washing the blot three times, for 5 min each, in washing buffer [1x TBS (#1706435, Bio-Rad) with 0.001% (v/v) Tween®20 (10%; #1610781, Bio-Rad) in Milli-Q® $H_2O$]. To detect the target protein (NDUFS4) and loading control [voltage dependent anion channel subunit 1 (VDAC1)], the blot was incubated overnight at 4°C, in immunodetection solvent [1x TBS with 1% (w/v) Casein] containing the following primary antibodies in a 1:1 000 dilution: A mouse monoclonal antibody, reactive against mouse NDUFS4 (#ab87399, Abcam, Cambridge, UK), and a rabbit polyclonal antibody, reactive to mouse VDAC1 (#ab15895, Abcam).

On the following day, the blot was incubated for 1.5 h in immunodetection solvent containing secondary antibodies (at a 1:10 000 dilution) directed against the primary antibodies and the molecular weight marker (the molecular weight marker contained an integral Strep-tag® sequence, which enabled its detection with a Strep-tactin® secondary antibody). To avoid possible interaction between the different secondary antibodies, two incubations were performed. The first included a goat polyclonal horse radish peroxidase (HRP)-conjugated antibody, reactive against mouse (#ab97023, Abcam), as well as Precision Protein™ StrepTactin®-HRP Conjugate

(#1610782, Bio-Rad), reactive against the molecular weight marker. The second incubation included the goat polyclonal HRP-conjugated antibody, reactive against rabbit (#ab97051, Abcam). Following a final wash, the gel was incubated in 1x TBS for 5 min to remove the Tween®20, after which it was covered by Clarity™ Western Enhanced Chemiluminescence (ECL) Substrate (#1705060, Bio-Rad). The latter consisted of a 1:1 solution of $H_2O_2$ and luminol/enhancer. During this reaction the HRP enzyme oxidises luminol in the presence of its substrate, $H_2O_2$, to produce light, while the enhancer serves to increase the longevity and intensity of the emission.

Following 1 min of incubation, the blot was photographed using the ChemiDoc™ MP system and Image Lab software (v5.2.1). A Chemi Hi Resolution protocol was set up, and the image was obtained using signal accumulation mode (SAM).

### 4.3.8 QUANTIFYING THE STEADY STATE LEVEL & ACTIVITY OF FULLY ASSEMBLED CI WITH BN-PAGE + WESTERN BLOT & IGA ANALYSES – *Objective 1.8*

#### 4.3.8.1 METHODS

To analyse the stability and activity of fully assembled (i.e. not denatured) CI, enriched mitochondrial fractions were first separated via BN-PAGE. This method, originally described by Schagger and von Jagow (1991), employs non-denaturing conditions to allow the separation of protein complexes while maintaining their native conformations (Wittig *et al.*, 2006). Following protein separation, the gel was cut into three parts (see Figure 4.3) to enable western blot assessment, IGA analysis, and staining with Coomassie brilliant blue (CBB) R-250.

##### 4.3.8.1.a BN-PAGE ANALYSIS OF CI

Duplicate samples consisting of 20 µg of protein, 1x NativePAGE™ Sample Buffer (4x; #BN2003, Life Technologies™, Thermo Fisher Scientific™)[33], 1% (v/v) of the non-ionic detergent *n*-dodecyl-β-D-maltoside (DDM, 10%; #BN2005, Life Technologies™, Thermo Fisher Scientific™) and Milli-Q® $H_2O$ were prepared and incubated at 0°C for 10 min, to allow the preferential solubilisation of membrane proteins. Any remaining cell debris was then collected by centrifugation at 20 000 x *g* and 4°C for 20 min, after which the supernatant was transferred to a clean PCR tube and combined with 0.22% (v/v) of the NativePAGE™ G-250 Sample Additive (5%; #BN2004, Life Technologies™, Thermo Fisher Scientific™). The BN-PAGE system was set up according to the manufacturer's instructions (Life Technologies™: NativePAGE™ Novex® Bis-Tris Gel System,

[33] The 4x NativePAGE™ Sample Buffer contains 50 mM Bis-Tris, 6 N HCl, 50 mM NaCl, 10% (w/v) Glycerol, and 0.001% Ponceau S adjusted to pH 7.2.

P/N 25-0894), using a 1 mm 4% to 16% gradient gel (NativePAGE™ 4-16% Bis-Tris Protein Gel, 1.0 mm, 10-well; #BN1002BOX, Life Technologies™, Thermo Fisher Scientific™), cathode buffer [1x NativePAGE™ Running Buffer (20x; #BN2001, Life Technologies™, Thermo Fisher Scientific™) and 1x NativePAGE™ Cathode Additive (20x; #BN2002, Life Technologies™, Thermo Fisher Scientific™) in Milli-Q® $H_2O$] and anode buffer [1x NativePAGE™ Running Buffer in Milli-Q® $H_2O$]. The latter two buffers were respectively added to the upper and lower buffer chambers of the XCell SureLock™ Mini-Cell system (#EI0001, Life Technologies™, Thermo Fisher Scientific™).

Hereafter, 20 µL volumes of the samples, as well as a molecular weight marker [prepared like the samples, but with 22.4% (v/v) NativeMark™ Unstained Protein Standard (#LC0725, Life Technologies™, Thermo Fisher Scientific™) instead of protein] were added to their respective wells (see Figure 4.3). To promote the even running of the stacking front, the remaining unfilled well was loaded with 20 µL of a blank sample (prepared like the samples, but with Milli-Q® $H_2O$ instead of protein). The gel was then run at 100 V for 10 min to allow samples a smooth exit from the wells. The Coomassie blue G-250 anionic dye, present in the sample additive and cathode buffer, endowed the protein complexes with a net negative charge without denaturing them. This allowed their migration to the anode as they separated according to size. The voltage was then adjusted to 150 V until the electrophoretic dye front had travelled one third of the gel length. To limit the quantity of Coomassie blue G-250 in the gel, the cathode buffer was then replaced with anode buffer, and the gel was allowed to run to completion at 150 V. Since a 4% to 16% gradient gel was used, protein complexes ranging from 15 kDa to 10 000 kDa could be separated and retained as soon as they reached their size-dependent specific pore-size limit (Life Technologies™: NativePAGE™ Novex® Bis-Tris Gel System, P/N 25-0894) (Wittig *et al.*, 2006). Following BN-PAGE the gel was cut into three parts as depicted in Figure 4.3:

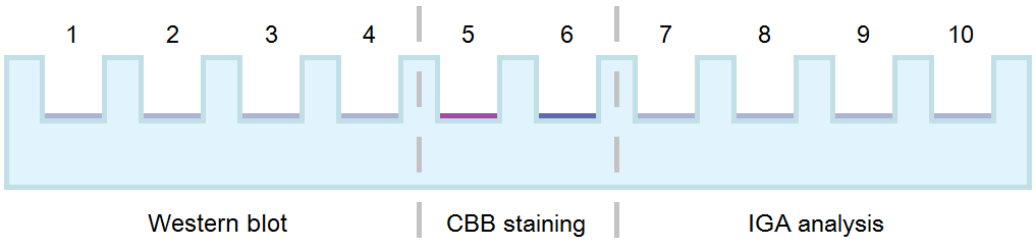


**Figure 4.3: Illustration of the BN-PAGE well layout.** Samples corresponding to WT 1, OVER 1, KO 1, and KO OVER 1 were respectively loaded in lanes 1, 2, 3 and 4, as well as in lanes 7, 8, 9 and 10. The molecular weight marker was added to lane 6, while the blank sample was loaded in lane 5. Dashed lines indicate where the gel was cut.

#### 4.3.8.1.b WESTERN BLOT ANALYSIS OF CI

By adhering to the methods described in Section 4.3.7.1.b, the gel was electroblotted, and the resulting blot was blocked. As before, the blot was washed following this (and every succeeding) step and then incubated overnight at 4°C in immunodetection solvent containing a 1:250 dilution of Total OXPHOS Blue Native Western Blot Antibody Cocktail (#ab110412, Abcam). The mouse monoclonal primary antibodies contained in this cocktail were directed against mouse NDUFA9 (a CI subunit), SDHA (a CII subunit), UQCRC2 (a CIII subunit), COXIV (a CIV subunit), and ATP5A (a CV subunit). For the 1.5 h secondary antibody incubation, immunodetection solvent containing a 1:10 000 dilution of goat polyclonal HRP-conjugated antibody, reactive against mouse, was used. The blot was then washed as before, overlaid with Clarity™ Western ECL Substrate for 1 min, and imaged using the ChemiDoc™ MP system and Image Lab software (v5.2.1). To achieve this, a Chemi Hi Resolution protocol was used, employing SAM to obtain the blot photograph.

#### 4.3.8.1.c IGA ANALYSIS OF CI ACTIVITY

Since OXPHOS complexes separated by BN-PAGE retain their enzymatic activity, it was further possible to use IGA analysis to determine the activity of CI (Schagger & von Jagow, 1991). It should however be noted that IGA measurements are imprecise and therefore only allow a qualitative estimation of the activity (Wittig *et al.*, 2006). While more quantitative results may have been obtained via a spectrophotometric enzymatic assay, IGA analysis was sufficient for the purpose of this study (Pretorius, 2011).

To detect the activity of CI, the method of Nijtmans *et al.* (2002) was followed. Accordingly, the gel was histochemically stained in a CI substrate mixture consisting of 2 mM Tris-HCl (pH 7.4), 0.1 mg/mL NADH (#10107735001, Roche, Sigma-Aldrich), and 2.5 mg/mL nitro-blue tetrazolium (NBT; #24823, Merck, MA, USA) prepared in Milli-Q® $H_2O$. Provided the N module of CI was active and connected to the rest of CI, NADH would then be oxidised to $NAD^+$ and $H^+$ (Sabar *et al.*, 2005). This, in turn, would allow the reduction of NBT by the liberated $H^+$ to produce blue-purple crystals at the position in the gel where CI had migrated. Incubation with the substrate mixture lasted 30 min, after which the gel was photographed using the ChemiDoc™ MP system and Image Lab software (v5.2.1).

#### 4.3.8.1.d COOMASSIE STAINING OF THE PROTEIN LADDER

To visualise the molecular weight marker, the lane containing the ladder was first fixed with fixative solution [25% (v/v) isopropanol and 10% (v/v) acetic acid in Milli-Q® $H_2O$] by gentle agitation at 26 rpm on a waving platform shaker for 20 min at RT. The solution was then replaced

with CBB stain [10% (v/v) acetic acid and 0.006% (w/v) CBB R-250 (#12553, Merck) in Milli-Q® $H_2O$] and incubated as before, for 1 h. Hereafter, the stain was discarded and the gel was destained for 2 h with 10% (v/v) acetic acid in Milli-Q® $H_2O$ (replacing the destaining solution every hour). Finally, the ladder was photographed using the ChemiDoc™ MP system and Image Lab software (v5.2.1).

## 4.4 PART 2: INVESTIGATING THE EFFECT OF MTI OVEREXPRESSION ON THE BIOENERGETICS CONSEQUENCES OF CI DEFICIENCY

Fibroblasts are known to exhibit an inherently glycolytic metabolism (van den Heuvel *et al.*, 2004). In addition, most cells cultured *in vitro* tend to favour glycolysis over OXPHOS to realise their ATP requirements (i.e. the Crabtree effect) (Mot *et al.*, 2016; Rodriguez-Enriquez *et al.*, 2001). This contradicts the general behaviour *in vivo* and has been observed even when culture medium with a low glucose concentration (~5 mM) is employed. To overcome this limitation and allow the more pronounced expression of OXPHOS defects *in vitro*, cells may instead be cultured in galactose-containing medium (Valsecchi *et al.*, 2012; van den Heuvel *et al.*, 2004). However, since these conditions are usually too harsh for standard culturing, van den Heuvel *et al.* (2004) suggest using glucose-containing medium for routine culturing, and switching to galactose-containing medium one to two days prior to experimental evaluation.

Thus, the eight primary fibroblast cell lines (see Table 4.2) were restarted and cultured to passage four, using glucose-containing medium, as described in Section 4.3.3.1.c. Depending on the assay, the complete growth medium was then replaced with galactose-containing medium one or two days before analysis. Galactose-containing medium consisted of 1 mM sodium pyruvate (100x; #11360039, Gibco®, Thermo Fisher Scientific™), 1% (v/v) P/S, 20% (v/v) FBS, 10 mM galactose (pH 7.4; #G0750, Sigma-Aldrich) and 44 mM sodium bicarbonate (pH 7.4) prepared in the same low buffered medium stock used for the Seahorse XF analyses[34]. *To avoid microtiter plate-related differences, all eight cell lines were seeded and analysed on a single microtiter plate for each of the following analyses.*

### 4.4.1 DETERMINING CELL VIABILITY WITH THE MTT ASSAY – *Objective 2.1*

#### 4.4.1.1 METHODS

To determine how cell survival was influenced by the genotype, the viability of each cell culture was measured and compared to that of the WT cell line. This was accomplished by performing the quantitative, colorimetric 3-(4,5-dimethylthiazolyl-2)-2,5-diphenyltetrazolium bromide (MTT)

[34] The content of the low buffered medium stock may be found in Section 4.4.6.3.a.

assay, originally described by Mosmann (1983), which distinguishes between living and dead cells by utilising the degree of MTT reduction.

#### 4.4.1.1.a SEEDING CELLS

In preparation for the assay, each cell culture was harvested by trypsinisation, as explained in Section 4.3.3.1.c, and resuspended in galactose-containing medium. Hereafter, 100 µL of the cell suspension was added to 900 µL of 1x PBS, and the cells were counted using the Scepter 2.0 Handheld Automated Cell Counter (with 60 µm sensors; #PHCC20060, purchased from Millipore™, Merck). The amount of cells/µL was then calculated and the appropriate volumes of cell suspension and galactose-containing medium were added together to obtain a final seeding density of 12 500 cells/100 µL/well (the cell density was chosen to be similar to that employed in Section 4.4.6). Each cell line was then seeded in eight wells of a 96-well microtiter plate, as indicated in Appendix D. Additionally, eight wells of a negative control (prepared using cells from WT 1), as well as eight wells containing only galactose-containing medium (blank, no cells, used for background correction), were seeded. To promote even cell distribution and reduce edge effects, the cells were left to adhere to the microtiter plate in the laminar flow hood for 1 h, after which the plate was incubated under standard conditions for 24 h.

#### 4.4.1.1.b MTT ASSAY

On the following day, 30 min before the end of the initial incubation period, the medium in the negative control wells was replaced by 100 µL of galactose-containing medium containing 6% (v/v) acetic acid. The plate was then incubated for 30 min, ensuring cell death in these wells. To limit cell loss by pipetting, the microtiter plate was subsequently centrifuged at 1 000 x *g* for 5 min. Hereafter, each well was washed by carefully replacing the medium with 200 µL 1x PBS/well and the plate was centrifuged again. The PBS was then replaced by 100 µL of a 1:10 dilution of 5 mg/mL MTT (prepared in 1x PBS):galactose-containing medium, after which the microtiter plate was incubated for 5 h, under standard conditions.

During this time, the yellow tetrazolium salt, MTT, is taken up via endocytosis (Liu *et al.*, 1997). Inside the cells, its tetrazolium ring is cleaved to yield an amount of reduced, blue-purple formazan product, directly proportional to the number of living cells (Mosmann, 1983). While this reaction is thought to be primarily mediated by extramitochondrial NAD(P)H-dependent oxidoreductases, rotenone-independent mitochondrial RC involvement has also been demonstrated (Berridge & Tan, 1993). Upon production, the insoluble formazan crystals then accumulate as intracellular granules in perinuclear (either endosomal or lysosomal) compartments (formazan crystals may

also be transferred to the cell's surface by exocytosis following prolonged periods) (Liu *et al.*, 1997).

After incubation, the plate was centrifuged and the solution was removed. To each well, 100 µL of DMSO was added to lyse the cells and solubilise the formazan crystals. The plate was then mixed by tapping for 1 min and the absorbance was measured at a wavelength of 560 nm (and a reference wavelength of 630 nm) using the Synergy™ HT Multi-detection microtiter plate reader and Gen5™ Data Analysis software (v1.11.5).

### 4.4.2 DETERMINING THE RMCN BY qPCR ANALYSIS – *Objective 2.2*

#### 4.4.2.1 METHODS

To determine the effect of the genetic modifications on mtDNA replication (as indicator of mitochondrial biogenesis), the RMCN was assessed. In preparation hereof, cell pellets from each primary fibroblast culture (switched to galactose-containing medium three to eight days prior) were collected, stored and used for DNA isolation, via the methods in Sections 4.3.4.1.a and 4.3.4.1.b. The pure DNA of each sample, as well as that of an mtDNA-depleted control [rho0 ($\rho^0$) cells generated from a human osteosarcoma cell line (143B)], were then quantified as before. Hereafter, the mitochondrial *Nd2* (*mt-Nd2*; target) gene was relatively quantified to the nuclear *Actb* (reference) gene, using a qPCR method similar to that in Section 4.3.4.1.d. Finally, the $2^{-\Delta CT}$ method was used to determine the RMCN. As somatic mouse nDNA contains two copies of the *Actb* gene in comparison to the single copy of *mt-Nd2*, the answer was multiplied by two to obtain the final RMCN.

For each cell line, for the $\rho^0$ control and for an NTC, triplicate and separate reactions of 20 µL were set up exactly as described in Section 4.3.4.1.d. The 1x TaqMan® Gene Expression Assays (20x) used for the target and reference genes, respectively included those directed against mouse *mt-Nd2* (#4331182, Mm04225288_s1, Applied Biosystems, Thermo Fisher Scientific™) and mouse nuclear *Actb*[35]. As before, amplification was performed using the QuantStudio™ 5 Real-Time PCR system and QuantStudio™ Design and Analysis Desktop Software (v1.4). The cycling conditions included those mentioned in Section 4.3.4.1.d.

To determine whether the $2^{-\Delta CT}$ method could be used, the optimal concentration of input template DNA, the PCR amplification efficiency percentage of each gene, and the relative efficiency of the target and reference qPCR amplification reactions were determined (see Appendix B for results).

[35] Each TaqMan® Gene Expression Assay (20x) contains two primers (18 µM each), a 6-FAM™ dye-labelled TaqMan® MGB probe (5 µM), and an NFQ in an optimised reaction mix.

While the results obtained for the PCR efficiency and relative efficiency differed slightly from those advised, they were still regarded as applicable for the purpose of this method.

### 4.4.3 QUANTIFYING THE RELATIVE NADH/NAD$^+$ RATIO – *Objective 2.3*

#### 4.4.3.1 METHODS

To determine the cellular redox status of each cell line, the total NADH/NAD$^+$ ratio was measured using the bioluminescent NAD/NADH-Glo™ Assay (#G9061, Promega, WI, USA). In accordance with the assay's specifications, the optimal seeding density and final incubation time were determined as 17 500 cells/well and 45 min (not shown)[36].

##### 4.4.3.1.a SEEDING CELLS

Prior to analysis, cells were harvested, counted, and seeded in triplicate wells (at 17 500 cells/100 µL/well) according to the method described in Section 4.4.1.1.a (see Appendix D for the plate layout). In addition, three wells comprising only galactose-containing medium (blank, no cells, used for background correction) were set up. To maximize the light output signal and reduce the inter-well crosstalk, a white-walled, clear-bottom 96-well microtiter plate was used for seeding.

##### 4.4.3.1.b NAD/NADH-GLO™ ASSAY

The experimental protocol followed was in accordance with the instructions provided by the supplier (Promega: NAD/NADH-Glo™ Assay, TM399). After an initial incubation period of 26 h, 50 µL of a positive control, containing 400 nM NAD$^+$ (#N7004, Sigma-Aldrich) in 1x PBS, was set up in triplicate on the microtiter plate (triplicate values were chosen due to reagent restrictions). The galactose-containing medium of the sample- and blank wells was then replaced by 50 µL of 1x PBS. To ensure cell lysis while preserving the stability of the dinucleotides, 50 µL of a base solution [0.2 N NaOH with 1% (w/v) dodecyltrimethylammonium bromide (DTAB; #D8638, Sigma-Aldrich)] was added to each well (samples, blanks and positive controls) and gently mixed by tapping for 1 min. Since NAD$^+$ and NADH have differential stabilities in heated solutions of acidic and basic pH, this offered a means to separately measure the NAD$^+$ and NADH

[36] Optimisation included cell seeding densities ranging of 7 500 cells/well to 22 500 cells/well, and incubation periods ranging from 30 min to 70 min. Due to limited reagents, one replicate per well was analysed per cell seeding density. The optimal incubation time was chosen based on the linearity of the relative light unit (RLU) against cell seeding density curve generated (i.e. the most linear curve), while optimal seeding density was taken as the most linear position on the aforementioned curve.

levels of every well. To achieve this, 50 µL of each well volume was transferred to an empty well on the same plate (see Appendix D). These volumes were then treated with 25 µL of an acid solution (0.4 N HCl). Hereafter, the plate was covered, sealed with parafilm and carefully heated for 15 min at 60°C in a water bath. This permitted the selective destruction of $NAD^+$ in the original basic wells, and NADH in the new acidic wells. Following equilibration to RT for 10 min, the base and acid solutions were respectively neutralised by the addition of either 50 µL of HCl/Tris (consisting of 0.4 N HCl and 0.5 M Tris in a 1:1 ratio), or 25 µL of 0.5 M Tris. Ultimately, each neutralised well contained $NAD^+$ or NADH in the same final buffer formulation, thereby allowing the direct comparison of these molecules.

Hereafter, the NAD/NADH-Glo™ Detection Reagent was added to each well in a 1:1 ratio. The solution was then mixed by tapping for 1 min and the plate was incubated at RT for a final period of 45 min. During this time, $NAD^+$ is converted to NADH by the NAD Cycling Enzyme. In the presence of NADH, the Reductase Enzyme is then able to reduce its proluciferin Reductase Substrate to form luciferin. The latter was consequently quantified by its light-producing reaction with the Ultra-Glo™ Recombinant Luciferase component of the Luciferin Detection Reagent (the luciferase reaction is described in Section 4.4.4). Following incubation, luminescence was measured using the Synergy™ HT Multi-detection microtiter plate reader (with an integration time of 1 s) and Gen5™ Data Analysis software (v1.11.5). The relative light units (RLUs) obtained from the base-treated and acid-treated wells were thus respectively proportional to the amount of total cellular NADH or $NAD^+$, while the NADH/$NAD^+$ ratio could be determined by dividing the former by the latter. Since a ratio was calculated, there was no need for further normalisation.

### 4.4.4 QUANTIFYING THE RELATIVE ATP/ADP RATIO – *Objective 2.4*

#### 4.4.4.1 METHODS

The cellular energy status of each genotype was evaluated by measuring the ATP/ADP ratio using the ADP/ATP Assay Kit (#MAK135, Sigma-Aldrich). While the recommended seeding density was $10^3$ to $10^4$ cells per well, it was decided to use the same seeding density as in Section 4.4.3 (i.e. 17 500 cells/100 µL/well), since the latter fell within the linear range of the assay.

#### 4.4.4.1.a SEEDING CELLS

On the day before the analysis, each cell line was harvested (from the same flasks used for the NAD/NADH-Glo™ assay), counted, and seeded in triplicate wells, as described in Section 4.4.1.1.a (see Appendix D for the plate layout). In addition, three wells containing only galactose-containing medium (blank, no cells, used for background correction) were prepared. For the

reasons mentioned in Section 4.4.3.1.a, cells were seeded in a white-walled, clear-bottom 96-well microtiter plate.

#### 4.4.4.1.b ADP/ATP RATIO ASSAY

The experiment was performed according to the manufacturer's instructions. After 25 h[37] of incubation under standard conditions, 10 µL of a positive control, consisting of 500 nM ATP (#A2383, Sigma-Aldrich) in 1x PBS, was added to three wells of the microtiter plate. This was followed by removing the galactose-containing medium from the samples and blank wells and adding 90 µL of ATP reagent to each well (samples, blanks and positive controls). The solution was then mixed by tapping and the plate was incubated at RT for 1 min (Table 4.6 shows the composition of the two reagents used).

**Table 4.6: Composition of the ATP- and ADP reagents required for one reaction**

| ATP Reagent | |
|---|---|
| **Constituents** | **Volume per reaction (µL)** |
| Assay Buffer | 95 |
| Substrate | 1 |
| Co-substrate | 1 |
| ATP Enzyme | 1 |
| **ADP Reagent** | |
| **Constituents** | **Volume per reaction (µL)** |
| $H_2O$ | 5 |
| ADP Enzyme | 1 |

The table displays the volumes of each component of the ATP- and ADP reagents for one reaction.

During this time, the cells are lysed and the total cellular ATP is liberated. In the presence of ATP, $O_2$ and $Mg^{2+}$, luciferase converts its substrate luciferin to the energetically excited oxyluciferin (additional products included AMP, inorganic pyrophosphate, and $CO_2$) (DeLuca & McElroy, 1978). The light signal produced from oxyluciferin's subsequent decay was then measured using the Synergy™ HT Multi-detection microtiter plate reader and Gen5™ Data Analysis software (v1.11.5). This signal ($RLU_A$) was therefore directly proportional to the quantity of cellular ATP.

Following a 10 min incubation at RT, the luminescence of the residual ATP signal ($RLU_B$) was determined as background for the final ADP measurement. 5 µL of the ADP reagent was then added to each well, mixed as before and incubated at RT for 1 min. During this step, ADP was converted to ATP to react with luciferase as mentioned above. To determine the total ADP

[37] The difference in incubation time between Section 4.4.3 (26 h) and Section 4.4.4 (25 h) was due to the fact that the two experiments were performed on cells seeded at the same time.

concentration of each well, the luminescence produced as a result of the converted ADP, was measured one last time ($RLU_C$). Finally, Equation 4.2 was used to obtain the ATP/ADP ratio. Since a ratio was calculated, no normalisation was required.

$$\text{ATP/ADP ratio} = \text{RLU}_\text{A} / (\text{RLU}_\text{C} - \text{RLU}_\text{B}) \quad (4.2)$$

### 4.4.5 DETERMINING ROS LEVELS USING THE BD FACSVerse™ FLOW CYTOMETER – *Objective 2.5*

In order to quantitatively evaluate the intracellular oxidative status of each cell line, the ROS levels were assessed by flow cytometry, following sample treatment with the fluorescent probe, 6-carboxy-2',7'-dichlorodihydrofluorescein diacetate di(acetoxymethyl ester) (hereafter referred to as C-DCFH-DA-AM; #C2938, purchased from Molecular Probes®, Thermo Fisher Scientific™). A brief description of the techniques used is given, followed by the specific methodology pertaining to each.

#### 4.4.5.1 FLUORESCENCE-BASED QUANTIFICATION OF ROS USING FLOW CYTOMETRY

Due to its extremely short half-life, the measurement of ROS has always been considered problematic (du Plessis *et al.*, 2010). A method that has gained increasing popularity since its development in 1983, is the use of the cell permeable probe, 2',7'-dichlorodihydrofluorescein diacetate (DCFH-DA) (Bass *et al.*, 1983). Upon entering the cell, the non-fluorescent probe is quickly deacetylated by esterases to yield the relatively polar, cell impermeable product, 2',7'-dichlorodihydrofluoroscein (DCFH). This non-fluorescent molecule, which accumulates intracellularly and can remain stable for a few hours, is then subsequently oxidised by ROS to produce the highly fluorescent 2',7'-dichlorofluorescein (DCF). Although DCFH-DA is commonly used to measure intracellular $H_2O_2$, it may perhaps be more accurately described as a generalised oxidative stress assay, since (i) DCFH can only react with peroxides following their decomposition to radicals, and (ii) DCFH can also be oxidised by nitric oxide and $O_2^{\bullet -}$ (Eruslanov & Kusmartsev, 2010). Therefore, following excitation at 488 nm, DCF's emission of green fluorescence is proportional to the degree of intracellular ROS, instead of intracellular $H_2O_2$. Moreover, since the DCF product is membrane permeable, analogues have been developed to increase its cellular retention (Eruslanov & Kusmartsev, 2010). An example is the probe used in this analysis, C-DCFH-DA-AM. Following its cleavage and oxidation, the final fluorescent product (carboxydichlorofluorescein) will have two additional negative charges at physiological pH, thereby preventing its leakage.

The DCFH-DA assay may further be combined with flow cytometry to determine quantitative data on the number of cells producing intracellular ROS (du Plessis *et al.*, 2010). Briefly stated, flow cytometry is an analytical technique that utilises light to identify, count, and characterise single cells (or other particles, e.g. nuclei, etc.) in a heterogeneous population. This technique is capable of yielding information on the physical properties of cells (or other particles), including their size and complexity (Ibrahim & van den Engh, 2007). Additionally, by using different lasers and filters, the instrument can provide the user with chemical or physiological information concerning the analysed sample, based on the fluorescence emission spectra exhibited by the population. The technique has been successfully used to quantify cellular ROS in diverse cell types of different disease states and offers many advantages, including superior accuracy and speed (du Plessis *et al.*, 2010). Of importance is the fact that flow cytometry can quantitatively determine the characteristics of a specific subpopulation of cells, as opposed to merely assessing the mean of the total population. Since primary cell cultures often exhibit slight morphological differences, this was beneficial to the study. While the process used to obtain single cells in suspension (e.g. trypsinisation) may theoretically contribute to oxidative stress and potentially interfere with the analysis, it should be mentioned that these effects are limited by optimising the system via the use of controls (Eruslanov & Kusmartsev, 2010).

#### 4.4.5.2 METHODS

##### 4.4.5.2.a SAMPLE PREPARATION

Two days prior to the analysis (at times corresponding to the assay of each sample), the complete growth medium was removed from each culture, and cells were rinsed with 8 mL 1x PBS. To each T25 flask, a volume of 5 mL galactose-containing medium was then added and cells were incubated under standard conditions. To ensure the complete elimination of residual medium glucose (contained in the routine culture medium), a 48 h incubation period was chosen. Since the fibroblasts of WT 1 (see Table 4.2) would be used as controls, two flasks of this cell line were cultured.

On the day of the analysis, each culture (at ± 90% confluency) was trypsinised, followed by the addition of galactose-containing medium, and the cell pellets were collected by centrifugation at 600 x *g* and 20°C for 5 min. The supernatant was then discarded and each cell line was resuspended in 5 mL 1x PBS. At this point, the fibroblasts of WT 1 were pooled and each cell line was pelleted again. Hereafter, samples were resuspended in 1x PBS.

A cell control and positive control, as well as triplicate samples of each cell line were then prepared in a final volume of 500 µL 1x PBS in FACS (fluorescence-activated cell sorting) tubes (#352052, Becton Dickinson, CA, USA). Whereas the cell control consisted of only cells, the positive control was additionally pre-incubated with 4 mM $H_2O_2$ (#H-1009, Sigma-Aldrich) for 1 h at RT. The

positive control and samples were then treated with 10 µM C-DCFH-DA-AM (reconstituted in DMSO) for 30 min at RT, protected from light. It should be noted that the triplicate stained samples of WT 1 were used as negative controls.

#### 4.4.5.2.b ANALYSING THE ROS LEVELS USING THE BD FACSVERSE™ FLOW CYTOMETER

Hereafter, the cells were analysed by Prof Lissinda du Plessis from the Pharmaceutics Department of the NWU (Potchefstroom Campus), by using a bench top flow cytometer (BD FACSVerse™, Becton Dickinson) equipped with blue (488 nm) and red (640 nm) lasers. The method followed was essentially as described by Wentzel *et al.* (2017), with some assay-specific differences. To identify rare events, cells were assessed using the high sensitivity mode (with a flow rate of 0 µL/min to 55 µL/min) of the BD FACSuite™ Software (v1). Prior to sample analysis, the instrument was calibrated with BD FACSuite™ CS&T research beads (#650622, Becton Dickinson) as advised by the manufacturer. Detection was then optimised by using the cell-, positive- and negative controls, after which each sample was analysed in triplicate.

A total of 100 000 events were counted per control or sample, during which signal amplification data was collected at a logarithmic scale for forward scatter (FSC), side scatter (SSC) and green fluorescence (FITC) events. The data was subsequently analysed by using the FCS Express™ Flow Research software (2017 edition; De Novo Software, CA, USA) to produce dot blots (SSC against FSC, FSC against FITC and SSC against FITC) and histograms (cell count against FITC). As shown in Figure 4.4.a, the cell control was used to set a specific user-defined threshold (called a *gate)* in order to exclude debris and identify the cell population of interest. This gated region was applied to all samples and used for the analysis of all subsequent dot plots and histograms. To analyse the fluorescent properties of the cells, dot blots of FSC against FITC (Figure 4.4.b) were employed, whereas cell count against FITC histograms (Figure 4.4.c) were used to calculate the geometric mean (defined as the $n^{th}$ root of the product of n numbers) fluorescence intensity (gMFI) of each analysed sample or control, according to Equation 4.3:

$$\left(\prod_{i=1}^{n} x_i\right)^{\frac{1}{n}} = \sqrt[n]{x_1 \cdot x_2 \cdots x_n} \qquad (4.3)$$

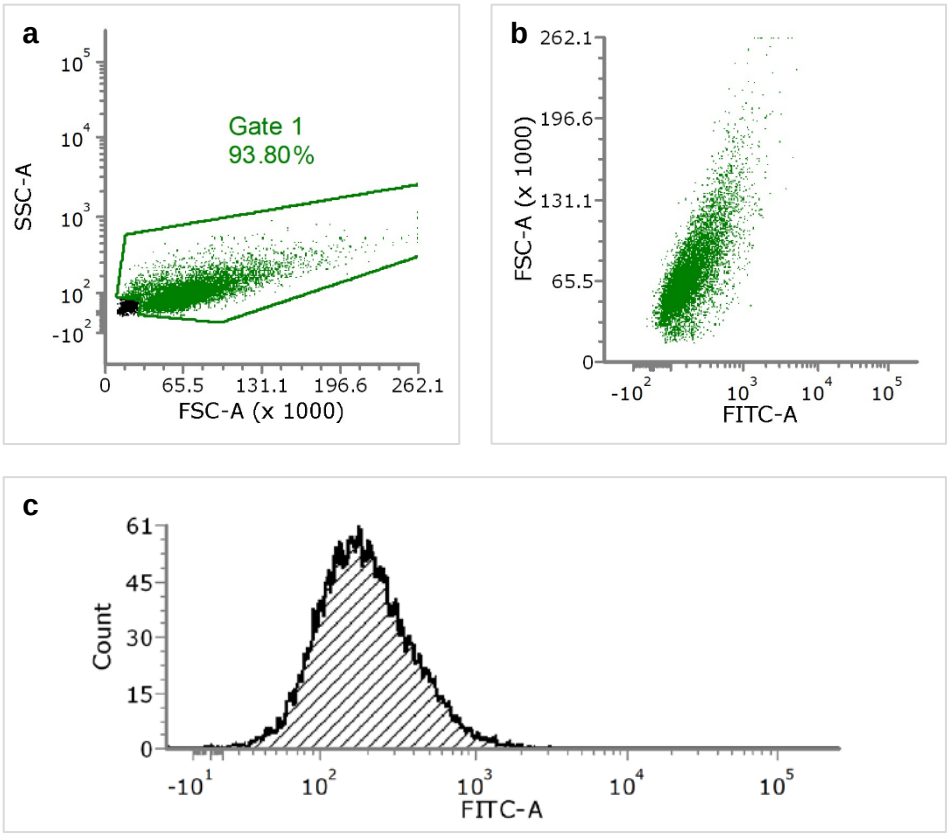


**Figure 4.4: Flow cytometric dot plots and histogram depicting the gating method employed for this study.** Data was collected for 100 000 events and plotted as described above. As an example, the graphs obtained for the cell control are shown. **(a)** Dot plot of SSC against FSC depicting the set gate (in green) used to identify the cell population of interest and exclude cell debris. **(b)** Dot plot of FSC against FITC illustrating only the events gated in a. **(c)** Histogram of cell count against FITC depicting the data used to calculate the gMFI.

### 4.4.6 DETERMINING THE BIOENERGETICS PROFILE USING THE SEAHORSE XF$^e$96 ANALYSER – *Objective 2.6*

To assess the bioenergetics profile of each cell line, the Seahorse XF$^e$96 Analyser (Seahorse Bioscience, MA, USA) was used. In this Section, the general operation of the XF Analyser is given. This is followed by a description of the parameters calculated in this study, as well as the experimental methods employed to evaluate the mitochondrial respiration (Mito Stress Test).

#### 4.4.6.1 OPERATION OF THE EXTRACELLULAR FLUX ANALYSER

The XF Analyser (or Seahorse XF Analyser) is a bioenergetics platform, allowing the simultaneous evaluation of mitochondrial respiration and glycolysis (the two primary energy-yielding pathways of the cell) of cells or organelles in real-time (Brand & Nicholls, 2011; Zhang *et al.*, 2012). Under aerobic conditions, the cell consumes energy-substrates, as well as $O_2$, to

produce ATP via mitochondrial OXPHOS (Section 2.2.2). By contrast, ATP is produced by substrate-level phosphorylation during glycolysis, when glucose is converted to pyruvate. If the downstream processing of the latter is however obstructed, or $O_2$ is absent, pyruvate will be shunted to lactate with the concomitant release of $NAD^+$ and $H^+$. The XF Analyser can determine mitochondrial respiration and glycolysis, by respectively measuring the rate at which $O_2$ is taken up from- (the *oxygen consumption rate*; OCR), and $H^+$ is expelled to (the *extracellular acidification rate*; ECAR), the surrounding medium. Together, the OCR and ECAR are known as the *extracellular flux (XF)* (Agilent, 2017).

Each analysis is performed by using a 24- or 96-well cell culture plate (depending on the instrument) and a sensor cartridge, the latter of which is composed of one probe surrounded by four injection ports for each well (Agilent, 2017). Embedded in polymer, at the base of each probe, are two fluorophores. While the first is quenched by $O_2$ to determine the OCR, the second is responsive to $H^+$, enabling it to measure the ECAR. During each measurement, fibre optic bundles of the instrument are simultaneously lowered into each probe to emit light. This excites the fluorophores, which in turn read back their own light emission signals relative to the change in medium-$O_2$ and -$H^+$ content. To achieve these measurements, the sensor cartridge is lowered 200 µm above the sample in each well to create a transient micro chamber (2 µL in the 96-well format) with limited diffusion (Agilent, 2017; Brand & Nicholls, 2011). For this reason, accurate data can only be obtained by seeding samples in uniform monolayers (Zhang *et al.*, 2012). While monolayer formation is spontaneous for adherent cells, isolated mitochondria (or other organelles) and cells grown in suspension require centrifugation or treatment with specialised chemicals (e.g. Cell-Tak™) (Agilent, 2017; Zhang *et al.*, 2012).

The XF Analyser allows different aspects of cellular bioenergetics to be assessed by loading up to four compounds in the drug injection ports surrounding the probe (Agilent, 2017). Here, they are held by capillary action until their pneumatic injection, at time points specified by the user during the analysis. These components are then mixed into the medium of each well by raising and lowering the sensor cartridge, and kinetic measurements are made as described above. Following each measurement, the sensor cartridge is raised again to allow the re-equilibration of the medium (to prevent the medium from becoming anoxic or too acidic) and the process is repeated (Agilent, 2017). To perform a Mito Stress Test, specific modulators of the relevant metabolic pathway are loaded into the drug injection ports. The serial injection of these compounds subsequently permits the user to observe specific parameters of OXPHOS under stressed conditions as shown in Figure 4.5.

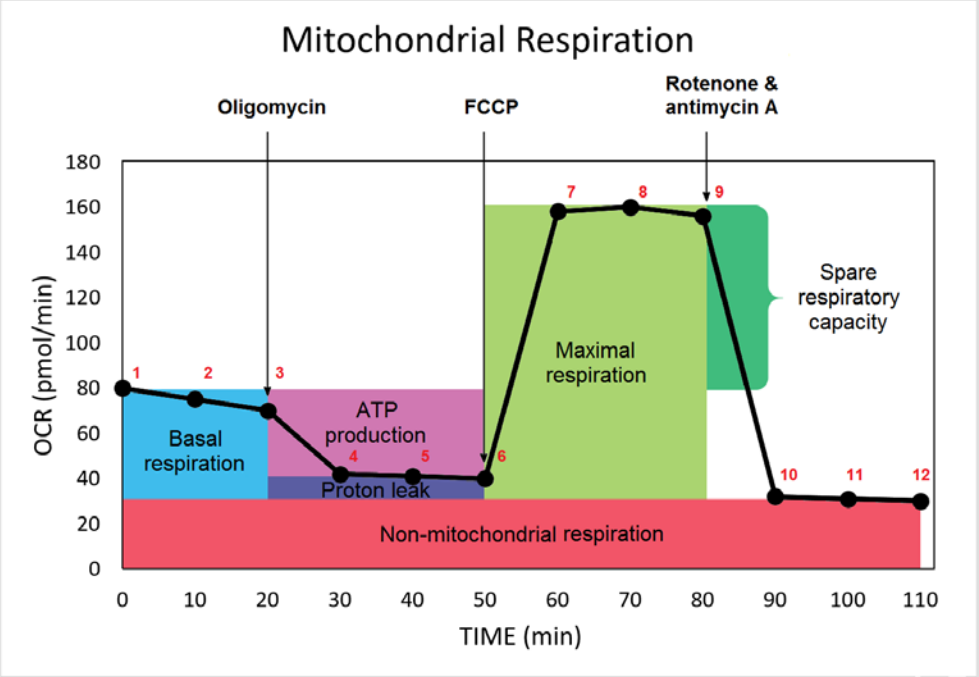


**Figure 4.5: Mito Stress Test profile.** The change in OCR following the injection of oligomycin, FCCP, and rotenone and antimycin A is depicted. Measured parameters (basal respiration, ATP production, proton leak, maximal respiration, spare respiratory capacity, and non-mitochondrial respiration) are also shown. The annotations, 1 to 12, represent default measurement intervals during the analysis. Based on a figure by Agilent (2017).

In a typical Mito Stress Test, the Analyser begins by measuring the basal respiration (Brand & Nicholls, 2011). Oligomycin is then injected. As this compound binds to and blocks the proton channel of the $F_0$ portion of CV, CV-mediated proton re-entry and -ATP synthesis are precluded. This decreases the OCR, with residual values attributable to the inherent proton leak and non-mitochondrial respiration. Next, carbonyl cyanide-4-(trifluoromethoxy) phenylhydrazone (FCCP) is injected. This protonophore consequently uncouples mitochondrial respiration by transporting $H^+$ across the IMM, as opposed to through CV (Brand & Nicholls, 2011). The result is a collapsed $\Delta\psi$ and a consequent increase in OCR and energy consumption. Additionally, ECAR increases as metabolism shifts to glycolysis in an attempt to uphold the cell's energy balance. Finally, all remaining mitochondrial respiration is eradicated by the simultaneous injection of rotenone and antimycin A. While the first functions as a CI inhibitor[38] by obstructing electron transfer from CI's Fe-S clusters to Q, the second inhibits CIII and thus the formation of a proton gradient. Any residual OCR is therefore solely due to non-mitochondrial respiration, whereas ECAR increases for the aforementioned reason.

[38] Rotenone binds to the NDUFS2 subunit, located in the Q module, and should therefore not be influenced by a lack of NDUFS4 (Mimaki *et al.*, 2012; Pineau *et al.*, 2005; Prieur *et al.*, 2001).

#### 4.4.6.2 DESCRIPTION OF THE PARAMETERS EVALUATED

While much information is obtainable from a Mito Stress Test (as indicated in Figure 4.5), only the basal respiration, ATP production, and maximal respiration were evaluated. The reason for this was that previous studies at this institution had demonstrated that those parameters obtained from very small values (falling below the level of sensitivity of the instrument; i.e. proton leak and non-mitochondrial respiration), as well as those parameters calculated from more than one other parameter or the ratios of parameters [i.e. spare respiratory capacity, % spare respiratory capacity, % coupling efficiency, and bioenergetics health index], displayed poor repeatability (van Dyk, 2016). As previously determined by van Dyk (2016), the three parameters reported in this dissertation (as discussed in Chapter 6) were considered to be consistent with regards to the instrument.

The first, *basal respiration*, may be regarded as the cell's baseline oxygen consumption prior to the injection of OXPHOS-altering compounds. It is primarily controlled by the cell's ATP demand, and partially by the endogenous proton leak and substrate supply (Brand & Nicholls, 2011). Additionally, basal respiration is sensitive to the substrates and hormones contained in the incubation medium.

Following the addition of oligomycin, CV is inhibited and electron flux through the RC decreases due to an increase in $\Delta\psi$. The rate of *ATP production* via CV may be determined from this decrease (Brand & Nicholls, 2011). While increased ATP production implies a higher energy demand, decreased ATP production may result from a reduced energy demand, insufficient substrate, or a severely damaged OXPHOS system. Therefore, the parameter will also be negatively influenced by increased oxidative stress (van Dyk, 2016).

*Maximal respiration* is obtained after the injection of the uncoupler, FCCP. Since CV is already inhibited at this point, and saturating levels of ADP are unachievable in experiments involving intact cells (due to the inability of ADP and $P_i$ to cross the plasma membrane), the maximal respiration described here refers to RC (and not OXPHOS) capacity (Brand & Nicholls, 2011; van Dyk, 2016). Apart from the rate of substrate absorption and catabolism, this parameter is limited by the activity of the RC. Consequently, a decrease in maximal respiration can indicate an inadequate substrate supply, or OXPHOS impairment.

Most cells further exhibit a low percentage (~10%) of *non-mitochondrial oxidative respiration* brought about by the activity of certain detoxification-, desaturase-, and pro-inflammatory enzymes (Brand & Nicholls, 2011; van Dyk, 2016). While this rate has been shown to differ in the presence of stressors (e.g. increasing due to ROS), it is primarily used in the calculation of other parameters.

#### 4.4.6.3 METHODS

##### 4.4.6.3.a DETERMINING THE BIOENERGETICS PROFILE USING A MITO STRESS TEST

Prior to its utilisation, the XF Analyser necessitates the optimisation of each new cell type (Zhang *et al.*, 2012). Critical considerations include cell seeding density and the FCCP concentration used. The optimisation of these parameters may be found in Appendix E.

The final XF analysis required three days to execute. To perform the Mito Stress Test, the protocol described below was followed. The methods and reagents used were as advised by the supplier.

DAY 1

Each cell line was harvested, counted, and seeded in 11 or 12 wells (depending on the background wells) of a Seahorse XF96 Cell Culture Microtiter plate (#101085-004, Agilent Technologies, CA, USA), as explained in Section 4.4.1.1.a (see Appendix D for the plate layout). To the four corner wells (A1, A12, H1, and H12) the same volume, containing only galactose-containing medium, was added (blank, no cells, used for background- and temperature correction). The optimal seeding density employed (see Appendix E) was taken as 12 500 cells/80 µL/well (the recommended volume). The cells were then left to adhere to the microtiter plate in the laminar flow hood for 1 h to promote even cell distribution and reduce edge effects, after which the plate was incubated under standard conditions for 47 h. This period was chosen to guarantee the complete elimination of residual medium glucose (contained in the routine culture medium) from the cells.

DAY 2

For the proper function of the sensor cartridge fluorophores, hydration is required prior to use. This was achieved by adding 200 µL of XF Calibrant (pH 7.4; #100840-000, Agilent Technologies) to each well of the utility plate supplied with the Seahorse XF$^{e}$96 FluxPak (#102416-100, Agilent Technologies). The sensor cartridge was then lowered onto the utility plate, covered with the lid, and incubated at 37°C in a humidified atmosphere containing 0% $CO_2$ (in the XF Prep Station) 24 h prior to the assay. The XF Analyser was also switched on at this time to allow the temperature to equilibrate to 37°C, and the protocol was designed using the Wave Controller software (v2.4). To ensure that cells had sufficient nutriment, an additional 50 µL of galactose-containing medium was added to each well of the cell culture plate and incubation was resumed.

DAY 3

In order to accurately measure ECAR, the pH of the medium must be equilibrated. This necessitates the use of a 0% $CO_2$ incubator (to remove $CO_2$ from the cells, medium, and cell culture plate) and low buffered medium. Consequently, a stock solution of low buffered medium, consisting of a bottle of DMEM powder (#D5030, Sigma-Aldrich), 1.85 g/L filter-sterilised NaCl, 2 mM GlutaMAX (#35050038, Gibco®, Thermo Fisher Scientific™), 0.85 mM NaOH, and 3 mg/L

phenol red (#P0290, Sigma-Aldrich), was prepared in 1 L of autoclaved Milli-Q® $H_2O$, and stored at 4°C (for up to 3 months). On the third day of the analysis, 150 mL of assay medium was prepared for the Mito Stress Test. This was done by supplementing the low buffered medium stock with 10 mM filter-sterilised galactose (pH 7.4) and 1 mM sodium pyruvate. The medium was then warmed to 37°C in a water bath and the pH was adjusted to 7.4 using 0.5 M NaOH.

Following 47 h of incubation, the XF Prep Station (Seahorse Bioscience) was used to remove the galactose-containing medium in the cell culture plate, to wash the cells, and to add a final volume of assay medium to each well. To achieve this, Milli-Q® $H_2O$, 70% (v/v) ethanol, and 138 mL of the assay medium were respectively added to the "$H_2O$", "Clean", and "Medium" bottles. The Seahorse XF Prep Station software (v1.0.0.2) was then set up to perform the following steps: The manifold was firstly primed with "Clean" and then "$H_2O$". Hereafter, three media changes were performed. This involved a third priming step with "Medium", followed by two aspiration and dispense cycles, using 200 µL assay medium/well. A final aspiration and dispense cycle left each well containing 175 µL of assay medium. Cell adherence was then microscopically verified, after which the cell culture plate was incubated at 37°C and 0% $CO_2$ (in the XF Prep Station), 1 h before the assay (total incubation time: 48 h).

The injectable compounds were then reconstituted and made up to their recommended (or optimised) concentrations using the assay medium. Hereafter, 25 µL of each compound was pipetted into the corresponding injection ports of all 96 wells of the sensor cartridge from Day 2. For the Mito Stress Test, this included 1 µM oligomycin in port A, 0.75 µM FCCP (as optimised) in port B, and 0.5 µM rotenone and antimycin A in port C (#103015-100, Agilent Technologies).

The loaded sensor cartridge and utility plate were then inserted into the XF Analyser, the relevant protocol was initiated, and the sensor cartridge was calibrated (~25 min). Hereafter, the utility plate was exchanged for the cell culture plate, and the assay was run (~2 h to 3 h). The latter consisted of four steps (one basal reading and one reading following the injection of ports A, B and C), each comprising three measurement cycles (3 min mix, 3 min measure), for a total of 12 measurements per well (as depicted in Figure 4.5). After the run, the medium was removed from the cell culture plate, and the plate was frozen at -80°C for 24 h in preparation for the CyQUANT® assay.

#### 4.4.6.3.b NORMALISING TO CELL NUCLEIC ACID CONTENT USING THE CYQUANT® CELL PROLIFERATION ASSAY KIT

To account for inter-well differences in the cell seeding density of each cell line, the CyQUANT® Cell Proliferation Assay Kit (#C7026, Molecular Probes®, Thermo Fisher Scientific™) was used

to normalise cells in the Mito Stress Test microtiter plate, according to the total cellular nucleic acid content/well (Jones *et al.*, 2001). This was achieved by following the manufacturer's instructions (Molecular Probes®: CyQUANT® Cell Proliferation Assay Kit, MP07026).

The microtiter plate, which had previously been frozen at -80°C for 24 h to aid in efficient cell lysis during the CyQUANT® assay, was allowed to equilibrate to RT. A sufficient reaction volume was then prepared (100 µL/well) by adding together 1x Cell-lysis buffer (20x), 1x CyQUANT® GR dye (400x) and nuclease-free $H_2O$. The suspension was mixed by vortexing and 100 µL thereof was added per well (including the blank wells). Hereafter, the plate was incubated, protected from light, for 5 min at RT, during which cells were lysed, allowing the green fluorescent CyQUANT® GR dye to bind to the total cellular nucleic acid and fluoresce (Jones *et al.*, 2001). Each sample was then mixed by gentle pipetting and 95 µL was transferred to the corresponding well of a black 96-well microtiter plate (used to absorb light, and reduce crosstalk and background signal). Using the Synergy™ HT Multi-detection microtiter plate reader and Gen5™ Data Analysis software (v1.11.5), the sample fluorescence (which correlates linearly with cell number) was then measured in the black 96-well plate, at a 480 nm excitation- and 520 nm emission wavelength. To obtain values of appreciable size, the sensitivity was set to 100.

### 4.4.7 STATISTICAL ANALYSES & INTERPRETATION – *Objective 2.7.*

#### 4.4.7.1 STATISTICAL ANALYSES

In order to answer the questions set for Objectives 1.5, 1.6, and 2.1 to 2.6, statistical analyses were performed by using SPSS Statistics (v.24.0; IBM) and Microsoft Excel 2013. A schematic representation of the strategy followed to achieve this is given in Figure 4.6. Since Objectives 1.1 to 1.4, 1.7, and 1.8 were carried out on single replicates or yielded no countable data, their statistical analysis was unnecessary.

As a first step, outliers which could potentially skew the data were identified and removed using Tukey's method. This method defines outliers as those data values respectively lying 1.5 interquartile ranges below or above the first- ($25^{th}$ percentile; Q1) and third quartiles ($75^{th}$ percentile; Q3) of the data set[39] (Tukey, 1977). In cases where outliers were apparent but not identifiable by Tukey's method due to the small number of replicates analysed, outliers causing a coefficient of variance (CV%) ≥20% were excluded from the data set (van der Westhuizen, 2017b, personal communication). The remaining values were then processed if necessary, after which the data from the two sets of cell lines (see Table 4.2) were analysed

[39] In this chapter, "data points" refer to the individual data values (replicates), whereas "data set" implies the collection of values obtained per mouse for each analysis. Note that this differs from the meaning given in Chapters 5, 6 and 7.

separately to determine whether or not significant differences existed between the four genotypes within each set. This was done only for Objectives 2.1 and 2.3 to 2.6.

To compare the four genotypes within each set of cell lines, the type of statistical test to employ (parametric or non-parametric) was first determined by assessing the assumptions of normality and the homogeneity of variances. While the former was determined by employing the Shapiro-Wilk test, the latter was assessed by Levene's test (Field, 2009b:144-152). If both assumptions held for both sets of cell lines ($p \geq 0.05$), parametric tests were performed. Conversely, if either assumption was violated, a non-parametric approach was followed.

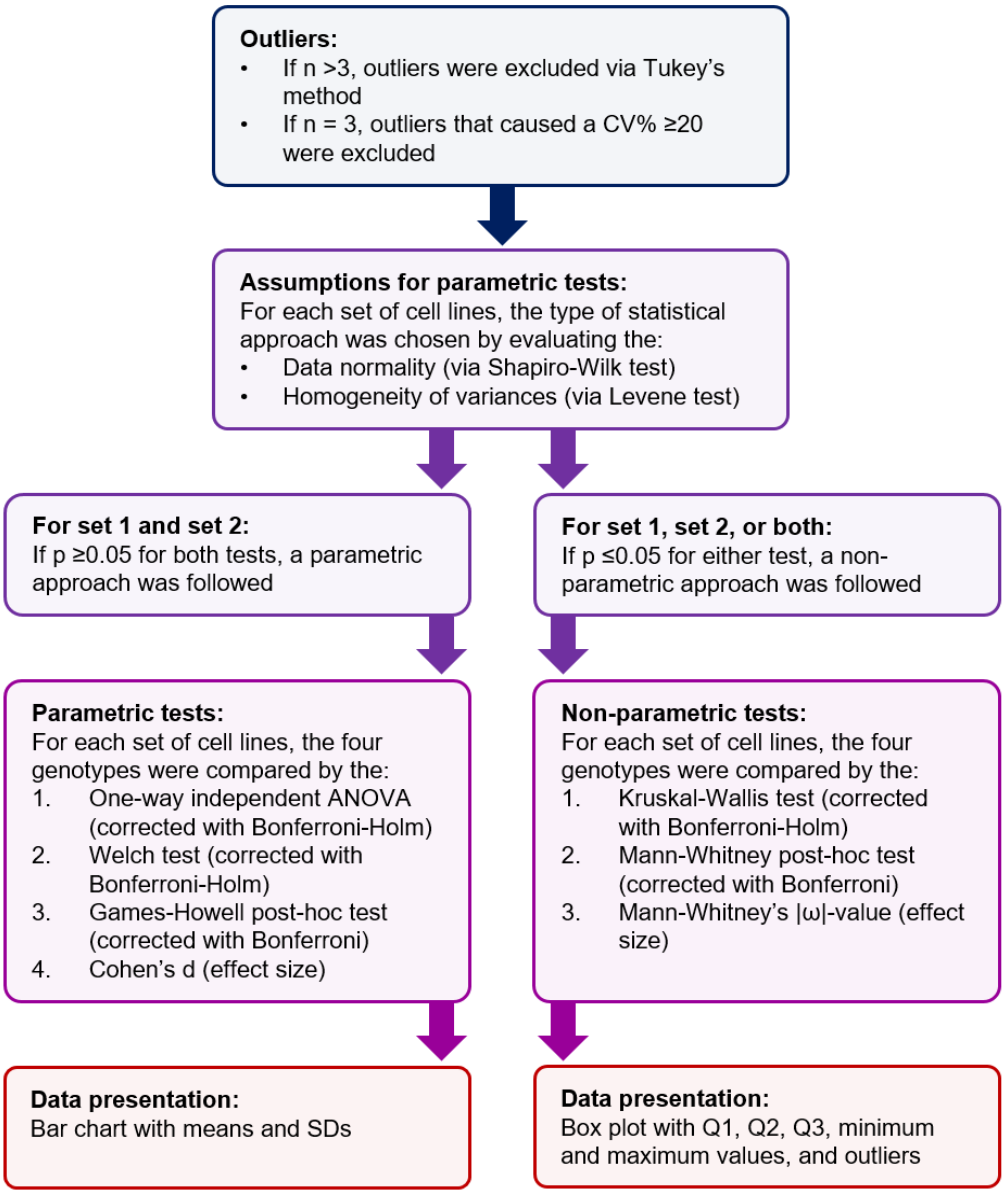


**Figure 4.6: Strategy depicting the statistical analyses performed on the data obtained from Objectives 2.1 and 2.3 to 2.6.**

By following the parametric approach, the data obtained from the four genotypes of each cell line set were firstly analysed using a one-way independent ANOVA (analysis of variance). This type of test may be used to determine whether significant differences exist between three or more groups (i.e. the four genotypes) (Field, 2009d:349). Since the Levene p-values of some data sets were very close to 0.05, the ANOVA's results were confirmed by Welch's test, a more robust parametric test which better compensates for heterogeneous variances (Field, 2009c:308).

When multiple groups are compared for statistical analysis (referred to in this study as *multiple testing*), e.g. when the data of more than two groups are compared or the data of two groups are repeatedly compared, the *Type I error rate* is inflated (Field, 2009a:56). This error may be described as the false assumption of a significant difference in the population, and can be controlled by adjusting the α-value (i.e. the p threshold; the probability of making a Type I error) via data correction. For the ANOVA and Welch's test, the α-value of each variable (experiment) was adjusted by using the Bonferroni-Holm correction to correspond to an estimated false discovery rate of 5% and 10% (Holm, 1979). In other words, these α-values served as new p thresholds to indicate statistical significance with 95% and 90% certainty, respectively. In order to simplify the data interpretation in Chapter 6, the p-values were then multiplied by a constant factor, so that $p = 0.05$ and $p = 0.10$ would once again respectively indicate statistical significance at 95% and 90% certainty.

To establish between which genotypes the statistical significance lay, Games-Howell's *post hoc* test was performed (Games & Howell, 1976). This *post hoc* test was selected as it has been specifically designed for cases in which variances (indicated by Levene's test) and sample sizes are different. To correct for multiple testing within the *post hoc* test, the α-value was once again adjusted to correspond to an estimated false discovery rate of 5% and 10%, this time however using the more conservative Bonferroni method (Field, 2009d:373). Once again, the p-values were multiplied by a constant factor, so that $p = 0.05$ = significance at 95% and $p = 0.10$ = significance at 90%. Overall, two genotypes were considered significantly different from each other if statistical significance was indicated by the ANOVA, Welch's test and the Games-Howell's *post hoc* test. To establish the practical significance of the observed differences (i.e. the importance of the observed effect), the effect size was then determined using Cohen's d. Here, a d-value ≥0.5 indicated practically visible differences, whereas a d-value ≥0.8 implied practically significant differences (Ellis & Steyn, 2003).

To perform non-parametric tests, the non-parametric counterpart of the ANOVA, termed the Kruskal-Wallis test, was applied to the data. This test once again allowed for the comparison of three or more groups (Kruskal & Wallis, 1952). To correct for multiple testing, the α-value was adjusted for each variable (experiment) by employing the Bonferroni-Holm correction, and multiplication, as before (Holm, 1979). As a *post hoc* test, the Mann-Whitney test was then

employed, in which the differences between two groups (i.e. genotypes) within a variable (i.e. experiment) were assessed to determine which groups were significantly different in comparison to each other (Mann & Whitney, 1947). The α-value was adjusted using the Bonferroni correction, after which the p-values were multiplied as described. Two genotypes were considered significantly different from each other if statistical significance was observed for both the Kruskal-Wallis and Mann-Whitney tests. Finally, the effect size was determined by calculating Mann-Whitney's |ω|-value from the z-values. While practically visible differences were indicated by an |ω|-value ≥0.3, practically significant differences were designated by an |ω|-value ≥0.5 (Ellis & Steyn, 2003).

To present the parametric data, bar charts were constructed using the means of the samples and/or controls, with the error bars representing the standard deviation (SD; as a measure of variation) within the data from each. Where applicable, the CV% was also determined per sample and/or control as a measure of assay precision or repeatability. By contrast, the non-parametric data was plotted using box plots. Here, the bottom and top whiskers represented the minimum and maximum values respectively (i.e. the range), whereas the bottom and top edges of the box denoted Q1 and Q3. Therefore, the box itself represented the interquartile range (50% of the data, ranging from Q1 to Q3), with the median (second quartile; $50^{th}$ percentile; Q2) located by a line in the box. In these plots, outliers (1.5 interquartile ranges below or above Q1 and Q3) and extreme outliers (three interquartile ranges below or above Q1 and Q3) were depicted by circles and asterisks, respectively.

#### 4.4.7.2 INTERPRETATION

To present the results of Objectives 1.1 to 1.8 (Chapter 5), a traditional approach was followed in which all eight cell lines were portrayed in the same graph(s). Since these objectives focussed on characterising the mouse fibroblast models, each cell line was compared with its genetic counterpart (e.g. WT 1 and WT 2), while the four genotype groups (i.e. WT, OVER, KO and KO OVER) were compared with each other to evaluate the effect of the genetic modifications.

For Objectives 2.1 to 2.6 (Chapter 6), a different strategy was followed. Since slight genetic differences and the process of cell culture can lead to variability which may affect the results of otherwise genetically identical samples, the reproducibility of the findings within a specific genotype group was assessed by comparing the trend in the data of the first set of cell lines to that of the second set. To this end two separate graphs were constructed, one for each set of cell lines. *While it should be noted that this comparison is not a specific objective of the study*, it is considered good practice when using primary fibroblasts to evaluate whether the results obtained for each genotype are reproducible. In doing so, it is possible to assess whether the results are repeatable or the consequence of genotype-unrelated variability. If the same tendency was

observed between the two sets of cell lines, the statistically significant differences (and effect sizes) of the first set of cell lines (WT 1, OVER 1, KO 1, and KO OVER 1) were discussed, with the purpose of investigating the effect of MTI overexpression on CI deficiency. Conversely, if no trend was observed between the two graphs, possible explanations, suggestions, and a hypothesis of the expected outcome were given. Therefore, the second set of cell lines only served to evaluate the reproducibility of the results within a genotype and were not used to make deductions.

# CHAPTER 5:

## RESULTS & DISCUSSION

## PART 1: ESTABLISHING & CHARACTERISING Ndufs4:TgMTI MICE

### 5.1 INTRODUCTION

In Chapter 4, a detailed description of the methods used to generate and process the data required to achieve the proposed objectives was given. Recall that this study has been divided into two parts, each corresponding to a specific aim (Section 3.3.2). In this chapter, the final results pertaining to the first aim (part one) of this study, namely "Establishing & characterising Ndufs4:TgMTI mice", will be presented and discussed. This will entail the comparability of the genetic backgrounds of the Ndufs4 and TgMTI strains to that of C57BL6/J, followed by a brief overview of the effectiveness of the breeding strategy and cell culture procedures employed. Hereafter, results concerning the genetic and protein characterisation of each of the cell lines will be given and examined, to serve as validation of the experimental models developed.

For the discussion of those results concerning the second aim (part two) of this study, namely "Investigating the effect of MTI overexpression on the bioenergetics consequences of CI deficiency", the reader is referred to Chapter 6.

Note: In Chapters 5, 6, and 7, the terms "significant" and "statistically significant" were used when referring to data points with p-values of ≤0.05 or ≤0.1, calculated as described in Section 4.4.7.
To indicate the final mean (average) value(s) determined for a single sample, the term "data point(s)" was used throughout.
By contrast, the terms "data set" and "group(s)" were generally used when referring to a collection of data points for the samples or controls of a specific genotype.
All DNA base pair sizes and protein molecular weights (respectively presented in bp or kDa) imply the theoretical or approximate values, and have been derived following careful comparison with size markers (ladders).
For descriptions of each sample name (e.g. WT 1, WT 2, OVER 1, OVER 2, etc.) the reader is referred to Table 4.2, whereas control names have been explained in the text.
Lastly, words like "association", "correlation", "range", "dependent", "trend", and "tendency" were used for descriptive purposes only, and bear no relation to any statistical functions.

## 5.2 GENOTYPING THE WHOLE GENOME OF THE Ndufs4 & TgMTI STRAINS – *Objective 1.1*

### 5.2.1 INTRODUCTION

Much research has shown that discrepancies in the genetic backgrounds of mouse models can affect the desired presentation of a particular phenotype by altering the penetrance or expressivity of the genetic modification, or by changing the degree of its pathogenicity (Schauwecker, 2011). In particular, studies have reported genetic differences even in mice that have been backcrossed on a specific strain (JAX, 2006). It was therefore vital for this study, as well as for those studies related to it, to ensure that the genetic backgrounds of the contributing strains were uniform and corresponded to the C57BL6/J genome (Petkov *et al.*, 2004). In doing so, not only could the characteristics of the strains be confirmed, but an accurate breeding strategy could be set up to ensure the production of reproducible genotypes.

Prior to the commencement of this study, the first step was thus to verify the comparability of the genetic backgrounds of the two strains of interest (Ndufs4 and TgMTI mice) to the C57BL6/J genome. To achieve this, DNA from nine *TgMTI*$^{+/-}$ or *TgMTI*$^{+/+}$ mice, as well as two *Ndufs4*$^{+/-}$ mice (see Table 4.1 for details) were sent to the Jackson Laboratory for evaluation on a 1 500 SNP Panel, as explained in Section 4.3.1. Accordingly, samples were analysed against a set of 1 453 validated and polymorphic (i.e. highly informative) SNP markers, which are specific to the C57BL6/J background genome, and spaced evenly across all 19 autosomes and the X chromosome (JAX, 2014). The data was subsequently processed by calculating the percentage equivalence between the SNPs of each sample and the C57BL6/J reference genome, as well as determining the percentage heterozygous SNPs identified for each mouse. Since the number of no-calls (misreads) were few (having a mean of 1.67% across both strains), they were individually excluded from the total number of SNPs analysed for each sample. Additionally, no wrong-calls (mismatches) were found. Lastly, the mean and SD of the percentage equivalence and heterozygous SNPs, were determined for each strain.

### 5.2.2 RESULTS

The final results obtained for each mouse, following the analysis of their DNA on the 1 500 SNP Panel, are displayed in Table 5.1.

**Table 5.1: Comparability of the Ndufs4 and TgMTI strains' genetic background to a reference C57BL6/J genome, as determined by SNP analysis**

| Animal ID | Genotype | Gender | Equivalence to C57BL6/J genetic background (%) | Heterozygous SNPs detected (%) |
|---|---|---|---|---|
| 7964 | *TgMTI*$^{+/-}$ or $^{+/+}$ | Male | 99.4 | 0.58 |
| 2282 | *TgMTI*$^{+/-}$ or $^{+/+}$ | Male | 99.7 | 0.28 |
| 2273 | *TgMTI*$^{+/-}$ or $^{+/+}$ | Male | 99.7 | 0.28 |
| 7691 | *TgMTI*$^{+/-}$ or $^{+/+}$ | Male | 99.7 | 0.35 |
| 2278 | *TgMTI*$^{+/-}$ or $^{+/+}$ | Female | 99.5 | 0.48 |
| 2277 | *TgMTI*$^{+/-}$ or $^{+/+}$ | Female | 99.8 | 0.21 |
| 2269 | *TgMTI*$^{+/-}$ or $^{+/+}$ | Female | 99.7 | 0.28 |
| 2271 | *TgMTI*$^{+/-}$ or $^{+/+}$ | Female | 99.7 | 0.28 |
| 2279 | *TgMTI*$^{+/-}$ or $^{+/+}$ | Female | 99.4 | 0.62 |
| | | **Mean (%)** | **99.6** | **0.37** |
| | | **SD** | **0.15** | **0.15** |
| Q4036 | *Ndufs4*$^{+/-}$ | Female | 99.6 | 0.44 |
| Q4037 | *Ndufs4*$^{+/-}$ | Female | 99.4 | 0.63 |
| | | **Mean (%)** | **99.5** | **0.53** |
| | | **SD** | **0.13** | **0.13** |

The table displays the percentage equivalence obtained when comparing the genetic background of the Ndufs4 and TgMTI mouse strains to 1 453 C57BL6/J-specific SNPs. The percentage heterozygous SNPs discovered in these 11 mice are also shown. Lastly, the mean and SDs for the percentage equivalence and heterozygous SNPs are given for each strain ($n_{TgMTI}$ = 9 and $n_{Ndufs4}$ = 2).

### 5.2.3 DISCUSSION

As shown in Table 5.1, ≥99.4% of the C57BL6/J-specific SNPs could be detected in the DNA of the individual mice from both strains, with each strain displaying an average C57BL6/J comparability of ≥99.5%. In addition, however, an average of ≤0.53% heterozygous SNPs, corresponding to only one allele of the C57BL6/J reference genome, were discovered per strain. From the high percentage of equivalence and small percentage of differences (i.e. heterozygous SNPs), it was therefore concluded by the author, and confirmed by the technician at the Jackson Laboratory, that the mice from the Ndufs4 and TgMTI strains shared enough of the C57BL6/J genetic background, to consider their individual genetic modifications [i.e. the deletion of *Ndufs4*'s second exon (Ndufs4 mouse), and insertion of 56 *Mtl** transgenes per allele (TgMTI mouse)] the only significant differences between them. These results were as expected, as both strains had been backcrossed on the C57BL6/J genetic background (JAX, 2017a; Kruse *et al.*, 2008). Since only 1 453 SNPs were analysed, further conclusions concerning the similarity of the rest of the

genetic background, as well as the effect of crossbreeding the two strains on the genetic background, cannot be made (JAX, 2006).

Fewer samples were analysed from the Ndufs4 strain than the TgMTI strain. The reason for this was that the Ndufs4 colony had not yet been established at this facility at the time of the analysis. The DNA of these mice were thus kindly provided by Prof Albert Quintana. While the results shown above are definitive, a more inclusive distribution might have been obtained if more *Ndufs4*$^{+/-}$ mice (and in particular, males) were to have been analysed. Despite this, the method yielded satisfactory results to continue with the breeding and crossbreeding of these strains.

## 5.3 CROSSBREEDING THE Ndufs4 & TgMTI MOUSE LINES & ESTABLISHING & CULTURING PRIMARY MOUSE FIBROBLAST CELL LINES – *Objectives 1.2 & 1.3*

### 5.3.1 RESULTS & DISCUSSION

After confirming the uniformity of the C57BL6/J genetic backgrounds in the Ndufs4 and TgMTI strains, the breeding strategy explained in Section 4.3.2 was set up (Objective 1.2). This enabled the acquisition of mice of the four specific genotypes at the highest possible efficiency and probability. As discussed in Section 4.3.3, primary fibroblast cells were subsequently cultured from the skin samples of specific mice (see Tables 4.2 and 4.5 for details; Objective 1.3). As shown in Figure 5.1, the culture procedure yielded cells of similar fusiform morphology (indicative of fibroblasts), as anticipated, with an approximate doubling time of 72 h.

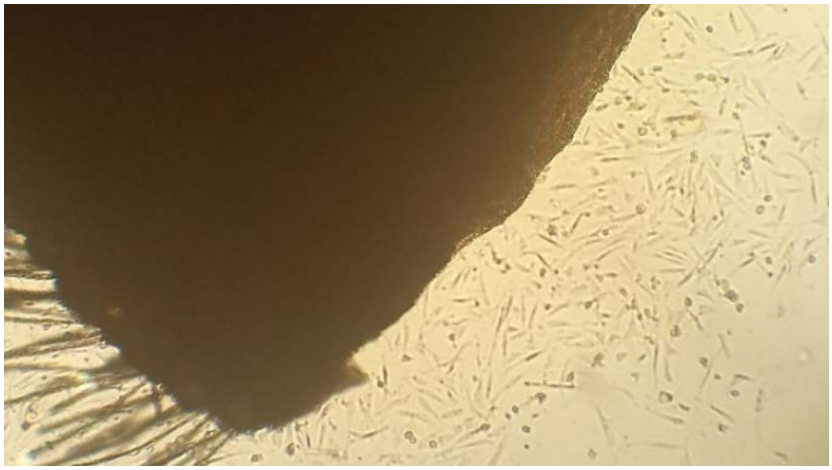

**Figure 5.1: Image depicting mouse skin fibroblasts with fusiform morphology, exiting the skin explant after three days of culture.** Cells with a spherical morphology indicate dividing fibroblasts.

*It should however be noted that those fibroblasts with an Ndufs4*$^{-/-}$ *genotype grew at a rate comparable to, if not slightly higher than, the Ndufs4*$^{+/+}$ *fibroblasts, when cultured in glucose-containing medium.* This was in contrast with the expected result, as seen *in vivo*, and indicated

that the disease phenotype did not result in a limited/stressed growth rate under these culture conditions. Nevertheless, these findings complied with many studies on fibroblast cultures, reporting on their inherent glycolytic nature (Valsecchi *et al.*, 2012; van den Heuvel *et al.*, 2004). Therefore, the ability of fibroblasts to shift their energy metabolism from OXPHOS to glycolysis under normal conditions, and as an adaptive mechanism (i.e. the Crabtree effect) when faced with a challenge like CI deficiency, was considered (Reinecke *et al.*, 2009). In order to allow the more pronounced expression of CI deficiency *in vitro*, it was thus decided to evaluate the bioenergetics consequences (discussed in Chapter 6) on cells that had been pre-incubated in galactose-containing medium for one to two days prior to their experimental analysis (see Section 4.4 for a more detailed explanation). Thus, by switching the cell culture medium from glucose-containing to galactose-containing medium, the cells would be forced to rely more heavily on ATP production via the OXPHOS system, due to the slow conversion of galactose to G-6-P (via glucose-1-phosphate) (Mot *et al.*, 2016; van den Heuvel *et al.*, 2004; Voets *et al.*, 2012). For routine cell culture and the analyses discussed in this chapter, the use of glucose-containing culture medium (which allows the rapid production of ATP via the glycolytic pathway) was sufficient.

## 5.4 GENOTYPING Ndufs4:TgMTI MICE – *Objectives 1.4 & 1.5*

As mentioned in Section 4.3.4, it was necessary to characterise the genotype of each mouse before its inclusion into the study, since each step of the breeding strategy (see Figure 4.2) had the potential to yield pups with at least two possible Ndufs4 and/or TgMTI genotypes. The process was then repeated on the primary fibroblast cell lines established from the skin samples of the selected mice, prior to executing further experimental analyses, in order to validate the genotypes and confirm that there was no sample mix up. Since both the initial and repeated (final) PCR and qPCR amplification methods produced the same results, only the final (and most recent) results will be discussed.

### 5.4.1 CHARACTERISING THE Ndufs4 GENOTYPE – *Objective 1.4*

#### 5.4.1.1 INTRODUCTION

The Ndufs4 genotype was determined by amplifying DNA from each of the eight cell lines, as explained in Section 4.3.4.1.c. Concurrently, the tail-snip DNA of an *Ndufs4*$^{+/+}$, *Ndufs4*$^{+/-}$, and *Ndufs4*$^{-/-}$ mouse were amplified to serve as controls. Following amplification, the eight samples and three controls were then separated via agarose gel electrophoresis. In addition, a DNA size marker (ladder) was included on the gel to provide standard DNA fragments of known lengths to which the sample- and control bands could be compared for size estimation.

### 5.4.1.2 RESULTS

Following band separation, the gel was photographed to yield the final results displayed in Figure 5.2:

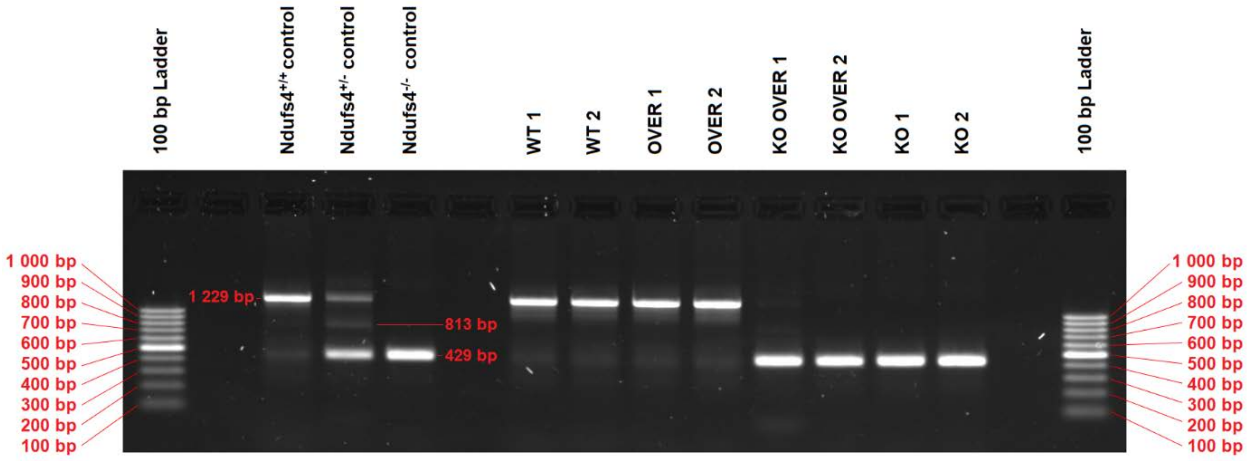


**Figure 5.2: Agarose gel electrophoresis image depicting the bands produced by each sample and three Ndufs4 controls.** The size (in bp) of the PCR products of the eight samples and the three controls used (*Ndufs4*$^{+/+}$, *Ndufs4*$^{+/-}$, and *Ndufs4*$^{-/-}$; see Table 4.3 for details), are shown, together with that of a 100 bp DNA size marker (ladder; on either side of the gel).

Given that the primer pair used was as described by Valsecchi *et al.* (2012), the expected band size of the Ndufs4 WT allele was 1 229 bp. Since the Ndufs4 KO genotype was produced by deleting an 800 bp DNA region (which included the second exon of the *Ndufs4* gene), the band size of the KO allele was anticipated to be 429 bp. Consequently, a heterozygous sample possessing both allele types would display both bands.

As shown in Figure 5.2, each control displayed its anticipated band(s). In addition, however, faint, non-specific bands corresponding to ~429 bp and ~813 bp were respectively seen in the lanes containing the *Ndufs4*$^{+/+}$ control and the *Ndufs4*$^{+/-}$ control. For the WT and OVER samples, a band of 1 229 bp was observed, together with a very faint, non-specific band of ~429 bp, whereas only a 429 bp band was seen for the KO OVER and KO samples.

### 5.4.1.3 DISCUSSION

The band(s) displayed by each control corresponded to the results reported by Valsecchi *et al.* (2012). Additionally, the Ndufs4 genotyping results of each WT, OVER, KO OVER, and KO sample observed in Figure 5.2 corroborated the initial PCR results used to select the eight mice employed in this study (gel results not shown; see Table 4.2 for genotype results). Specifically, the bands displayed in Figure 5.2 indicated that the WT and OVER samples exhibited an *Ndufs4*$^{+/+}$ genotype, whereas the KO OVER and KO samples possessed an *Ndufs4*$^{-/-}$ genotype, as

expected. It can therefore be said that each fibroblast cell culture corresponded to the correct mouse, i.e. the mice and/or samples were not mixed up.

While the non-specific band observed in the lanes containing the *Ndufs4*$^{+/+}$ control and WT and OVER samples was the same size as that of the KO band, the intensity of the bands in these lanes (a more intense 1 229 bp band and a very faint ~429 bp non-specific band) was clearly different from that of the *Ndufs4*$^{+/-}$ control (a less intense 1 229 bp band and a more intense 429 bp band). The non-specific band was also consistently observed in each *Ndufs4*$^{+/+}$ sample genotyped throughout the entire breeding process, even when different preparations of the primers were used. Therefore, this non-specific band may be regarded as the result of non-specific PCR amplification, rather than primer or sample contamination. Similarly, the non-specific band observed in the lane containing the *Ndufs4*$^{+/-}$ control (~813 bp) may also be described as a non-specific PCR artefact, since this band was consistently observed in the genotyping results of each *Ndufs4*$^{+/-}$ mouse throughout the breeding process.

Though various methods were tested to prevent non-specific amplification of the DNA [i.e. new primer preparations, optimisation of the annealing temperature via a temperature gradient, employing a DMSO gradient, adhering to the cycling times and concentrations indicated by the manufacturer, and maximising the ramp rate of the thermal cycler (to 4°C/s; not shown in this dissertation)], none were successful. In the future, it might be considered to decrease the number of cycles to <35. However, as it was still possible to clearly distinguish *Ndufs4*$^{+/+}$ samples from *Ndufs4*$^{+/-}$ samples in this experiment, these results, albeit with the presence of two very faint non-specific bands, were regarded as sufficient for the purpose of meeting Objective 1.4.

### 5.4.2 CHARACTERISING THE TgMTI GENOTYPE – *Objective 1.5*

#### 5.4.2.1 INTRODUCTION

As explained in Section 4.3.4.1.d, a novel method was developed to determine the TgMTI genotype of each of the eight samples, as well as three TgMTI controls, by measuring the $C_T$-values for the amplification of the *MtI* (target) and *Actb* (reference) genes in triplicate. These values were then processed as discussed and substituted into the $2^{-\Delta CT}$ formula. Finally, the answer was multiplied by two to yield the copy number of nuclear *MtI* (here *MtI* copy number collectively refers to the number of *MtI** transgenes and inherent *MtI* genes), quantified relative to that of a single copy of nuclear *Actb*. To further quantify the degree of variation within the data point of each sample, the pooled SD of each copy number was calculated by using the Gauß error propagation, as displayed in Equation 5.1:

$$\text{Pooled SD} = \sqrt{(\text{SD}_{\text{CT}_{\text{target}}})^2 + (\text{SD}_{\text{CT}_{\text{reference}}})^2} \qquad (5.1)$$

### 5.4.2.2 RESULTS

The *MtI* copy number results obtained for each of the eight samples, as well as the three TgMTI controls, are depicted together with each pooled SD (as error bars), in Figure 5.3:

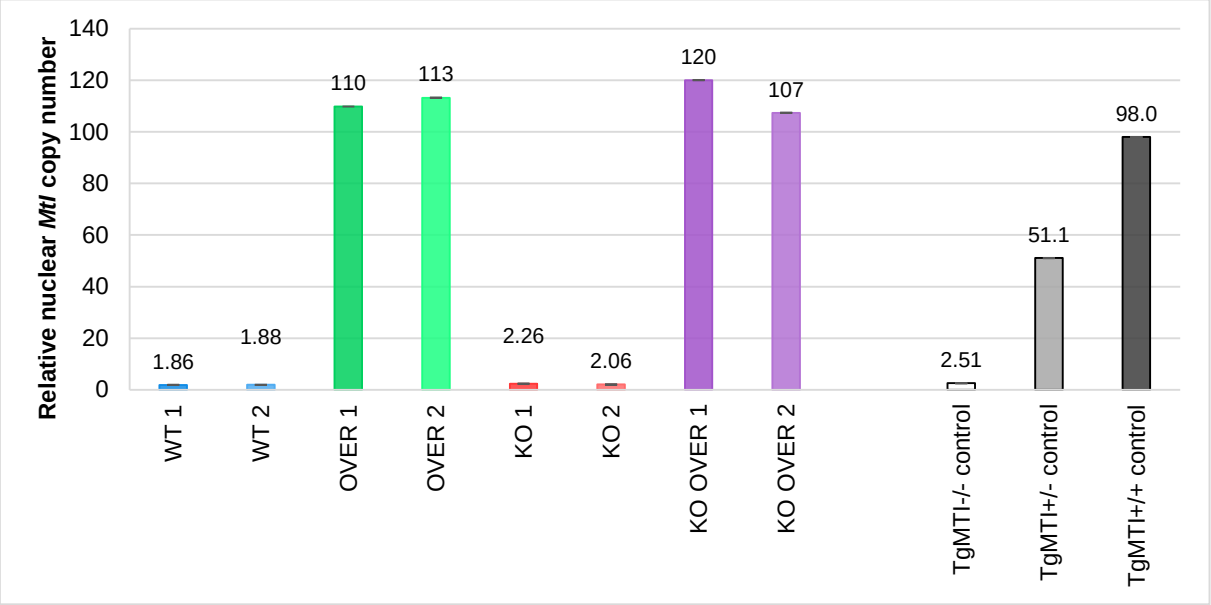


**Figure 5.3: Bar chart depicting the nuclear *MtI* copy number, relative to *Actb*, for each sample and three TgMTI controls.** The number of *MtI* copies contained in the diploid nDNA, expressed relative to that of nuclear *Actb*, is shown for all eight cell lines, as well as the three controls used (*TgMTI*$^{-/-}$, *TgMTI*$^{+/-}$, and *TgMTI*$^{+/+}$; see Table 4.3 for control details). The exact copy number is indicated above the respective bar. (n = 3) ± SD.

While no comparable published data existed at the onset of this study to describe exactly where the *MtI** transgenes are located within the mouse genome, it was theorised that 56 copies per allele of the *MtI** transgene are transferred to the progeny mice, for the reason discussed in Section 4.3.4.1.d. In addition to this, each diploid mouse genome contains two inherent copies of *MtI* (Beach & Palmiter, 1981). Therefore, while *TgMTI*$^{-/-}$ mice are suspected to have only two copies of *MtI*, *TgMTI*$^{+/-}$ and *TgMTI*$^{+/+}$ mice should exhibit 58 copies (two inherent *MtI* genes and 56 *MtI** genes) and 114 copies (two inherent *MtI* genes and 2x 56 *MtI** genes), respectively.

### 5.4.2.3 DISCUSSION

As shown in Figure 5.3, a clear comparison could be drawn between the WT and KO samples and the *TgMTI*$^{-/-}$ control. Since these values were further all extremely close to the anticipated copy number of 2, it indicated that these samples indeed possessed a *TgMTI*$^{-/-}$ genotype. Similarly, the results of the OVER and KO OVER samples correlated very closely with that of the *TgMTI*$^{+/+}$ control. With copy numbers close to 114, it was therefore possible to deduce that these

samples exhibited a *TgMTI*$^{+/+}$ genotype. Additionally, the copy number of the *TgMTI*$^{+/-}$ control was close to the expected value of 58.

While the results of each sample and control were not identical to the anticipated values, a factor that may be ascribed to the decimal-level differences between the quantity of the starting template DNA concentration of different samples of a specific genotype (e.g. decimal-level differences between the DNA quantities of WT 1 and WT 2), the obtained copy numbers could clearly be grouped close to the expected values of the three genotypes. Moreover, the small SDs indicated limited variability between the replicates of a single sample. With this method it was thus possible to meet Objective 1.5. Additionally, in the process, a new, simple, quick and accurate means to distinguish between the *TgMTI*$^{-/-}$ and overexpressing (*TgMTI*$^{+/-}$ and *TgMTI*$^{+/+}$) genotypes was developed. More specifically however, this method allowed for the distinction between the *TgMTI*$^{+/-}$ and *TgMTI*$^{+/+}$ genotypes – which had not been possible using conventional end-point PCR.

## 5.5 QUANTIFYING THE RELATIVE *MtI* mRNA – *Objective 1.6*

### 5.5.1 INTRODUCTION

In order to validate the TgMTI model for use in this study, it was necessary to confirm that the presence of the *MtI** transgenes resulted in MTI overexpression. For this reason, the level of *MtI* expression (mRNA level) exhibited by each cell line was determined according to the RT-qPCR method described in Section 4.3.5. At the same time, four controls were analysed. These included primary skin fibroblasts of an *Ndufs4*$^{+/+}$*:TgMTI*$^{-/-}$ and *Ndufs4*$^{+/+}$*:TgMTI*$^{+/+}$ mouse, which were either untreated (termed the *WT control* and *OVER control* in Figure 5.4), or treated with 12.5 µM $CdCl_2$ (a known *MtI* inducer; termed the *WT $CdCl_2$ control* and *OVER $CdCl_2$ control* in Figure 5.4) for 24 h prior to trypsinisation (see Table 4.5 for details).

To evaluate the expression of *MtI* mRNA in those samples with a *TgMTI*$^{-/-}$ or *TgMTI*$^{+/+}$ genotype, the WT and OVER controls were respectively used as positive controls. On the other hand, the WT $CdCl_2$ control was included to assess whether the *TgMTI*$^{+/+}$ model yielded suitably high MTI overexpression. Lastly, the WT $CdCl_2$ control and OVER $CdCl_2$ control were used to determine the inducibility of the *MtI** transgenes by Cd.

For each sample and control, triplicate $C_T$-values were obtained for the amplification of the *MtI* (target) and *B2m* (reference) cDNA. The data was then processed and substituted into the $2^{-\Delta CT}$ formula to yield the expression of *MtI* (here *MtI* collectively refers to inherent *MtI* and the *MtI** transgenes), quantified relative to that of *B2m.* Hereafter, the *MtI* mRNA level of each sample and control was expressed relative to that of WT 1, which was arbitrarily assigned the value of 1.00. To determine the variation within each data point, the pooled SD was calculated via Equation 5.1.

Finally, the pooled CV% was determined, by using the Gauß error propagation as displayed in Equation 5.2, yielding values of ≤1.33 for each sample and control:

$$\text{Pooled CV\%} = \sqrt{(\text{CV\%}_{\text{CT}_{\text{target}}})^2 + (\text{CV\%}_{\text{CT}_{\text{reference}}})^2} \qquad (5.2)$$

### 5.5.2 RESULTS

The *Mtl* mRNA expression obtained for each sample, as well as the four controls, may be found in Figure 5.4.

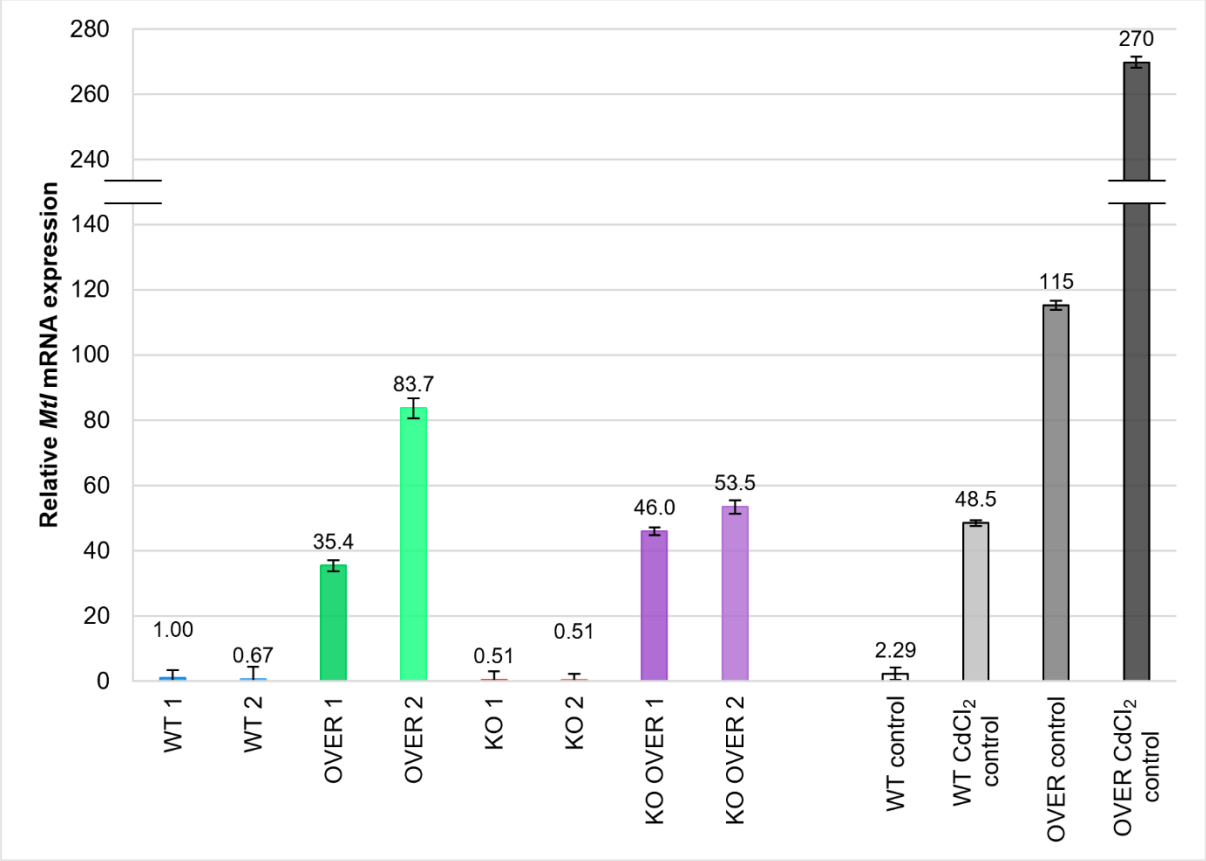


**Figure 5.4: Bar chart depicting the mRNA expression of *Mtl*, relative to *B2m*, for each sample and four controls.** For all eight cell lines, as well as four controls (WT and OVER fibroblasts, untreated or treated with 12.5 µM of the *Mtl* inducer, $CdCl_2$, for 24 h), the level of nuclear *Mtl* (inherent *Mtl* and *Mtl** transgenes) mRNA is shown, as expressed relative to nuclear *B2m*. The exact copy number is indicated above the respective bar. (n = 3) ± SD.

From Figure 5.4, it was observed that the WT and KO samples compared well to the WT control. By contrast, the OVER and KO OVER samples displayed *Mtl* mRNA expression ranging from ~16 to ~37 times that of the WT control. Although variation was evident, these four values were comparable with each other and the OVER control. Additionally, none of the obtained values were comparable to the OVER $CdCl_2$ control, which yielded the highest *Mtl* mRNA expression, as

expected. Finally, it may be seen that each $CdCl_2$-treated control displayed increased *MtI* mRNA expression when compared to its untreated counterpart.

### 5.5.3 DISCUSSION

As mentioned in Section 2.6.6, *MtI* may be induced by several heavy metals including Cd, which act on the MREs situated in the gene's proximal promotor (Penkowa *et al.*, 2006). By studying the controls depicted in Figure 5.4, the effect hereof was evident, since each $CdCl_2$-treated control displayed increased *MtI* mRNA expression in comparison with its untreated counterpart (the WT $CdCl_2$ control: ~21-fold increase, and the OVER $CdCl_2$ control: ~two-fold increase). With these results it was thus possible to confirm that *MtI** transgenes are regulated by Cd, as first reported by Palmiter *et al.* (1993). Additionally, it was shown that the $TgMTI^{+/+}$ genotype (OVER control) resulted in a higher expression of *MtI* mRNA than chemically induced MTI overexpression (WT $CdCl_2$ control). This indicated that the model was particularly suitable for the purpose of this study.

The *MtI* mRNA expression displayed by the WT and KO samples further resembled that of the WT control as expected, and thereby corroborated the $TgMTI^{-/-}$ genotype of each of these samples (as depicted in Figure 5.3). By contrast, MTI was clearly overexpressed in the $TgMTI^{+/+}$ genotype, as was evident from the increased *MtI* mRNA levels exhibited by the OVER and KO OVER samples, as well as the OVER control, in comparison to the WT control. While the results yielded by the OVER and KO OVER samples were in a similar range, significant variation was observed between them and the OVER control, as well as within the OVER genotype group. However, no clear trend was observed to link this variability to the Ndufs4 genotype.

Therefore, to explain the variability observed between samples of the same genotype, the nature of the method (experimental variability) was first considered. Since a specific quantity of total RNA, instead of pure mRNA, was used as starting template, the percentage mRNA within the template RNA was unknown. The variability in the amount of mRNA present in each sample could therefore possibly have contributed to slightly higher or lower mRNA expression values. Secondly, the existence of inherent variability between similar cell lines was considered. Research has shown that gene expression is stochastic by nature (Raj & van Oudenaarden, 2008). In other words, the mRNA expression of a specific gene fluctuates in the individual cells of a genetically homogeneous population (i.e. clones). This occurs since mRNA synthesis is not a continuous process, but rather a series of brief periods during which the gene of interest is transcriptionally active. In the cell, stochastic gene expression may be caused by extrinsic (e.g. the varying levels of transcription activators) or intrinsic factors (e.g. the inherent randomness associated with the transcription and translation process). While it is true that the effect of stochastic gene expression will become statistically less significant as the population size of the analysed sample increases, it was still possible that these extrinsic and intrinsic factors could

have contributed to the small differences observed (Raj & van Oudenaarden, 2008). As both the SD (Figure 5.4) and CV% (≤1.33) of each sample and control were low, respectively indicating little variation between the measurements of each data point and a high assay repeatability (a CV% of ≤10% indicates sufficient repeatability), technical error was disregarded as a potential cause of the varying mRNA levels.

It is important to note that *MtI* mRNA will not necessarily result in comparable quantities of the protein, as mentioned in Section 4.3.5.1 (Dabrio *et al.*, 2002; Vasconcelos, 2002). RT-qPCR therefore only allows a semi-quantitative measure of putative MTI protein expression. However, as the objective of this method was not to quantify MTI, but simply to observe if the *TgMTI*$^{+/+}$ genotype led to *MtI* mRNA overexpression, the results were considered satisfactory.

## 5.6 QUANTIFYING THE STEADY STATE LEVEL OF NDUFS4 WITH SDS-PAGE + WESTERN BLOT ANALYSIS – *Objective 1.7*

### 5.6.1 INTRODUCTION

Although initial studies have classified the *Ndufs4*$^{-/-}$ mouse as a putative whole-body KO, and while the protein's synthesis has further specifically been shown to be precluded in immortalised mouse embryonic fibroblasts of the strain, it was still considered thorough to verify that the changes in the Ndufs4 genotype were being translated to the protein level in the four models used in this study (Kruse *et al.*, 2008; Valsecchi *et al.*, 2012). This was especially important for the *Ndufs4*$^{-/-}$*:TgMTI*$^{+/+}$ genotype, as this cell model is the first of its kind. Furthermore, since transgene integration is a random process and the *MtI** insertion sites are as of yet unknown, it was important to establish that the *Ndufs4* gene was not disrupted by the *MtI** transgenes (Pilbrough *et al.*, 2009). Thus, the steady state level of NDUFS4 was determined to characterise each model, and to verify that *MtI**'s presence did not reduce NDUFS4's expression.

As discussed in Section 4.3.7, the denatured cytosolic extracts of four cell lines representing each genotype (WT 1, OVER 1, KO 1, and KO OVER 1), as well as a molecular weight marker, were separated by SDS-PAGE, electroblotted to a PVDF membrane, and probed with primary antibodies reactive to NDUFS4 and the mitochondrial housekeeping protein, VDAC1. Following incubation with HRP-conjugated secondary antibodies, the bands in each sample lane, as well as the lane containing the molecular weight marker, were detected by chemiluminescence. Using the Image Lab software (v5.2.1), those bands corresponding to the expected molecular weights of NDUFS4 (18 kDa) and VDAC1 (31 kDa) were identified by comparison with the molecular weight marker. Concurrently, the background was subtracted and the intensity of NDUFS4 was quantified relative to that of VDAC1. The NDUFS4 band intensities of OVER 1, KO 1, and KO OVER 1 were then expressed as a percentage of that of WT 1.

### 5.6.2 RESULTS

Figure 5.5.a-b displays an image of the western blot, as well as a bar chart depicting the final quantity of NDUFS4 protein of each sample:

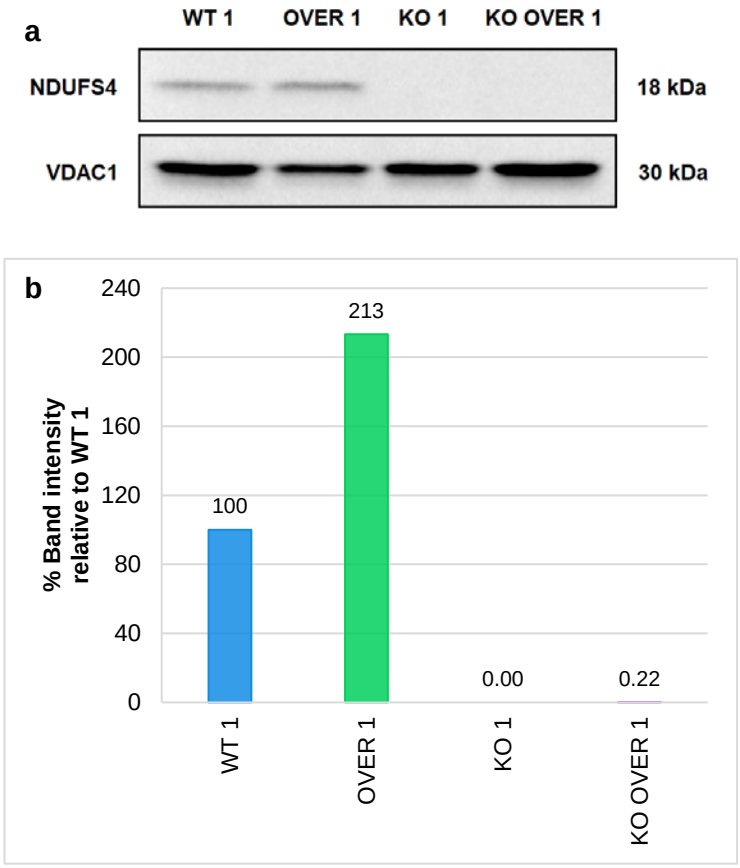


**Figure 5.5.a-b: Western blot of NDUFS4 and VDAC1 following separation by SDS-PAGE, and a bar chart depicting normalised NDUFS4 band intensity. (a)** Sections of the western blot depicting the NDUFS4 (target) and VDAC1 (loading control) proteins and their molecular weights (in kDa) for each genotype (WT 1, OVER 1, KO 1, and KO OVER 1). **(b)** Bar chart displaying the NDUFS4 band intensity of each sample, normalised to the VDAC1 band intensity and expressed as a percentage of WT 1.

As shown in Figure 5.5.a, an NDUFS4 band (size ~18 kDa) was present in the lanes containing the WT 1 and OVER 1 samples, but absent from those of KO 1 and KO OVER 1. Furthermore, the quantity of the band corresponding to VDAC1 (size ~30 kDa) appeared to be consistent across all samples except OVER 1, where a fainter band was observed. Following normalisation, the results depicted in Figure 5.5.b revealed a ~113% increase in the expression of NDUFS4 of the OVER 1 sample when compared to WT 1, while the band intensities of both the KO 1 and KO OVER 1 samples were ~0%.

### 5.6.3 DISCUSSION

As shown in Figure 5.5.a, the presence of the NDUFS4 band in the lanes containing WT 1 and OVER 1 (*Ndufs4*$^{+/+}$ genotypes), as well as its absence from the lanes comprising KO 1 and KO OVER 1 (*Ndufs4*$^{-/-}$ genotypes), corresponded to the genotype of each sample (shown in Figure 5.2). This confirmed that each Ndufs4 genotype was translated to the protein level. Consequently, it may be said that the deletion of exon two from the *Ndufs4* gene results in a lack of the mature protein in primary mouse skin fibroblasts.

What was interesting, however, was the ~113% increase in NDUFS4 expression displayed by OVER 1 in comparison to WT 1 (Figure 5.5.b). While it could have been argued that MTI overexpression leads to a decreased production of VDAC1, a similar decrease was not observed in the KO OVER 1 sample. Although this experiment was not repeated to confirm its reproducibility, the possibility that that MTI overexpression may have increased the production of NDUFS4 was considered.

As mentioned in Section 2.6.6, MTs participate in the cellular transport of $Zn^{2+}$, an essential metal ion required as a cofactor by more than 300 enzymes. The latter includes numerous TFs and Zn-finger proteins. MTs may therefore regulate the expression of various genes, by activating or inhibiting TFs and/or Zn-finger proteins via their provision or removal of $Zn^{2+}$ (Babula *et al.*, 2012). According to a study by Kindermann *et al.* (2004), Zn-availability also affects the expression of NDUFS4. Since the authors reported a decreased transcription of *NDUFS4* in the case of Zn-depletion, it could thus be argued that the opposite is also true, i.e. that increased Zn will result in augmented NDUFS4.

While the method in which NDUFS4 is increased cannot be deduced from the limited data yielded in the current study, the possibility does exist that MTI overexpression might indirectly augment the steady state level of NDUFS4 by increasing the provision of Zn to those proteins involved in *Ndufs4*'s transcription. It should, however, again be noted that only one *Ndufs4*$^{+/+}$*:TgMTI*$^{+/+}$ sample was analysed. More definitive results concerning the level of steady state NDUFS4 may therefore be obtained in the future by analysing and comparing more samples and/or replicates.

## 5.7 QUANTIFYING THE STEADY STATE LEVEL & ACTIVITY OF FULLY ASSEMBLED CI WITH BN-PAGE + WESTERN BLOT & IGA ANALYSES – *Objective 1.8*

### 5.7.1 INTRODUCTION

In order to evaluate the validity of the CI deficiency model in primary skin fibroblasts, the effect of the absence of mature NDUFS4 on both the structure and activity of fully assembled CI was assessed. Accordingly, enriched mitochondrial fractions of cell lines corresponding to the four genotypes (WT 1, OVER 1, KO 1, and KO OVER 1) were separated via non-denaturing

BN-PAGE. This was followed by detecting each of the five OXPHOS complexes via immunostaining and determining the activity of CI as described in Section 4.3.8. The bands corresponding to CI and CII were then identified and sized by comparison with the molecular weight marker.

Using the Image Lab software (v5.2.1), the western blot results were subsequently processed by subtracting the background and quantifying the intensity of CI, relative to that of CII. The latter complex was present and comparable in all lanes and served as a loading control. The normalised CI band intensity of each sample was then presented as a percentage of that of WT 1.

For the IGA detection of CI, no reference activity (loading control) was present. Therefore, the CI activity was determined by subtracting the background and expressing each CI band intensity (representing CI activity) as a percentage of that of WT 1.

### 5.7.2 RESULTS

An image of the blot, as well as a bar chart depicting the normalised expression of fully assembled CI, may be found in Figure 5.6.a-b, whereas Figure 5.7.a-b displays the same information for the activity of fully assembled CI.

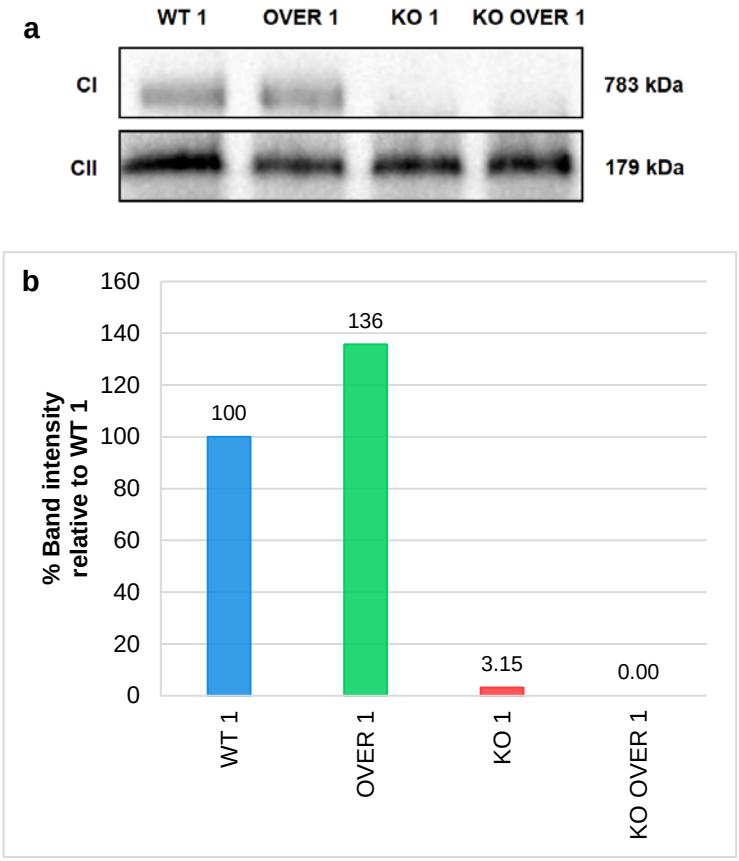


**Figure 5.6.a-b: Western blot of CI and CII following separation by BN-PAGE, and a bar chart depicting normalised CI band intensity. (a)** Sections of the western blot depicting CI (target) and CII (loading control), together with their molecular weights (in kDa), for each genotype (WT 1, OVER 1, KO 1, and KO OVER 1). **(b)** Bar chart displaying the CI band intensity of each sample, normalised to the CII band intensity and expressed as a percentage of WT 1.

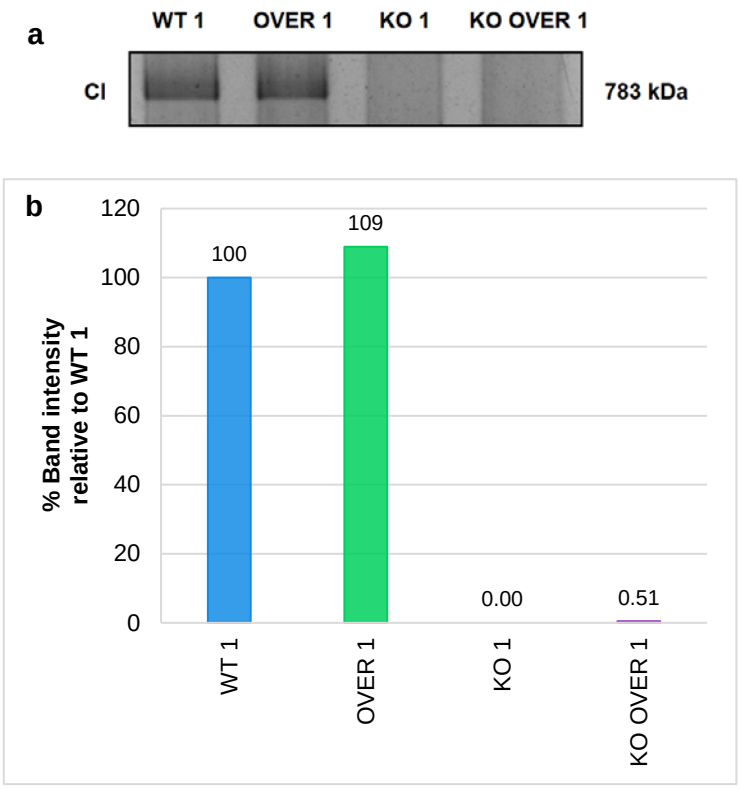


**Figure 5.7.a-b: In-gel activity analysis of CI following separation by BN-PAGE, and a bar chart depicting normalised CI band intensity. (a)** Section of the gel depicting the activity and molecular weight (in kDa) of CI, for each genotype (WT 1, OVER 1, KO 1, and KO OVER 1). **(b)** Bar chart displaying the CI band intensity of each sample, normalised to the gel background of each lane and expressed as a percentage of WT 1.

From Figure 5.6.a, it may be seen that the lanes comprising WT 1 and OVER 1 each contained a band corresponding to CI. Similarly, these lanes displayed a blue-purple coloured band, correlating with the size of CI, following IGA analysis (Figure 5.7.a). The CI band was however absent from those lanes containing the KO 1 and KO OVER 1 samples in both Figures 5.6.a and 5.7.a. Upon normalisation of the CI band intensity (Figure 5.6.b), it was further found that OVER 1 displayed a ~36.0% increase in CI expression when compared to WT 1, whereas the intensities measured in the KO 1 and KO OVER 1 samples were very low (≤3.50%). Conversely, the percentage CI activity observed in OVER 1 was only slightly higher (~9.00%) than that of WT 1 (Figure 5.7.b), while the KO 1 and KO OVER 1 samples once again exhibited nearly negligible (≤0.51%) results.

### 5.7.3 DISCUSSION

The presence of fully assembled CI in the WT 1 and OVER 1 lanes of Figure 5.6.a agreed with both the *Ndufs4*$^{+/+}$ genotype and the NDUFS4 protein expression previously shown for these

samples (see Figures 5.2 and 5.5.b). While the molecular weight of the complex differed from that reported in literature (~980 kDa in human and mouse), the use of a CI-specific antibody (reactive to the NDUFA9 subunit of CI) and the clear results obtained confirmed that the band detected was indeed CI. The difference in size could be attributed to the differential effects on the stability or migration of the complex, brought on by the specific conditions of the BN-PAGE method employed in this experiment (i.e. experimental variation, e.g. due to the choice of detergent) (Kruse *et al.*, 2008; Mimaki *et al.*, 2012; Valsecchi *et al.*, 2012). Furthermore, as shown in Figure 5.6.b, the increase in fully assembled CI observed for the OVER 1 sample corresponded to the relative increase in NDUFS4 expression seen for the same sample in Figure 5.5.b. This result therefore supported the observation made in Section 5.6, i.e. that MTI may increase NDUFS4 expression, and further suggests that MTI overexpression may increase the production of fully assembled CI. Interestingly, similar results concerning CI's expression have been found in patients with CI mutations, following treatment with the antioxidant Trolox (Distelmaier *et al.*, 2009). It is therefore possible that the mechanism employed by MTI to increase CI shares a common property with that of Trolox.

The CI band was, however, completely absent from the KO 1 and KO OVER 1 samples when compared to WT 1 (Figure 5.6.a-b). Since the anti-CI primary antibody employed in this study was reactive against the NDUFA9 subunit of CI's Q module, it was therefore theorised that CI's stability was affected by the lack of NDUFS4. In a study by Calvaruso *et al.* (2012), in which BN-PAGE + western blot analyses were performed using the same anti-CI primary antibody, various tissues (pancreas, kidney, liver, lung, brain, heart, and muscle) of the *Ndufs4*$^{-/-}$ mouse also failed to display fully assembled CI when compared to mice with an *Ndufs4*$^{+/+}$ or *Ndufs4*$^{+/-}$ genotype. Instead, the authors reported the presence of a lower molecular weight sub-assembly of CI. This sub-assembly was also observed for immortalised mouse embryonic fibroblasts of the Ndufs4 strain, as well as fibroblasts of patients with *NDUFS4* mutations (Scacco *et al.*, 2003; Ugalde *et al.*, 2004; Valsecchi *et al.*, 2012). Following further analyses, Calvaruso *et al.* (2012) identified this sub-assembly as CI lacking the N module, and reported that the absence of NDUFS4 led to a decreased stability of CI, which in turn increased the dissociation of the N module from the holo-complex. While fully assembled CI was absent from the blot produced in this experiment as mentioned, the lower molecular weight sub-assembly of CI could not be observed. Since each of the other complexes were however detected (data not shown), this was once again attributed to experimental variation between ours and the BN-PAGE method employed by other laboratories (e.g. the use of 1x PBS with 1x cOmplete™, Mini, EDTA-free Protease inhibitor Cocktail, instead of milder sucrose buffers) (Wittig *et al.*, 2006).

As explained in Section 4.3.8.1.c, the presence of a blue-purple band following IGA analysis occurs when the CI N module is functional and connected to the rest of the complex. The presence of a band in Figure 5.7.a, corresponding in size to the CI band observed in Figure 5.6.a, therefore

indicated functional and fully assembled CI. This band was observed in the lanes containing WT 1 and OVER 1, a result which corresponded to both the *Ndufs4*$^{+/+}$ genotype (Figure 5.2) and the successful expression of the NDUFS4 protein (Figure 5.5.b) previously demonstrated for these samples. These results further agreed with those reported by Valsecchi *et al.* (2012) for immortalised mouse embryonic fibroblasts of the Ndufs4 strain. While the band intensity of OVER 1 was slightly higher than that of WT 1, these results could not be used as a quantitative measure of CI activity due to the qualitative nature of IGA analysis. Since the main objective of this experiment was to observe the qualitative difference in CI activity between cells with an *Ndufs4*$^{+/+}$ and *Ndufs4*$^{-/-}$ genotype, the method was however entirely sufficient.

Conversely, no CI activity was observed for those lanes comprising KO 1 and KO OVER 1. These results corroborated previous findings by Valsecchi *et al.* (2012) and Calvaruso *et al.* (2012) and were not considered surprising, as the KO 1 and KO OVER 1 samples did not display fully assembled CI following western blot analysis (Figure 5.6.a). The absence of a CI band following IGA analysis should however not be mistaken for the inability of *Ndufs4*$^{-/-}$ cells to utilise CI, but merely indicates that CI, as a single complex, is instable and unable to oxidise NADH in cells with an *Ndufs4*$^{-/-}$ genotype. As mentioned in Section 2.3.3, CI may exist in supercomplexes by combining with CIII and CIV (Stroud *et al.*, 2016). In a study evaluating the IGA of individual CI and CI-containing supercomplexes, CI activity was observed in *Ndufs4*$^{-/-}$ mouse tissues when the complex was present as the CI+CIII$^2$ supercomplex (Calvaruso *et al.*, 2012). Additionally, the authors demonstrated that all investigated *Ndufs4*$^{-/-}$ tissues displayed some residual, albeit greatly reduced, CI activity, as determined by spectrophotometric analyses. The same result was obtained at this institution when using liver samples (unpublished results).

From the results shown in Figure 5.7.a-b, it may thus be deduced that CI requires NDUFS4 for its proper functioning. Literature however reports that the complex may be stabilised by the formation of respiratory supercomplexes with CIII, thereby enabling the survival of cells with an *Ndufs4*$^{-/-}$ genotype, as well as the transitory viable phenotype of the *Ndufs4*$^{-/-}$ mouse. While the results displayed by this part of the study were unable to elaborate on the finer aspects of CI's structure and assembly, they were able to clearly demonstrate that the NDUFS4 subunit of CI was knocked out, thereby resulting in the destabilised structure of CI in the fibroblasts used.

# CHAPTER 6:

## RESULTS & DISCUSSION

## PART 2: INVESTIGATING THE EFFECT OF MTI OVEREXPRESSION ON THE BIOENERGETICS CONSEQUENCES OF CI DEFICIENCY

### 6.1 INTRODUCTION

In the following chapter, the results concerning the second aim (part two) of this study, namely "Investigating the effect of MTI overexpression on the bioenergetics consequences of CI deficiency", will be presented and discussed. This will include an evaluation of the effects of the varied genotypes on cell viability, RMCN, redox- ($NADH/NAD^+$) and energy (ATP/ADP) status, and ROS levels. Finally, the bioenergetics profile, as determined using the Seahorse $XF^e96$ Analyser, will be given and discussed.

*Unless otherwise stated, the data of Objectives 2.1 to 2.6 were discussed by following the approach outlined in Section 4.4.7.2.* In short, the trend of the data belonging to the first set of cell lines (i.e. WT 1, OVER 1, KO 1, and KO OVER 1) was compared to that of the second set (i.e. WT 2, OVER 2, KO 2, and KO OVER 2) to evaluate the reproducibility of the results obtained for each genotype. If the trend in the results of the contributing cell lines of a specific genotype was similar, the data was regarded as repeatable. Consequently, the statistically significant differences (and effect sizes) of the first set of cell lines were then discussed to evaluate the effect of MTI overexpression on CI deficiency. Conversely, if no similarity was found the data was regarded as inconclusive and the result of genotype-unrelated variability. In this case, possible explanations, suggestions, and the expected hypothesis were given.

As mentioned in Chapter 4, all eight cell lines were restarted for culture at the same time, cultured under identical conditions, and seeded and analysed in a single microtiter plate for each analysis. This was done to limit time-, microplate-, and obvious cell culture-related differences from affecting the results. Furthermore, to allow for the more pronounced expression of CI deficiency *in vitro*, the cell culture medium was switched from glucose-containing medium (used for routine culture) to galactose-containing medium (used to promote the use of the OXPHOS system) one or two days prior to analysis (as discussed in Section 5.3.1).

### 6.2 DETERMINING CELL VIABILITY WITH THE MTT ASSAY – *Objective 2.1*

#### 6.2.1 INTRODUCTION

In order to assess whether the overall growth of skin fibroblasts was influenced by the absence of NDUFS4, overexpression of MTI, or both of the mutations, the viability of each genotype was

assessed by using the reductive MTT assay, as described in Section 4.4.1. To account for any non-specific background produced as a result of the reagents used, blank wells comprising only galactose-containing medium were included on the microtiter plate. Additionally, WT cells, treated and killed with 6% acetic acid (in galactose-containing medium), were included to serve as a negative control for cell viability. The results obtained were subsequently processed by subtracting the mean of the blank wells from the absorbance at 560 nm and 630 nm (reference wavelength). To further account for non-specific background produced by external factors (e.g. plate variability or fingerprints), the absorbance at 630 nm was then subtracted from that at 560 nm. Hereafter, outliers were identified and removed using the Tukey method. The data was presented as the percentage cell viability by expressing the values of each sample, as well as the negative control, to the mean of WT 1.

### 6.2.2 RESULTS

Figure 6.1.a shows the results obtained for the negative control, as well as the first set of cell lines, whereas the results of the second set of cell lines are depicted in Figure 6.1.b. To allow for an unbiased comparison, the y-axis range was kept identical (the same was done for Sections 6.3 to 6.7).

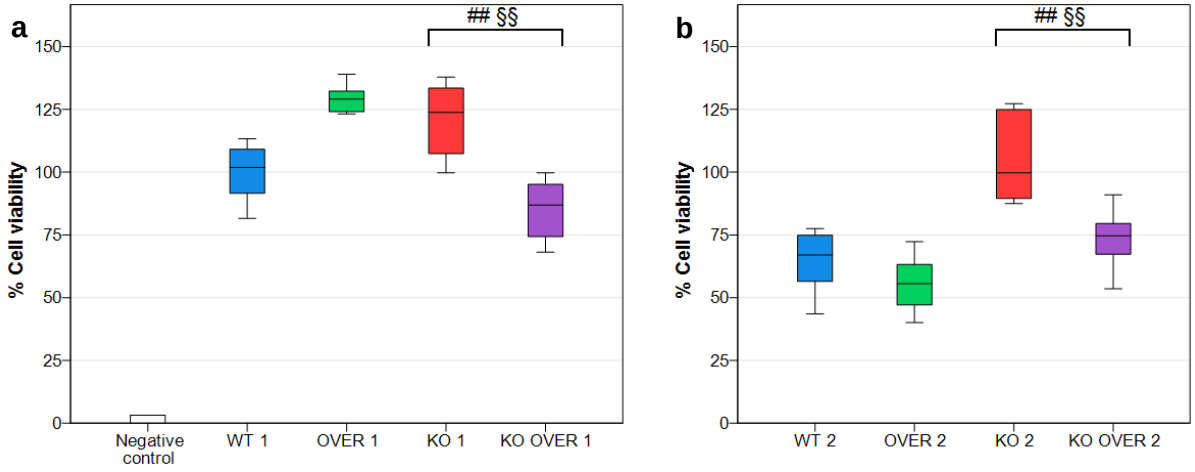


**Figure 6.1.a-b: Box plots depicting the percentage cell viability of two sets of cell lines, each comprising the four genotypes of interest. (a)** For the negative control (WT 1 cells, treated with 6% acetic acid), as well as the samples in the first and **(b)** second set of cell lines, the cell viability is shown as a percentage of WT 1, following analysis by the MTT assay. (n = 8) ± SD. Hashes indicate significant differences between genotype groups within a set of cell lines (## p ≤0.05; # p ≤0.1), whereas effect size is shown as § (§ |ω| ≥0.3; §§ |ω| ≥0.5). Statistical analyses were performed according to non-parametric tests, as explained in Section 4.4.7.1.

### 6.2.3 DISCUSSION

As shown in Figure 6.1.a-b, the data did not produce a repeatable trend over both sets of cell lines when comparing the samples of each genotype (i.e. WT 1 against WT 2, etc.). Instead, the percentage cell viability differed between those cell lines belonging to the WT genotype group and the OVER genotype group. From this, it was concluded that the data was not reproducible between more than one cell line of the same genotype. The results were therefore inconclusive, and no inferences regarding the statistically significant difference observed between the KO 1 and KO OVER 1 cell lines (Figure 6.1.a: $p = 0.017$, $|\omega| = 0.828$) could be drawn from the assay.

To explain the inconsistency observed within the WT and OVER genotype groups, two factors were considered: (i) The technical error associated with seeding cells, and (ii) the inherent variability observed in cell culture. (i) To limit inter-well variances in cell density from affecting the results, it is common practice to normalise data to the total cellular nucleic acid- or protein content per well of the analysed microtiter plate. However, since the last step of the MTT protocol involves the addition of DMSO – a known apoptotic inducer – cell integrity is lost, thereby eliminating the possibility of single-plate normalisation (Aita *et al.*, 2005). As an alternative, it was considered to normalise the data to an identically seeded second microtiter plate (Reinecke, 2004). In doing so, it was found that the inter-plate differences inflated the variance observed in the cell viability data and, therefore, the method was not used. In order to confirm that the experiment was repeatable, the assay was performed again. Subsequently, the same trends as those depicted in Figure 6.1.a-b were obtained (data not shown). Thus, since the cell viability was not altered by any additional factor other than the cell biological consequences of the specific genetic modifications [i.e. the deletion of *Ndufs4*'s second exon (Ndufs4 mouse), and insertion of 56 *MtI** transgenes per allele (TgMTI mouse)], and the assay proved to be repeatable, the use of unnormalised data was regarded as acceptable for the purpose of this experiment. In addition, the SDs (not shown) accompanying each data point were considered satisfactory.

(ii) Instead, the intra-genotype variance was attributed to the inherent variability known to occur in cell culture. The source of this variability is wide-reaching and many studies have reported on the development of heterogeneous phenotypes in clonal cells, due to minor changes to the cells' *physical environment* (e.g. type of culture flask and lot of FBS), the *cell culture techniques* used (e.g. enzymatic versus manual techniques), and the *time spent in culture* (i.e. passage number and sub-culturing frequency) (Baker, 2016; Hughes *et al.*, 2007). During the course of this study, special care was taken to treat the cell lines as uniformly as possible, e.g. by thawing new aliquots of cells for each assay, keeping the physical environment constant, analysing cells at low and equivalent passage numbers, and sub-culturing cells at similar densities using a single method (see Section 4.3.3). The cause of variation therefore seemed to stem from the cells themselves. This argument is corroborated by other authors, who have reported on the variation observed between genetically identical cells due to *varying proliferation rates* between genetically identical

cultures (possibly leading to differences in the cultures' position on the growth curve), as well as the *differential (stochastic) expression of genes*, even between single cells (Baker, 2016; Neildez-Nguyen *et al.*, 2008; Raj & van Oudenaarden, 2008). Indeed, small variations in cell proliferation were observed throughout this study, with some cell lines of the same genotype constantly appearing to grow slightly quicker, thereby reaching the desired passaging confluency earlier than others. While this was accounted for by varying the sub-culturing ratio to an appropriate degree, it could be argued that the time spent culturing the cells after thawing (eight to nine days) was not long enough to completely correct for these differences. Furthermore, as shown in Section 5.5, intra-genotype differences were observed in the expression of the *Mtl* genes. Therefore, it is possible that gene expression as a whole might have differed between the cell lines and thus contributed to the variation observed in Figure 6.1.a-b. Additionally, *modifier genes*, which may lead to varying levels of mutational expressivity, have been identified in various inbred mouse models and could therefore have contributed if present (Distelmaier *et al.*, 2009; JAX, 2006). It should further be considered that the cells used in this study were primary cell cultures obtained from different mice. Although the *biological variation between animals* should theoretically be reduced by the use of cell cultures, it cannot be ignored that inter-mouse differences are observed when comparing the life span, phenotype and metabolome of the animals (Johnson *et al.*, 2013; Kruse *et al.*, 2008; Louw, 2017, personal communication). Another important factor to consider is the *purity* of the cell culture. Although the fibroblasts in this study appeared to be morphologically identical, and while the growth of fibroblasts is reported to outcompete that of other cell types (e.g. keratinocytes) at very early passages (first and second), primary lines are not entirely pure (Auburger *et al.*, 2012; Takashima, 1998:2.2.11). In support hereof, differences were observed in the cell size within a genotype following inspection by flow cytometry (refer to Figures 6.6.b and 6.6.c, discussed in Section 6.6). Since the cell type was not explicitly tested for in this study, the question of the effect of purity remained a possibility.

Had the results not been influenced by intra-genotype variability, the cell viability displayed by the WT and OVER cell lines would have been expected to be similar. Moreover, as the loss of NDUFS4 was shown to interfere with the stability of CI (see Section 5.7), it would have been reasonable to anticipate that the KO cell lines would exhibit lowered cell viability in comparison to the WT and OVER samples. While no change in cell growth was reported by Valsecchi *et al.* (2013) in their analyses of the cell cycle of *Ndufs4*$^{-/-}$ fibroblasts (cultured in glucose-containing medium) when compared to *Ndufs4*$^{+/+}$ cells, it could be argued that the use of the OXPHOS-promoting galactose-containing medium would have allowed for the decrease in the viability of the KO cells used in this study, due the forced increase of OXPHOS usage imposed by galactose. Finally, as a result of their ROS scavenging abilities, the overexpression of MTI would have been expected to return, or at least increase, the lowered cell viability of the KO OVER cell lines to that of the WT samples.

Although it is not possible to identify the source of variability from the experiments conducted in this study, unaccounted variability between cell lines of similar genotypes might be reduced in the future by increasing the period of cell culture ranging from thawing to experimental analysis. Additionally, the reproducibility may be improved by assessing the identity (purity) of the cell line, and constructing growth curves to ensure that analyses are performed on cells occurring in the same growth state (Baker, 2016; Hughes *et al.*, 2007).

## 6.3 DETERMINING THE RMCN BY qPCR ANALYSIS – *Objective 2.2*

### 6.3.1 INTRODUCTION

The effect of each of the four genotypes on mtDNA replication (as an indicator of mitochondrial biogenesis) was assessed by measuring the RMCN, as explained in Section 4.4.2. This was accomplished by determining the $C_T$-values of all eight cell lines, yielded by the amplification of the *mt-Nd2* (target) and nuclear *Actb* (reference) genes. To evaluate the specificity of the *mt-Nd2* TaqMan® Gene Expression Assay to mtDNA, the DNA from a $\rho^0$ cell line was amplified as a negative control for mtDNA. Since no outliers were present, the data obtained was then processed as discussed, substituted into the $2^{-\Delta CT}$ formula and multiplied by two. In this manner, the mtDNA copy number, quantified relative to a single copy of nuclear *Actb,* was obtained. Additionally, the pooled SDs were calculated for each data set according to Equation 5.1.

### 6.3.2 RESULTS

Figure 6.2.a depicts the RMCN values for the negative control and the first set of cell lines, while the RMCN of the second set of cell lines is shown in Figure 6.2.b:

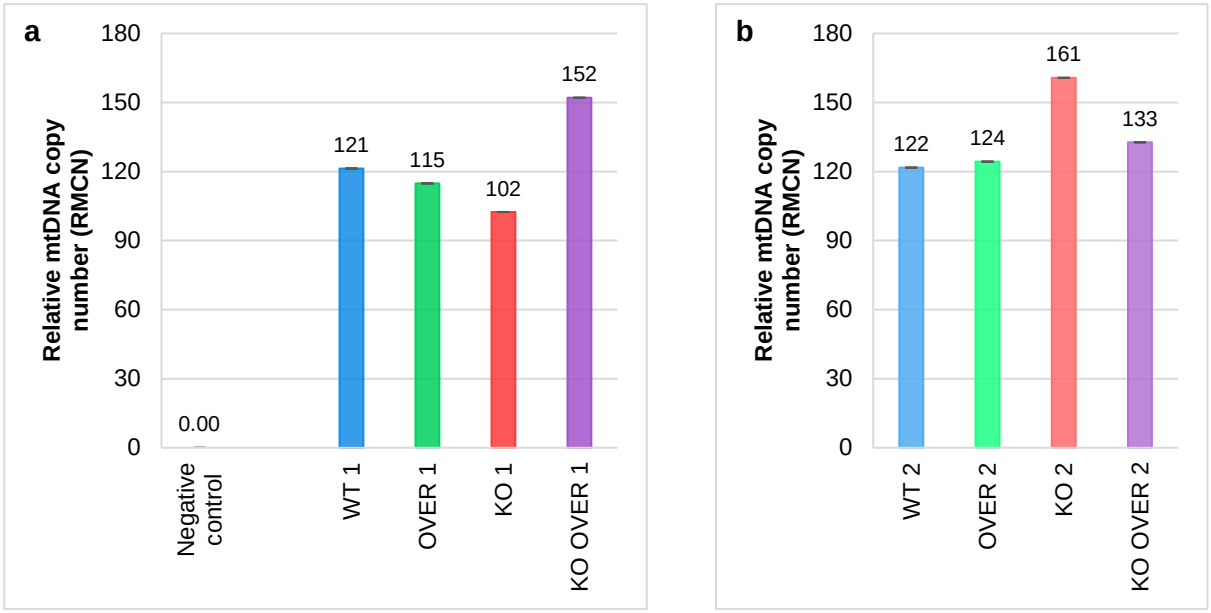


**Figure 6.2.a-b: Bar charts depicting the RMCN of two sets of cell lines, each comprising the four genotypes of interest.** The copy number of the *mt-Nd2* gene (representing the mtDNA), quantified relative to a single copy of nuclear *Actb,* is shown for **(a)** the negative control ($\rho^0$ cells), as well as the first and **(b)** second set of cell lines. The exact copy number is indicated above the respective bar. (n = 3) ± SD.

As shown in Figure 6.2.a, no mtDNA copies were detected for the negative control. This was due to the lack of *mt-Nd2* target gene amplification observed for this sample. Since $\rho^0$ cells lack mtDNA, the result indicated that the *mt-Nd2* TaqMan® Gene Expression Assay was specific for mtDNA.

### 6.3.3 DISCUSSION

As explained in Section 4.4.2, the results shown in Figure 6.2.a-b were obtained by calculations involving the means (n = 3) of the target and reference genes of each sample. Moreover, only one DNA sample was analysed per cell line. Therefore, as a single RMCN value was obtained for each sample, it was not possible to perform statistical analyses on the data. However, since the pooled SDs determined for each sample were extremely small, the results could therefore be interpreted with confidence and it was decided to discuss the data of all eight cell lines.

As may be seen from Figure 6.2.a-b, the WT and OVER samples exhibited comparable mtDNA copy numbers (ranging from 115 to 124), with very little intra-genotype variation. It was therefore concluded that the overexpression of MTI did not influence the replication of mtDNA in the OVER

genotype. The RMCN was, however, clearly increased in KO 2 and both of the KO OVER cell lines. As mentioned in Section 2.6.2, mitochondrial biogenesis, which includes the replication of mtDNA, is modulated by the cell's energy requirement and oxidative stress level (Butow & Avadhani, 2004; Jones *et al.*, 2012). Both these factors are further known to be affected by mutations in the OXPHOS complexes (Reinecke *et al.*, 2009). While no significant differences were observed for the ATP/ADP ratio (Section 6.5.3) or ATP production (Section 6.7.3), the possible effect of oxidative stress could not be ruled out due to the lack of reproducibility observed for this parameter. It was therefore plausible that the RMCN could have been increased in fibroblasts with an *Ndufs4*$^{-/-}$ genotype due to the oxidative stress imposed on the cell by the lack of the NDUFS4 subunit.

While the RMCN in the KO OVER group was less than that of the KO 2 sample, no definite conclusions could be drawn about the effect of MTI overexpression on CI deficiency due to the large intra-genotype variation within the KO group. To assess whether this intra-genotype variation was due to experimental error, the assay was performed again using new DNA samples of each cell line. Subsequently, the same trends as those shown in Figure 6.2.a-b were observed. For this reason, as well as the fact that the SD of each data point was almost negligible in both assays, the variation between the individual cell lines of a particular genotype group was instead attributed to the variation associated with cell culture, as explained in Section 6.2. The difference in the RMCN values of KO 1 and KO 2 were therefore interpreted as the difference in cellular stress experienced by each of the cell lines, possibly due to factors inherent to the cells themselves or the culture process. The reduced RMCN observed for KO 1 could therefore be explained in one of two ways: Either the cellular stress exerted on KO 1 (due to the knockout of the *Ndufs4* gene) was not severe enough to elicit an increase in mtDNA copy number (as seen in KO 2), or the cellular stress experienced by KO 1 was much more severe than that experienced by KO 2, thereby resulting in mtDNA degradation or mitophagy (Lee & Wei, 2005). Since KO 1 exhibited a high cell viability (Figure 6.1.a), the former applied in this case. It was therefore hypothesised that KO 1 was not as severely affected by *Ndufs4*'s knockout as KO 2. Since both an increase and decrease in mtDNA copy number have been observed during CI deficiency, and as the life span, phenotype and metabolome of the animals do differ, this was considered plausible (Johnson *et al.*, 2013; Kruse *et al.*, 2008; Louw, 2017, personal communication; Reinecke *et al.*, 2009).

## 6.4 QUANTIFYING THE RELATIVE NADH/NAD$^+$ RATIO – *Objective 2.3*

### 6.4.1 INTRODUCTION

As explained in Section 4.4.3, the redox status of the eight cell lines was determined by measuring the total cellular NADH and NAD$^+$ of each sample in triplicate. In order to correct for non-specific

background, three blank wells containing only reagent were included on the microtiter plate. In addition, triplicate wells of a positive control, comprising 400 nM $NAD^+$ (in 1x PBS), were prepared to evaluate the cycling enzyme. Following analysis, the data of each well was then processed by respectively subtracting the mean of the blank wells' NADH measurements and $NAD^+$ measurements (in RLUs) from the NADH and $NAD^+$ values of each sample and the positive control. Hereafter, the NADH/$NAD^+$ ratio was calculated for each well. Since no outliers were present, the mean and SD of the NADH/$NAD^+$ ratios were then determined for each sample and the positive control. To present the results, the NADH/$NAD^+$ ratio of each sample was expressed as a percentage of that of WT 1, while the percentage $NAD^+$ was calculated by doing the same for the positive control, using the mean $NAD^+$ of WT 1 as a reference.

### 6.4.2 RESULTS

The final data points of each genotype of the two sets of cell lines as well as the positive control may be found in Figure 6.3.a-c:

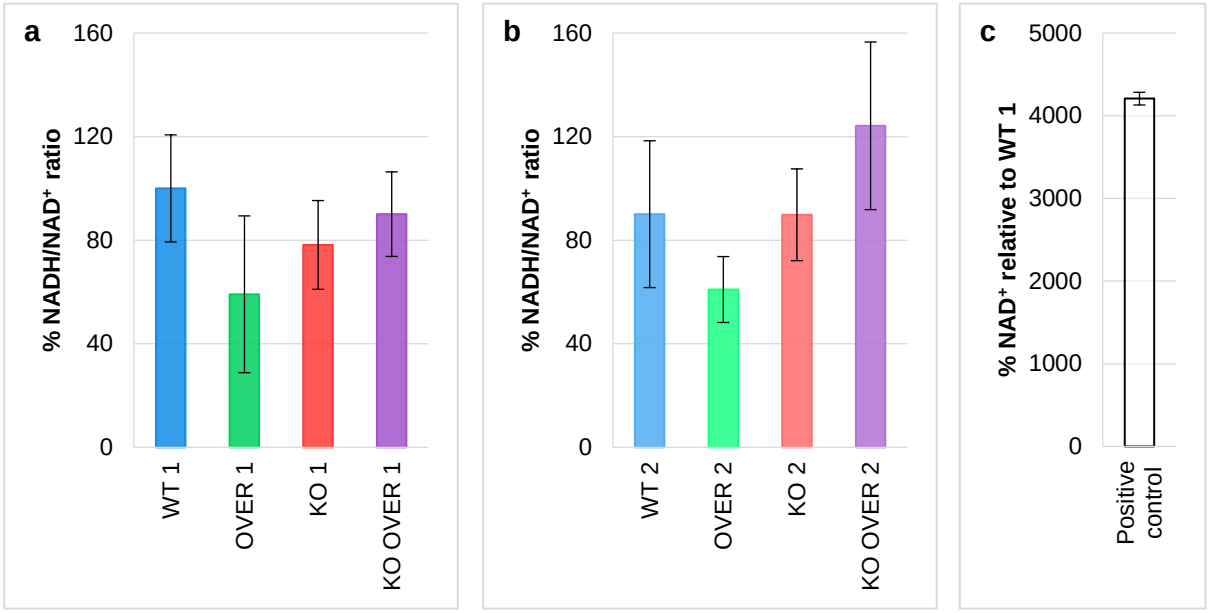


**Figure 6.3.a-c: Bar charts depicting the percentage NADH/$NAD^+$ ratio of two sets of cell lines, each comprising the four genotypes of interest, as well as the percentage $NAD^+$ of the positive control. (a)** For the first and **(b)** second set of cell lines the NADH/$NAD^+$ ratio is shown as a percentage of WT 1, following analysis by the NAD/NADH-Glo™ assay. **(c)** In addition, the $NAD^+$ measurement of the positive control (400 nM $NAD^+$ in 1x PBS) is shown as a percentage of that of WT 1. (n = 3) ± SD. Statistical analyses were performed according to parametric tests, as explained in Section 4.4.7.1.

As shown in Figure 6.3.c, the high signal obtained for the positive control (relative to WT 1) indicated that the cycling enzyme used was functional.

### 6.4.3 DISCUSSION

From Figures 6.3.a and 6.3.b, a similar tendency was observed across the four genotypes for the two sets of cell lines analysed. This indicated that the results between the cell lines of a single genotype were reproducible and that conclusions could be drawn from the data. Upon comparison to WT 1, the NADH/$NAD^+$ ratio displayed by the OVER 1 sample was found to be reduced by ~40%, whereas the KO 1 and KO OVER 1 samples yielded decreases of ~20% and ~10% each. However, none of these relationships were of statistical significance when comparing the genotype groups, possibly due to the high SD observed within each data point. Since ratios, which are internally normalised, were compared in this assay, the reason for the high variance in the data was attributed to the small number of replicates (n = 3) analysed (due to reagent restrictions).

As various studies (as well as the results of Section 5.6 of this study) have indicated that CI's activity is decreased by the absence of NDUFS4, it was expected that the NADH/$NAD^+$ ratio of KO 1 would be increased in comparison to WT 1 due to the accumulation of CI's substrate, NADH (Calvaruso *et al.*, 2012; Papa *et al.*, 2010; Quintana *et al.*, 2010; Scacco *et al.*, 2003). Indeed, such an increase was observed by Valsecchi *et al.* (2012) when the group compared the redox couple in the immortalised embryonic fibroblasts of *Ndufs4*$^{+/+}$ and *Ndufs4*$^{-/-}$ mice. It should be considered that the assay employed in this study detected the total cellular NADH and $NAD^+$ in lysed cells (i.e. the NAD pool, consisting of free and protein-bound forms of NADH and $NAD^+$ in all cellular compartments). According to Bilan and Belousov (2016), the NADH/$NAD^+$ ratio of the NAD pool can vary considerably in different cellular organelles. Whereas cytoplasmic NADH/$NAD^+$ may range from 1 to 700 in mammalian cells, the ratio has a much smaller range (1 to 8) within an organelle like the mitochondrion. It is therefore conceivable that the mitochondrial NADH/$NAD^+$ ratio was not affected to such an extent in this study as to significantly influence the total cellular NADH/$NAD^+$ ratio.

While no significant difference was observed, it was expected that the overexpression of MTI in KO OVER 1 would decrease the NADH/$NAD^+$ ratio in comparison to the KO 1 sample in this experiment. This was based on the observation by Lindeque (2011) that MTI and MTII display a protective effect on rotenone-induced CI-deficient cells: In this study it was found that *MtI + MtII* KO mice displayed an increased concentration of lactate when compared to WT mice. Since the production of lactate from pyruvate replenishes $NAD^+$, an increased lactate concentration suggested more depleted $NAD^+$ and thus increased NADH in the absence of MTI and MTII.

In the future, this hypothesis, as well as the notion that NADH increases in CI deficiency, may be better studied by specifically analysing the mitochondrial NADH/$NAD^+$ ratio. In addition, the variance observed within the data may be reduced by the use of more replicates.

## 6.5 QUANTIFYING THE RELATIVE ATP/ADP RATIO – *Objective 2.4*

### 6.5.1 INTRODUCTION

The total cellular energy status (ATP/ADP ratio) was evaluated in triplicate for each sample, by using a bioluminescent assay, as explained in Section 4.4.4. Additionally, non-specific background was accounted for by analysing three blank wells containing only reagent. On the same microtiter plate, a positive control consisting of 500 nM ATP (in 1x PBS) was prepared to evaluate the ATP reagent. The data obtained was subsequently processed by subtracting the mean of the blank from each value across all three measurements of the samples and the $RLU_A$ (i.e. ATP measurement) measurement of the positive control. Hereafter, the ATP/ADP ratio of each well was determined as shown in Equation 4.2. Due to the small number of replicates analysed (n = 3), outliers could not be identified and removed according to Tukey's method. As an alternative, outliers were taken as those values causing a CV% of ≥20% in the data point (van der Westhuizen, 2017b, personal communication). Using the remaining values, the mean and SD within each data point were then calculated and the ATP/ADP ratio of each sample was expressed as a percentage of that of WT 1. A similar approach was followed to determine the percentage ATP of the positive control, using the mean $RLU_A$ measurement of WT 1 as a reference.

### 6.5.2 RESULTS

While non-parametric tests were performed to assess the statistical difference in the data, the number of replicates (n = 3) was too small to construct box plots. Results were therefore presented as bar charts, as shown in Figure 6.4.a-c:

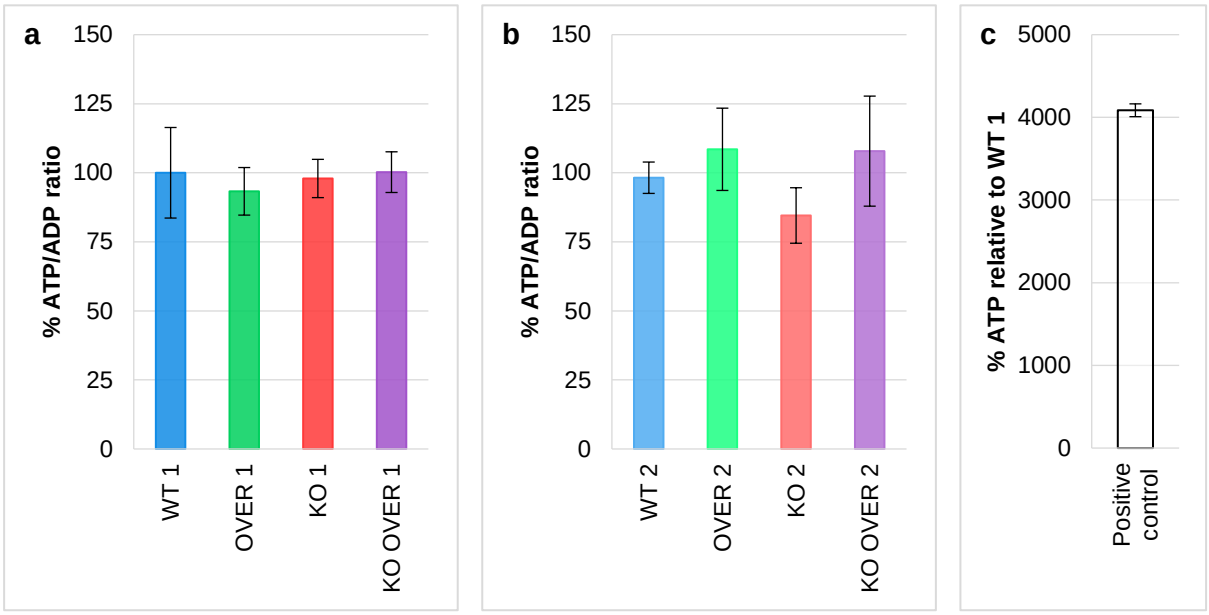


**Figure 6.4.a-c: Bar charts depicting the percentage ATP/ADP ratio of two sets of cell lines, each comprising the four genotypes of interest, as well as the percentage ATP of the positive control. (a)** For the first and **(b)** second set of cell lines, the ATP/ADP ratio is shown as a percentage of WT 1 following analysis by the ADP/ATP Assay Kit. **(c)** The quantity of ATP of the positive control (500 nM ATP in 1x PBS) is shown as a percentage of that of WT 1. (n = 3) ± SD. Statistical analyses were performed according to non-parametric tests, as explained in Section 4.4.7.1.

The high percentage ATP yielded by the positive control in comparison to the WT 1 sample (Figure 6.4.c) was interpreted as the accurate functioning of the ATP reagent.

### 6.5.3 DISCUSSION

As depicted in Figures 6.4.a and 6.4.b, no discernible trend was evident when comparing the results obtained for the first and second set of cell lines. Instead, the ATP/ADP ratio of all eight samples fell within a similar range (from 84.5% to 108%) with overlapping SDs. Additionally, since these SDs were small and no statistically significant differences were observed between the genotypes of a set of cell lines, it was concluded that the results were reproducible and that the genetic modifications had not disturbed the cellular ATP homeostasis. In support hereof, the obtained results corresponded to a study by Valsecchi *et al.* (2012) in which the total cellular ATP,

determined using a bioluminescent assay, was not found to be markedly altered between the immortalised embryonic fibroblasts of *Ndufs4*$^{+/+}$ and *Ndufs4*$^{-/-}$ mice.

Recall that fibroblasts are considered to be mainly glycolytic (Section 4.4 and 5.3) (Voets *et al.*, 2012). As a result, this cell type relies more heavily on glycolysis to produce ATP when cultured in glucose-containing medium. In this experiment, cells were deprived of glucose by switching to galactose-containing medium prior to analysis. Since the conversion of galactose to the glycolysis substrate G-6-P (via glucose-1-phosphate) occurs very slowly, galactose-containing medium forces the fibroblasts to produce ATP via the oxidation of alternative substrates (like pyruvate and glutamine). The majority of catabolic products generated in this manner ultimately culminate on the OXPHOS-system, thereby increasing the reliance of fibroblasts on OXPHOS-derived ATP production (Melcher *et al.*, 2017; Voets *et al.*, 2012). Since no significant difference was observed in the cellular ATP/ADP ratio of the KO 1 sample in comparison to WT 1, it may therefore be concluded that this cell line was able to effectively adjust to *Ndufs4*'s knockout. While mechanisms cannot be inferred from the results of this experiment, possible methods might include the increased use of metabolic pathways or shuttles that enable CII-derived ATP production (e.g. $FADH_2$ generation via fatty acid β-oxidation, or the irreversible glycerophosphate shuttle), the increased use of pathways that donate electrons to Q, and/or the use of CI, despite its lack of NDUFS4, via the formation of CI-containing supercomplexes like $CI+CIII^2$, as shown by Calvaruso *et al.* (2012). The formation of supercomplexes corresponds to the lack of a significant increase observed in the $NADH/NAD^+$ ratio of KO 1 (Section 6.4). Another possibility is that selection had occurred against the KO phenotype to favour the growth of less severely affected- or better adjusted cells (explained in detail in Section 6.7.3). Since the ATP/ADP ratio of OVER 1 and KO 1 were not altered in relation to WT 1, no change was expected to occur in the ATP/ADP ratio of the KO OVER 1 sample.

## 6.6 DETERMINING THE ROS LEVELS USING THE BD FACSVerse™ FLOW CYTOMETER – *Objective 2.5*

### 6.6.1 INTRODUCTION

As described in Section 4.4.5, the intracellular oxidative status of all eight cell lines was determined in triplicate by quantifying the ROS production using the BD FACSVerse™ flow cytometer. To optimise the sample- and fluorescence detection, an unstained cell control and stained positive ROS control (pre-treated with 4 mM $H_2O_2$) were prepared from WT 1 cells. Following data analysis, a gMFI value representing the fluorescence of the ROS sensitive probe (C-DCFH-DA-AM) was obtained for each replicate. Since the number of replicates analysed was too small to use Tukey's method (n = 3), outliers were removed as described in Section 6.5. For

each sample, as well as the controls, the mean gMFI together with the SD within each data point, was calculated, after which the data was expressed as a percentage of WT 1.

### 6.6.2 RESULTS

Figure 6.5.a depicts the results obtained for the cell- and positive controls, as well as the first set of cell lines, whereas the results of the second set of cell lines are shown in Figure 6.5.b:

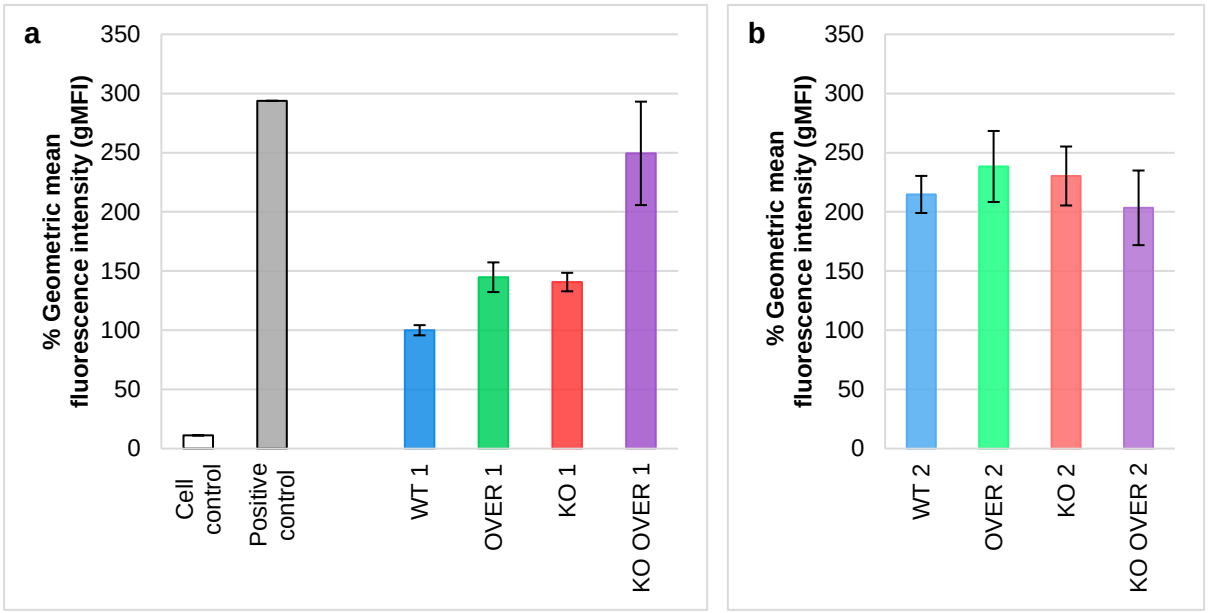


**Figure 6.5.a-b: Bar charts depicting the percentage ROS, expressed as the gMFI, of two sets of cell lines, each comprising the four genotypes of interest. (a)** The fluorescence intensity of ROS is reported as a percentage of WT 1 for the cell- and positive controls, as well as the first and **(b)** second set of cell lines. (n = 3) ± SD. Statistical analyses were performed according to parametric tests, as explained in Section 4.4.7.1.

To depict the difference in fluorescence yielded by the cell- and positive controls, a histogram of the cell count against fluorescence is shown in Figure 6.6.a. In Figures 6.6.b and 6.6.c the difference in cell size (as an indicator of possible variances in cell purity) is illustrated between two cell lines of the same genotype, OVER 1 and OVER 2.

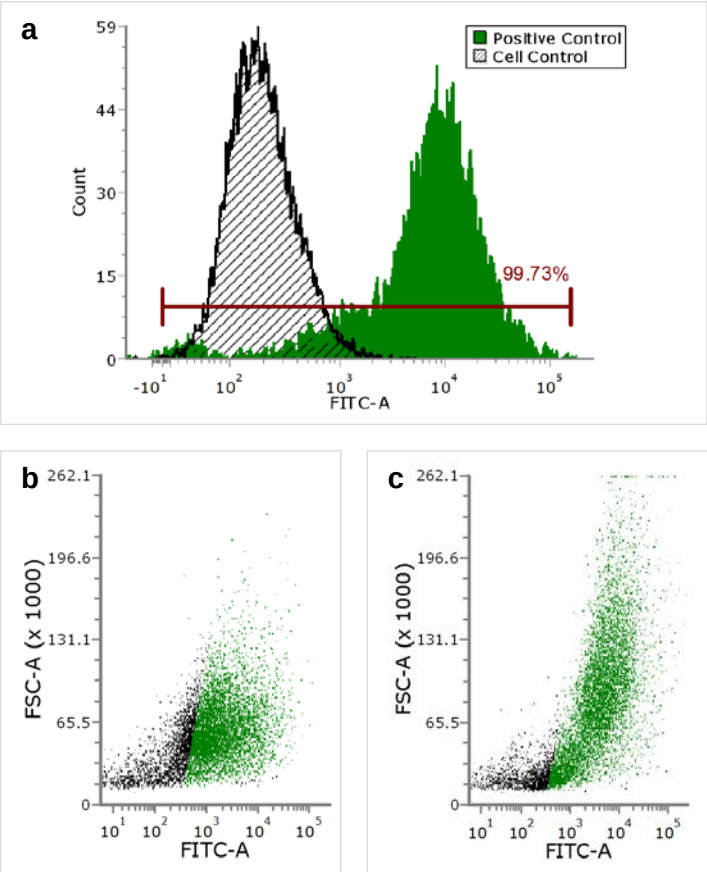


**Figure 6.6.a-c: Histogram depicting the fluorescence of the cell- and positive controls, and two dot blots illustrating the differences in cell size between two genetically identical cell lines.** Data was collected for 100 000 events and plotted as described in Section 4.4.5. **(a)** The difference between the fluorescence of the cell control (in black) and positive control (in green) are depicted in a histogram of cell count against FITC. The percentage gated cells is displayed in maroon, and the data has been normalised to the number of events. To illustrate the difference in cell size (as an indicator of variances in cell purity) between cell lines of the same genotype, dot blots of FSC against FITC are shown for **(b)** OVER 1 and **(c)** OVER 2. Here, cell size increases to the top of the y-axis and gated areas (in green) represent the specific cell population analysed. All measurements are given in relative units.

### 6.6.3 DISCUSSION

Considering the validity of the controls used in this experiment, the cell control shown in Figures 6.5.a and 6.6.a yielded a very low level of fluorescence in contrast to the samples and positive control. As the cell control was unstained, this value was interpreted as autofluorescence displayed by the cells themselves. The positive control, in turn, did not produce as high a level of fluorescence as expected. This was attributed to the highly reactive nature of $H_2O_2$ which, in a cellular suspension, would react with the residual medium and the external surface of the cells,

thereby resulting in less available $H_2O_2$ to enter the cell and react (in radical form) with the activated ROS-sensitive probe. Since the positive control was only used to optimize the detection of fluorescence by the flow cytometer, and as it still displayed a higher fluorescence than any of the samples analysed, its degree of fluorescence did not affect the results. Considering that, although widely used, the DCFH-DA probe and its analogues have limitations with regards to specificity, it was concluded that the probe was indeed sensitive to ROS due to the difference in fluorescence observed between the cell control and positive control, as well as the increased fluorescence displayed by the positive control in comparison to the samples (Kalyanaraman *et al.*, 2012). Furthermore, while the variance in the KO OVER 1 sample was higher than ideal, as indicated by its calculated SD in Figure 6.5.a, it was regarded as acceptable for the purpose of this experiment since the sample's CV% was below 20%.

As shown in Figure 6.5.a-b, a repeatable trend was not observed when comparing the four genotypes between each set of cell lines. Whereas well-defined differences existed among the genotypes of the first set of cell lines (e.g. the ~150% increase in gMFI observed for KO OVER 1, in comparison with WT 1), the fluorescence values measured for each genotype in the second set of cell lines (Figure 6.5.b) all fell within a similar range. This example clearly illustrates the importance of evaluating the reproducibility of the findings between different cultures of genetically identical primary fibroblasts. Thus, as a result of the lack of repeatability between cell lines of the same genotype, no inferences could be made from the data concerning the effect of *Ndufs4*'s knockout, the overexpression of MTI, or both mutations on ROS production.

Instead, it was concluded that the variation associated with cell culture, as discussed before, had contributed appreciably to the production of ROS, thereby possibly masking the effect of the genotype on the cellular oxidative stress. Indeed, studies have shown that ROS production is frequently influenced by the cell culture conditions employed (Rodenburg, 2016). Moreover, the level of cellular oxidative stress has been reported to vary due not only to the severity of CI dysfunction, but also as a result of the adaptive response program, both of which may further be cell type-specific (Koopman *et al.*, 2013; Reinecke *et al.*, 2009). Since the purity of the primary fibroblasts used in this study was not explicitly investigated (as explained in Section 6.2), it is therefore possible that the variances observed between the genetically identical cell lines were influenced by this. In support hereof, dot blots of FSC against FITC (Figures 6.6.b and 6.6.c) displaying two representative cell lines of the same genotype, OVER 1 and OVER 2, are shown. In these graphs, the FSC (y) and FITC (x) axes respectively indicate cell size and ROS-sensitive fluorescence, with an increase in each parameter occurring to the top and right of the corresponding axes (du Plessis *et al.*, 2010). The green area in turn represents the gate that was set, and thus the cell population that was analysed in this experiment. From the figures, it is clear that there is a difference in the number of cells corresponding to certain sizes between the two cell lines, with OVER 2 displaying a greater population of larger cells (≥131 relative units). This

inconsistency could thus be interpreted as small differences in the purity of the cell lines used in this experiment. While many studies report on the differential ROS production occurring in the primary fibroblasts of patients with *NDUFS4* mutations, discrepancies have also been observed in different cell- and tissue types of the Ndufs4 mouse model itself, e.g. between immortalised mouse embryonic-, primary skin-, and primary muscle fibroblasts (Iuso *et al.*, 2006; Koopman *et al.*, 2013; Melcher *et al.*, 2017; Valsecchi *et al.*, 2012). Consequently, although it is possible that the production of ROS was simply not affected by the genotype in this experiment, its cellular concentration might have been influenced by natural (differences in cellular processes) and/or experimental factors (cell culture differences).

If the genotype had influenced ROS production, the following results would have been expected: Firstly, since neither the WT or OVER cells were under increased oxidative stress, their levels would have been expected to be similar and low. In comparison with these genotypes, the fluorescence displayed by the KO cell lines would have been anticipated to increase, due to the decreased activity displayed by CI (discussed in Section 5.7). Indeed, this result was observed by Valsecchi *et al.* (2013) for immortalised embryonic fibroblasts of *Ndufs4*$^{-/-}$ mice when compared to those from *Ndufs4*$^{+/+}$ mice. Lastly, as illustrated in HeLa cells by Reinecke *et al.* (2006), the ROS scavenging properties of MTI would ideally have been expected to lower the cellular ROS produced by the KO OVER cell lines to values closer to or comparable with that produced by the WT and OVER genotypes (Babula *et al.*, 2012; Penkowa *et al.*, 2006).

In the future, the methodology of ROS analysis in fibroblasts might be revised in several ways. As done by Reinecke *et al.* (2006), ROS could be measured in microtiter plate format (i.e. measuring the population effect instead of the individual effect on a subpopulation of cells), with and without a stressor such as the CI inhibitor, rotenone. In this manner, the cells might be subjected to less experimental variation than that possibly encountered in this experiment (e.g. variation possibly caused by harvesting cells close to the time of analysis). While the use of galactose in this study led to a state of increased cellular oxidative stress [in comparison with previous attempts using glucose (results not shown)] and was therefore suspected to enhance the distinction between the WT and KO-produced ROS, rotenone is more specific to CI (binding to the NDUFS2 subunit)[40] (Voets *et al.*, 2012). Therefore, the use of rotenone instead of galactose will give a better indication of CI-, and thus mitochondrial-, produced ROS. Finally, considering the reported lack of specificity of DCFH-DA (and its analogues) as a ROS probe, more specific probes such as Amplex® Red, hydroethidine or MitoSOX™ Red could be used (Kalyanaraman *et al.*, 2012).

[40] NDUFS2 is located in the Q module of CI and should therefore not be influenced by a lack of NDUFS4 (Mimaki *et al.*, 2012; Pineau *et al.*, 2005; Prieur *et al.*, 2001).

## 6.7 DETERMINING THE BIOENERGETICS PROFILE USING THE SEAHORSE XF$^e$96 ANALYSER – *Objective 2.6*

### 6.7.1 INTRODUCTION

As described in Section 4.4.6, the bioenergetics profile of each of the four mouse fibroblast genotypes was evaluated in an intact cellular environment by performing an optimised Mito Stress Test, using the XF Analyser. Since Seahorse Bioscience[41] reports a coefficient of variation of up to 20% for inter-day (and thus inter-plate) experiments, all eight cell lines were analysed on the same plate (Dranka *et al.*, 2011). In addition, four blank wells (containing no cells) were included on each microtiter plate (see Appendix D) to serve as both temperature- (for the temperature-sensitive $O_2$-fluorophore) and background correction controls (Dranka *et al.*, 2011). Using the information gathered by these wells, the Wave Controller software (v2.4) was consequently able to automatically correct the data for temperature drift and non-specific background readings. Moreover, inter-well differences in cell seeding density were accounted for by normalising each well to its total nucleic acid content, using the CyQUANT® Cell Proliferation Assay Kit. Since cellular nucleic acid content is reported to be tightly regulated, the information could be interpreted as an indication of cell number (Jones *et al.*, 2001; van den Bossche *et al.*, 2015).

The data obtained was processed by exporting the measurements (normalised to cell number and multiplied by a scale factor of $10^4$ to obtain values of appreciable size) of the Mito Stress Test (OCR values) into Microsoft Excel 2013, where outliers were identified via the Tukey method. Using the Wave Desktop software (v2.4), these outlier wells were subsequently removed across all measurements of the Stress Test. The data was then exported into Microsoft Excel 2013 via the Seahorse XF Cell Mito Stress Test Report Generator (Agilent, 2017). This enabled the automatic calculation of the parameters, as shown in Table 6.1, from the normalised, outlier-free values.

While more information is obtainable from the Mito Stress Tests (as depicted in Figure 4.5), only the parameters shown in Table 6.1 were reported. This was done for the reasons given in Section 4.4.6.2. As previously shown by van Dyk (2016), the parameters reported in this dissertation were considered to be consistent with regards to the instrument.

[41] The Seahorse XF Analyser was originally developed, manufactured, and supplied by Seahorse Bioscience Inc. In 2015, the company was acquired by Agilent Technologies.

**Table 6.1: Equations used by the Seahorse XF Cell Mito Stress Test Report Generator to obtain the reported parameters**

| Parameter | Equation |
|---|---|
| **Non-mitochondrial respiration** | Minimum rate measurement after rotenone and antimycin A injection |
| **Basal respiration** | Measurement 3 - Non-mitochondrial respiration |
| **Maximal respiration** | Maximum rate measurement after FCCP injection - Non-mitochondrial respiration |
| **ATP production** | Measurement 3 - Minimum rate measurement after oligomycin injection |

The table displays the calculations used to obtain the parameters reported for the Mito Stress Test, as shown in Figures 6.7.a-f. As a reference for the measurements, Figure 4.5 may be consulted. Measurement equations were obtained from the Seahorse XF Cell Mito Stress Test Report Generator (Agilent, 2017).

### 6.7.2 RESULTS

The calculated values were subsequently used to perform statistical analyses and to construct the box plots depicted in Figures 6.7.a-f:

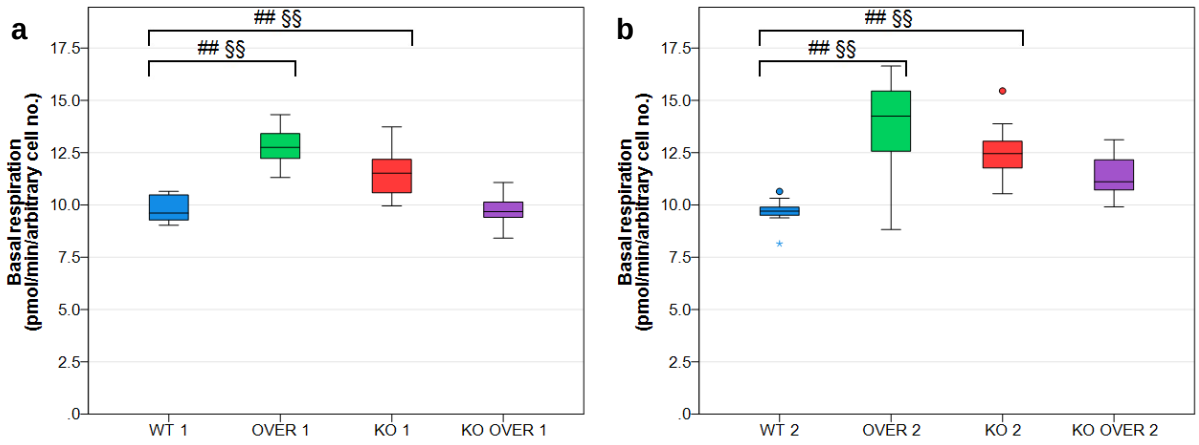


**Figure 6.7.a-b: Box plots depicting the basal respiration of two sets of cell lines, each comprising the four genotypes of interest. (a)** The OCR values for the basal respiration are shown for the first and **(b)** second set of cell lines. (n = 11 to 12) ± SD. Circles and asterisks represent outliers and extreme outliers, respectively. Hashes indicate significant differences between genotype groups within a set of cell lines (## p ≤0.05; # p ≤0.1), whereas effect size is shown as § (§ |ω| ≥0.3; §§ |ω| ≥0.5). Statistical analyses were performed according to non-parametric tests, as explained in Section 4.4.7.1.

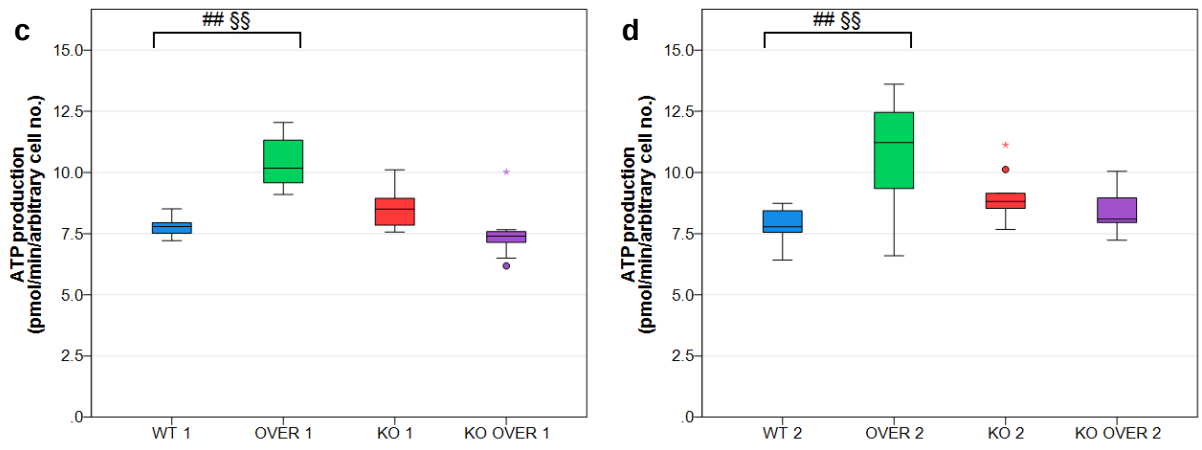


**Figure 6.7.c-d: Box plots depicting the ATP production of two sets of cell lines, each comprising the four genotypes of interest. (c)** The OCR values for the ATP production are shown for the first and **(d)** second set of cell lines. (n = 11 to 12) ± SD. Circles and asterisks represent outliers and extreme outliers, respectively. Hashes indicate significant differences between genotype groups within a set of cell lines (## p ≤0.05; # p ≤0.1), whereas effect size is shown as § (§ |ω| ≥0.3; §§ |ω| ≥0.5). Statistical analyses were performed according to non-parametric tests, as explained in Section 4.4.7.1.

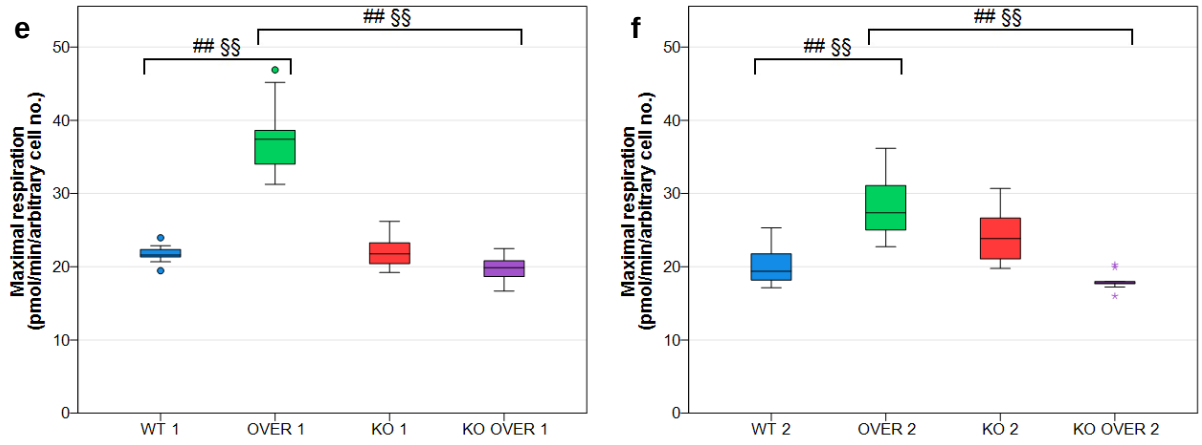


**Figure 6.7.e-f: Box plots depicting the maximal respiration of two sets of cell lines, each comprising the four genotypes of interest. (e)** The OCR values for the maximal respiration are shown for the first and **(f)** second set of cell lines. (n = 11 to 12) ± SD. Circles and asterisks represent outliers and extreme outliers, respectively. Hashes indicate significant differences between genotype groups within a set of cell lines (## p ≤0.05; # p ≤0.1), whereas effect size is shown as § (§ |ω| ≥0.3; §§ |ω| ≥0.5). Statistical analyses were performed according to non-parametric tests, as explained in Section 4.4.7.1.

### 6.7.3 DISCUSSION

Upon comparing the data of the Mito Stress Test parameters between the two sets of cell lines analysed (i.e. Figures 6.7.a versus 6.7.b, Figures 6.7.c versus 6.7.d, and Figures 6.7.e versus 6.7.f), a repeatable trend was observed for each. The results between two cell lines of a genotype were therefore regarded as reproducible, and consequently conclusions could be drawn from the first set of cell lines. In general the spread of the data, indicated by the box of the plot (i.e. the interquartile range), across Figures 6.7.a-f was also considered acceptable for the first set of cell lines.

From Figure 6.7.a, a statistically significant increase ($p = 0.011$, $|\omega| = 0.731$) was seen in the basal respiration of KO 1 in comparison to WT 1. In addition, a very slight, but non-significant increase was observed for the ATP production (Figure 6.7.c) and maximal respiration (Figure 6.7.e) of KO 1. In the Mito Stress Test, OCR was measured in low buffered medium containing galactose (instead of glucose) and sodium pyruvate. While galactose could be used for the glycolytic production of ATP, the process occurred very slowly (as explained in Section 6.5) and consequently cells were forced to depend more on OXPHOS. Sodium pyruvate, on the other hand, fed directly into the TCA cycle to yield NADH as a substrate for CI-driven ATP production. Since oxygen consumption was therefore largely dependent on CI's ability to transfer electrons via a functional N module – the stability of which has been shown to be reduced in the *Ndufs4*$^{-/-}$ mouse – the basal respiration, ATP production, and maximal respiration displayed by KO 1 were expected to be lower than that of WT 1 (Calvaruso *et al.*, 2012; Kruse *et al.*, 2008; Valsecchi *et al.*, 2012). While these parameters have been shown to be significantly decreased in the isolated mitochondria of *Ndufs4*$^{-/-}$ mice when compared to *Ndufs4*$^{+/+}$ mice, the same was not observed for this study (Chen *et al.*, 2017; Kayser *et al.*, 2013; Song *et al.*, 2017; van Wyk, 2016). In order to explain the difference between the results obtained for fibroblasts and mitochondria, the effect of cell culture on the expression of the KO phenotype was considered. Since cells cultured *in vitro*, especially those obtained from a primary explant, differ in their individual fitness and proliferation rates, a degree of competition will occur over time among neighbouring cells for access to substrates. This competition, which might e.g. present as differences in cellular gene expression, -proliferation, and/or -adaptation, will ultimately result in the selection against weaker, more damaged, and/or slower-proliferating cells (e.g. via apoptosis or the rate of cell division) (Raj & van Oudenaarden, 2008; Sancho *et al.*, 2013; Shakiba & Zandstra, 2017). Consequently, a culture of stronger cells, more inclined to adapt to the harsh conditions of CI deficiency, will remain and can therefore yield results that differ from those observed *in vivo*. By contrast, mitochondria are assessed immediately following their isolation. The *in vivo* phenotype is thus maintained, and the result is a clear decrease in the bioenergetics profiles of *Ndufs4*$^{-/-}$ mice compared to *Ndufs4*$^{+/+}$ mice. While cultures were used at very low

passage numbers in this study (i.e. passage four), it is nevertheless possible that a less severely affected- or better adjusted phenotype was unknowingly selected for during cell culture.

Interestingly, a significant increase was observed in the basal respiration (Figure 6.7.a: $p = 0.002$, $|\omega| = 0.845$), ATP production (Figure 6.7.c: $p = 0.002$, $|\omega| = 0.845$) and maximal respiration (Figure 6.7.e: $p = 0.002$, $|\omega| = 0.845$)[42] of OVER 1 in comparison to WT 1. Since no experiments were conducted to evaluate the specific mechanism of MTI's putative effect on CI, the RC, or the OXPHOS system, the reason behind these results can only be speculated on. Many studies have reported on the ability of MTs to transfer metals (mainly $Zn^{2+}$ and $Cu^{+}$) within the cell (Section 2.6.6.2). Since $Zn^{2+}$ and $Cu^{+}$ are required as cofactors for the function of many enzymes, including members of the OXPHOS system, and as MTs can translocate to the IMS, it is plausible that MTI may directly provide metal ions to these proteins (e.g. CI, CIII to CV and cyt c) (Lindeque *et al.*, 2010). Additionally, MTs located in the IMS have been reported to donate metal ions to IMM-metal transporters, thereby supplying cofactors to proteins located on the matrix side of the IMM (e.g. CII) (Costello *et al.*, 2004). It is thus conceivable that MTs *could increase the electron-flux through the RC via the provision of metal ions*, and thereby enhance the basal- and maximal respiration as well as the translocation of $H^{+}$, and thus the production of ATP. A study by Merten *et al.* (2005) further suggests that MTs may induce a post-translational modification in the cytochrome c oxidase-Va (CCO-Va) subunit of CIV that *improves the RC's utilisation of $O_2$* (and thus the OCR). The results displayed by OVER 1 in Figures 6.7.a, 6.7.c, and 6.7.e further corresponded to the enhanced expression observed for NDUFS4 (~113%) and CI (~36.0%) of the same sample in comparison to WT 1 [see Sections 5.6 (Figure 5.5.b) and 5.7 (Figure 5.6.b)]. Here it was argued that the increased expression of NDUFS4 (and CI) could be the result of MTI's *donation of metal ions to the TFs and/or Zn-finger proteins* participating in *Ndufs4*'s transcriptional pathways (Babula *et al.*, 2012). As also mentioned in Section 5.7, a similar increase in CI's expression was reported in CI-deficient patients pre-treated with the antioxidant Trolox (Distelmaier *et al.*, 2009). As no obvious increase was found in the quantity of the other complexes (following BN-PAGE + western blot analysis; data not shown), and since the basal- and maximal respiration and ATP production of KO OVER 1 was similar to that of WT 1, it is very plausible that the increased respiration observed for OVER 1 was caused by a *CI-specific effect of* MTI. This can however only be confirmed if more samples are analysed via western blot analysis. A final possibility is the *effect of* MTI *on those enzymes* (e.g. α-KGDH and *m*-aconitase) *participating in the metabolic reactions that yield substrates* for the RC (Brown *et al.*, 2000; Feng *et al.*, 2005; Ye

[42] The p-values and effect sizes obtained for Figures 6.7.a, 6.7.c, and 6.7.e were identical. Since these values remained unchanged when the statistical analyses were repeated, this may be regarded as purely coincidental.

*et al.*, 2001). As before, this may proceed via MTI's donation of metal ions to the enzymes involved or the transcriptional machinery encoding them (Babula *et al.*, 2012; Hathout *et al.*, 2001).

Another statistically significant difference was observed between the maximal respiration of OVER 1 and KO OVER 1 (Figure 6.7.e: $p = 0.001$, $|\omega| = 0.847$). This result was as expected. However, since the respiration of KO OVER 1 was very similar to that of WT 1 throughout the entire experiment (in Figures 6.7.a, 6.7.c, and 6.7.e), the difference between OVER 1 and KO OVER 1 was interpreted as the result of the increased respiration observed for OVER 1, and not due to the respiration displayed by the KO OVER 1 sample.

While many studies report on the ROS scavenging ability of MTs, no conclusions regarding the production of ROS could be made in this study (Section 6.6). As a result, no hypotheses regarding MTI's influence on oxidative respiration via the mitigation of ROS could be made. To test the hypothesis of MTI's promotion of cellular survival (via e.g. the reduction of ROS or prevention of apoptosis) and thus its effect on mitochondrial respiration in *Ndufs4*$^{-/-}$ mice, future Seahorse studies would benefit more from using isolated mitochondria from the mice in question (Penkowa *et al.*, 2006; Reinecke *et al.*, 2006).

# CHAPTER 7:

# SUMMARY & CONCLUSIONS

## 7.1 INTRODUCTION

Considering its role in energy metabolism and the number of genes involved, deficiency of CI is the most debilitating and frequently encountered disorder of the OXPHOS system. Due to its progressive and devastating course, as well as the exceptional genetic and clinical heterogeneity accompanying the disorder, no curative treatment is available as of yet. Despite contradicting evidence, the excessive production of ROS and ensuing oxidative damage are accepted as being among the most destructive consequences of CI deficiency (Distelmaier *et al.*, 2009). Previous studies at this institution have elaborated on the adaptive responses involved in CI deficiency, including the increased expression and protective effect of MTs against ROS-mediated cell damage and -death (Lindeque, 2011; Pretorius, 2011; Reinecke *et al.*, 2006; van der Westhuizen *et al.*, 2003). In addition, therapeutic studies involving antioxidants have shown great promise (de Haas *et al.*, 2017). However, in order to properly investigate MT as a putative therapeutic intervention, a *suitable experimental model* has been lacking. To this end, the *Ndufs4* whole-body KO mouse model – a nuclear-encoded genetic animal model for CI deficiency which became commercially available in 2015 – and the MTI overexpressing mouse model (TgMTI) were used in this study. Furthermore, as *fibroblasts* proved to be an effective model in the pre-clinical development of therapeutic drugs (Trolox and its derivatives) against LS, a similar *in vitro* approach was followed (Koopman *et al.*, 2016). This study formed the first part of a larger, ongoing study in which the effect of MTI overexpression on CI deficiency is evaluated on several biological levels in mice (biochemical, metabolic and phenotypic) with the aim of investigating a putative protective effect *in vivo.* The rationale behind the present study was to prove the protective effect of MTI overexpression on CI-deficient primary fibroblasts (while *in vivo* investigations were ongoing in parallel), as was done in genetically modified HeLa cells using recombinant DNA technology and rotenone treatment in 2006 (Reinecke *et al.*, 2006).

The first aim of the present study was thus to crossbreed the Ndufs4 and TgMTI mouse strains to develop a model with which the effects of MTI overexpression on CI deficiency could be studied in fibroblasts. Primary skin fibroblasts were then cultured from the resulting mice and characterised on a genetic and protein level. As a second aim, the effect of MTI overexpression on the bioenergetics consequences of CI deficiency was then evaluated on the same fibroblast cell lines. In Chapters 5 and 6, a detailed discussion regarding the results obtained for each objective of the respective aims was given. This chapter will therefore serve to provide a summary of the key findings of this study, as well as the final conclusions of each aim and the proposed future prospects.

## 7.2 PART 1: ESTABLISHING & CHARACTERISING Ndufs4:TgMTI MICE – *Aim 1*

As a first step in this study, the genetic background of the individual mouse strains (Ndufs4 and TgMTI) were compared to that of a *bona fide* C57BL6/J background **(Objective 1.1)**. From the obtained results, it could be concluded that each strain displayed sufficient comparability (an average of ≥99.5%) to consider their specific genetic modifications [i.e. the deletion of *Ndufs4*'s second exon (Ndufs4 mouse), and insertion of 56 *MtI** transgenes per allele (TgMTI mouse)] the only variables of importance between them. Since both strains were thoroughly backcrossed on a C57BL6/J genetic background prior to their acquisition from the Jackson Laboratory, this result was as expected (JAX, 2017a; JAX, 2017b; Kruse *et al.*, 2008; Palmiter *et al.*, 1993). Consequently, the characteristics of each strain (as informed by the Jackson Laboratory) were confirmed, and an accurate breeding strategy could be set up **(Objective 1.2)**. From the latter, it was possible to obtain mice with the four genotypes of interest [WT (*Ndufs4*$^{+/+}$*:TgMTI*$^{-/-}$), KO (*Ndufs4*$^{-/-}$*:TgMTI*$^{-/-}$), OVER (*Ndufs4*$^{+/+}$*:TgMTI*$^{+/+}$), and KO OVER (*Ndufs4*$^{-/-}$*:TgMTI*$^{+/+}$)] at the highest practical efficiency and probability.

Fibroblast cell lines were then successfully established from the skin biopsies of two mice of each genotype (as well as two control mice) using an explant culture technique **(Objective 1.3)** (Keira *et al.*, 2004). When cultured in glucose-containing medium, it was found that the growth rate exhibited by those cell lines with an *Ndufs4*$^{-/-}$ genotype (i.e. KO and KO OVER) was comparable to, if not slightly higher than, that of the *Ndufs4*$^{+/+}$ genotype (i.e. WT and OVER). While this was unexpected for the *Ndufs4*$^{-/-}$ genotype, it could be attributed to adaptive responses such as the inherent glycolytic phenotype of fibroblasts as a whole (Mot *et al.*, 2016; Valsecchi *et al.*, 2012; van den Heuvel *et al.*, 2004; Voets *et al.*, 2012). Consequently, it was concluded that, on the background of a CI deficiency and as a putative retrograde adaptive response, the glucose-containing medium had contributed to a compensatory shift in the energy metabolism of the fibroblasts from OXPHOS to glycolysis, thereby resulting in a less pronounced disease phenotype for the *Ndufs4*$^{-/-}$ cells compared to *in vivo* conditions (Reinecke *et al.*, 2009). Since the disease phenotype was especially important in the second aim (part two) of this study, cell lines were consequently incubated in galactose-containing medium one or two days prior to analysing their bioenergetics parameters (examined in Section 7.3), as suggested by van den Heuvel *et al.* (2004). This was done to allow for a more pronounced *in vitro* expression of CI deficiency as a result of a higher reliance on OXPHOS-produced ATP, which in turn was due to the slow rate of glycolytic substrate entrance when using galactose.

The genotyping methods employed and developed in this study were further able to successfully distinguish between WTs, heterozygotes, and homozygotes of both the Ndufs4 **(Objective 1.4)** and TgMTI **(Objective 1.5)** genotypes. Consequently, each sample corresponded to its previously determined and expected genotype. While the Ndufs4 genotyping results exactly resembled those described for the Ndufs4 mice by Valsecchi *et al.* (2012), the results yielded by

the novel qPCR TgMTI genotyping method grouped very closely to the anticipated *MtI* copy numbers (Beach & Palmiter, 1981; JAX, 2017a). The latter was particularly noteworthy, as no published method existed at the start of this study with which *TgMTI*$^{+/-}$ and *TgMTI*$^{+/+}$ mice could be differentiated. This method may therefore be used in the future as a simple, quick, and accurate means to distinguish between TgMTI genotypes.

In this study, it was further possible to confirm that the presence of *MtI** transgenes in the *TgMTI*$^{+/+}$ genotype resulted in the overexpression of *MtI* mRNA (and by extension, the MTI protein) when compared to the *TgMTI*$^{-/-}$ genotype **(Objective 1.6)**. Although a different method was used, the results corresponded to the overexpression and copy number as first determined by Palmiter *et al.* (1993). While *MtI* mRNA was clearly overexpressed, variation was observed between identical genotypes. Possible explanations included experimental variability (i.e. experimental sensitivity to small variations in the mRNA content of the total RNA samples) or the inherent variability associated with the gene expression of different cell cultures (Raj & van Oudenaarden, 2008). While it should be noted that mRNA levels do not imply an equivalent protein quantity, the results obtained were sufficient for this objective, especially in the absence of a robust protein analysis for MTs (Dabrio *et al.*, 2002; Vasconcelos, 2002). Since the level of overexpression in those cell lines with a *TgMTI*$^{+/+}$ genotype further exceeded that of chemically induced *MtI* mRNA, and as there were no adverse effects (e.g. growth reduction) evident from the MTI overexpressing cell lines, it could be concluded that the model was particularly suitable for the purpose of this study.

With regards to the steady state protein level of NDUFS4 **(Objective 1.7)**, the four models produced in this study corresponded to the previously mentioned genotypes, as well as to the results of the original Ndufs4 mice, as demonstrated by Kruse *et al.* (2008). It could therefore be concluded with confidence that the absence of the second exon of *Ndufs4* (i.e. the *Ndufs4*$^{-/-}$ genotype) resulted in a lack of the mature NDUFS4 protein in primary mouse skin fibroblasts. Of interest, was the finding that OVER 1 yielded a two-fold increase in NDUFS4 when compared to WT 1. While the precise mechanism responsible for this could not be deduced from this study, evidence linking NDUFS4's expression to $Zn^{2+}$-availability suggested that MTI's role in metal-transfer (e.g. to those proteins responsible for *Ndufs4*'s transcription) could be involved (Babula *et al.*, 2012; Kindermann *et al.*, 2004).

Additionally, primary mouse skin fibroblasts with an *Ndufs4*$^{-/-}$ genotype (i.e. KO 1 and KO OVER 1) failed to display fully assembled CI or CI activity when compared to the *Ndufs4*$^{+/+}$ cell lines (i.e. WT 1 and OVER 1) **(Objective 1.8)**. This agreed with both the Ndufs4 genotype and protein expression results described above, as well as the reports concerning CI expression in tissues and immortalised embryonic fibroblasts of the Ndufs4 mouse, and patient fibroblasts with *NDUFS4* mutations (Calvaruso *et al.*, 2012; Scacco *et al.*, 2003; Ugalde *et al.*, 2004; Valsecchi *et al.*, 2012). While these authors further reported on the presence of an inactive lower

molecular weight sub-assembly of CI lacking the N module, the same result was not seen in this study – a factor which was attributed to experimental variation between ours and other laboratories' BN-PAGE methods (Mimaki *et al.*, 2012). From the BN-PAGE + western blot analysis, it could thus be concluded that NDUFS4 is required for the stability of CI, and consequently for the proper functioning of its N module. Since spectrophotometric results by Calvaruso *et al.* (2012) as well as by this institution (unpublished data) indicate that *Ndufs4*$^{-/-}$ tissues display residual activity (albeit greatly reduced and ranging between 9% and 44%, depending on the tissue), the results obtained in this study should not be mistaken for the inability of *Ndufs4*$^{-/-}$ cells to utilise CI, but rather that CI as a single complex is incapable of oxidising NADH in these cells. Indeed, studies have shown that CI of the Ndufs4 mouse is active in the CI+CIII$^2$ supercomplex, which offers an explanation for the survival of *Ndufs4*$^{-/-}$ cells, as well as the transitory viable phenotype displayed by *Ndufs4*$^{-/-}$ mice (Calvaruso *et al.*, 2012). Finally, in agreement with the previous finding that MTI overexpression increased the expression of NDUFS4 in OVER 1, this experiment further showed an increase in the expression, as well as the activity (albeit small), of fully assembled CI in OVER 1 when compared to WT 1. Interestingly, patients with CI mutations displayed a similar increase in CI expression following treatment with the antioxidant Trolox (Distelmaier *et al.*, 2009). It is therefore possible that MTI and Trolox may increase the expression of CI in a similar manner.

From these results, it could thus be concluded that all the objectives relating to the development and characterisation of the primary mouse fibroblasts were successfully met. Furthermore, due to the undeniable genetic and protein correspondence between the four fibroblast models and the original Ndufs4 and TgMTI mouse strains, the models were regarded as very promising. For these reasons, it was decided to commence with the biochemical evaluation (part two).

## 7.3 PART 2: INVESTIGATING THE EFFECT OF MTI OVEREXPRESSION ON THE BIOENERGETICS CONSEQUENCES OF CI DEFICIENCY – *Aim 2*

In the second part of this study, it was important to evaluate the repeatability of the results between cell lines of the same genotype prior to discussing the findings. While not a specific objective, it was considered good practice – especially for primary cell lines – and enabled the discovery of genotype-unrelated variability (i.e. unrepeatable results). Indeed, the cell viability **(Objective 2.1)** and ROS levels **(Objective 2.5)** – both determined via commonly used methodologies – differed among genetically identical cell lines. Consequently, no conclusions regarding statistically significant differences could be reached for these objectives. The reason for the inconsistency observed was rationalised by considering the inherent variability associated with cell culture. Since cells were cultured under uniform conditions with regards to time, as well as the physical environment and techniques used, it was hypothesised that the variances were the result of cell-specific occurrences (Baker, 2016; Neildez-Nguyen *et al.*, 2008). While it should

be mentioned that it was not possible to identify the precise cause from the experiments conducted in this study, certain factors were considered. These included (i) the varying proliferation rates between genetically identical cultures, (ii) the differential (stochastic) expression of genes, (iii) the possible presence of modifier genes, (iv) the observation of inter-mouse differences, and (v) the purity of the cell culture.

Briefly stated, differences were observed in the cell proliferation of identical genotypes. While this was accounted for by varying the sub-culturing ratio, the period spent in culture might have been insufficient to allow for the complete equalisation of the proliferation rates. Secondly, the expression of the *MtI* genes were shown to vary between identical genotypes (Objective 1.6). While not affecting the results, this implied sample-specific variance in the gene expression as a whole (Baker, 2016; Neildez-Nguyen *et al.*, 2008; Raj & van Oudenaarden, 2008). Thirdly, studies have reported on the existence of modifier genes capable of affecting the mutational expressivity and phenotype of inbred strains (JAX, 2006). While it was unknown whether these genes were present in the mice used in this study, it remained a possibility. A fourth option included the biological variability (in the life span, phenotype, and metabolome) observed in genetically identical mice employed in this study (Johnson *et al.*, 2013; Kruse *et al.*, 2008; Louw, 2017, personal communication). Although this variance was lessened by the use of cell cultures, it was possible that some degree of individuality could have remained, thereby affecting the results. Lastly, an important consideration was the cell culture purity. While studies have reported primary fibroblasts to outcompete other cell types at very early passages, and the fibroblasts used in this study appeared to be morphologically similar, clear differences in the cell size between cultures of identical genotypes were observed following analysis by flow cytometry **(Objective 2.5)**. Indeed studies have shown cell viability and ROS production to differ between different cell types of the same organism (e.g. due to differences in the severity of CI deficiency and the adaptive responses employed) (Koopman *et al.*, 2013; Reinecke *et al.*, 2009). In fact, discrepancies in the ROS production have specifically been demonstrated in different cell- and tissue types of the Ndufs4 mouse model itself, e.g. between immortalised mouse embryonic-, primary skin-, and primary muscle fibroblasts (Iuso *et al.*, 2006; Kalyanaraman *et al.*, 2012; Koopman *et al.*, 2013; Melcher *et al.*, 2017; Valsecchi *et al.*, 2012). Therefore, as cell type was not explicitly tested for in this study, the effect of purity remained a possibility.

The trends of the results were more reproducible for the rest of the analysed parameters, thus enabling conclusions to be drawn from statistically significant differences. While the RMCN results were not statistically analysed, the low level of intra-sample variance (i.e. SDs) allowed for the confident comparison of results and therefore both sets of cell lines could be discussed **(Objective 2.2)**. Consequently, it was concluded that the overexpression of MTI did not appreciably affect the mtDNA copy number in OVER cells. By contrast, mtDNA copy number was increased in KO 2 and both KO OVER cell lines when compared to WT 1. As a cause, cellular

stress brought on by the absence of NDUFS4 and the resultant strain on CI was considered (Butow & Avadhani, 2004; Jones *et al.*, 2012; Reinecke *et al.*, 2009). While no significant differences were observed in the ATP/ADP ratio or ATP production of these samples (which would have indicated bioenergetics stress), it was not possible to rule out the effect of excessive ROS (which indicated oxidative stress) since no inferences could be made regarding the ROS levels of the four genotypes. Regrettably, no conclusions concerning the putative protective effect of MTI overexpression on CI deficiency could be reached, due to the intra-group variation observed for the KO genotype. To clarify the latter, the possibility that the two KO cell lines might have been affected to different extents by the absence of NDUFS4, due to the abovementioned cell culture variability, was contemplated (Lee & Wei, 2005).

Following the analysis of the $NADH/NAD^+$ ratio **(Objective 2.3)** and ATP/ADP ratio **(Objective 2.4)**, no statistically significant differences were observed when comparing the four genotypes. In contrast with the former, Valsecchi *et al.* (2012) had reported a statistically significant increase in the $NADH/NAD^+$ ratio of immortalised embryonic fibroblasts of *Ndufs4*$^{-/-}$ mice when compared to WT animals. For the present $NADH/NAD^+$ results, the lack of significant differences was attributed to the high variance (i.e. SD) present within each data point, which in turn was thought to be caused by the small number of replicates analysed. Furthermore, since the total cellular $NADH/NAD^+$ ratio was measured, for which large variation has been reported to occur (a reference which unfortunately was only noted after the completion of this study), it was further hypothesised that the mitochondrial $NADH/NAD^+$ ratio was not influenced to such a degree as to significantly alter the $NADH/NAD^+$ ratio of the total cell (Bilan & Belousov, 2016). Considering the ATP/ADP ratio, the results obtained in this study corresponded to that shown by Valsecchi *et al.* (2012). It was therefore concluded that the KO genotype was able to effectively adjust to the absence of NDUFS4. Speculations concerning the possible mechanisms included (i) the increased use of metabolic shuttles or pathways that enable CII-driven ATP production, (ii) the increased use of metabolic pathways resulting in electron-donation to Q, (iii) the effective use of CI as part of a CI-containing supercomplex, and (iv) the possibility of selection against the KO genotype during cell culture to favour the survival of better adjusted, stronger cells (Calvaruso *et al.*, 2012; Sancho *et al.*, 2013; Shakiba & Zandstra, 2017).

Finally, the bioenergetics profile of each genotype was obtained by investigating the basal respiration, ATP production, and maximal respiration parameters of the Mito Stress Test **(Objective 2.6)**. Surprisingly, a statistically significant increase was observed in the basal respiration of KO 1, in comparison with WT 1. As NDUFS4's absence had been shown to lead to a decreased stability of CI (Objective 1.8), this was in contrast with the expected result. Indeed, studies have demonstrated isolated mitochondria of the *Ndufs4*$^{-/-}$ mice to display a decreased basal respiration when compared to *Ndufs4*$^{+/+}$ mice (Chen *et al.*, 2017; Kayser *et al.*, 2013; Song *et al.*, 2017; van Wyk, 2016). To explain the difference observed between fibroblasts and

mitochondria, it was hypothesised that selection had unknowingly occurred during cell culture (perhaps via differences in cellular gene expression, -proliferation, and/or -adaptation) against weaker, more damaged, and/or slower proliferating KO cells, thereby favouring the survival of stronger cells that were more able to adapt to the harsh conditions of CI deficiency (Raj & van Oudenaarden, 2008; Sancho *et al.*, 2013; Shakiba & Zandstra, 2017). As a result, the bioenergetics phenotype analysed in cells differed from that observed *in vivo*, whereas mitochondria – assessed immediately following their isolation – displayed the defective *in vivo* phenotype. Secondly, a statistically significant increase was observed in the basal respiration, ATP production, and maximal respiration of OVER 1 when compared to WT 1. Since the specific mechanism of MTI's putative effect on CI, the RC, or the OXPHOS system could not be inferred from the study, various causes were considered. These included (i) MTI's direct or indirect donation of metal cofactors to members of the OXPHOS system, thereby increasing their function and the flux of electrons through the RC (Costello *et al.*, 2004; Lindeque *et al.*, 2010), (ii) MTI's post-translational modification of CIV to increase the $O_2$-consumption of the RC (Merten *et al.*, 2005), and/or (iii) MTI's effect on the enzymes involved in the provision of substrates to the RC (perhaps via metal donation to the enzymes or factors promoting the enzymes' expression) (Brown *et al.*, 2000; Feng *et al.*, 2005; Ye *et al.*, 2001). A particularly interesting observation was that the increased basal respiration, ATP production, and maximal respiration of OVER 1 coincided with the increased expression of NDUFS4, CI, and the CI activity observed for the same sample (Objectives 1.7 and 1.8). Therefore, a final possibility was that (iv) MTI had been able to specifically enhance the expression of CI, either via its metal-donating ability, or a mechanism similar to that employed by Trolox (as explained for Objective 1.8) (Distelmaier *et al.*, 2009).

From the results, it could therefore be concluded that all the objectives set to investigate the effect of MTI overexpression on the bioenergetics consequences of CI deficiency, using fibroblasts, were addressed using appropriate methodologies. However, since the variability associated with cell culture had contributed appreciably to the obtained results, it was not possible to investigate the effect of the genotype alone on each parameter. Primary skin fibroblasts are therefore not considered a suitable model to investigate the effect of MTI overexpression on CI deficiency.

If it were possible to demonstrate the protective effect of MTI overexpression on CI deficiency in this study, e.g. as previously described by Reinecke *et al.* (2006), the following results would ideally have been obtained: Due to MTI's putative protective effect, the OVER genotype would not have been expected to display increased bioenergetics or oxidative stress. For this reason, the cell viability, RMCN, and ROS levels would have corresponded to that of the WT. Furthermore, as this study had shown MTI to augment the expression of NDUFS4 and CI, the Mito Stress Test parameters observed for the OVER genotype in this study would have been anticipated, whereas the $NADH/NAD^+$ ratio and ATP/ADP ratio might have been predicted to respectively decrease and increase as a result of improved CI usage. By contrast, the reduced CI stability observed for

the KO genotype would have been expected to decrease the functionality of CI (as observed for *in vivo* studies; unpublished data). This would have resulted in lowered RC and OXPHOS function, leading to a decrease in the Mito Stress Test parameters and ATP/ADP ratio, as well as an increase in the NADH/$NAD^+$ ratio. Depending on the severity of the bottleneck at CI, ROS production via CI would then have been anticipated to increase, causing the cell to recede into a bioenergetics and oxidative crisis. In an attempt to rescue the cell from apoptosis, retrograde and anterograde responses could then have been expected to increase mitochondrial biogenesis, indicated in this study by the RMCN. However, were the oxidative stress to be too severe, a decrease in cell viability (possibly as a result of apoptosis) would then have occurred. As a result of MT's protective effect against the destructive properties of ROS and apoptosis, as well as its positive influence on the OXPHOS system, the overexpression of MTI would have been expected to return (or at least improve) the results observed for the KO genotype to those of the WT.

## 7.4 FINAL CONCLUSIONS & FUTURE PROSPECTS

In this study, primary skin fibroblasts, cultured from mice obtained from crossbreeding the Ndufs4 and TgMTI mouse models, were characterised and used to investigate the effect of MTI overexpression on CI deficiency. As mentioned in Section 7.1, fibroblasts were chosen based on the promising results obtained by Koopman *et al.* (2016) when using this cell type in the pre-clinical development of therapeutic drugs against LS. As a research model, the use of primary fibroblasts also presents many practical benefits over tissues. These include the ease of sample collection, the ability to culture large quantities from little starting material, the option of storage and re-culture for future use (e.g. when new knowledge or technology becomes available), the ability to easily manipulate the experimental milieu, and a general robustness (Auburger *et al.*, 2012; van den Heuvel *et al.*, 2004). In addition, the fact that both investigated mutations (i.e. the knockout of *Ndufs4* and the *Mtl** transgenes) were nuclear meant that CI deficiency and the overexpression of MTI would be expressed systemically, thus bypassing the obvious problems associated with fibroblasts when investigating mtDNA- (i.e. variability due to heteroplasmy) or X-linked mutations (i.e. gender-specific results due to allele-specific expression) (van den Heuvel *et al.*, 2004). Indeed, it was possible to accurately characterise the primary fibroblast genotypes on both the genetic and protein level (Aim 1). The results obtained for this part of the study were comparable to the anticipated and original findings, and consequently the expectation was that a suitable *in vitro* model had been developed to investigate the second aim.

However, upon evaluating the effect of genotype on the bioenergetics consequences of CI deficiency (Aim 2), inconsistent results attributable to the influence of cell culture were obtained for Objectives 2.1 and 2.5. In addition, it appeared as though selection had unknowingly occurred against weaker, more damaged, and/or slower proliferating KO cells, thereby interfering with the original *in vivo* bioenergetics phenotype (Objective 2.6). Therefore, while a more

reproducible experimental milieu is often presented as an advantage of using fibroblasts (van den Heuvel *et al.*, 2004), it was definitely not the case in this study. Other papers have reported problems associated with the use of fibroblasts. These include varying culture purity, e.g. cultures consisting of both mitotic and post-mitotic fibroblasts, as well as an inherent predisposition to clonal selection and genetic drift (Auburger *et al.*, 2012). It was thus possible that these factors may have contributed to the heterogeneity among genetically similar samples, thereby producing the variable results obtained in this study. An investigation regarding the precise cause for the observed inconsistencies was, however, beyond the scope of this dissertation. Studies have further shown that CI deficiencies do not always present in fibroblasts, despite a clear phenotype in both muscle and neuronal tissue (Hoefs *et al.*, 2012; van den Heuvel *et al.*, 2004). It is also generally agreed that functional mutations of the OXPHOS system (such as *Ndufs4*$^{-/-}$) are not as pronounced in fibroblasts as in other tissues. While the precise reason for this is unknown, it is suggested that the glycolytic phenotype of fibroblasts, and thus their lower dependence on OXPHOS-produced ATP, may contribute to this observed difference from other tissues (van den Heuvel *et al.*, 2004).

In conclusion, the aims formulated at the onset of this dissertation were investigated via an extensive study design including current methodology and technology, as explained in Section 3.4. Notably, from the first aim, a novel method was developed with which *TgMTI*$^{+/-}$ and *TgMTI*$^{+/+}$ mice could be distinguished. This method is simple, quick, and accurate, and proved to be particularly useful and time-saving throughout the breeding process. From the second aim, it was evident that primary fibroblasts are not a suitable model to investigate the effect of MTI overexpression on the bioenergetics consequences of CI deficiency, since these cells are particularly susceptible to cell culture variation. As clear systemic effects have been observed by colleagues in tissues and biological fluids of the mice developed in this study (unpublished results), it is therefore recommended that future studies investigating the effect of MTI overexpression on CI deficiency be conducted on the animal models themselves (i.e. phenotypic studies) or their tissues and/or biological fluids (i.e. *in vivo* studies), to thereby obtain a better representation of the steady state *in vivo* conditions. Indeed, this is currently underway in a parallel investigation.

# REFERENCES


Abcam. 2016. Sample preparation for western blot. http://docs.abcam.com/pdf/protocols/sample-preparation-for-western-blot.pdf Date of access: 11 Aug. 2017.

Acin-Perez, R. & Enriquez, J.A. 2014. The function of the respiratory supercomplexes: the plasticity model. *Biochimica et Biophysica Acta (BBA) - Bioenergetics*, 1837(4):444-450.

Acin-Perez, R., Fernandez-Silva, P., Peleato, M.L., Perez-Martos, A. & Enriquez, J.A. 2008. Respiratory active mitochondrial supercomplexes. *Molecular Cell*, 32(4):529-539.

Agarwal, R., Goel, S.K. & Behari, J.R. 2010. Detoxification and antioxidant effects of curcumin in rats experimentally exposed to mercury. *Journal of Applied Toxicology*, 30(5):457-468.

Agilent. 2017. Cell Analysis (Seahorse). http://www.agilent.com/en-us/products/cell-analysis-(seahorse) Date of access: 11 Aug. 2017.

Aita, K., Irie, H., Tanuma, Y., Toida, S., Okuma, Y., Mori, S. & Shiga, J. 2005. Apoptosis in murine lymphoid organs following intraperitoneal administration of dimethyl sulfoxide (DMSO). *Experimental and Molecular Pathology*, 79(3):265-271.

Aiuchi, T., Mihara, S., Nakaya, M., Masuda, Y., Nakajo, S. & Nakaya, K. 1998. Zinc ions prevent processing of caspase-3 during apoptosis induced by geranylgeraniol in HL-60 cells. *Journal of Biochemistry*, 124(2):300-303.

Alam, M.T., Manjeri, G.R., Rodenburg, R.J., Smeitink, J.A., Notebaart, R.A., Huynen, M., Willems, P.H. & Koopman, W.J. 2015. Skeletal muscle mitochondria of NDUFS4-/- mice display normal maximal pyruvate oxidation and ATP production. *Biochimica et Biophysica Acta (BBA) - Bioenergetics*, 1847(6-7):526-533.

Alder, N.N. & Theg, S.M. 2003. Energy use by biological protein transport pathways. *Trends in Biochemical Sciences*, 28(8):442-451.

Alessandrini, M. 2003. Evaluation of the effects of coenzyme Q10 and succinate in a rotenone-induced complex I deficient rat model. Potchefstroom: NWU. (Thesis – PhD).

Almeida, L.S., Nogueirao, C. & Vilarinho, L. 2012. (*In* Cseri, J., *ed.* Skeletal muscle - from myogenesis to clinical relations. InTech. p. 293-316).

Alston, C.L., Rocha, M.C., Lax, N.Z., Turnbull, D.M. & Taylor, R.W. 2017. The genetics and pathology of mitochondrial disease. *Journal of Pathology*, 241(2):236-250.

Andreu, A.L., Martinez, R., Marti, R. & Garcia-Arumi, E. 2009. Quantification of mitochondrial DNA copy number: pre-analytical factors. *Mitochondrion*, 9(4):242-246.

Andrews, B., Carroll, J., Ding, S., Fearnley, I.M. & Walker, J.E. 2013. Assembly factors for the membrane arm of human complex I. *Proceedings of the National Academy of Sciences of the United States of America*, 110(47):18934-18939.

Andrews, G.K. 2000. Regulation of metallothionein gene expression by oxidative stress and metal ions. *Biochemical Pharmacology*, 59(1):95-104.

Asin-Cayuela, J. & Gustafsson, C.M. 2007. Mitochondrial transcription and its regulation in mammalian cells. *Trends in Biochemical Sciences*, 32(3):111-117.

Auburger, G., Klinkenberg, M., Drost, J., Marcus, K., Morales-Gordo, B., Kunz, W.S., Brandt, U., Broccoli, V., Reichmann, H., Gispert, S. & Jendrach, M. 2012. Primary skin fibroblasts as a model of Parkinson's disease. *Molecular Neurobiology*, 46(1):20-27.

Babula, P., Masarik, M., Adam, V., Eckschlager, T., Stiborova, M., Trnkova, L., Skutkova, H., Provaznik, I., Hubalek, J. & Kizek, R. 2012. Mammalian metallothioneins: properties and functions. *Metallomics*, 4(8):739-750.

Baehrecke, E.H. 2003. Autophagic programmed cell death in Drosophila. *Cell Death and Differentiation*, 10(9):940-945.

Baker, M. 2016. Reproducibiity: respect you cells! *Nature*, 537(7620):433-435.

Bakker, B.M., Bro, C., Kotter, P., Luttik, M.A., van Dijken, J.P. & Pronk, J.T. 2000. The mitochondrial alcohol dehydrogenase Adh3p is involved in a redox shuttle in Saccharomyces cerevisiae. *Journal of Bacteriology*, 182(17):4730-4737.

Balsa, E., Marco, R., Perales-Clemente, E., Szklarczyk, R., Calvo, E., Landazuri, M.O. & Enriquez, J.A. 2012. NDUFA4 is a subunit of complex IV of the mammalian electron transport chain. *Cell Metabolism*, 16(3):378-386.

Banerjee, D., Onosaka, S. & Cherian, M.G. 1982. Immunohistochemical localization of metallothionein in cell nucleus and cytoplasm of rat liver and kidney. *Toxicology*, 24(2):95-105.

Baradaran, R., Berrisford, J.M., Minhas, G.S. & Sazanov, L.A. 2013. Crystal structure of the entire respiratory complex I. *Nature*, 494(7438):443-448.

Barrientos, A. & Moraes, C.T. 1999. Titrating the effects of mitochondrial complex I impairment in the cell physiology. *Journal of Biological Chemistry*, 274(23):16188-16197.

Barrow, J.J., Balsa, E., Verdeguer, F., Tavares, C.D., Soustek, M.S., Hollingsworth IV, L.R., Jedrychowski, M., Vogel, R., Paulo, J.A., Smeitink, J.A., Gygi, S.P., Doench, J., Root, D.E. &

Puigserver, P. 2016. Bromodomain inhibitors correct bioenergetic deficiency caused by mitochondrial disease complex I mutations. *Molecular Cell*, 64(1):163-175.

Bass, D.A., Parce, J.W., Dechatelet, L.R., Szejda, P., Seeds, M.C., & Thomas, M. 1983. Flow cytometric studies of oxidative product formation by neutrophils: a graded response to membrane stimulation. *Journal of Immunology*, 130(4):1910-1917.

Bayona-Bafaluy, M.P. 2003. Revisiting the mouse mitochondrial DNA sequence. *Nucleic Acids Research*, 31(18):5349-5355.

Beach, L.R. & Palmiter, R.D. 1981. Amplification of the metallothionein-I gene in cadmium-resistant mouse cells. *Proceedings of the National Academy of Sciences of the United States of America*, 78(4):2110-2114.

Berridge, M.V. & Tan, A.S. 1993. Characterization of the cellular reduction of 3-(4,5-dimethylthiazol-2-yl)-2,5-diphenyltetrazolium bromide (MTT): subcellular localization, substrate dependence, and involvement of mitochondrial electron transport in MTT reduction. *Archives of Biochemistry and Biophysics*, 303(2):474-482.

Bibb, M.J., van Etten, R.A., Wright, C.T., Walberg, M.W. & Clayton, D.A. 1981. Sequence and gene organization of mouse mitochondrial DNA. *Cell*, 26(2 Pt 2):167-180.

Bilan, D.S. & Belousov, V.V. 2016. Genetically encoded probes for $NAD^+$/NADH monitoring. *Free Radical Biology and Medicine*, 100:32-42.

Boggess, D., Silva, K.A., Landel, C.P., Mobraaten, L. & Sundberg, J.P. 2004. 1- Approaches to handling, breeding, strain preservation, genotyping, and drug administration for mouse models of cancer. (*In* Holland, E.C., *ed.* Mouse models of human cancer. Hoboken, NJ: John Wiley & Sons. p. 1-14).

Bourgeron, T., Rustin, P., Chretien, D., Birch-Machin, M., Bourgeois, M., Viegas-Pequignot, E., Munnich, A. & Rotig, A. 1995. Mutation of a nuclear succinate dehydrogenase gene results in mitochondrial respiratory chain deficiency. *Nature Genetics*, 11(2):144-149.

Brand, M.D. & Nicholls, D.G. 2011. Assessing mitochondrial dysfunction in cells. *Biochemical Journal*, 435(2):297-312.

Brandt, U. 1997. Proton-translocation by membrane-bound NADH:ubiquinone-oxidoreductase (complex I) through redox-gated ligand conduction. *Biochimica et Biophysica Acta (BBA) - Bioenergetics*, 1318(1-2):79-91.

Brandt, U., Kerscher, S., Drose, S., Zwicker, K. & Zickermann, V. 2003. Proton pumping by NADH:ubiquinone oxidoreductase. A redox driven conformational change mechanism? *FEBS Letters*, 545(1):9-17.

Breeuwer, M. & Goldfarb, D.S. 1990. Facilitated nuclear transport of histone H1 and other small nucleophilic proteins. *Cell*, 60(6):999-1008.

Brenmoehl, J. & Hoeflich, A. 2013. Dual control of mitochondrial biogenesis by sirtuin 1 and sirtuin 3. *Mitochondrion*, 13(6):755-761.

Breuer, M.E., Koopman, W.J., Koene, S., Nooteboom, M., Rodenburg, R.J., Willems, P.H. & Smeitink, J.A. 2013a. The role of mitochondrial OXPHOS dysfunction in the development of neurologic diseases. *Neurobiology of Disease*, 51:27-34.

Breuer, M.E., Willems, P.H., Smeitink, J.A., Koopman, W.J. & Nooteboom, M. 2013b. Cellular and animal models for mitochondrial complex I deficiency: a focus on the NDUFS4 subunit. *IUBMB Life*, 65(3):202-208.

Brouwer, M., Hoexum-Brouwer, T. & Cashon, R.E. 1993. A putative glutathione-binding site in CdZn-metallothionein identified by equilibrium binding and molecular-modelling studies. *Biochemical Journal*, 294(Pt 1):219-225.

Brown, A.M., Kristal, B.S., Effron, M.S., Shestopalov, A.I., Ullucci, P.A., Sheu, K.R., Blass, J.P. & Cooper, A.J. 2000. $Zn^{2+}$ inhibits α-ketoglutarate-stimulated mitochondrial respiration and the isolated α-ketoglutarate dehydrogenase complex. *Journal of Biological Chemistry*, 275(18):13441-13447.

Butow, R.A. & Avadhani, N.G. 2004. Mitochondrial signaling: the retrograde response. *Molecular Cell*, 14(1):1-15.

Cagin, U. & Enriquez, J.A. 2015. The complex crosstalk between mitochondria and the nucleus: what goes in between? *International Journal of Biochemistry and Cell Biology*, 63:10-15.

Cai, L., Wang, Y., Zhou, G., Chen, T., Song, Y., Li, X. & Kang, Y.J. 2006. Attenuation by metallothionein of early cardiac cell death via suppression of mitochondrial oxidative stress results in a prevention of diabetic cardiomyopathy. *Journal of the American College of Cardiology*, 48(8):1688-1697.

Calvaruso, M.A., Willems, P., van den Brand, M., Valsecchi, F., Kruse, S.E., Palmiter, R.D., Smeitink, J.A. & Nijtmans, L. 2012. Mitochondrial complex III stabilizes complex I in the absence of NDUFS4 to provide partial activity. *Human Molecular Genetics*, 21(1):115-120.

Calvo, S.E., Clauser, K.R. & Mootha, V.K. 2016. MitoCarta2.0: an updated inventory of mammalian mitochondrial proteins. *Nucleic Acids Research*, 44(D1):D1251-D1257.

Carilla-Latorre, S., Annesley, S.J., Munoz-Braceras, S., Fisher, P.R. & Escalante, R. 2013. Ndufaf5 deficiency in the Dictyostelium model: new roles in autophagy and development. *Molecular Biology of the Cell*, 24(10):1519-1528.

Carroll, C.J., Brilhante, V. & Suomalainen, A. 2014. Next-generation sequencing for mitochondrial disorders. *British Journal of Pharmacology*, 171(8):1837-1853.

Chan, F.K., Shisler, J., Bixby, J.G., Felices, M., Zheng, L., Appel, M., Orenstein, J., Moss, B. & Lenardo, M.J. 2003. A role for tumor necrosis factor receptor-2 and receptor-interacting protein in programmed necrosis and antiviral responses. *Journal of Biological Chemistry*, 278(51):51613-51621.

Chen, B., Hui, J., Montgomery, K.S., Gella, A., Bolea, I., Sanz, E., Palmiter, R.D. & Quintana, A. 2017. Loss of mitochondrial Ndufs4 in striatal medium spiny neurons mediates progressive motor impairment in a mouse model of Leigh syndrome. *Frontiers in Molecular Neuroscience*, 10:265.

Chinnery, P.F. & Hudson, G. 2013. Mitochondrial genetics. *British Medical Bulletin*, 106:135-159.

Choi, C. 2003. Cloning and functional study of a novel human metallothionein-I isoform induced by paraquat. *Biochemical and Biophysical Research Communications*, 304(2):236-240.

Clay Montier, L.L., Deng, J.J. & Bai, Y. 2009. Number matters: control of mammalian mitochondrial DNA copy number. *Journal of Genetics and Genomics*, 36(3):125-131.

Costello, L.C., Guan, Z., Franklin, R.B. & Feng, P. 2004. Metallothionein can function as a chaperone for zinc uptake transport into prostate and liver mitochondria. *Journal of Inorganic Biochemistry*, 98(4):664-666.

Coyle, P., Philcox, J.C., Carey, L.C. & Rofe, A.M. 2002. Metallothionein: the multipurpose protein. *Cellular and Molecular Life Sciences*, 59(4):627-647.

Crabtree, H.G. 1929. Observations on the carbohydrate metabolism of tumours. *Biochemical Journal*, 23(3):536-545.

Cutler, R.G., Plummer, J., Chowdhury, K. & Heward, C. 2005. Oxidative stress profiling: part II. Theory, technology, and practice. *Annals of the New York Academy of Sciences*, 1055:136-158.

Dabrio, M., Rodriguez, A.R., Bordin, G., Bebianno, M.J., de Ley, M., Sestakova, I., Vasak, M. & Nordberg, M. 2002. Recent developments in quantification methods for metallothionein. *Journal of Inorganic Biochemistry*, 88(2):123-134.

Danielson, S.R., Carelli, V., Tan, G., Martinuzzi, A., Schapira, A.H., Savontaus, M. & Cortopassi, G.A. 2005. Isolation of transcriptomal changes attributable to LHON mutations and the cybridization process. *Brain*, 128(5):1026-1037.

Darin, N., Oldfors, A., Moslemi, A., Holme, E. & Tulinius, M. 2001. The incidence of mitochondrial encephalomyopathies in childhood: clinical features and morphological, biochemical, and DNA abnormalities. *Annals of Neurology*, 49(3):377-383.

Das, K., de Groof, A., Jauniaux, T. & Bouquegneau, J.M. 2006. Zn, Cu, Cd and Hg binding to metallothioneins in harbour porpoises Phocoena phocoena from the southern North Sea. *BioMed Central Ecology*, 6:2.

Day, E.K., Sosale, N.G. & Lazzara, M.J. 2016. Cell signaling regulation by protein phosphorylation: a multivariate, heterogeneous, and context-dependent process. *Current Opinions in Biotechnology*, 40:185-192.

de Haas, R., Das, D., Garanto, A., Renkema, H.G., Greupink, R., van den Broek, P., Pertijs, J., Collin, R.W., Willems, P., Beyrath, J., Heerschap, A., Russel, F.G. & Smeitink, J.A. 2017. Therapeutic effects of the mitochondrial ROS-redox modulator KH176 in a mammalian model of Leigh disease. *Scientific Reports*, 7(1):11733.

DeLuca, M. & McElroy, W.D. 1978. Purification and properties of firefly luciferase. *Methods in Enzymology*, 57:3-15.

Ding, H.Q., Zhou, B.J., Liu, L. & Cheng, S. 2002. Oxidative stress and metallothionein expression in the liver of rats with severe thermal injury. *Burns*, 28(3):215-221.

Distelmaier, F., Koopman, W.J., van den Heuvel, L.P., Rodenburg, R.J., Mayatepek, E., Willems, P.H. & Smeitink, J.A. 2009. Mitochondrial complex I deficiency: from organelle dysfunction to clinical disease. *Brain*, 132(Pt 4):833-842.

Dranka, B.P., Benavides, G.A., Diers, A.R., Giordano, S., Zelickson, B.R., Reily, C., Zou, L., Chatham, J.C., Hill, B.G., Zhang, J., Landar, A. & Darley-Usmar, V.M. 2011. Assessing bioenergetic function in response to oxidative stress by metabolic profiling. *Free Radical Biology & Medicine*, 51(9):1621-1635.

du Plessis, L., Laubscher, P., Jooste, J., du Plessis, J., Franken, A., van Aarde, N. & Eloff, F. 2010. Flow cytometric analysis of the oxidative status in human peripheral blood mononuclear cells of workers exposed to welding fumes. *Journal of Occupational and Environmental Hygiene*, 7(6):367-374.

Edinger, A.L. & Thompson, C.B. 2004. Death by design: apoptosis, necrosis and autophagy. *Current Opinion in Cell Biology*, 16(6):663-669.

Efremov, R.G. & Sazanov, L.A. 2012. The coupling mechanism of respiratory complex I - A structural and evolutionary perspective. *Biochimica et Biophysica Acta (BBA) - Bioenergetics*, 1817(10):1785-1795.

Elder, P.K., French, C.L., Subramaniam, M., Schmidt, L.J. & Getz, M.J. 1988. Evidence that the functional β-actin gene is single copy in most mice and is associated with 5' sequences capable of conferring serum- and cycloheximide-dependent regulation. *Molecular and Cellular Biology*, 8(1):480-485.

Ellis, S.M. & Steyn, H.S. 2003. Practical significance (effect sizes) versus or in combination with statistical significance (p-values). *Management Dynamics*, 12(4):51-53.

Elmore, S. 2007. Apoptosis: a review of programmed cell death. *Toxicologic Pathology*, 35(4):495-516.

Erickson, J.C., Hollopeter, G., Thomas, S.A., Froelick, G.J. & Palmiter, R.D. 1997. Disruption of the metallothionein-III gene in mice: analysis of brain zinc, behavior, and neuron vulnerability to metals, aging, and seizures. *Journal of Neuroscience*, 17(4):1271-1281.

Erickson, J.C., Masters, B.A., Kelly, E.J., Brinster, R.L. & Palmiter, R.D. 1995. Expression of human metallothionein-III in transgenic mice. *Neurochemistry International*, 27(1):35-41.

Eruslanov, E. & Kusmartsev, S. 2010. Identification of ROS using oxidized DCFDA and flow-cytometry. *Methods in Molecular Biology*, 594:57-72.

Esterhuizen, K., van der Westhuizen, F.H. & Louw, R. 2017. Metabolomics of mitochondrial disease. *Mitochondrion*, 35:97-110.

Fato, R., Bergamini, C., Bortolus, M., Maniero, A.L., Leoni, S., Ohnishi, T. & Lenaz, G. 2009. Differential effects of mitochondrial complex I inhibitors on production of reactive oxygen species. *Biochimica et Biophysica Acta (BBA) - Bioenergetics*, 1787(5):384-392.

Felsenfeld, G. 1992. Chromatin as an essential part of the transcriptional mechanism. *Nature*, 355(6357):219-224.

Feng, W., Cai, J., Pierce, W.M., Franklin, R.B., Maret, W., Benz, F.W. & Kang, Y.J. 2005. Metallothionein transfers zinc to mitochondrial aconitase through a direct interaction in mouse hearts. *Biochemical and Biophysical Research Communications*, 332(3):853-858.

Fiedorczuk, K., Letts, J.A., Degliesposti, G., Kaszuba, K., Skehel, M. & Sazanov, L.A. 2016. Atomic structure of the entire mammalian mitochondrial complex I. *Nature*, 538(7625):406-410.

Field, A. 2009a. Discovering statistics using SPSS. 3rd ed. London: SAGE. p. 31-60.

Field, A. 2009b. Discovering statistics using SPSS. 3rd ed. London: SAGE. p. 131-165.

Field, A. 2009c. Discovering statistics using SPSS. 3rd ed. London: SAGE. p. 264-315.

Field, A. 2009d. Discovering statistics using SPSS. 3rd ed. London: SAGE. p. 347-394.

Forman, H.J., Zhang, H. & Rinna, A. 2009. Glutathione: overview of its protective roles, measurement, and biosynthesis. *Molecular Aspects of Medicine*, 30(1-2):1-12.

Freisinger, E. 2008. Plant MTs-long neglected members of the metallothionein superfamily. *Dalton Transactions,* (47):6663-6675.

Friedrich, T. 2001. Complex I: a chimaera of a redox and conformation-driven proton pump? *Journal of Bioenergetics and Biomembranes*, 33(3):169-177.

Friedrich, T. & Bottcher, B. 2004. The gross structure of the respiratory complex I: a Lego system. *Biochimica et Biophysica Acta (BBA) - Bioenergetics*, 1608(1):1-9.

Galluzzi, L., Kepp, O. & Kroemer, G. 2012. Mitochondria: master regulators of danger signalling. *Nature Reviews Molecular Cell Biology*, 13(12):780-788.

Games, P.A. & Howell, J.F. 1976. Pairwise multiple comparison procedures with unequal N's and/or variances: a Monte Carlo study. *Journal of Educational Statistics*, 1(2):113-125.

Garrett, R.H. & Grisham, C.M. 2013a. (*In* McGahey, P., *ed.* Biochemistry. 6th ed. Belmont, CA: Brooks/Cole. p. 643-682).

Garrett, R.H. & Grisham, C.M. 2013b. (*In* McGahey, P., *ed.* Biochemistry. 6th ed. Belmont, CA: Brooks/Cole. p. 891-918).

Garrett, R.H. & Grisham, C.M. 2013c. (*In* McGahey, P., *ed.* Biochemistry. 6th ed. Belmont, CA: Brooks/Cole. p. 919-946).

Ghiasi, P., Hosseinkhani, S., Noori, A., Nafissi, S. & Khajeh, K. 2012. Mitochondrial complex I deficiency and ATP/ADP ratio in lymphocytes of amyotrophic lateral sclerosis patients. *Neurological Research*, 34(3):297-303.

Gorman, G.S., Chinnery, P.F., DiMauro, S., Hirano, M., Koga, Y., McFarland, R., Suomalainen, A., Thorburn, D.R., Zeviani, M. & Turnbull, D.M. 2016. Mitochondrial diseases. *Nature Reviews Disease Primers*, 2:16080.

Gorman, G.S., Schaefer, A.M., Ng, Y., Gomez, N., Blakely, E.L., Alston, C.L., Feeney, C., Horvath, R., Yu-Wai-Man, P., Chinnery, P.F., Taylor, R.W., Turnbull, D.M. & McFarland, R. 2015. Prevalence of nuclear and mitochondrial DNA mutations related to adult mitochondrial disease. *Annals of Neurology*, 77(5):753-759.

Gourlay, C.W. & Ayscough, K.R. 2005. The actin cytoskeleton: a key regulator of apoptosis and ageing? *Nature Reviews Molecular Cell Biology*, 6(7):583-589.

Gropper, S.S. & Smith, J.L. 2013. (*In* Feldman, E., *ed.* Advanced nutrition and human metabolism. Belmont, CA: Wadsworth. p. 1-32).

Guerrero-Castillo, S., Baertling, F., Kownatzki, D., Wessels, H.J., Arnold, S., Brandt, U. & Nijtmans, L. 2017. The assembly pathway of mitochondrial respiratory chain complex I. *Cell Metabolism*, 25(1):128-139.

Haack, T.B., Haberberger, B., Frisch, E.M., Wieland, T., Iuso, A., Gorza, M., Strecker, V., Graf, E., Mayr, J.A., Herberg, U., Hennermann, J.B., Klopstock, T., Kuhn, K.A., Ahting, U., Sperl, W., Wilichowski, E., Hoffmann, G.F., Tesarova, M., Hansikova, H., Zeman, J., Plecko, B., Zeviani, M., Wittig, I., Strom, T.M., Schuelke, M., Freisinger, P., Meitinger, T. & Prokisch, H. 2012. Molecular diagnosis in mitochondrial complex I deficiency using exome sequencing. *Journal of Medical Genetics*, 49(4):277-283.

Haase, H. & Maret, W. 2008. Partial oxidation and oxidative polymerization of metallothionein. *Electrophoresis*, 29(20):4169-4176.

Hackenbrock, C.R., Chazotte, B. & Gupte, S.S. 1986. The random collision model and a critical assessment of diffusion and collision in mitochondrial electron transport. *Journal of Bioenergetics and Biomembranes*, 18(5):331-368.

Hance, N., Ekstrand, M.I. & Trifunovic, A. 2005. Mitochondrial DNA polymerase gamma is essential for mammalian embryogenesis. *Human Molecular Genetics*, 14(13):1775-1783.

Haq, F., Mahoney, M. & Koropatnick, J. 2003. Signaling events for metallothionein induction. *Mutation Research/Fundamental and Molecular Mechanisms of Mutagenesis*, 533(1-2):211-226.

Hathout, Y., Fabris, D. & Fenselau, C. 2001. Stoichiometry in zinc ion transfer from metallothionein to zinc finger peptides. *International Journal of Mass Spectrometry*, 204(1-3):1-6.

Hauser-Davis, R.A., Bastos, F.F., Tuton, B., Chavez Rocha, R., Saint' Pierre, T., Ziolli, R.L. & Arruda, M.A. 2014. Bile and liver metallothionein behavior in copper-exposed fish. *Journal of Trace Elements in Medicine and Biology*, 28(1):70-74.

Hayflick, L. 1965. The limited in vitro lifetime of human diploid cell strains. *Experimental Cell Research*, 37(3):614-636.

Heid, C.A., Stevens, J., Livak, K.J. & Williams, P.M. 1996. Real time quantitative PCR. *Genome Research*, 6(10):986-994.

Hock, M.B. & Kralli, A. 2009. Transcriptional control of mitochondrial biogenesis and function. *Annual Review of Physiology*, 71:177-203.

Hoefs, S.J., Rodenburg, R.J., Smeitink, J.A. & van den Heuvel, L.P. 2012. Molecular base of biochemical complex I deficiency. *Mitochondrion*, 12(5):520-532.

Hofhaus, G., Johns, D.R., Hurko, O., Attardi, G. & Chomyn, A. 1996. Respiration and growth defects in transmitochondrial cell lines carrying the 11778 mutation associated with Leber's hereditary optic neuropathy. *Journal of Biological Chemistry*, 271(22):13155-13161.

Holler, N., Zaru, R., Micheau, O., Thome, M., Attinger, A., Valitutti, S., Bodmer, J., Schneider, P., Seed, B. & Tschopp, J. 2000. Fas triggers an alternative, caspase-8-independent cell death pathway using the kinase RIP as effector molecule. *Nature Immunology*, 1(6):489-495.

Holm, S. 1979. A simple sequentially rejective multiple test procedure. *Scandinavian Journal of Statistics*, 6:65-70.

Holt, I.J., Harding, A.E. & Morgan-Hughes, J.A. 1988. Deletions of muscle mitochondrial DNA in patients with mitochondrial myopathies. *Nature*, 331(6158):643-730.

Hudson, G., Keers, S., Man, P.Y., Griffiths, P., Huoponen, K., Savontaus, M., Nikoskelainen, E., Zeviani, M., Carrara, F., Horvath, R., Karcagi, V., Spruijt, L., de Coo, I.F., Smeets, H.J. & Chinnery, P.F. 2005. Identification of an X-chromosomal locus and haplotype modulating the phenotype of a mitochondrial DNA disorder. *American Journal of Human Genetics*, 77(6):1086-1091.

Hughes, P., Marshall, D., Reid, Y., Parkes, H. & Gelber, C. 2007. The costs of using unauthenticated, over-passaged cell lines: how much more data do we need? *BioTechniques*, 43(5):575-586.

Hunte, C., Zickermann, V. & Brandt, U. 2010. Functional modules and structural basis of conformational coupling in mitochondrial complex I. *Science*, 329(5990):448-451.

Hunziker, P.E. & Kagi, J.H. 1985. Isolation and characterization of six human hepatic isometallothioneins. *Biochemical Journal*, 231(2):375-382.

Hussain, S., Slikker, W.J. & Ali, S.F. 1996. Role of metallothionein and other antioxidants in scavenging superoxide radicals and their possible role in neuroprotection. *Neurochemistry International*, 29(2):145-152.

Ibrahim, S.F. & van den Engh, G. 2007. Flow cytometry and cell sorting. *Advances in Biochemical Engineering/Biotechnology*, 106:19-39.

Indo, H.P., Davidson, M., Yen, H.C., Suenaga, S., Tomita, K., Nishii, T., Higuchi, M., Koga, Y., Ozawa, T. & Majima, H.J. 2007. Evidence of ROS generation by mitochondria in cells with impaired electron transport chain and mitochondrial DNA damage. *Mitochondrion*, 7(1-2):106-118.

Ingraham, C.A., Burwell, L.S., Skalska, J., Brookes, P.S., Howell, R.L., Sheu, S.S. & Pinkert, C.A. 2009. NDUFS4: creation of a mouse model mimicking a complex I disorder. *Mitochondrion*, 9(3):204-210.

Irwin, M.H., Parameshwaran, K. & Pinkert, C.A. 2013. Mouse models of mitochondrial complex I dysfunction. *International Journal of Biochemistry and Cell Biology*, 45(1):34-40.

Iszard, M.B., Liu, J. & Klaassen, C.D. 1995. Effect of several metallothionein inducers on oxidative stress defense mechanisms in rats. *Toxicology*, 104(1-3):25-33.

Iuso, A., Scacco, S., Piccoli, C., Bellomo, F., Petruzzella, V., Trentadue, R., Minuto, M., Ripoli, M., Capitanio, N., Zeviani, M. & Papa, S. 2006. Dysfunctions of cellular oxidative metabolism in patients with mutations in the NDUFS1 and NDUFS4 genes of complex I. *Journal of Biological Chemistry*, 281(15):10374-10380.

Jacob, C., Maret, W. & Vallee, B.L. 1998. Control of zinc transfer between thionein, metallothionein, and zinc proteins. *Proceedings of the National Academy of Sciences of the United States of America*, 95(7):3489-3494.

Jain, I.H., Zazzeron, L., Goli, R., Alexa, K., Schatzman-Bone, S., Dhillon, H., Goldberger, O., Peng, J., Shalem, O., Sanjana, N.E., Zhang, F., Goessling, W., Zapol, W.M. & Mootha, V.K. 2016. Hypoxia as a therapy for mitochondrial disease. *Science*, 352(6281):54-61.

JAX. 2006. The importance of genetic background in mouse-based biomedical research. https://www.jax.org/news-and-insights/2006/june/the-importance-of-genetic-background-in-mouse-based-biomedical-research Date of access: 20 Sept. 2017.

JAX. 2014. JAX® Mice, Clinical & Research Services Catalog: June 2014 – May 2015. http://www.scanburresearch.com/media/30968/2014-15-JAX-Mice-Services-Catalog.pdf Date of access: 20 Sept. 2017.

JAX. 2017a. Mouse strain datasheet - 002210. https://www.jax.org/strain/002210 Date of access: 29 Jun. 2017.

JAX. 2017b. Mouse strain datasheet - 027058. https://www.jax.org/strain/027058 Date of access: 29 Jun. 2017.

Jin, W., Penington, C.J., McCue, S.W. & Simpson, M.J. 2017. A computational modelling framework to quantify the effects of passaging cell lines. *PLOS ONE*, 12(7):e0181941.

Johnson, K.R., Zheng, Q.Y., Bykhovskaya, Y., Spirina, O. & Fischel-Ghodsian, N. 2001. A nuclear-mitochondrial DNA interaction affecting hearing impairment in mice. *Nature Genetics*, 27(2):191-194.

Johnson, S.C., Yanos, M.E., Kayser, E., Quintana, A., Sangesland, M., Castanza, A., Uhde, L., Hui, J., Wall, V.Z., Gagnidze, A., Oh, K., Wasko, B.M., Ramos, F.J., Palmiter, R.D., Rabinovitch, P.S., Morgan, P.G., Sedensky, M.M. & Kaeberlein, M. 2013. mTOR inhibition alleviates mitochondrial disease in a mouse model of Leigh syndrome. *Science*, 342(6165):1524-1528.

Jones, A.W., Yao, Z., Vicencio, J.M., Karkucinska-Wieckowska, A. & Szabadkai, G. 2012. PGC-1 family coactivators and cell fate: roles in cancer, neurodegeneration, cardiovascular disease and retrograde mitochondria-nucleus signalling. *Mitochondrion*, 12(1):86-99.

Jones, L.J., Gray, M., Yue, S.T., Haugland, R.P. & Singer, V.L. 2001. Sensitive determination of cell number using the CyQUANT® cell proliferation assay. *Journal of Immunological Methods*, 254(1-2):85-98.

Kagi, J.H. & Schaffer, A. 1988. Biochemistry of metallothionein. *Biochemistry*, 27(23):8509-8515.

Kahlhofer, F., Kmita, K., Wittig, I., Zwicker, K. & Zickermann, V. 2017. Accessory subunit NUYM (NDUFS4) is required for stability of the electron input module and activity of mitochondrial complex I. *Biochimica et Biophysica Acta (BBA) - Bioenergetics*, 1858(2):175-181.

Kalman, B. 2006. Role of mitochondria in multiple sclerosis. *Current Neurology and Neuroscience Reports*, 6(3):244-252.

Kalyanaraman, B., Darley-Usmar, V., Davies, K.J., Dennery, P.A., Forman, H.J., Grisham, M.B., Mann, G.E., Moore, K., Roberts II, L.J. & Ischiropoulos, H. 2012. Measuring reactive oxygen and nitrogen species with fluorescent probes: challenges and limitations. *Free Radical Biology & Medicine*, 52(1):1-6.

Kang, Y.J. 1999. The antioxidant function of metallothionein in the heart. *Proceedings of the Society for Experimental Biology and Medicine*, 222(3):263-273.

Kang, Y.J., Chen, Y., Yu, A., Voss-McCowan, M. & Epstein, P.N. 1997. Overexpression of metallothionein in the heart of transgenic mice suppresses doxorubicin cardiotoxicity. *Journal of Clinical Investigation*, 100(6):1501-1506.

Kayser, E., Johnson, S.C., Kaeberlein, M.R., Sedensky, M.M. & Morgan, P.G. 2013. Capacity for oxidative phosphorylation does not decline with age in mitochondria from Ndufs4 knockout mice. *Mitochondrion*, 13(6):915.

Keira, S.M., Ferreira, L.M., Gragnani, A., Duarte, I.S. & Santos, I.A. 2004. Experimental model for fibroblast culture. *Acta Cirúrgica Brasileira*, 19:11-16.

Kelso, G.F., Porteous, C.M., Coulter, C.V., Hughes, G., Porteous, W.K., Ledgerwood, E.C., Smith, R.A. & Murphy, M.P. 2001. Selective targeting of a redox-active ubiquinone to mitochondria within cells: antioxidant and antiapoptotic properties. *Journal of Biological Chemistry*, 276(7):4588-4596.

Kerr, J.F., Wyllie, A.H. & Currie, A.R. 1972. Apoptosis: a basic biological phenomenon with wide-ranging implications in tissue kinetics. *British Journal of Cancer*, 26(4):239-257.

Kindermann, B., Doring, F., Pfaffl, M. & Daniel, H. 2004. Identification of genes responsive to intracellular zinc depletion in the human colon adenocarcinoma cell line HT-29. *Journal of Nutrition*, 134(1):57-62.

Koene, S., Willems, P.H., Roestenberg, P., Koopman, W.J. & Smeitink, J.A. 2011. Mouse models for nuclear DNA-encoded mitochondrial complex I deficiency. *Journal of Inherited Metabolic Disease*, 34(2):293-307.

Kondo, Y., Yanagiya, T., Himeno, S., Yamabe, Y., Schwartz, D., Akimoto, M., Lazo, J.S. & Imura, N. 1999. Simian virus 40-transformed metallothionein null cells showed increased sensitivity to cadmium but not to zinc, copper, mercury or nickel. *Life Sciences*, 64(11):PL145-PL150.

Koopman, W.J., Distelmaier, F., Smeitink, J.A. & Willems, P.H. 2013. OXPHOS mutations and neurodegeneration. *EMBO Journal*, 32(1):9-29.

Koopman, W.J., Verkaart, S., Visch, H.J., van der Westhuizen, F.H., Murphy, M.P., van den Heuvel, L.W., Smeitink, J.A. & Willems, P.H. 2005. Inhibition of complex I of the electron transport chain causes $O_2^{\cdot-}$-mediated mitochondrial outgrowth. *American Journal of Physiology - Cell Physiology*, 288(6):C1440-C1450.

Koopman, W.J., Beyrath, J., Fung, C., Koene, S., Rodenburg, R.J., Willems, P.H. & Smeitink, J.A. 2016. Mitochondrial disorders in children: toward development of small-molecule treatment strategies. *EMBO Molecular Medicine*, 8(4):311-327.

Koopman, W.J., Nijtmans, L.G., Dieteren, C.E., Roestenberg, P., Valsecchi, F., Smeitink, J.A. & Willems, P.H. 2010. Mammalian mitochondrial complex I: biogenesis regulation and reactive oxygen species generation. *Antioxidants and Redox Signalling*, 12(12):1431-1470.

Krezel, A. & Maret, W. 2007. Different redox states of metallothionein/thionein in biological tissue. *Biochemical Journal*, 402(3):551-558.

Kruse, S.E., Watt, W.C., Marcinek, D.J., Kapur, R.P., Schenkman, K.A. & Palmiter, R.D. 2008. Mice with mitochondrial complex I deficiency develop a fatal encephalomyopathy. *Cell Metabolism*, 7(4):312-320.

Kruskal, W.H. & Wallis, W.A. 1952. Use of ranks in one-criterion variance analysis. *Journal of the American Statistical Association*, 47(260):583-621.

Kulinsky, V.I. & Kolesnichenko, L.S. 2007. Mitochondrial glutathione. *Biochemistry (Moscow)*, 72(7):698-701.

Laemmli, U.K. 1970. Cleavage of structural proteins during the assemby of the head of bacteriophage T4. *Nature*, 227(5259):645-760.

Lagouge, M. & Larsson, N.G. 2013. The role of mitochondrial DNA mutations and free radicals in disease and ageing. *Journal of Internal Medicine*, 273(6):529-543.

Lake, N.J., Bird, M.J., Isohanni, P. & Paetau, A. 2015. Leigh syndrome: neuropathology and pathogenesis. *Journal of Neuropathology and Experimental Neurology*, 74(6):482-492.

Lamont, R.E., Beaulieu, C.L., Bernier, F.P., Sparkes, R., Innes, A.M., Jackel-Cram, C., Ober, C., Parboosingh, J.S. & Lemire, E.G. 2017. A novel NDUFS4 frameshift mutation causes Leigh disease in the Hutterite population. *American Journal of Medical Genetics Part A*, 173(3):596-600.

Lee, H. & Wei, Y. 2005. Mitochondrial biogenesis and mitochondrial DNA maintenance of mammalian cells under oxidative stress. *International Journal of Biochemistry & Cell Biology*, 37(4):822-834.

Lee, H., Yin, P., Lu, C., Chi, C. & Y., W. 2000. Increase of mitochondria and mitochondrial DNA in response to oxidative stress in human cells. *Biochemical Journal*, 348(Pt 2):425-432.

Lestienne, P. & Ponsot, G. 1988. Kearns-Sayre syndrome with muscle mitochondrial DNA deletion. *Lancet*, 1(8590):885.

Lim, D., Jocelyn, K.M., Yip, G.W. & Bay, B.H. 2009. Silencing the metallothionein-2A gene inhibits cell cycle progression from G1- to S-phase involving ATM and cdc25A signaling in breast cancer cells. *Cancer Letters*, 276(1):109-117.

Lindeque, J.Z. 2007. Expression and mass spectrometric analysis of recombinant human metallothionein 2A. Potchefstroom: NWU. (Dissertation – M.Sc.).

Lindeque, J.Z. 2011. Metallothionein involvement in mitochondrial function and disease: a metabolomics investigation. Potchefstroom: NWU. (Thesis – PhD).

Lindeque, J.Z., Levanets, O., Louw, R. & van der Westhuizen, F.H. 2010. The involvement of metallothioneins in mitochondrial function and disease. *Current Protein and Peptide Science*, 11(4):292-309.

Liu, Y., Peterson, D.A., Kimura, H. & Schubert, D. 1997. Mechanism of cellular 3-(4,5-dimethylthiazol-2-yl)-2,5-diphenyltetrazolium bromide (MTT) reduction. *Journal of Neurochemistry*, 69(2):581-593.

Loeffen, J.L., Smeitink, J.A., Triepels, R.H., Smeets, R., Schuelke, M., Sengers, R.C., Trijbels, F., Hamel, B., Mullaart, R. & van den Heuvel, L. 1998. The first nuclear-encoded complex I mutation in a patient with Leigh syndrome. *American Journal of Human Genetics*, 63(6):1598-1608.

Loeffen, J.L., Smeitink, J.A., Trijbels, J.M., Janssen, A.J., Triepels, R.H., Sengers, R.C. & van den Heuvel, L.P. 2000. Isolated complex I deficiency in children: clinical, biochemical and genetic aspects. *Human Mutation*, 15(2):123-134.

Louw, R. 2017. Metabolomics of the Ndufs4 mouse [personal communication]. 16 Oct., Potchefstroom: NWU.

Ma, H. 2005. Simultaneous determination of metallothionein and thionein with cadmium-hemoglobin saturation method. *Journal of American Science*, 1(1):28-33.

Maldonado, E.N. & Lemasters, J.J. 2014. ATP/ADP ratio, the missed connection between mitochondria and the Warburg effect. *Mitochondrion*, 19 Pt A:78-84.

Mann, H.B. & Whitney, D.R. 1947. On a test of whether one of two random variables is stochastically larger than the other. *Annals of Mathematical Statistics*, 18(1):50-60.

Mannella, C.A. 2006. Structure and dynamics of the mitochondrial inner membrane cristae. *Biochimica et Biophysica Acta (BBA) - Molecular Cell Research*, 1763(5-6):542-548.

Maret, W. 1994. Oxidative metal release from metallothionein via zinc-thiol/disulfide interchange. *Proceedings of the National Academy of Sciences of the United States of America*, 91(1):237-241.

Maret, W., Jacob, C., Vallee, B.L. & Fischer, E.H. 1999. Inhibitory sites in enzymes: zinc removal and reactivation by thionein. *Proceedings of the National Academy of Sciences of the United States of America*, 96(5):1936-1940.

Margoshes, M. & Vallee, B.L. 1957. A cadmium protein from equine kidney cortex. *Journal of the American Chemical Society*, 79(17):4813-4814.

Marquez, J., Lee, S.R., Kim, N. & Han, J. 2016. Post-translational modifications of cardiac mitochondrial proteins in cardiovascular disease: not lost in translation. *Korean Circulation Journal*, 46(1):1-12.

Masters, B.A., Kelly, E.J., Quaife, C.J., Brinster, R.L. & Palmiter, R.D. 1994. Targeted disruption of metallothionein I and II genes increases sensitivity to cadmium. *Proceedings of the National Academy of Sciences of the United States of America*, 91(2):584-588.

Mehus, A.A., Muhonen, W.W., Garrett, S.H., Somji, S., Sens, D.A. & Shabb, J.B. 2014. Quantitation of human metallothionein isoforms: a family of small, highly conserved, cysteine-rich proteins. *Molecular and Cellular Proteomics*, 13(4):1020-1033.

Meissner-Roloff, M. 2009. The occurrence of mitochondrial DNA polymerase gamma gene mutations in mitochondrial deficiencies, in a selection of South African paediatric patients. Potchefstroom: NWU. (Dissertation – M.Sc.).

Melcher, M., Danhauser, K., Seibt, A., Degistirici, O., Baertling, F., Kondadi, A.K., Reichert, A.S., Koopman, W.J., Willems, P.H., Rodenburg, R.J., Mayatepek, E., Meisel, R. & Distelmaier, F. 2017. Modulation of oxidative phosphorylation and redox homeostasis in mitochondrial NDUFS4 deficiency via mesenchymal stem cells. *Stem Cell Research & Therapy*, 8(1):150.

Merten, K.E., Feng, W., Zhang, L., Pierce, W., Cai, J., Klein, J.B. & Kang, Y.J. 2005. Modulation of cytochrome C oxidase-Va is possibly involved in metallothionein protection from doxorubicin cardiotoxicity. *Journal of Pharmacology and Experimental Therapeutics*, 315(3):1314-1329.

Michalska, A.E. & Choo, K.H. 1993. Targeting and germ-line transmission of a null mutation at the metallothionein I and II loci in mouse. *Proceedings of the National Academy of Sciences of the United States of America*, 90(17):8088-8092.

Mimaki, M., Wang, X., McKenzie, M., Thorburn, D.R. & Ryan, M.T. 2012. Understanding mitochondrial complex I assembly in health and disease. *Biochimica et Biophysica Acta (BBA) - Bioenergtics*, 1817(6):851-862.

Min, K., Horie, T., Tetsutchikawahara, N. & Onosaka, S. 2005. Metallothionein suppresses the formation of 8-hydroxy-2'-deoxyguanosine in DNA induced by ferric nitrilotracetate in vitro. *Journal of Health Science*, 51(4):497-503.

Mitchell, P. 1961. Coupling of phosphorylation to electron and hydrogen transfer by a chemi-osmotic type of mechanism. *Nature*, 191(4784):144-148.

Miyahara, T., Nemoto, M., Tukamoto, S., Yamada, H., Kozuka, H., Kuze, S., Sudo, H. & Yamamoto, S. 1991. Induction of metallothionein and stimulation of calcification by dexamethasone in cultured clonal osteogenic cells, MC3T3-E1. *Toxicology Letters*, 57(3):257-267.

Molto, E., Bonzon-Kulichenko, E., Gallardo, N. & Andres, A. 2007. MTPA: a crustacean metallothionein that affects hepatopancreatic mitochondrial functions. *Archives of Biochemistry and Biophysics*, 467(1):31-40.

Mootha, V.K., Bunkenborg, J., Olsen, J.V., Hjerrild, M., Wisniewski, J.R., Stahl, E., Bolouri, M.S., Ray, H.N., Sihag, S., Kamal, M., Patterson, N., Lander, E.S. & Mann, M. 2003. Integrated analysis of protein composition, tissue diversity and gene regulation in mouse mitochondria. *Cell*, 115(5):629-640.

Mosmann, T. 1983. Rapid colorimetric assay for cellular growth and survival: application to proliferation and cytotoxicity assays. *Journal of Immunological Methods*, 65(1-2):55-63.

Mot, A.I., Liddell, J.R., White, A.R. & Crouch, P.J. 2016. Circumventing the Crabtree effect: a method to induce lactate consumption and increase oxidative phosphorylation in cell culture. *International Journal of Biochemistry and Cell Biology*, 79:128-138.

Mullis, K., Faloona, F., Scharf, S., Saiki, R., Horn, G. & Erlich, H. 1986. Specific enzymatic amplification of DNA in vitro: the polymerase chain reaction. *Cold Spring Harbor Symposia on Quantitative Biology*, 51(Pt 1):263-273.

Murai, M., Murakami, S., Ito, T. & Miyoshi, H. 2015. Amilorides bind to the quinone binding pocket of bovine mitochondrial complex I. *Biochemistry*, 54(17):2739-2746.

Nagano, T., Itoh, N., Ebisutani, C., Takatani, T., Miyoshi, T., Nakanishi, T. & Tanaka, K. 2000. The transport mechanism of metallothionein is different from that of classical NLS-bearing protein. *Journal of Cellular Physiology*, 185(3):440-446.

NCBI. 2017a. Mus musculus mitochondrion, complete genome. https://www.ncbi.nlm.nih.gov/nuccore/NC_005089 Date of access: 02 Feb. 2017.

NCBI. 2017b. Ndufs4 NADH dehydrogenase (ubiquinone) Fe-S protein 4 [ Mus musculus (house mouse) ]. https://www.ncbi.nlm.nih.gov/gene/?term=17993 Date of access: 19 Feb. 2017.

NCBI. 2017c. NDUFS4 NADH:ubiquinone oxidoreductase subunit S4 [ Homo sapiens (human) ]. https://www.ncbi.nlm.nih.gov/gene/4724 Date of access: 19 Feb. 2017.

Neildez-Nguyen, T.M., Parisot, A., Vignal, C., Rameau, P., Stockholm, D., Picot, J., Allo, V., Le Bec, C., Laplace, C. & Paldi, A. 2008. Epigenetic gene expression noise and phenotypic diversification of clonal cell populations. *Differentiation*, 76(1):33-40.

Nicholls, D.G. & Ferguson, J.L. 2002a. Bioenergetics. 3rd ed. San Diego, CA: Elsevier Science, Academic Press. p. 3-14.

Nicholls, D.G. & Ferguson, J.L. 2002b. Bioenergetics. 3rd ed. San Diego, CA: Elsevier Science, Academic Press. p. 89-154.

Nicholls, D.G. & Ferguson, J.L. 2002c. Bioenergetics. 3rd ed. San Diego, CA: Elsevier Science, Academic Press. p. 219-248.

Nijtmans, L.G., Henderson, N.S. & Holt, I.J. 2002. Blue native electrophoresis to study mitochondrial and other protein complexes. *Methods*, 26(4):327-334.

Niyazov, D.M., Kahler, S.G. & Frye, R.E. 2016. Primary mitochondrial disease and secondary mitochondrial dysfunction: importance of distinction for diagnosis and treatment. *Molecular Syndromology*, 7(3):122-137.

Obre, E. & Rossignol, R. 2015. Emerging concepts in bioenergetics and cancer research: metabolic flexibility, coupling, symbiosis, switch, oxidative tumors, metabolic remodeling, signaling and bioenergetic therapy. *International Journal of Biochemistry and Cell Biology*, 59:167-181.

Ohnishi, T. & Salerno, J.C. 2005. Conformation-driven and semiquinone-gated proton-pump mechanism in the NADH-ubiquinone oxidoreductase (complex I). *FEBS Letters*, 579(21):4555-4561.

OMIM. 2016a. Leigh syndrome; LS. https://www.omim.org/entry/256000?search=256000&highlight=256000 Date of access: 01 Mar. 2017.

OMIM. 2016b. Mitochondrial complex I deficiency. http://omim.org/entry/252010?search=mitochondrial%20deficiencies&highlight=deficiency%20mitochondrial Date of access: 18 Feb. 2017.

Palmiter, R.D., Sandgren, E.P., Koeller, D.M. & Brinster, R.L. 1993. Distal regulatory elements from the mouse metallothionein locus stimulate gene expression in transgenic mice. *Molecular and Cellular Biology*, 13(9):5266-5275.

Papa, S., Scacco, S., de Rasmo, D., Signorile, A., Papa, F., Panelli, D., Nicastro, A., Scaringi, R., Santeramo, A., Roca, E., Trentadue, R. & Larizza, M. 2010. cAMP-dependent protein kinase regulates post-translational processing and expression of complex I subunits in mammalian cells. *Biochimica et Biophysica Acta (BBA) - Bioenergetics*, 1797(6-7):649-658.

Park, C.B. & Larsson, N.G. 2011. Mitochondrial DNA mutations in disease and aging. *Journal of Cell Biology*, 193(5):809-818.

Parker, J. 2001. ATP (Adenosine Triphosphate) (*In* Miller, J.H. & Brenner, S., *eds.* Encyclopedia of Genetics, volume 1. New York, NY: Academic Press. p. 115-116).

Penkowa, M., Caceres, M., Borup, R., Nielsen, F.C., Poulsen, C.B., Quintana, A., Molinero, A., Carrasco, J., Florit, S., Giralt, M. & Hidalgo, J. 2006. Novel roles for metallothionein-I + II (MT-I + II) in defense responses, neurogenesis, and tissue restoration after traumatic brain injury: insights from global gene expression profiling in wild-type and MT-I + II knockout mice. *Journal of Neuroscience Research*, 84(7):1452-1474.

Penkowa, M., Camats, J., Giralt, M., Molinero, A., Hernandez, J., Carrasco, J., Campbell, I.L. & Hidalgo, J. 2003. Metallothionein-I overexpression alters brain inflammation and stimulates brain repair in transgenic mice with astrocyte-targeted interleukin-6 expression. *Glia*, 42(3):287-306.

Petkov, P.M., Cassell, M.A., Sargent, E.E., Donnelly, C.J., Robinson, P., Crew, V., Asquith, S., Haar, R.V. & Wiles, M.V. 2004. Development of a SNP genotyping panel for genetic monitoring of the laboratory mouse. *Genomics*, 83(5):902-911.

Pfaffl, M.W., Horgan, G.W. & Dempfle, L. 2002. Relative expression software tool (REST©) for group-wise comparison and statistical analysis of relative expression results in real-time PCR. *Nucleic Acids Research*, 30(9):e36.

Pilbrough, W., Munro, T.P. & Gray, P. 2009. Intraclonal protein expression heterogeneity in recombinant CHO cells. *PLOS ONE*, 4(12):e8432.

Pineau, B., Mathieu, C., Gerard-Hirne, C., de Paepe, R. & Chetrit, P. 2005. Targeting the NAD7 subunit to mitochondria restores a functional complex I and a wild type phenotype in the Nicotiana sylvestris CMS II mutant lacking nad7. *Journal of Biological Chemistry*, 280(28):25994-26001.

Porcelli, A.M., Calvaruso, M.A., Iommarini, L., Kurelac, I., Zuntini, R., Ferrari, S. & Gasparre, G. 2016. A unique combination of rare mitochondrial ribosomal RNA variants affects the kinetics of complex I assembly. *International Journal of Biochemistry and Cell Biology*, 75:117-122.

Pretorius, M. 2011. Evaluation of metallothionein involvement in the modulation of mitochondrial respiration in mice. Potchefstroom: NWU. (Dissertation – M.Sc.).

Prieur, I., Lunardi, J. & Dupuis, A. 2001. Evidence for a quinone binding site close to the interface between NUOD and NUOB subunits of complex I. *Biochimica et Biophysica Acta (BBA) - Bioenergetics*, 1504(2-3):173-178.

Quaife, C.J., Findley, S.D., Erickson, J.C., Froelick, G.J., Kelly, E.J., Zambrowicz, B.P. & Palmiter, R.D. 1994. Induction of a new metallothionein isoform (MT-IV) occurs during differentiation of stratified squamous epithelia. *Biochemistry*, 33(23):7250-7259.

Quesada, A.R., Byrnes, R.W., Krezoski, S.O. & Petering, D.H. 1996. Direct reaction of $H_2O_2$ with sulfhydryl groups in HL-60 cells: zinc-metallothionein and other sites. *Archives of Biochemistry and Biophysics*, 334(2):241-250.

Quintana, A., Kruse, S.E., Kapur, R.P., Sanz, E. & Palmiter, R.D. 2010. Complex I deficiency due to loss of Ndufs4 in the brain results in progressive encephalopathy resembling Leigh syndrome. *Proceedings of the National Academy of Sciences of the United States of America*, 107(24):10996-11001.

Quiros, P.M., Mottis, A. & Auwerx, J. 2016. Mitonuclear communication in homeostasis and stress. *Nature Reviews Molecular Cell Biology*, 17(4):213-226.

Raj, A. & van Oudenaarden, A. 2008. Nature, nurture, or chance: stochastic gene expression and its consequences. *Cell*, 135(2):216-226.

Reinecke, F. 2004. Functional properties of metallothionein expression in mitochondrial NADH:ubiquinone oxidoreductase deficiency. Potchefstroom: NWU. (Dissertation – M.Sc.).

Reinecke, F., Levanets, O., Olivier, Y., Louw, R., Semete, B., Grobler, A., Hidalgo, J., Smeitink, J.A., Olckers, A. & van der Westhuizen, F.H. 2006. Metallothionein isoform 2A expression is inducible and protects against ROS-mediated cell death in rotenone-treated HeLa cells. *Biochemical Journal*, 395(2):405-415.

Reinecke, F., Smeitink, J.A. & van der Westhuizen, F.H. 2009. OXPHOS gene expression and control in mitochondrial disorders. *Biochimica et Biophysica Acta (BBA) - Molecular Basis of Disease*, 1792(12):1113-1121.

Reznik, E., Miller, M., Senbabaoglu, Y., Riaz, N., Lee, W. & Sander, C. 2015. Mitochondrial DNA copy number variation across human cancers. *Elife*, 5(2016):1-23.

Rigby, K.E. & Stillman, M.J. 2004. Structural studies of metal-free metallothionein. *Biochemical and Biophysical Research Communications*, 325(4):1271-1278.

Rodenburg, R.J. 2011. Biochemical diagnosis of mitochondrial disorders. *Journal of Inherited Metabolic Disease*, 34(2):283-292.

Rodenburg, R.J. 2016. Mitochondrial complex I-linked disease. *Biochimica et Biophysica Acta (BBA) - Bioenergetics*, 1857(7):938-945.

Rodriguez-Enriquez, S., Juarez, O., Rodriguez-Zavala, J.S. & Moreno-Sanchez, R. 2001. Multisite control of the Crabtree effect in ascites hepatoma cells. *European Journal of Biochemistry*, 268(8):2512-2519.

Rofe, A.M., Philcox, J.C. & Coyle, P. 1996. Trace metal, acute phase and metabolic response to endotoxin in metallothionein-null mice. *Biochemical Journal*, 314(Pt 3):793-797.

Rossignol, R. 2015. Energy metabolism disorders in rare and common diseases. Toward bioenergetic modulation therapy and the training of a new generation of European scientists. *International Journal of Biochemistry and Cell Biology*, 63:2-9.

Rossignol, R., Faustin, B., Rocher, C., Malgat, M., Mazat, J. & Letellier, T. 2003. Mitochondrial threshold effects. *Biochemical Journal*, 370(Pt 3):751-762.

Rub, C., Wilkening, A. & Voos, W. 2017. Mitochondrial quality control by the Pink1/Parkin system. *Cell and Tissue Research*, 367(1):111-123.

Rubin, H. 1997. Cell aging in vivo and in vitro. *Mechanisms of Ageing and Development*, 98(1):1-35.

Rubio-Osornio, M., Orozco-Ibarra, M., Diaz-Ruiz, A., Brambila, E., Boll, M.C., Monroy-Noyola, A., Guevara, J., Montes, S. & Rios, C. 2017. Copper sulfate pretreatment prevents mitochondrial electron transport chain damage and apoptosis against $MPP^+$-induced neurotoxicity. *Chemico-Biological Interactions*, 271:1-8.

Sabar, M., Balk, J. & Leaver, C.J. 2005. Histochemical staining and quantification of plant mitochondrial respiratory chain complexes using blue-native polyacrylamide gel electrophoresis. *Plant Journal*, 44(5):893-901.

Sanchez-Caballero, L., Guerrero-Castillo, S. & Nijtmans, L. 2016. Unraveling the complexity of mitochondrial complex I assembly: a dynamic process. *Biochimica et Biophysica Acta (BBA) - Bioenergetics*, 1857(7):980-990.

Sancho, M., Di-Gregorio, A., George, N., Pozzi, S., Sanchez, J.M., Pernaute, B. & Rodriguez, T.A. 2013. Competitive interactions eliminate unfit embryonic stem cells at the onset of differentiation. *Developmental Cell*, 26(1):19-30.

Sazanov, L.A. 2015. A giant molecular proton pump: structure and mechanism of respiratory complex I. *Nature Reviews Molecular Cell Biology*, 16(6):375-388.

Scacco, S., Petruzzella, V., Budde, S., Vergari, R., Tamborra, R., Panelli, D., van den Heuvel, L.P., Smeitink, J.A. & Papa, S. 2003. Pathological mutations of the human NDUFS4 gene of the 18-kDa (AQDQ) subunit of complex I affect the expression of the protein and the assembly and function of the complex. *Journal of Biological Chemistry*, 278(45):44161-44167.

Schagger, H. & Pfeiffer, K. 2000. Supercomplexes in the respiratory chains of yeast and mammalian mitochondria. *EMBO Journal*, 19(8):1777-1783.

Schagger, H. & von Jagow, G. 1991. Blue native electrophoresis for isolation of membrane protein complexes in enzymatically active form. *Analytical Biochemistry*, 199(2):223-231.

Schauwecker, P.E. 2011. The relevance of individual genetic background and its role in animal models of epilepsy. *Epilepsy Research*, 97(1-2):1-11.

Schmittgen, T.D. & Livak, K.J. 2008. Analyzing real-time PCR data by the comparative $C_T$ method. *Nature Protocols*, 3(6):1101-1108.

Seddon, A.M., Curnow, P. & Booth, P.J. 2004. Membrane proteins, lipids and detergents: not just a soap opera. *Biochimica et Biophysica Acta (BBA) - Biomembranes*, 1666(1-2):105-117.

Seelert, H., Dani, D.N., Dante, S., Hauss, T., Krause, F., Schafer, E., Frenzel, M., Poetsch, A., Rexroth, S., Schwassmann, H.J., Suhai, T., Vonck, J. & Dencher, N.A. 2009. From protons to OXPHOS supercomplexes and Alzheimer's disease: structure-dynamics-function relationships of energy-transducing membranes. *Biochimica et Biophysica Acta (BBA) - Bioenergetics*, 1787(6):657-671.

Seluanov, A., Vaidya, A. & Gorbunova, V. 2010. Establishing primary adult fibroblast cultures from rodents. *Journal of Visualized Experiments,* (44):e2033.

Shakiba, N. & Zandstra, P.W. 2017. Engineering cell fitness: lessons for regenerative medicine. *Current Opinion in Biotechnology*, 47:7-15.

Sharpley, M.S., Marciniak, C., Eckel-Mahan, K., McManus, M., Crimi, M., Waymire, K., Lin, C.S., Masubuchi, S., Friend, N., Koike, M., Chalkia, D., MacGregor, G., Sassone-Corsi, P. & Wallace, D.C. 2012. Heteroplasmy of mouse mtDNA is genetically unstable and results in altered behavior and cognition. *Cell*, 151(2):333-343.

Shimoda, R., Achanzar, W.E., Qu, W., Nagamine, T., Takagi, H., Mori, M. & Waalkes, M.P. 2003. Metallothionein is a potential negative regulator of apoptosis. *Toxicological Sciences*, 73(2):294-300.

Smeitink, J.A., van den Heuvel, L. & DiMauro, S. 2001. The genetics and pathology of oxidative phosphorylation. *Nature Reviews Genetics*, 2(5):342-352.

Smeitink, J.A., van den Heuvel, L.W., Koopman, W.J., Nijtmans, L.G., Ugalde, C. & Willems, P.H. 2004. Cell biological consequences of mitochondrial NADH:ubiquinone oxidoreductase deficiency. *Current Neurovascular Research*, 1(1):29-40.

Smith, P.K., Krohn, R.I., Hermanson, G.T., Mallia, A.K., Gartner, F.H., Provenzano, M.D., Fujimoto, E.K., Goeke, N.M., Olson, B.J. & Klenk, D.C. 1985. Measurement of protein using bicinchoninic acid. *Analytical Biochemistry*, 150(1):76-85.

Song, L., Yu, A., Murray, K. & Cortopassi, G. 2017. Bipolar cell reduction precedes retinal ganglion neuron loss in a complex 1 knockout mouse model. *Brain Research*, 1657:232-244.

Stroud, D.A., Surgenor, E.E., Formosa, L.E., Reljic, B., Frazier, A.E., Dibley, M.G., Osellame, L.D., Stait, T., Beilharz, T.H., Thorburn, D.R., Salim, A. & Ryan, M.T. 2016. Accessory subunits are integral for assembly and function of human mitochondrial complex I. *Nature*, 538(7623):123-126.

Takashima, A. 1998. Unit 2.1 - Establishment of fibroblast cultures. Current protocols in cell biology. p. 2.1.1-2.1.12.

Tarasov, A.I., Griffiths, E.J. & Rutter, G.A. 2012. Regulation of ATP production by mitochondrial $Ca^{2+}$. *Cell Calcium*, 52(1):28-35.

Torraco, A., Diaz, F., Vempati, U.D. & Moraes, C.T. 2009. Mouse models of oxidative phosphorylation defects: powerful tools to study the pathobiology of mitochondrial diseases. *Biochimica et Biophysica Acta (BBA) - Molecular Cell Research*, 1793(1):171-180.

Trifunovic, A., Wredenberg, A., Falkenberg, M., Spelbrink, J.N., Rovio, A.T., Bruder, C.E., Bohlooly-Y, M., Gidlof, S., Oldfors, A., Wibom, R., Tornell, J., Jacobs, H.T. & Larsson, N. 2004. Premature ageing in mice expressing defective mitochondrial DNA polymerase. *Nature*, 429(6990):417-423.

Tukey, J.W. 1977. Some thoughts on clinical trials, especially problems of multiplicity. *Science*, 198(4318):679-684.

Tyynismaa, H., Mjosund, K.P., Wanrooij, S., Lappalainen, I., Ylikallio, E., Jalanko, A., Spelbrink, J.N., Paetau, A. & Suomalainen, A. 2005. Mutant mitochondrial helicase Twinkle causes multiple mtDNA deletions and a late-onset mitochondrial disease in mice. *Proceedings of the National Academy of Sciences of the United States of America*, 102(49):17687-17692.

Ugalde, C., Janssen, R.J., van den Heuvel, L.P., Smeitink, J.A. & Nijtmans, L.G. 2004. Differences in assembly or stability of complex I and other mitochondrial OXPHOS complexes in inherited complex I deficiency. *Human Molecular Genetics*, 13(6):659-667.

Valko, M., Leibfritz, D., Moncol, J., Cronin, M.T., Mazur, M. & Telser, J. 2007. Free radicals and antioxidants in normal physiological functions and human disease. *International Journal of Biochemistry and Cell Biology*, 39(1):44-84.

Valsecchi, F., Grefte, S., Roestenberg, P., Joosten-Wagenaars, J., Smeitink, J.A., Willems, P.H. & Koopman, W.J. 2013. Primary fibroblasts of NDUFS4$^{-/-}$ mice display increased ROS levels and aberrant mitochondrial morphology. *Mitochondrion*, 13(5):436-443.

Valsecchi, F., Monge, C., Forkink, M., de Groof, A.J., Benard, G., Rossignol, R., Swarts, H.G., van Emst-de Vries, S.E., Rodenburg, R.J., Calvaruso, M.A., Nijtmans, L.G., Heeman, B., Roestenberg, P., Wieringa, B., Smeitink, J.A., Koopman, W.J. & Willems, P.H. 2012. Metabolic consequences of NDUFS4 gene deletion in immortalized mouse embryonic fibroblasts. *Biochimica et Biophysica Acta (BBA) - Bioenergetics*, 1817(10):1925-1936.

van den Bossche, J., Baardman, J. & de Winther, M.P. 2015. Metabolic characterization of polarized M1 and M2 bone marrow-derived macrophages using real-time extracellular flux analysis. *Journal of Visualized Experiments,* (105):e53424.

van den Heuvel, L.P., Smeitink, J.A. & Rodenburg, R.J. 2004. Biochemical examination of fibroblasts in the diagnosis and research of oxidative phosphorylation (OXPHOS) defects. *Mitochondrion*, 4(5-6):395-401.

van der Lee, R., Szklarczyk, R., Smeitink, J.A., Smeets, H.J., Huynen, M.A. & Vogel, R. 2015. Transcriptome analysis of complex I-deficient patients reveals distinct expression programs for subunits and assembly factors of the oxidative phosphorylation system. *BioMed Central Genomics*, 16:691.

van der Westhuizen, F.H. 2017a. Detection of metallothionein I protein [personal communication]. 15 May., Potchefstroom: NWU.

van der Westhuizen, F.H. 2017b. Outlier removal from limited replicates [personal communication]. 24 Oct., Potchefstroom: NWU.

van der Westhuizen, F.H., van den Heuvel, L.P., Smeets, R., Veltman, J.A., Pfundt, R., van Kessel, A.G., Ursing, B.M. & Smeitink, J.A. 2003. Human mitochondrial complex I deficiency: investigating transcriptional responses by microarray. *Neuropediatrics*, 34(1):14-22.

van Dyk, H.C. 2013. Development of cytoplasmic hybrid cells to evaluate mitochondrial DNA mutation pathogenicity. Potchefstroom: NWU. (Mini-dissertation – Honours).

van Dyk, H.C. 2016. Evaluating the involvement of mtDNA variants in patients diagnosed with myalgic encephalomyelitis. Potchefstroom: NWU. (Dissertation – M.Sc.).

van Wyk, R. 2016. The effects of a complex I knockout on the bioenergetics of NDUFS4 knockout mice heart tissue. Potchefstroom: NWU. (Mini-dissertation – Honours).

Vasak, M. 2005. Advances in metallothionein structure and functions. *Journal of Trace Elements in Medicine and Biology*, 19(1):13-17.

Vasava, A.A. & Mashiyava, P.H. 2016. Electron transport chain: role in reactive oxygen species production and aging. *Scholars Journal of Agriculture and Veterinary Sciences*, 3(5):378-388.

Vasconcelos, M. 2002. Metal- and tissue-dependent relationship between metallothionein mRNA and protein. *Toxicology and Applied Pharmacology*, 182(2):91-97.

Vempati, U.D., Torraco, A. & Moraes, C.T. 2008. Mouse models of oxidative phosphorylation dysfunction and disease. *Methods*, 46(4):241-247.

Voets, A.M., Huigsloot, M., Lindsey, P.J., Leenders, A.M., Koopman, W.J., Willems, P.H., Rodenburg, R.J., Smeitink, J.A. & Smeets, H.J. 2012. Transcriptional changes in OXPHOS complex I deficiency are related to anti-oxidant pathways and could explain the disturbed calcium homeostasis. *Biochimica et Biophysica Acta (BBA) - Molecular Basis of Disease*, 1822(7):1161-1168.

Wallace, D.C., Singh, G., Lott, M.T., Hodge, J.A., Schurr, T.G., Lezza, A.M., Elsas II, L.J. & Nikoskelainen, E.K. 1988. Mitochondrial DNA mutation associated with Leber's hereditary optic neuropathy. *Science*, 242(4884):1427-1430.

Warburg, O., Wind, F. & Negelein, E. 1927. The metabolism of tumors in the body. *Journal of Biological Chemistry*, 8(6):519-530.

Wentzel, J.F., Lombard, M.J., du Plessis, L.H. & Zandberg, L. 2017. Evaluation of the cytotoxic properties, gene expression profiles and secondary signalling responses of cultured cells exposed to fumonisin B1, deoxynivalenol and zearalenone mycotoxins. *Archives of Toxicology*, 91(5):2265-2282.

Weydert, C.J. & Cullen, J.J. 2010. Measurement of superoxide dismutase, catalase and glutathione peroxidase in cultured cells and tissue. *Nature Protocols*, 5(1):51-66.

Willems, P.H., Smeitink, J.A. & Koopman, W.J. 2009. Mitochondrial dynamics in human NADH:ubiquinone oxidoreductase deficiency. *International Journal of Biochemistry and Cell Biology*, 41(10):1773–1782.

Wittig, I., Braun, H.P. & Schagger, H. 2006. Blue native PAGE. *Nature Protocols*, 1(1):418-428.

Woese, C.R., Olsen, G.J., Ibba, M. & Soll., D. 2000. Aminoacyl-tRNA synthetases the genetic code and the evolutionary process. *Microbiology and Molecular Biology Reviews*, 64(1):202-236.

Wong, D.L., Merrifield-MacRae, M.E. & Stillman, M.J. 2017. (*In* Sigel, A., Sigel, H. & Sigel, R.K., *eds*. Metal ions in life sciences, volume 17. Berlin: Walter de Gruyter GmbH. p. 241-269).

Woo, E.S., Dellapiazza, D., Wang, A.S. & Lazo, J.S. 2000. Energy-dependent nuclear binding dictates metallothionein localization. *Journal of Cellular Physiology*, 182(1):69-76.

Wortmann, S.B., Mayr, J.A., Nuoffer, J.M., Prokisch, H. & Sperl, W. 2017. A guideline for the diagnosis of pediatric mitochondrial disease: the value of muscle and skin biopsies in the genetics era. *Neuropediatrics*, 48(4):309-314.

Wu, H. & Kang, Y.J. 1998. Inhibition of buthionine sulfoximine-enhanced doxorubicin toxicity in metallothionein overexpressing transgenic mouse heart. *Journal of Pharmacology and Experimental Therapeutics*, 287(2):515-520.

Ye, B., Maret, W. & Vallee, B.L. 2001. Zinc metallothionein imported into liver mitochondria modulates respiration. *Proceedings of the National Academy of Sciences of the United States of America*, 98(5):2317-2322.

Yonekawa, T. & Thorburn, A. 2013. Autophagy and cell death. *Essays in Biochemistry*, 55:105-117.

Yousuf, S., Atif, F., Ahmad, M., Hoda, N., Ishrat, T., Khan, B. & Islam, F. 2009. Resveratrol exerts its neuroprotective effect by modulating mitochondrial dysfunctions and associated cell death during cerebral ischemia. *Brain Research*, 1250:242-253.

Zhang, J., Nuebel, E., Wisidagama, D.R., Setoguchi, K., Hong, J.S., van Horn, C.M., Imam, S.S., Vergnes, L., Malone, C.S., Koehler, C.M. & Teitell, M.A. 2012. Measuring energy metabolism in cultured cells, including human pluripotent stem cells and differentiated cells. *Nature Protocols*, 7(6):1068-1085.

# APPENDIX A:

## PUNNETT SQUARES

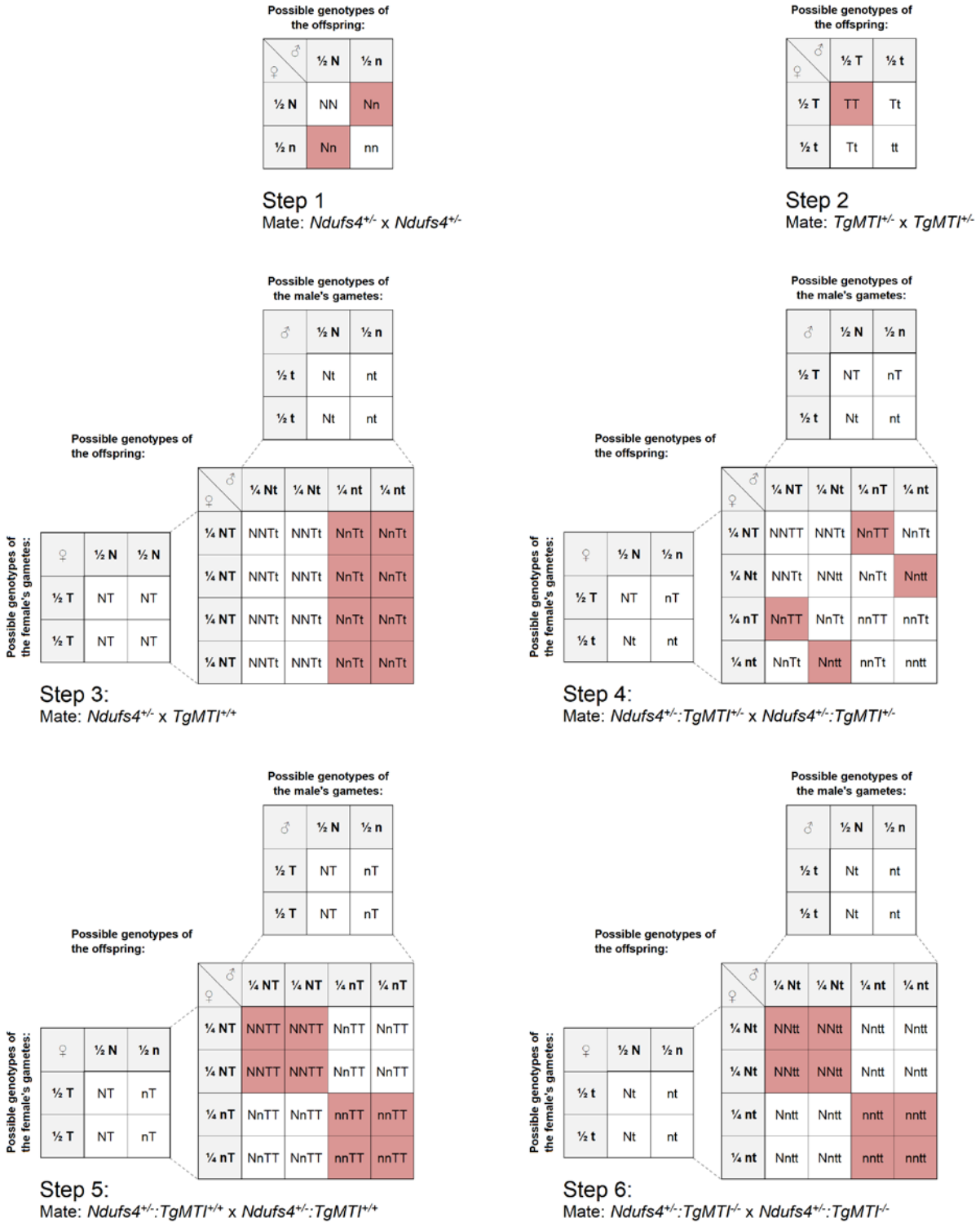


**Figure A.1: Punnett squares depicting how the probability of each genotype was determined as a fraction of 4 or 16.** For example, offspring from Step 1 have a 2 in 4 (50%)

chance of being born with an *Ndufs4*$^{+/-}$ genotype. NN and TT refer to *Ndufs4*$^{+/+}$ and *TgMTI*$^{+/+}$ respectively, while nn and tt signify *Ndufs4*$^{-/-}$ and *TgMTI*$^{-/-}$. *Ndufs4*$^{+/-}$ and *TgMTI*$^{+/-}$ are indicated by Nn and Tt. Red squares represent the desired genotype outcome of each step.

# APPENDIX B:

## OPTIMISATION OF THE qPCR AMPLIFICATION OF DNA & RNA

### INTRODUCTION

Prior to performing qPCR assays in which the quantity of a target gene is expressed relative to that of a reference gene (i.e. the $2^{-\Delta CT}$ method), it is necessary to determine: (i) The optimal concentration of input template DNA or RNA, as well as (ii) the individual efficiency and (iii) the relative efficiency of the target and reference qPCR amplification reactions. This appendix provides a short summary of each for the experiments described in Sections 4.3.4.1.d, 4.3.5.1.c and 4.4.2.1. For a more detailed explanation of the underlying principles, the reader is referred to van Dyk (2013).

### i. OPTIMISATION OF INPUT TEMPLATE DNA & RNA CONCENTRATION

To determine each parameter, reactions were prepared, in separate and triplicate wells, for the target [*MtI, mt-Nd2* or *MtI* (mRNA)] and reference [*Actb* or *B2m* (mRNA)] genes, according to the respective methods described in Sections 4.3.4.1.d, 4.3.5.1.c and 4.4.2.1. The DNA and RNA used were respectively isolated (as explained in Sections 4.3.4.1.b and 4.3.5.1.b) from the tail-snip (mouse ID 67) and liver tissue (mouse ID 66) samples of WT mice (see Table B.1).

**Table B.1: Mice used to optimise qPCR amplification**

| Animal ID | Genotype | Gender | DOB |
|---|---|---|---|
| 66 | *Ndufs4*$^{+/+}$*:TgMTI*$^{-/-}$ | Male | 2016-06-28 |
| 67 | *Ndufs4*$^{+/+}$*:TgMTI*$^{-/-}$ | Male | 2016-06-28 |

The table displays the ear punch identification number (ID), genotype, gender, and date of birth (DOB) of the mice.

To determine the optimal input template DNA or RNA concentration, a two-fold serial dilution range was set up for each experiment. As before, lack of reagent contamination was confirmed via an NTC, which yielded undefined $C_T$-values. For the DNA samples, the average $C_T$-values and SDs obtained for each gene may be found in Table B.2, while Figure B.1 depicts the standard curve for these results. For the RNA samples, the same information is displayed in Table B.3 and Figure B.2.

**Table B.2: Average $C_T$-values obtained for the *Mtl*, *mt-Nd2* and *Actb* genes using a serial dilution of DNA**

| | | | | | | |
|---|---|---|---|---|---|---|
| **Input template DNA (in ng)** | 3.13 | 6.25 | 12.5 | 25.0 | 50.0 | 100 |
| **log (ng input template DNA)** | 0.49 | 0.80 | 1.10 | 1.40 | 1.70 | 2.00 |
| **Average *Mtl* $C_T$-values** | 29.7 | 28.6 | 27.6 | 26.4 | 25.5 | 24.4 |
| **SD for *Mtl*** | 0.07 | 0.08 | 0.06 | 0.05 | 0.09 | 0.04 |
| **Average *mt-Nd2* $C_T$-values** | 23.9 | 22.9 | 21.8 | 20.8 | 19.5 | 18.4 |
| **SD for *mt-Nd2*** | 0.11 | 0.02 | 0.03 | 0.02 | 0.02 | 0.06 |
| **Average *Actb* $C_T$-values** | 30.6 | 29.6 | 28.4 | 27.5 | 26.4 | 25.3 |
| **SD for *Actb*** | 0.02 | 0.01 | 0.10 | 0.10 | 0.07 | 0.09 |

The table displays the serial dilution of input template DNA used, the log thereof, as well as the average $C_T$-values and SDs calculated for the qPCR amplification of each gene.

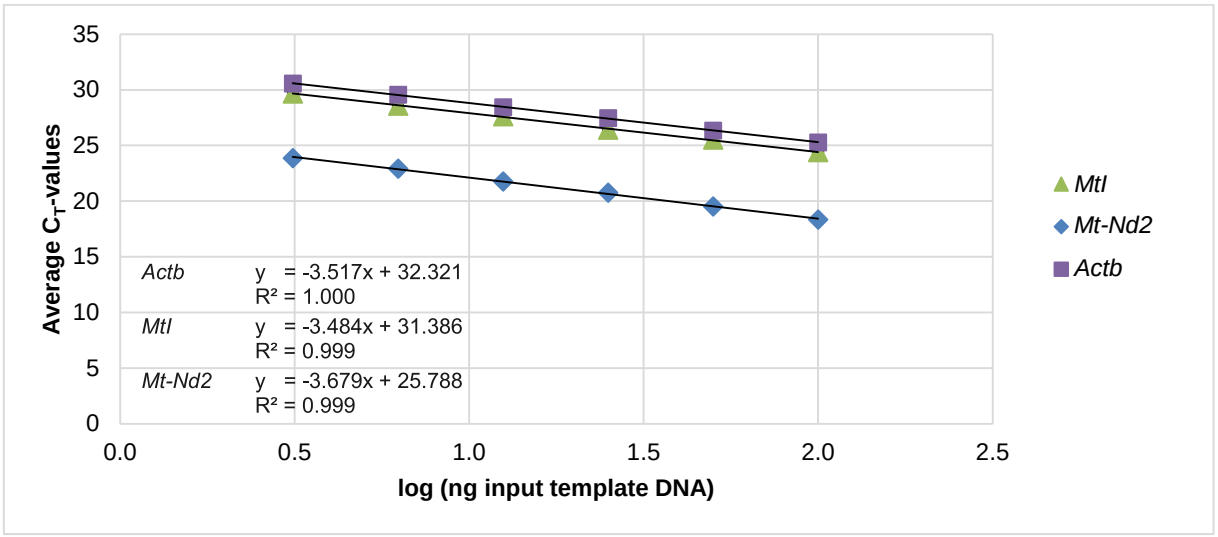


**Figure B.1: Standard curve depicting the results for *Mtl*, *mt-Nd2* and *Actb* in Table B.2.** The curve shows the average $C_T$-values obtained for the *Mtl* and *mt-Nd2* target genes and *Actb* reference gene, plotted against the log of the quantity (in ng) of input template DNA used for each reaction. The equation and $R^2$-value of each curve are also depicted.

**Table B.3: Average $C_T$-values obtained for the *Mtl* (mRNA) and *B2m* (mRNA) genes using a serial dilution of RNA**

| | | | | |
|---|---|---|---|---|
| **Input template RNA (in ng)** | 31.3 | 62.5 | 125 | 250 |
| **log (ng input template RNA)** | 1.49 | 1.80 | 2.10 | 2.40 |
| **Average *Mtl* (mRNA) $C_T$-values** | 24.5 | 23.0 | 21.8 | 21.0 |
| **SD for *Mtl* (mRNA)** | 0.41 | 0.71 | 0.32 | 0.35 |
| **Average *B2m* (mRNA) $C_T$-values** | 18.0 | 17.0 | 16.4 | 15.3 |
| **SD for *B2m* (mRNA)** | 0.35 | 0.20 | 0.38 | 0.22 |

The table shows the serial dilution of input template RNA used, the log thereof, as well as the average $C_T$-values and SDs calculated for the qPCR amplification of each gene.

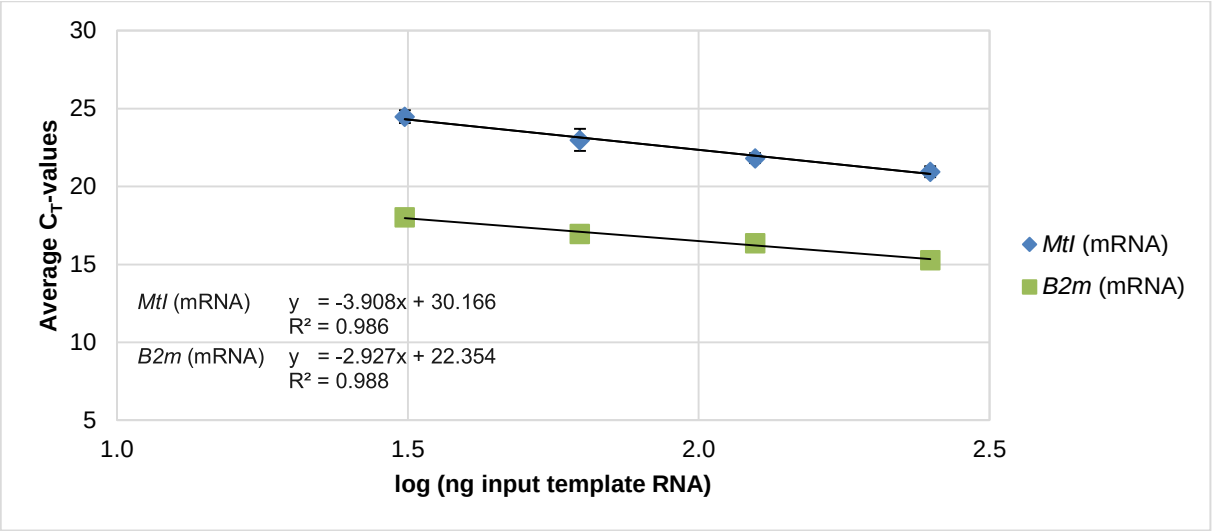


**Figure B.2: Standard curve depicting the results for *MtI* (mRNA) and *B2m* (mRNA) in Table B.3.** The curve displays the average $C_T$-values obtained for the *MtI* (mRNA) target gene and *B2m* (mRNA) reference gene, plotted against the log of the quantity (in ng) of input template RNA used for each reaction. The equation and $R^2$-value of each curve are also depicted.

When plotting data, the linearity thereof (i.e. how well the experimental data fits the regression line) is represented by the $R^2$-value. This linearity serves as a measure of the variability between samples and in this case, indicates whether the PCR amplification efficiency is similar across the DNA or RNA concentrations used. Since the $R^2$-values of each gene analysed in Figures B.1 and B.2 were above 0.980, and $R^2$-values >0.980 are generally deemed acceptable, any of the DNA or RNA concentrations may be used in the qPCR analyses. It was therefore decided to use a total of 10 ng DNA and 100 ng RNA per reaction.

### ii. PCR AMPLIFICATION EFFICIENCY

The Relative expression software tool (REST©), first described by Pfaffl *et al.* (2002), was used to determine the PCR amplification efficiency (E) of each gene. This was done by substituting the slope of each curve in Figures B.1 and B.2 into Equation B.1, which has a theoretical minimum and maximum of 1 and 2:

$$\mathrm{E} = 10^{(-1/\mathrm{slope})} \qquad (\mathrm{B.1})$$

Each PCR amplification efficiency was then further converted to a percentage according to Equation B.2 to indicate the percent of template DNA or cDNA that was successfully amplified in each cycle (with 0% signifying no amplification and 100% indicating perfect PCR product doubling) (Bio-Rad: Real-Time PCR Applications Guide, Bulletin 5279).

$$\% \text{ Efficiency} = (\text{E} - 1) \text{ x } 100\% \qquad \text{(B.2)}$$

Consequently, the percentage PCR efficiencies for the amplification of the *MtI, mt-Nd2, Actb, MtI* (mRNA), and *B2m* (mRNA) genes were respectively determined to be 93.65%, 86.98%, 92.47%, 80.27%, and 119.6%. In theory, amplification efficiencies of 90% to 105% are regarded as satisfactory. Therefore, the *MtI* and *Actb* reactions were deemed adequate. Even though the efficiency of *mt-Nd2* was below 90%, it was close enough to be regarded as sufficient. By contrast, the PCR amplification efficiencies of *MtI* (mRNA) and *B2m* (mRNA), deviated more than would normally be acceptable. Since the multiplex RT-qPCR assay included two steps (i.e. the reverse transcription of mRNA to cDNA, and the subsequent amplification of cDNA), this method displayed a larger capacity for error. Therefore, the poorer PCR amplification efficiencies were attributed to the shortcomings of the assay itself, and deemed acceptable for the purpose of simply displaying a clear difference between MTI expression in WT and MTI overexpressing mice.

### iii. RELATIVE EFFICIENCY OF COMPARED qPCR REACTIONS

To determine whether or not the target gene of choice could be expressed relative to a specific reference gene using the $\Delta C_T$ method, it was necessary to show that the PCR amplification efficiencies of both reactions were equivalent. This was achieved by examining the slope of the relative efficiency plot, as shown in Figures B.3, B.4, and B.5. (Applied Biosystems: User Bulletin No. 2, P/N 4303859).

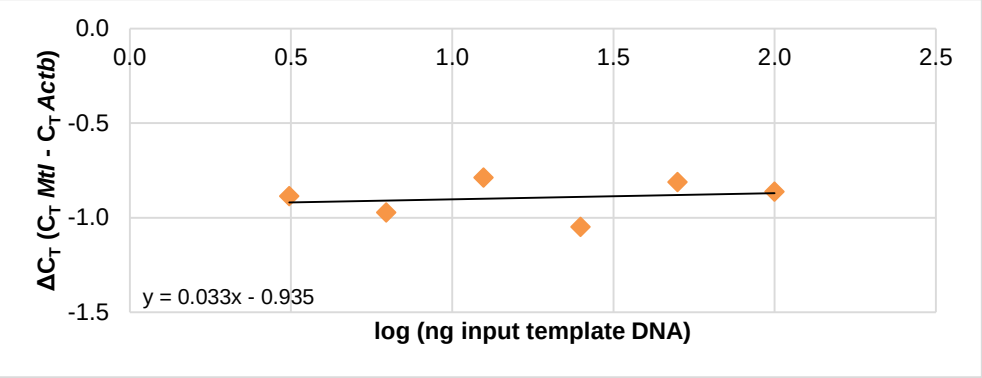


**Figure B.3: Relative efficiency plot for *MtI* and *Actb*.** The curve depicts the $\Delta C_T$-values obtained from the *MtI* target gene and *Actb* reference gene, plotted against the log of the quantity (in ng) of input template DNA used for each reaction (data from Table B.2). The equation of the curve is also displayed.

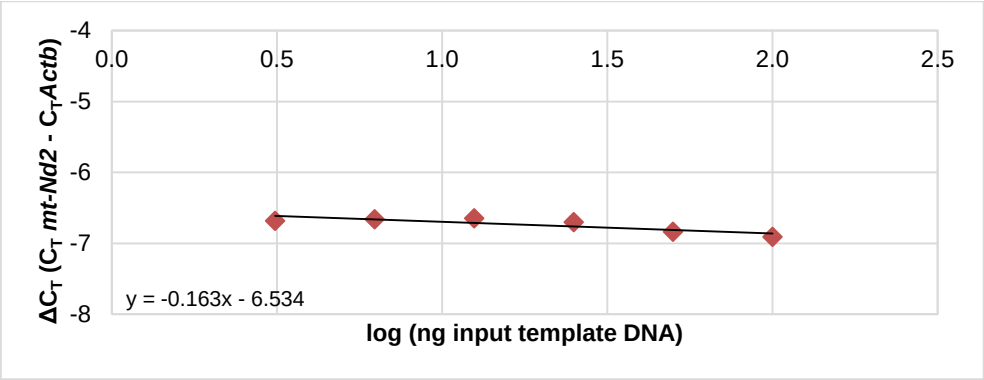


**Figure B.4: Relative efficiency plot for *mt-Nd2* and *Actb*.** The curve depicts the $\Delta C_T$-values obtained from the *mt-Nd2* target gene and *Actb* reference gene, plotted against the log of the quantity (in ng) of input template DNA used for each reaction (data from Table B.2). The equation of the curve is also displayed.

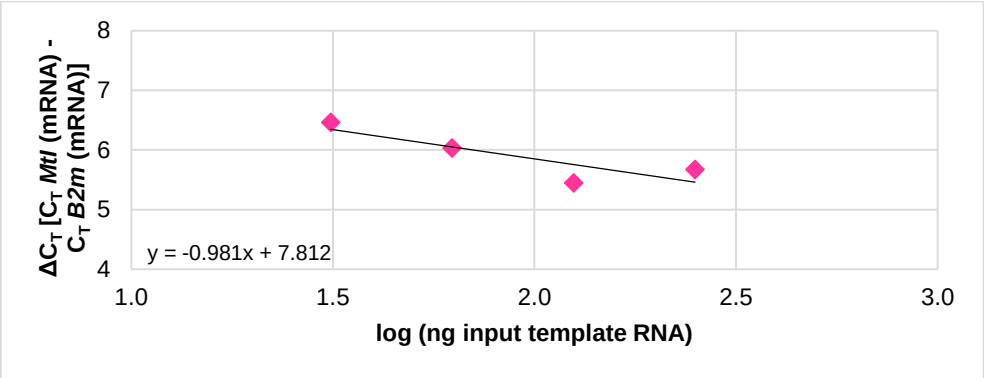


**Figure B.5: Relative efficiency plot for *MtI* (mRNA) and *B2m* (mRNA).** The curve depicts the $\Delta C_T$-values obtained from the *MtI* (mRNA) target gene and *B2m* (mRNA) reference gene, plotted against the log of the quantity (in ng) of input template RNA used for each reaction (data from Table B.3). The equation of the curve is also displayed.

For the PCR amplification efficiencies of the target and reference genes to be equivalent, the absolute value of the slope of the relative efficiency plot should ideally be <0.1. While this was the case for the *MtI* and *Actb* genes (Figure B.3) which yielded a value of 0.033, the |slope| of the relative efficiency curve for *mt-Nd2* and *Actb* (Figure B.4) was 0.163. Previous work by van Dyk (2013), however, reported that this slope was sufficient for the purpose of determining the RMCN. Similarly, the |slope| of the *MtI* (mRNA) and *B2m* (mRNA) strayed from the advised values (0.981; Figure B.5). It was however decided to continue with this analysis, and the deviation was attributed to the shortcomings of the multiplex RT-qPCR assay.

# APPENDIX C:

## PREPARATION OF SDS-PAGE GEL

The protein preparations isolated for NDUFS4 detection were separated on a 1 mm SDS-PAGE gel. The preparation of the constituting 4% stacking- and 10% resolving gels is shown in Table C.1.

**Table C.1: Content of the stacking- and resolving components of the SDS-PAGE gel**

| Reagent | Cat. no. & Company of purchase | Final concentration | |
|---|---|---|---|
| | | Stacking gel (4%) | Resolving gel (10%) |
| **Milli-Q® $H_2O$** | - | - | - |
| **Tris (pH 8.8)** | - | - | 0.375 M |
| **Tris (pH 6.8)** | - | 0.125 M | - |
| **Acrylamide-Bis (37.5:1; 30%)** | 100639100, Merck | 4 % (v/v) | 10 % (v/v) |
| **SDS** | L3771, Sigma-Aldrich | 0.10 % (w/v) | 0.10 % (w/v) |
| **APS** | A3678, Sigma-Aldrich | 0.05 % (w/v) | 0.05 % (w/v) |
| **TEMED** | T7024, Sigma-Aldrich | 0.10 % (w/v) | 0.10 % (w/v) |
| **Total volume prepared (in µL)** | | 3 000 | 5 000 |

The table displays the reagents (and their final concentrations) used to prepare the 4% stacking- and 10% resolving components of the SDS-PAGE gel. APS = ammonium persulphate, cat. no. = catalogue number, SDS = sodium dodecyl sulphate, TEMED = *N,N,N',N'*-tetramethylethylenediamine.

# APPENDIX D:

## 96-WELL MICROTITER PLATE LAYOUTS

The following figures depict the 96-well microtiter plate layouts used in Sections 4.4.1, 4.4.3, 4.4.4, and 4.4.6:

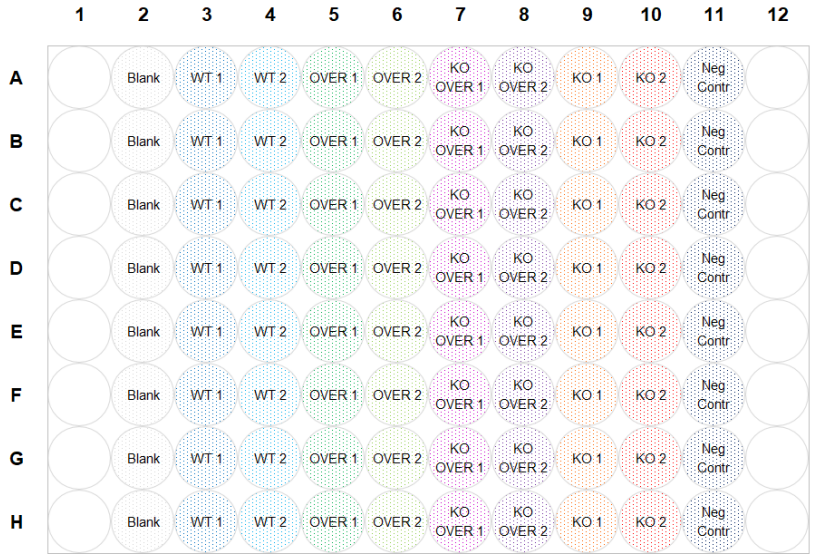


**Figure D.1: Microtiter plate layout used for the MTT assay.** Cells (see Table 4.2) were seeded as described in Section 4.4.1. In addition, blank wells (no cells), as well as negative controls (using cells from WT 1), were set up. The latter were treated with 6% (v/v) acetic acid in galactose-containing medium as explained. Neg Contr = negative control.

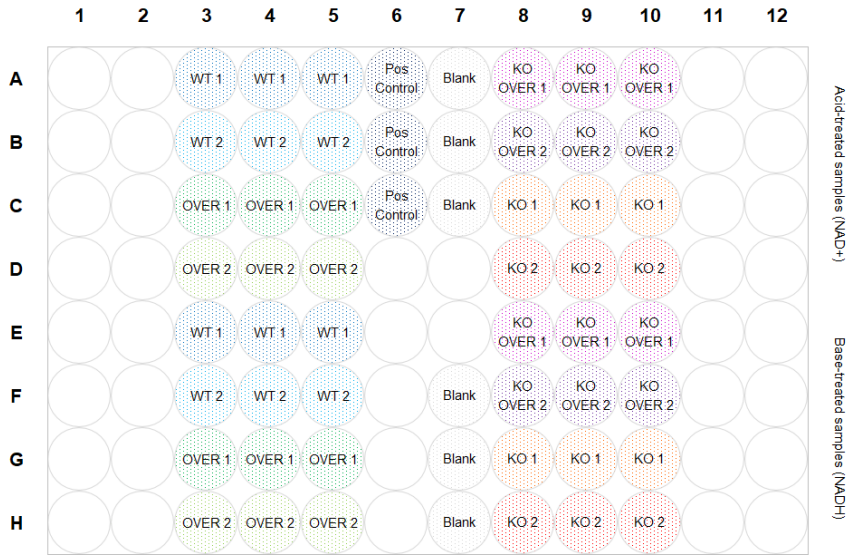


**Figure D.2: Microtiter plate layout used for the NAD/NADH-Glo™ assay.** As described in Section 4.4.3, cells (see Table 4.2) and blank wells (no cells) were prepared in rows E to H. Each cell solution was lysed, divided, and transferred to the corresponding columns of rows A to D for

acid treatment. Additionally, positive controls (containing 400 nM $NAD^+$ in 1x PBS) were set up in row 6. Pos Contr = positive control.

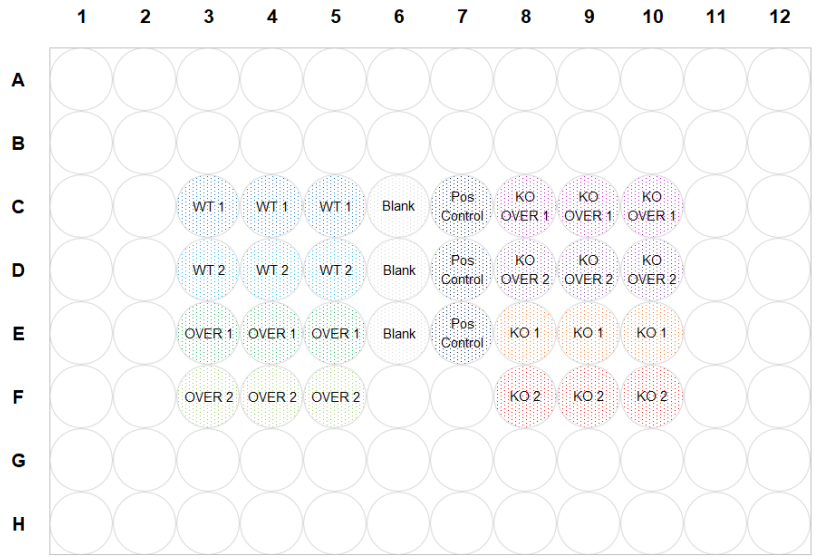


**Figure D.3: Microtiter plate layout used for the ADP/ATP assay.** Cells (see Table 4.2) were seeded as explained in Section 4.4.4. On the same plate, blank wells (no cells) as well as positive controls (containing 500 nM ATP in 1x PBS) were set up. Pos Contr = positive control.

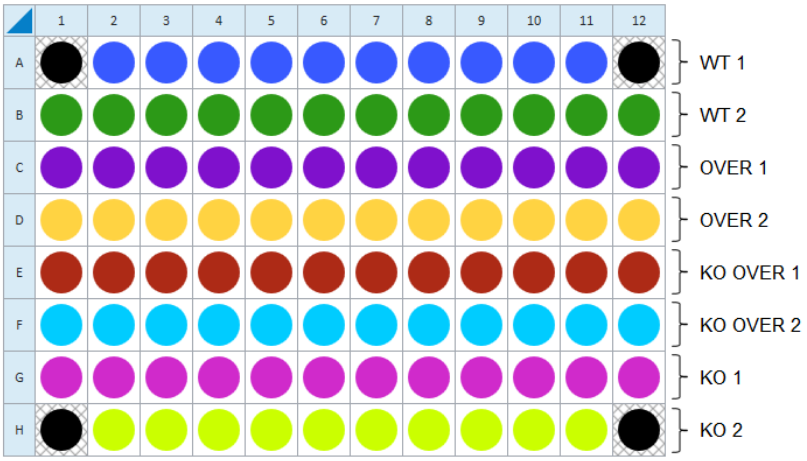


**Figure D.4: Microtiter plate layout used for the Mito Stress Test.** Cells (see Table 4.2) were seeded as explained in Section 4.4.6. Wells A1, A12, H1, and H12 were filled with galactose-containing medium only, to serve as background- and temperature correction. Following analysis on the Seahorse XF Analyser, normalisation was performed in the same microtiter plate.

# APPENDIX E:

## OPTIMISATION OF THE SEAHORSE XF$^e$96 ANALYSER CONDITIONS

### INTRODUCTION

As primary mouse fibroblast cultures have not previously been analysed at this institution using the Seahorse XF$^e$96 Analyser, the cell seeding density and FCCP concentration – two values that are specific to each cell type – were optimised prior to evaluating the different genotypes (Agilent, 2017). It was regarded unnecessary to optimise the oligomycin concentration, since a study by van Dyk (2016) had shown that 1 µM is sufficient for the complete inhibition of CV of various cell types. Additionally, there was no need to optimise the rotenone and antimycin A concentration, since the advised concentration (0.5 µM) was already considered saturating.

### i. SEEDING CELLS & ANALYSING THE BIOENERGETICS PROFILE USING THE SEAHORSE XF$^e$96 ANALYSER

The optimal cell seeding density per well and FCCP concentration were determined on a single plate, by following the method described for the Mito Stress Test in Section 4.4.6.3.a. On the first day, cells from mouse 79 (WT; see Table 4.5) were seeded at four different seeding densities (as shown in Figure E.1) based on recommendations by Agilent (2017). Since it had not yet been decided at this point to culture cells in galactose-containing medium prior to their analysis, cells were seeded in glucose-containing medium and incubated under standard conditions (see Section 4.3.3.1.b) for only 23 h (according to the general procedure followed at this institution). Similarly, no additional medium was added to the wells throughout this period.

On the second day, the growth medium was exchanged for assay medium, consisting of low buffered medium stock supplemented with 5 mM filter-sterilised glucose (pH 7.4; #G8644, Sigma-Aldrich) and 1 mM sodium pyruvate. Using the same assay medium, compounds were reconstituted and made up as described before. At this time, a range of four different FCCP concentrations (see Figure E.1) were prepared. The rest of the protocol proceeded as explained in Section 4.4.6.3.a (to wells A1, A12, H1, and H12, 0.25, 0.5, 0.75 and 1 µM FCCP were added respectively). Since the conditions being optimised could be determined relative to the theoretical cell seeding density, plates were not normalised by using the CyQUANT® Cell Proliferation Assay Kit.

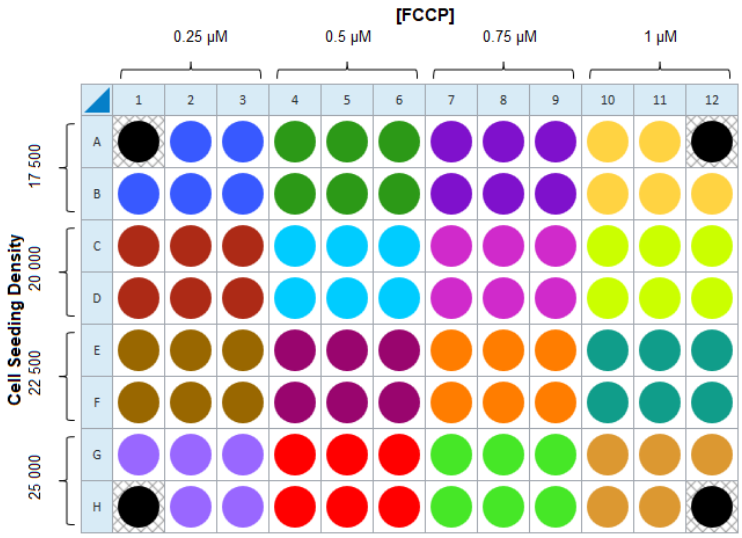


**Figure E.1: Microtiter plate layout depicting the different seeding densities and FCCP concentrations used for optimisation.** On the first day, WT cells were seeded at densities of 17 500, 20 000, 22 500, or 25 000 cells/80 µL/well. Wells A1, A12, H1, and H12 were filled with medium only to serve as background- and temperature correction. On the second day, FCCP was added to port B of the sensor cartridge at concentrations of 0.25 µM to 1 µM (in 0.25 µM increments). Each group (i.e. each seeding density or FCCP concentration) consisted of 22 or 24 wells.

### ii. OPTIMISING THE CELL SEEDING DENSITY & FCCP CONCENTRATION

The optimal cell seeding density and FCCP concentration were then determined using specific measurements (refer to Figure 4.5) of the bioenergetics profile obtained from the Mito Stress Test analysis. To process the data, the Wave Desktop software (v2.4) and Microsoft Excel 2013 were used. The mean and SD were calculated for a specific measurement of each group (i.e. each seeding density or FCCP concentration), after which outliers were removed according to the Tukey method.

The optimal cell seeding density was first approximated by visually inspecting the cells (at 23 h) under a microscope. Specifically, the following was evaluated: The confluency of each well had to be between 50% and 90%, and cells had to be evenly distributed within each well, as well as between the wells of a particular seeding group (Agilent, 2017; van Dyk, 2016). While this held true for all seeding densities, the confluency of the cells seeded at 25 000 cells/well was closer to 100%.

Using the data obtained from measurement 3 of the bioenergetics profile, the mean OCR was then determined for each seeding group. Measurement 3 was chosen, as the cells were still untreated and had unlimited access to substrates at this point. The mean OCR values were then

plotted against seeding density to produce the scatter plot in Figure E.2. From this figure, the optimal cell seeding density was estimated as the value at which the basal respiration was a maximum, yet still fell within the range of 20 pmol/min to 160 pmol/min [since the mean ECAR of each group was within its recommended range (10 mpH/min to 90 mpH/min), ECAR is not presented here].

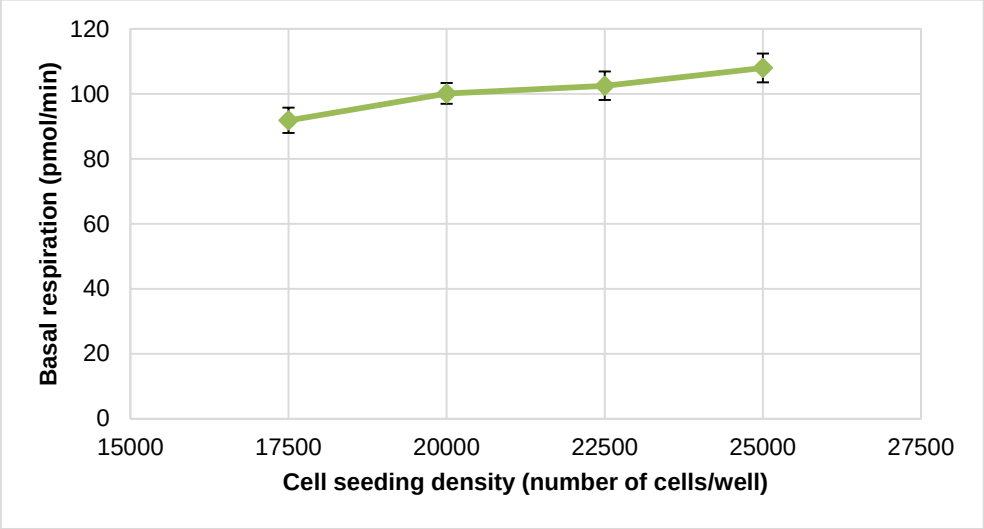


**Figure E.2: Scatter plot depicting the relationship between the basal respiration (OCR taken at measurement 3) and cell seeding density.** Data points represent the mean OCR (n = 22 or 24) ± SD.

Generally, the growth of a cell population is studied by employing a growth curve. The latter consists of four phases, including a lag-, exponential-, stationary-, and death phase. The lag phase describes a period of zero growth during which cells prepare to re-enter the cell cycle, and is brought on by the introduction of a new medium type, or the recovery of cells following previous stress (e.g. trypsinisation or overgrowth). Cells may then enter the exponential phase, in which they exhibit a constant and maximal growth rate, with regular cell population doubling. Here, growth is considered to be the most uniform and, consequently, the exponential phase is preferred for the study of cell biochemical characteristics. As substrates become limited or the critical population level is attained (e.g. when cells become over confluent), cells can withdraw from the cell cycle as they enter the stationary phase. During this time, cell morphology may change (e.g. fibroblasts can display cytoplasmatic prolongations), cells may still respire without division, and/or the division rate can equal the death rate (Keira *et al.*, 2004). Upon reaching the death phase, however, this balance will shift to mortality, as a result of nutrient depletion or programmed pathways.

As may be seen from Figure E.2, OCR increased with an increase in seeding density, as expected. The mitochondrial respiration did not reach a plateau, further indicating that cells seeded at the highest density (25 000 cells/well) had not yet entered the stationary phase (had

greater seeding densities been chosen, the curve would most likely have plateaued). Therefore, based on this graph alone, any of the seeding densities would have been sufficient.

To narrow this down, the OCR values were then normalised to the theoretical cell seeding density per well, and a second scatter plot was drawn (Figure E.3). Here the curve was expected to remain constant with increasing seeding density, while a decrease in OCR indicated that the maximum acceptable seeding density per well had been achieved (van Dyk, 2016).

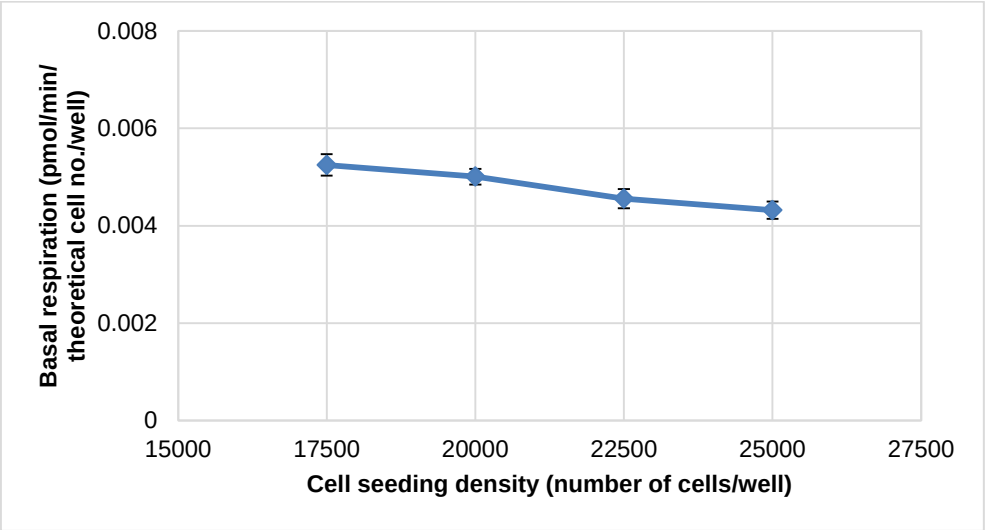


**Figure E.3: Scatter plot depicting the relationship between the basal respiration (OCR taken at measurement 3) and cell seeding density, normalised to the theoretical number of cells/well.** Data points represent the mean normalised OCR (n = 22 or 24) ± SD.

Figure E.3 displays a slow decrease in OCR from 17 500 cells/well to 20 000 cells/well. This decrease then becomes sharper as seeding density is increased to 25 000 cells/well. Thus, by taking into account the cell confluency, as well as the results shown in Figures E.2 and E.3, 20 000 cells/well was selected as the optimal seeding density.

It should however be noted that the reaction conditions employed differed between the optimisation and final experiments. Since the latter would require seeding cells in galactose-containing medium (instead of complete growth medium which contains glucose), and incubating the plate for 47 h (instead of 23 h), it was decided to decrease the seeding density of the final experiments to 12 500 cells/well.

To determine the optimal FCCP concentration, the mean OCR values were calculated for each FCCP concentration group by using the data obtained from measurement 7 of the bioenergetics profile at the optimal cell seeding density (determined as 20 000 cells/well above). The mean OCR values were then plotted against the FCCP concentration to yield the titration curve in Figure E.4.

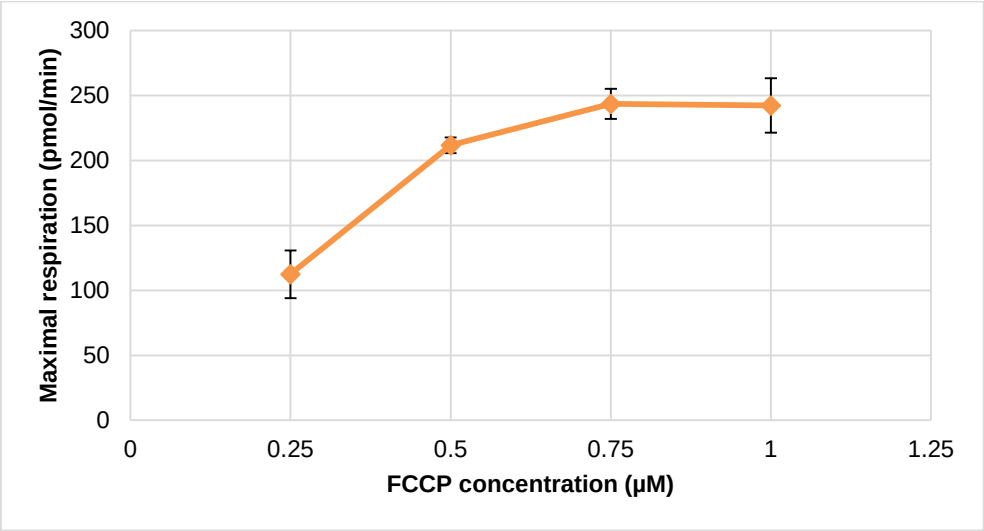


**Figure E.4: Titration curve depicting the relationship between the maximal respiration (OCR taken at measurement 7) and FCCP concentration.** Data points represent the mean OCR (n = 22 or 24) ± SD.

As shown in Figure E.4, OCR increased with increasing FCCP concentration, to reach a maximum at 0.75 µM, followed by a slight decrease to 1 µM FCCP. The latter may be attributed to a depolarised Δψ, which is influenced by FCCP's disruption of the endosome (and other organellar) function and acidification of the cytosol (since FCCP acts as a protonophore across all membranes) (Brand & Nicholls, 2011). The optimal FCCP concentration was therefore taken to be 0.75 µM; i.e. the FCCP concentration yielding the highest maximal respiration prior to a succeeding decrease in OCR.

# APPENDIX F:

## LANGUAGE EDITING CERTIFICATE

*This document serves to certify that the dissertation submitted in partial fulfilment of the degree,* ***Magister Scientiae*** *in* ***Biochemistry***

*of*

***Michelle Mereis***

*has been edited for grammar, linguistic accuracy, and authorial consistency*

*by*

*Helgard David Jordaan*

17/11/2017

**Wouter Stefanus Badenhorst**
Commissioner of Oaths
Practising Attorney - RSA
690 Ella Street, Rietfontein
Pretoria